Author:
Nielsen, Morten Lunde

Title:
Understanding biases in reconstructing ancient marine ecosystems through the early Cambrian Sirius Passet Lagerstätte, North Greenland

Understanding biases in reconstructing ancient marine ecosystems through the early Cambrian Sirius Passet Lagerstätte, North Greenland

by

Morten Lunde Nielsen

School of Earth Sciences
University of Bristol

with CASE partner

British Geological Survey

A dissertation submitted to the University of Bristol in accordance with the requirements for award of the degree of Doctor of Philosophy in the Faculty of Science

06/10/2022

Word count: 37326

Abstract

The early Cambrian (~538,8–509 Ma) marks the rapid radiation of modern animal life. ‘Burgess Shale-type’ (BST) Lagerstätte provide important windows into these early ecosystems. But how faithfully do they preserve them? Fossil assemblages have been through multiple taphonomic ‘filters’ before discovery that can each severely bias their biotas. In this thesis, I attempt to show how recognizing biases in the geologically complex and poorly understood lower Cambrian Sirius Passet Lagerstätte (North Greenland) can expose novel biological information. Each filter and its bias reflect processes that occur with different geological timing. First, I use petrographic and chemical analyses to show that quartz preserving labile soft tissues are a metamorphic replacement of originally phosphatized tissues. Then, I use a quantitative dataset of the distribution of these highly frequent phosphatized tissues to assess important controls and biases on phosphatization. I identify five controls: taxonomy, tissues, microenvironments, size, and diet. Each of them shows different biases. Then, I use an integrated bed-by-bed approach to determine the taphonomic and temporal biases of the depositional environment. I find that the benthic and pelagic components of Sirius Passet are minimally biased and capture temporal population dynamics due to highly frequent deposition. Since most macrofauna are likely preserved in Sirius Passet, I then attempt to reconstruct a qualitative food web for the pelagic biota. I find that the trophic structure has characteristics of a modern high-productivity ‘wasp-waist’ ecosystem, despite showing a significantly different taxonomic organization. Lastly, I speculate that the unique characteristics of Sirius Passet may be linked to a high-productivity paleoenvironment near a marine river plume. My thesis shows how detailed contextualization of a complex Lagerstätte (Sirius Passet) can reveal primary (biological) signals from secondary (biases/overprints) signals. Sirius Passet has potential to be a treasure trove of biological information from aftermath of the Cambrian Explosion.

Author’s declaration

I declare that the work in this dissertation was carried out in accordance with the requirements of the University's Regulations and Code of Practice for Research Degree Programmes and that it has not been submitted for any other academic award. Except where indicated by specific reference in the text, the work is the candidate's own work. Work done in collaboration with, or with the assistance of, others, is indicated as such. Any views expressed in the dissertation are those of the author.

Signed: Morten Lunde Nielsen   Date: 06/10/2022

Acknowledgements

First, I would like to sincerely thank my supervisors Jakob Vinther, Phil Wilby, Tae-Yoon Park and Arne Thorshøj Nielsen for their encouragement, training and support. I am especially grateful to Jakob for taking me on this journey and his generosity along the way.

I would also like to thank those who have supported my research: Stuart Kearns and Ben Buse at the School of Earth Sciences, University of Bristol. Sebastian Næsby Malkki at the Geological Survey of Denmark & Greenland. Collections manager Arden Roy Bashforth and curator Laura Cotton at the Natural History Museum of Denmark for access to previous Sirius Passet collections. The Department of Geosciences and Natural Resource Management, University of Copenhagen for a guest office during my time in Copenhagen, Denmark. My officemate Mads Engholm Jelby for sedimentological discussions. I am especially thankful for the generous help from Mirinae Lee, Jae-Ryong Oh, Ji-Hoohn Kihm, Yeongju Oh, Jikhan Jung, Pilmo Kang, and Jina Kim during my visits to Korea Polar Research Institute (KOPRI), Incheon, Korea.

I appreciate the support from my funding body Natural Environment Research Council (NERC) GW4+ Doctoral Training Partnership (DTP) and CASE-partner British Geological Survey. I also appreciate the additional support from KOPRI, especially the KOPRI Arctic Science Fellowship Program 2018 grant that enabled me to bring my family to Korea for 2½ months.

Lastly, I would like to thank Sarah, Eskild & Ronja for everything.

i. Thesis outline

The aim of this thesis is to improve ecosystem reconstructions by resolving taphonomic filters (biases) at different geological phases. We will here focus on cases from the Sirius Passet Lagerstätte that depict three principal biases: *(1)* biostratinomic temporal bias, *(2)* early diagenetic taphonomic bias, and *(3)* late diagenetic/metamorphic overprinting. Weathering is a fourth bias but (unfortunately) not treated independently herein. These biases are superimposed on each other as layers: effects of subsequent biases must be resolved before effects of preceding biases can be investigated. Only once every layer is removed can we get to the core: ecosystem reconstructions. In this thesis, I therefore treat the principal biases in reverse chronological order, each time peeling away a filter on the biota (Fig. i.1): Chapter 2 recognizes the metamorphic overprint on the primary taphonomic pathways. Only then can Chapter 3 recognize the primary biases of labile soft tissue phosphatisation. Chapter 4 (in part) recognizes the biostratinomic, temporal, and preservational biases in bed-by-bed fossil assemblages representing a given depositional environment. Then, once biases are recognized, Chapter 4 (in part) and Chapter 5 can finally present primary ecosystem reconstructions in form of temporal population dynamics (Chapter 4) and a food web for a Cambrian pelagic fauna (Chapter 5).

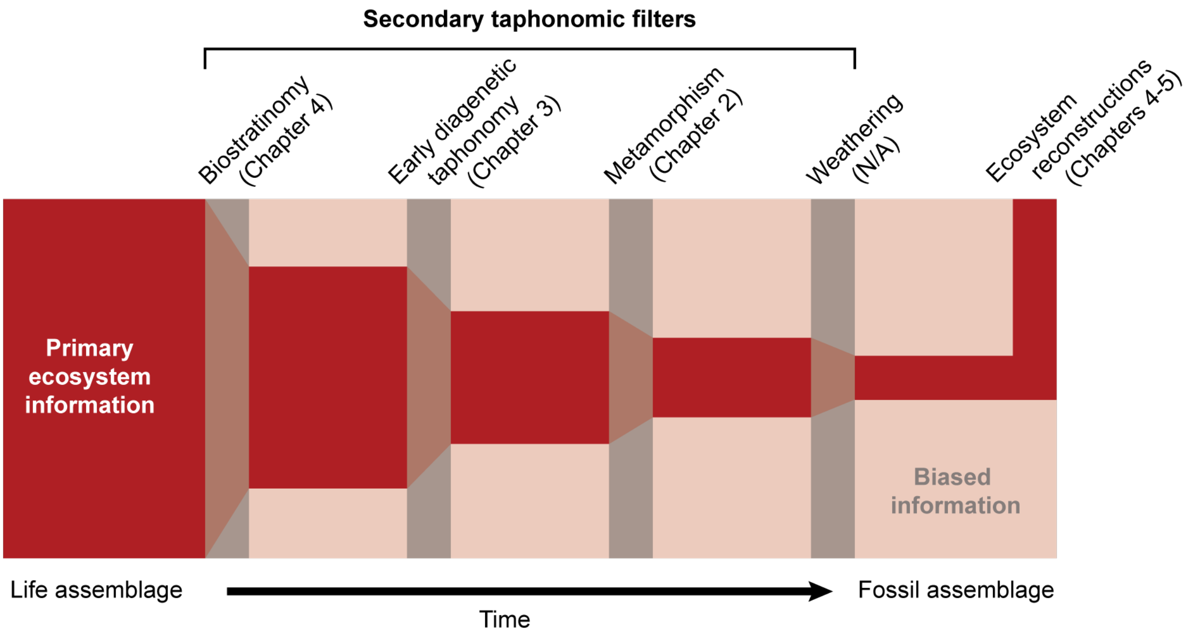

Figure i.1. Thesis overview. Conceptual overview of the principal taphonomic filters (grey bars) that bias (pale red) primary ecosystem information (dark red), and in which chapters they are treated.

Table of Contents

List of Figures

List of Tables

List of Electronic Data Tables

List of abbreviations

BST: ‘Burgess Shale-type’.

GEUS: Geological Survey of Denmark and Greenland.

GGU: Grønlands Geologiske Undersøgelse (now GEUS).

KOPRI: Korea Polar Research Institute.

MGUH: Institutional abbreviation for material deposited at the Natural History Museum of Denmark, Copenhagen, Denmark.

OMZ: Oxygen minimum zone.

SP: Field number for Sirius Passet material.

Chapter 1

Cambrian ‘Burgess Shale’-type Lagerstätten: their ecosystem windows, biases, and the Sirius Passet Lagerstätte

Author contributions

This chapter is not intended for publication. I wrote the chapter and produced the figure with minor input from Jakob Vinther.

1.1 How well do we understand ancient ecosystems?

Fossils are fundamental to answer this question since they record actual organismal history through geological time. However, the fossil record is essentially unreliable: quality, quantity and mode of preservation are highly variable between fossil sites (Kidwell and Holland, 2002). Highest quality of preservation is found in so-called Konservat-Lagerstätten—fossil sites with exceptional preservation of soft tissues (Seilacher et al., 1985; Allison, 1988a), but even they show limitations. If we want to better understand ancient ecosystems and their evolution, we must be capable of predicting these taphonomic limitations (i.e., bias). Mechanisms of taphonomic pathways for exceptional preservation have been extensively explored, for example for: organic preservation of compressed body fossils (e.g., Butterfield, 1990; Gaines et al., 2012; Anderson et al., 2020b) and associated pyritization (e.g., Briggs et al., 1996; Gabbott et al., 2004; Schiffbauer et al., 2014); phosphatization of labile soft tissues (e.g., Briggs and Kear, 1993; Wilby, 1993; Butterfield, 2002; McNamara et al., 2009) and external cellular tissues of microfossils (e.g., Muscente et al., 2015); silicification of external cellular tissues of microfossils (Muscente et al., 2015) and by entombment (e.g., Trewin et al., 2003); and aluminosilicification of labile soft tissues (Gabbott, 1998). However, the biases they each inflict upon preserved biotas are less well-understood but not less important (Allison, 1988c; Wilby and Briggs, 1997; Butterfield, 2003; Sansom et al., 2010; e.g., Wilson et al., 2016; Clements et al., 2017; Saleh et al., 2020b, 2021c). For example, loss of decay-susceptible tissues before fossilization may mimic evolutionary absences in early forms, a so-called 'stem-ward slippage' (Sansom et al., 2010). Or, phosphatization may favor preservation of certain organisms, such as fish and polychaetes, in one deposit but not the other (Wilby and Briggs, 1997). These biases distort the fossil record. Recognizing them requires a thorough understanding of the complex geological histories of Lagerstätten since numerous (also post-depositional) processes can significantly influence the taphonomy (e.g., Butterfield et al., 2007a). Biases especially impact interpretations of anatomy and morphology of early animals where relationships between (stem-lineage) taxa are not immediately obvious (Sansom et al., 2010). Much of our knowledge on early animals derives from Cambrian so-called 'Burgess Shale-type' (BST) Lagerstätte where the taxonomic relationships of some enigmatic taxa have been debated for a century due to their unusual morphologies (e.g., Vinther and Parry, 2019).

1.2 Why are Cambrian 'Burgess Shale-type' (BST) Lagerstätten important?

The 'Cambrian Explosion' marks the appearance of most modern phyla and modern-style ecosystems with infaunal, benthic, and pelagic lifestyles by the early Cambrian. This time interval therefore provides key evidence for evolutionary relationships between phyla. Evolution was likely escalated by ecological innovations such as carnivory (Sperling et al., 2013), but how were these early ecosystems actually structured? Cambrian Lagerstätten (Butterfield, 2003) are fundamental to answer this question. 'Burgess Shale-type' (BST) Lagerstätten are macrofossil sites where soft tissues are exceptionally preserved as carbonaceous compressions (i.e., BST preservation, Butterfield, 1990), providing the most complete records of soft-bodied biotas in the early Paleozoic (Conway Morris, 1989; Gaines, 2014). More than a dozen BST Lagerstätten have been reported worldwide (Holmes et al., 2018), but the most famous is the Burgess Shale Lagerstätte (Canada): it has since its relatively early discovery in 1909 epitomized BST Lagerstätten (Gould, 1989). BST Lagerstätten provide crucial information on evolution of e.g., arthropods (Daley et al., 2018) and numerous stem-group taxa for other phyla (Briggs and Fortey, 2005), some of which are still actively debated (e.g., *Amiskwia*: Caron and Cheung, 2019; Vinther and Parry, 2019). Ecosystem research has, however, received considerably less attention due to the geological nature of the Lagerstätten.

BST Lagerstätten captures biotas from a spectrum of marine depositional environments: from prodeltas (Chengjiang Lagerstätte, Saleh et al., 2022b) to more distal shelf environments (Burgess Shale, Gabbott et al., 2008). The Lagerstätten share some commonalities. The carbonaceous compressions are preserved in low-oxygen mudrocks (Butterfield, 1995; Gaines et al., 2008, 2012). Rapid burial is a prerequisite to reduce activity of decay-inducing bacteria by limiting oxygen availability (Butterfield, 1995). Encasing clay (such as kaolinite) minerals may aid preservation by either stabilizing tissues (Wilson and Butterfield, 2014) or inhibiting bacterial activity (McMahon et al., 2016) or both (Anderson et al., 2020b) (but see metamorphic overprints in Section 3.3). Fossils are mostly entombed within rapidly buried, catastrophic 'event beds' in e.g., Burgess Shale (Caron and Jackson, 2006; Gabbott et al., 2008) and Chengjiang (Zhao et al., 2009; MacKenzie et al., 2015), or, more rarely, on bedding surfaces as in Fezouata Lagerstätte (Saleh et al., 2021a). In the Burgess Shale, records of carbonaceous compressions are stratigraphically punctuated as they do not occur in all beds; instead, the fossiliferous beds are separated by non-fossiliferous beds (Caron and Jackson, 2006). In Burgess Shale and Chengjiang, fossils are relatively rare except for a few high-density beds (Caron et al., 2014 supplementary data 2; Vannier and Martin, 2017). The combination of punctuated records and low fossil densities are particularly adverse for ecosystem analyses which have been focused on broad-scale structures such as highly time-averaged food webs (Dunne et al., 2008) and communities (Caron and Jackson, 2008; Zhao et al., 2009; Nanglu et al., 2020). Still, food-web analyses (Dunne et al., 2008) and autecological interpretations (e.g., Vannier et al., 2007; Vinther et al., 2014) have indicated that modern-like food-web structures had already evolved by the early Cambrian.

1.3 Are BST biotas biased?

Understanding biases is crucial to predict what information is missing from fossil ecosystems. BST Lagerstätten have been subjected to several taphonomic processes (filters) that potentially have biased the fossil assemblages. How they are biased depends on the depositional environment and post-depositional (tectonic) history. Ignoring the important anthropocentric biases in fossil collection (Whitaker and Kimmig, 2020), the main processes of taphonomy are biostratinomy, early fossil diagenesis, metamorphism, and weathering (Parry et al., 2018 fig. 1). Each of these can introduce biases and the effects are cascading: the bias of a latter filter must be resolved before a former filter can be investigated. Incomplete understanding of the main taphonomic processes may eventually lead to invalid conclusions. In the following part, I briefly summarize these processes and their biases in reverse chronological order. Weathering will not be treated by itself in this thesis but is included here since it is common in BST Lagerstätten and shows a high potential for bias.

Weathering is the last process to affect fossils and likely also the most destructive. It is produced by percolating meteoric and/or groundwater (Forchielli et al., 2014). In BST Lagerstätten, effects are often restricted to pseudomorphing minerals of e.g., pyrite by iron oxide (e.g., Gabbott et al., 2004), but is also able to obscure primary taphonomic pathways completely (Butterfield, 2002; Lerosey-Aubril et al., 2018), or mimic biological structures (Saleh et al., 2020c). If weathering is restricted to specific bedding surfaces or intervals (e.g., Tarhan et al., 2018 for an Ediacaran example), it has potential to bias against those local depositional environments and distort bed-by-bed comparisons of fossil assemblages.

Metamorphism (and late diagenesis) can obscure primary taphonomic pathways by overprinting mineralogy of fossils. It can remove carbon from carbonaceous fossils by extensive volatilization (Butterfield et al., 2007a), alter it beyond recognition (Slater et al., 2018), and change mineralogy significantly. For example, in Burgess Shale, 'clay templating', originally thought to be the important taphonomic pathway for BST fossils (Orr et al., 1998; but see also Anderson et al., 2020b), and preservation of primary blood chemistry (Pushie et al., 2014), have both subsequently been argued to represent overprints by metamorphism (Butterfield et al., 2007b; Page et al., 2008) and late diagenetic fluid flows (Gaines et al., 2019), respectively.

Early fossil diagenesis of BST biotas is the most important window in which the organism becomes transformed into a geologically stable object. It also presents a good case for why it is important to consider the full taphonomic history of Lagerstätten as later overprints may get conflated into development of models of primary preservation. Once metamorphic and weathering effects (see above) have been identified, it is possible to understand the primary taphonomic pathways. Carbonaceous preservation (compressed later during diagenesis) (Butterfield, 1995; Gaines et al., 2008, 2012), +/- pyrite coatings (e.g., Gabbott et al., 2004; Saleh et al., 2020a), is the most important component in BST windows. It does, however, show taxonomic bias (Saleh et al., 2020a, 2022a); the underlying controls are uncertain but may partly relate to the original composition of the host tissues and the timing of decay versus stabilization (Parry et al., 2018; Saleh et al., 2022a). Carbonaceously preserved fossils may be accompanied by phosphatization (Butterfield, 2002; Lerosey-Aubril et al., 2012; Gaines, 2014), the replacement of labile soft tissues by authigenic apatite (Martill, 1988; Briggs et al., 1993). Phosphatization is intrinsically biased (Wilby and Briggs, 1997; Wilson et al., 2016; Clements et al., 2017) and only preserve commonly in a few types of BST organisms and tissues (mostly panarthropod guts; Butterfield, 2002; Lerosey-Aubril et al., 2012; Gaines, 2014), and hence strongly bias available anatomical information. Although phosphatization has received intense scrutiny (see e.g., Briggs, 2003), biases of phosphatization remain poorly known (but see Wilby and Briggs, 1997; Clements et al., 2017). Altogether, it is key to resolve primary taphonomic pathways and, importantly, recognize their biases before making predictions of missing elements from BST biotas and the fossil record in general.

Biostratinomy represents the (post-mortem) pre-diagenetic filters. It is strongly related to the depositional processes and can roughly be divided into accumulation and transportation (Kidwell and Bosence, 1991). Accumulation bias against less robust autochthonous fossils by the prolonged exposure of carcasses to decay, scavenging, and hydraulic fragmentation by e.g., winnowing (Kidwell and Bosence, 1991). It additionally biases temporal resolution by conflating successive communities into a single pooled community (Fürsich and Aberhan, 1990). Transportation likewise biases allochthonous fossil assemblages by distance-dependent size-sorting (Westrop, 1986) and fragmentation of (decayed) carcasses (Allison, 1986; Bath Enright et al., 2017). BST biotas are generally deposited within gravity flows and are in those cases biased by allochthonous transportation (Bath Enright et al., 2021; e.g., Saleh et al., 2021c), but may also be autochthonous (Zhao et al., 2009; Saleh et al., 2021a) and therefore mostly biased by accumulation mode (Zhao et al., 2009; Saleh et al., 2020b).

Each Lagerstätte is controlled by almost endless depositional variables that will create a distinct combination of biases. Information completely lost to bias is impossible to recover but if they are recognized, different Lagerstätten will likely provide different opportunities to understand early ecosystems.

1.4 Case site: the Sirius Passet Lagerstätte

The lower Cambrian Sirius Passet Lagerstätte (North Greenland) is a remarkable BST Lagerstätte, comparable in potential to Burgess Shale and Chengjiang (Conway Morris, 1989). It has provided enigmatic taxa that have improved our knowledge of particular phylogenetic relationships and stem-lineages, such as the so-called 'gilled lobopods' *Kerygmachela* (Budd, 1993) and *Pambdelurion* (Budd, 1997), the mollusc *Halkieria* (Conway Morris and Peel, 1995), and the large stem-loriciferan *Sirilorica* (Peel, 2010a). Additionally, it preserves astounding quantities of labile soft tissues as three-dimensional mineralizations (e.g., Young and Vinther, 2016) and carbonaceous compressions (e.g., Park et al., 2018). However, Sirius Passet has so far received much less attention than Burgess Shale and Chengjiang. The reasons are twofold: its remote location, that has made field collections expensive and impractical, and its complex geological history. Previous studies have primarily focused on taxonomical descriptions and their phylogenetic implications (Budd, 1995, 1997, 1998b; Stein, 2010; Vinther et al., 2011b; Stein et al., 2013), of which there are still numerous undescribed taxa. There has been less focus on resolving questions on ecology (Mángano et al., 2012; Vinther et al., 2014; Harper et al., 2019) and taphonomy (Budd, 2011; Strang et al., 2016b, 2016a; Topper et al., 2018). However, Sirius Passet is a natural laboratory for both: stacked fossiliferous beds with high densities of well-preserved fossils (Vinther et al., 2011b) have potential to reveal ecosystem dynamics, while the high frequencies of labile soft tissues (Young and Vinther, 2016) and extended geological history (Harper et al., 2019) is appropriate for resolving taphonomic biases and the potential effects of late-stage overprints. Consequently, much of Sirius Passet's potential to advance knowledge on Cambrian ecosystems has, so far, remained unrealized.

1.5 History of discovery

Material from Sirius Passet was first collected from scree in 1984 and 1985 during a regional mapping project of North Greenland by the Geological Survey of Greenland (GGU, now GEUS) (Peel, 1990; Peel and Ineson, 2011). However, its soft-bodied biota was not discovered until John Peel examined the collected material in 1986 (Peel, 1990). The implications of a new BST locality were immediately recognized (Conway Morris et al., 1987; Conway Morris, 1989), and the first Sirius Passet expedition, led by John Peel and Simon Conway Morris, commenced in 1989, collecting about 1500 slabs from the scree (Peel, 1990). Since then, nine expeditions have visited Sirius Passet under various leaderships: GGU/GEUS continued in 1991, 1991, 1994, 2006; Natural History Museum of Denmark (led by David Harper) in 2009, 2011; Korea Polar Research Institute (led by Tae-Yoon Park and Jakob Vinther) in 2016, 2017, 2018, and 2022 (Peel and Ineson, 2011; Harper et al., 2019). However, the actual outcrop was first uncovered in 2009 (Peel and Ineson, 2011). Before that, expeditions had collected (often weathered) scree material where fossil identification relied mostly upon their relief (e.g., Budd, 2011). Subsequent focus on *in situ* collection resulted in a much wider recognition of soft-bodied taxa preserved as entirely flat, reflective films (e.g., Vinther et al., 2011b). The *in situ* collection also led to the first attempts at quantifying the fossil density and variation in 10 cm bed-by-bed intervals (Harper et al., 2019). The late expeditions (2016–2022) had various aims but focused particularly on minimizing collection bias via thorough inspections after in-field cleaning of the rocks with water, in turn enhancing fossil reflectivity to find quality specimens for taxonomic descriptions. Another aim centered around my PhD thesis on collecting and identifying fossils in the field and in the laboratory for taphonomic and paleoecological quantification.

1.6 Geological setting

1.6.1 The Sirius Passet Lagerstätte

The Sirius Passet Lagerstätte is a collection of six sites with exceptionally preserved macrofossils located within a 1 km stretch of the informally dubbed 'Sirius Passet valley' (Peel & Ineson, 2011), just south of Nansen Landon the northern shore of the J.P. Koch Fjord in north-west Peary Land, North Greenland (Fig. 1.1A). It is part of the lowermost Buen Formation (Conway Morris et al., 1987; Harper et al., 2019) deposited in the Franklinian Basin (Higgins et al., 1991). The Buen Formation is exposed across an east-west outcrop belt in Peary Land that ranges from ~325–700 m in thickness and represents a northwards-trending onshore-offshore gradient, from sand-rich, onshore and shallow marine deposits in the south to mud-rich, deeper marine shelf deposits in the north (Ineson & Peel, 1997: Ineson & Peel, 2011). Buen Formation eventually transitions laterally into deeper basinal facies of the Polkorridoren Group (Ineson & Peel, 2011). In the 'Sirius Passet valley', the northern outcrop belt exposed these transitional deeper-marine facies (i.e., 'Transitional' Buen Formation in Ineson & Peel, 2011) adjacent to the Portfjeld Formation carbonates and permanent ice caps along the valley's southwestern-northeastern side (Ineson & Peel, 2011; Harper et al., 2019). The region around Sirius Passet then experienced two stages of regional tectonism: the Devonian Ellesmerian Orogeny produced a thrust-fold belt (Soper and Higgins, 1987; Higgins et al., 2000), while Mesozoic–Paleogene extensional-compressional tectonics caused dykes to intrude the local area around the Sirius Passet Lagerstätte (Soper and Higgins, 1987; Ineson and Peel, 2011).

Figure 1.1. The Sirius Passet Lagerstätte locality. (A) Location of Sirius Passet (red star) in Greenland. (B–E) Field photographs of Sirius Passet. (B) Main Sirius Passet locality (arrows) next to the carbonate Portfjeld Formation (light grey). Left arrow marks the stratigraphic top of the section, right arrow marks the stratigraphic base. (C) Closer view of the main section showing tilted beds. (D) Representative example of fissile, laminated mudrocks from a fossiliferous interval. (E) At least six exposed fossiliferous parting surfaces. Note the variation of weathering (iron oxide mineralization) between surfaces. Arrows mark fossils with labile soft tissue mineralization.

The Sirius Passet Lagerstätte is comprised of a main locality on a west-facing, scree-covered hillslope (Fig. 1B, latitude 82°47.6´N, longitude 42°13.7´W), with five subsidiary localities scattered within 1 km (Peel and Ineson, 2011). It only includes sites with BST preservation of macrofossils and does therefore not include the localities where preservation is restricted to small carbonaceous fossils found in the temporally younger parts of Buen Formation in southern outcrop belt (Slater et al., 2018). So far, research has mostly focused on the main locality since the other localities are mostly restricted to weathered scree (Peel and Ineson, 2011). Therefore, the name 'Sirius Passet' will from now on only refer to this particular main locality in the rest of this thesis. Here, an outcrop exposes a ~12 m thick section (Harper et al., 2019), with exceptional preservation in the upper ~8 m of the section, and is an isolated block between an older carbonate platform (Portfjeld Formation) and a thrust-fault (Ineson and Peel, 2011). It is therefore separated from the rest of the Buen Formation but is assumed to correlate to the lowermost mudrocks (Ineson and Peel, 2011).

The section is exposed with 48° tilting of the bedding planes (Ineson and Peel, 2011); it was previously suggested to be structurally right-way-up (Ineson and Peel, 2011), but the tectonic relationships and strong dominance of fossils oriented dorsal-down suggest it has been inverted (Harper et al., 2019). Age of Sirius Passet has been correlated to the *Nevadella* biozone in the early Cambrian (Stage 3, Series 2) based on the nevadiid trilobite *Buenellus higginsi* (Blaker, 1988; Babcock and Peel, 2007).

The section mainly consists of platy, laminated mudstones and siltstones (Fig. 1.1C; Ineson and Peel, 2011; Harper et al., 2019) in which the BST fossils occur. These fossiliferous beds are fissile and easily identified in the field by their mode of parting into distinct 2-5 mm beds. They are occasionally intervened by ~0,1–1 m thick massive, bioturbated beds (Ineson and Peel, 2011). The following description focuses solely on the fossiliferous beds and their appearance. Sedimentary structures are rarely reported in part because they are scant (Ineson and Peel, 2011), but planar lamination, fine grading and cross-lamination have been observed in thin sections (although the latter only below the fossiliferous intervals) (Strang et al., 2016b). Fossils are predominantly articulated (Babcock and Peel, 2007; Stein, 2010; Hammarlund et al., 2018). Microbial mats have been interpreted from clearly delimited, smooth surfaces of reflective films on the bedding surfaces sometimes associated with burrows from under-mat miners (Mángano et al., 2012; Harper et al., 2019), but their affinity has not yet been confirmed by microstructures from fossilized microbial cells or microbially induced sedimentary structures in thin sections.. Proposed microstructures are restricted to hollow vesicular and branching structures from trilobite molds (Strang et al., 2016b). However, these vesicles (Strang et al., 2016b, fig. 2E) are often angular and they could alternatively be molds after dissolved euhedral (pyrite?) crystals. Filamentous structures have not yet been identified on other fossils or surfaces. Trace fossils sometimes occur on parting surfaces as non-disruptive horizontal burrows most often associated with the ‘mats’ or fossils (Mángano et al., 2012). Mineralogy is a metapelite of predominantly quartz, micas, chlorite, and chloritoid (Strang et al., 2016b). Chloritoid needles cross-cut primary structures and represent greenschist-grade metamorphism (Ineson and Peel, 2011; Strang et al., 2016b) that has been estimated to have reached 409 ± 50 °C (Topper et al., 2018). Lastly, weathering often covers parting surfaces but their distribution and extent are uncertain (Fig. 1.1D; Harper et al., 2019).

The depositional environment is poorly understood due to the lack of unambiguous evidence. Initially, the laminated fossiliferous mudrock was interpreted to reflect sedimentation from suspension fall-out next to a carbonate platform scarp broadly similar to the setting of Burgess Shale (Ineson and Peel, 2011) possibly by windblown dust (Boudec et al., 2014). However, the sedimentological grading revealed by later analyses indicated that deposition was more likely by low-density gravity flows (Strang et al., 2016b), which is more consistent with such pristine exceptional preservation. Low-energy deposition is supported by the thin, fine-grained beds and a general paucity of fragmented or disturbed fossils (Budd, 1999; Babcock and Peel, 2007; Hammerlund et al., 2019). The muddy sediment was not fully anoxic as the presence of variable degrees of infaunal bioturbation suggests fluctuating oxygen levels (Ineson & Peel, 2011). Structural field relationships later indicated that the position next to the carbonate platform was likely a result of tectonic activity (Harper et al., 2019). Instead, the environment was interpreted as a low-oxygen environment on a low-gradient shelf-slope break correlative to the deeper parts of the 'Transitional' Buen Formation (Ineson & Peel, 2011; Harper et al., 2019). Paleobathymetry of Sirius Passet is uncertain, but the undisturbed sediments and fossils suggest it was below storm wave base (Strang et al., 2016b). The supposedly high densities of microbial mats were taken as an indication that the site was below the photic zone (Harper et al., 2019), but this remains speculative as the true extent of microbial mats has not yet been properly documented (see above). Compared to Burgess Shale (Walcott Quarry) and Chengjiang, deposition of Sirius Passet occurred in less energetic environment. In Burgess Shale and Chengjiang, exceptional preservation mainly occurs within centimeter-thick beds representing plug flows and low-density turbidity currents (Gabbott et al., 2008; Bath Enright et al., 2021; Saleh et al., 2022) with sufficient energy to transport engulfed animals away from their original habitats and deposit them in front of a distal shelf escarpment (at Burgess Shale, Caron & Jackson 2008) or, more proximally, at the edge of a prodelta (Chengjiang, Saleh et al., 2022). However, whether Sirius Passet is more distal or deeper than e.g. Burgess Shale requires a more extensive and in-depth description of its sedimentology.Paleogeographically, Sirius Passet was likely within the tropical or subtropical climate belt as part of Laurentia (Williams et al., 1996).

1.6.2 The Sirius Passet biota

Sirius Passet preserves a relatively low-diversity fossil assemblage (see Holmes et al., 2018 table 1) with 45 taxa described to date (Table 1.1). The biota is numerically dominated by arthropods (93% of field sampling in 2011 cf. Harper et al., 2019). It is taxonomically distinct from other Cambrian biotas (Holmes et al., 2018) and includes a range of unique taxa, such as articulated halkieriids (Conway Morris and Peel, 1990), 'gilled lobopods' (Budd, 1993, 1998a), and large-sized (up to 70 mm) stem-loriciferans (Peel et al., 2013). Other biomineralized shelly taxa are restricted to a single trilobite taxon (Babcock and Peel, 2007) and rare hyoliths (Peel, 2010b), in addition to a number of sponge taxa (Botting and Peel, 2016).

Isoxys volucris (Williams et al., 1996) is, by far, the most common fossil in Sirius Passet (see Hammarlund et al., 2018, fig. 6). It is a small bivalved panarthropod characterized by a carapace (<20 mm long) with long, thin anterior and posterior spines, a wrinkly dorsal surface, and a mostly smooth ventral surface bordered by a conspicuous doublure (Williams et al., 1996; Nielsen et al., 2017). Despite being ubiquitous, its ventral soft tissues are only known from a few specimens (Stein et al., 2010), likely due to highly variable, and evidently complex, taphonomic states. Observed ventral morphology comprises a pair of large eyes, frontal appendages (antennula cf. Stein et al., 2010); at least three rows of biramous limbs with almost equally-long endopods and paddle-shaped, setal-fringed exopods; and, possibly, a furca posteriorly (Stein et al., 2010). These features are broadly similar to *Isoxys auritus* from the Chengjiang Lagerstätte and possibly other species of *Isoxys* (Stein et al., 2010). Ecological niche of *Isoxys* (at the generic level) was likely as active swimmers in the water column based on morphological comparisons with modern bivalved arthropods (Vannier and Chen, 2000). *Isoxys volucris*, with its elongate carapace and long spines, likely inhabited the pelagic zone as such features are consistent with efficient long-distance swimming and vertical migration (Pates et al., 2021). This is supported by its relative eye size which is consistent with pelagic hunting interpreted for other *Isoxys* taxa (Vannier and Chen, 2000).

Table 1.1. Published taxa from the Sirius Passet Lagerstätte.

Taxa	Primary reference	Further references
Annelids		
Phragmochaeta canicularis	Conway Morris & Peel (2008)	Parry *et al.* (2015a)
Pygocirrus butyricampum	Vinther *et al.* (2011a)	Parry *et al.* (2015)

Arthropods		
Aaveqaspis inesoni	Peel & Stein (2009)	
Arthroaspis bergstroemi	Stein *et al.* (2013)	
Buenaspis forteyi	Budd (1999)	
Buenellus higginsi	Blaker (1988)	Babcock & Peel (2007)
Campanamuta mantonae	Budd (2011)	
Isoxys volucris	Williams *et al.* (1996)	Stein *et al.* (2010), Nielsen *et al.* (2017)
Kiisortoqia soperi	Stein (2010)	
Kleptothule rasmusseni	Budd (1995)	
Molaria steini	Peel (2017c)	
Pauloterminus spinodorsalis	Taylor (2002)	
Siriocaris trollae	Lagebro *et al.* (2009)	
Isoxys sp.	Peel (2010b)	
Sidneyia? sp.	Peel (2017b)	
Hyoliths		
Hyolithid sp.	Peel (2010b)	
Orthothetid sp.	Peel (2010b)	
Trapezovitus sp.	Peel (2010b)	
Scalidophorans		
Chalazoscolex pharkus	Conway Morris & Peel (2010)	
Singuuriqia simoni	Peel (2017a)	
Sirilorica carlsbergi	Peel (Peel, 2010a)	Peel *et al.* (2013)
Sirilorica pustulosa	Peel (2010b)	Peel *et al.* (2013)
Xystoscolex boreogyrus	Conway Morris & Peel (2010)	
Molluscs		
Halkieria evangelista	Conway Morris & Peel (1990)	Conway Morris & Peel (1995), Vinther & Nielsen (2005)
Non-euarthropod panarthropods		
Hadranax augustus	Budd & Peel (1998)	
Kerygmachela kierkegaardi	Budd (1993)	Budd (1998b), Park *et al.* (2018)
Pambdelurion whittingtoni	Budd (1997)	Budd (1998a), Vinther *et al.* (2016), Young *et al.* (2016)
Tamisiocaris borealis	Daley & Peel (2010)	Vinther *et al.* (2014)
Poriferans		
Choia cf. *carteri*	Botting *et al.* (2016)	
Constellatispongia canismajorii	Botting *et al.* (2016)	
Crassicoactum cucumis	Botting *et al.* (2016)	
Fieldospongia bellilineata	Botting *et al.* (2016)	
Hamptonia limatula	Botting *et al.* (2016)	
Lenica hindei	Rigby (1986)	Botting *et al.* (2016)
Lenica perversa	Botting *et al.* (2016)	
Lenica cf. unica	Botting *et al.* (2016)	
Saetaspongia cf. densa	Botting *et al.* (2016)	
Saetaspongia procera	Botting *et al.* (2016)	
Solactiniella cf. plumata	Botting *et al.* (2016)	
Demosponge indet.	Botting *et al.* (2014)	
Ethmophylloid archaeocyathan sp.	Peel (2010b)	
Silicean indet.	Botting *et al.* (2016)	
Stephanella? sp.	Botting *et al.* (2016)	

Fossils are mainly preserved as reflective films +/- low relief (Budd, 2011; Vinther et al., 2011b). Internal labile soft tissues are common: nervous tissues occur as reflective films (Park et al., 2018) while musculature and digestive systems occur as three-dimensional mineralizations. Muscle and guts (gut tracts and/or diverticula) have been reported from both ‘gilled lobopod’ taxa (*Kerygmachela* and *Pambdelurion*), six arthropod taxa (*Arthroaspis*, *Buenellus*, *Campanamuta*, *Kiisortoqia*, *Siriocaris*, and *Sidneyia*?), and a single polychaete (*Phragmochaeta*), while gut tracts furthermore have been reported from the arthropod *Pauloterminus* and both palaeoscolecid taxa (*Chalazoscolex* and *Xystoscolex*). Taphonomic pathways for Sirius Passet fossils have been debated due to their seemingly distinctive nature: *(1)* despite early recognition of Sirius Passet as an example of classic BST preservation (Butterfield, 1995), it was later suggested to represent a different taphonomic pathway due to the widespread three-dimensional soft tissue preservation (Gaines et al., 2008; Gaines, 2014). *(2)* reflective films generally lack substantial carbon concentrations (Budd, 2011) that have been suggested to reflect extensive carbon loss during metamorphism (Butterfield, 1995; Topper et al., 2018); however, Ediacaran-style ‘death-masks’ by microbial mat-derived authigenic silica veneers have also been proposed as a pathway for trilobites and perhaps others (Strang et al., 2016b). *(3)* Three-dimensional internal mineralizations show anatomically distinct mineralogy (Strang et al., 2016a): muscles are preserved by silica (Budd, 1998a, 1998b, 2011; Young and Vinther, 2016) and digestive structures are preserved in apatite (Vannier et al., 2014; Strang et al., 2016a). Pathways to explain this compositional variation have been surmised as primary phosphatization with metamorphic silica replacement of muscle (Butterfield, 2002), and, alternatively, proposed to be simultaneous phosphatization of guts and silicification of adjacent muscle (Strang et al., 2016b).

Ecological interpretations for Sirius Passet are scant. The biota has previously been surmised to capture two distinct communities: an autochthonous mat-dwelling community and an allochthonous community of mixed infaunal and nektonic taxa (Hammarlund et al., 2018; Harper et al., 2019), both representing extremely low-oxygen tolerant faunas (Hammarlund et al., 2018). The pelagic ecosystem was proposed to have a modern-like structure with high productivity, based on the suspension-feeding anomalocarid *Tamisiocaris borealis* (Vinther et al., 2014). Predator-prey interactions are preserved: gut contents reveal direct evidence of carnivorous predator-prey relationships for the arthropod *Sidneyia* and the palaeoscolecid worms *Chalazoscolex* and *Xystoscolex* that fed on *Isoxys* (*Sidneyia*?, palaeoscolecid worms) and *Halkieria* (*Sidneyia*?) (Peel, 2017b). Predation attempts have been inferred from deformed specimens of the trilobite *Buenellus* (Babcock and Peel, 2007) and stem-loriciferan *Sirilorica carlsbergi* (Peel et al., 2013).

1.7 Thesis aims

The overall goal of my thesis is to better understand the ecological context of early animals in the wake of the Cambrian 'Explosion'. To do this, taphonomic biases must be resolved first. It is therefore not an aim of this thesis to dwell on the details of the actual taphonomic processes, but instead to resolve the biases and reconstruct ecosystems. Sirius Passet is a natural laboratory to study late-diagenetic biases, taphonomic biases, and Cambrian ecology. Late-diagenetic biases from metamorphic (and weathering) overprints can be explored by a suite of mineral relationships. Taphonomic biases can be explored quantitatively by the high fossil densities and frequent preservation of labile soft tissues. Ecology can likewise be explored by the high fossil densities, with a temporal dimension since they occur continuously in stacked, thin beds. Here, I exploit this to illustrate the complex interplay between taphonomic biases and overprints, depositional environment, and ecosystems from a Cambrian paleoenvironment. First, I present a multidisciplinary series of cases that investigate the respective effects of metamorphism (Chapter 2), taphonomic pathways (Chapter 3), and biostratinomy (Chapter 4). Then, I attempt to reconstruct certain aspects of an early Cambrian ecosystem and link it to a possible paleoenvironment (Chapters 4–6).

In parallel to this, I aim to provide a depositional and taphonomic framework to interpret the Sirius Passet biota. So far, there has been ambiguity about its depositional environment and taphonomy due to the unique characteristics of Sirius Passet as both a Konservat (conservation) and Konzentrat (concentration) Lagerstätte (cf. Seilacher et al., 1985). Although many questions will be left unanswered, this thesis aims to present a coherent analysis of the general depositional and taphonomic setting.

Chapter 2

Metamorphism obscures primary taphonomic pathways

Author contributions

This chapter is published in *Geology*:

Nielsen, M.L., Lee, M., Ng, H.C., Rushton, J.C., Hendry, K.R., Kihm, J.H., Nielsen, A.T., Park, T.Y.S., Vinther, J. and Wilby, P.R., 2022. Metamorphism obscures primary taphonomic pathways in the early Cambrian Sirius Passet Lagerstätte, North Greenland. *Geology*, 50(1), pp.4-9.

My petrographic dataset is available at the University of Bristol Data Repository (data.bris) at https://doi.org/10.5523/bris.1imwjxezxgu332uqzlna2lugud.

The research for this chapter was developed by me, Jakob Vinther, and Philip R. Wilby. I selected, prepared, and analyzed material for scanning electron microscopy (petrography and elemental mapping), measured chloritoid angles, interpreted silicon isotopes, made the paragenetic sequence, and wrote most of the manuscript and produced most figures with input from other authors: Hong Chin Ng and Kathrine R. Hendry acquired silicon isotope data and wrote the isotope method section. Philip R. Wilby and Jeremy C. Rushton acquired bulk sediment composition data, analyzed them, produced Data Table E2.2 and Fig. 2.S1, and wrote the sections on bulk sediment compositions. Philip R. Wilby estimated mineral reactions on Fig. 2.7 and wrote the section on kaolinite. Mirinae Lee produced elemental maps for Fig. 2.1.

2.1 Abstract

Correct interpretation of soft-bodied fossils relies on a thorough understanding of their taphonomy. While the focus has often been on the primary roles of decay and early diagenesis, the impacts of deeper burial and metamorphism on fossil preservation are less well understood. Here, we document a sequence of late-stage mineral replacements in panarthropod fossils from the Sirius Passet Lagerstätte (North Greenland), an important early Cambrian 'Burgess Shale-type' biota. Muscle and gut diverticula were initially stabilized by early diagenetic apatite, prior to being pervasively replaced by quartz and then subordinate chlorite, muscovite and chloritoid during low-grade metamorphism (~400 °C). Each new mineral replicates the soft tissues with different precision and occurs in particular anatomical regions, imposing strong biases on the biological information retained. Muscovite and chloritoid largely obliterate the tissues' original detail, suggesting that aluminum-rich protoliths may have least potential for conserving mineralized soft tissues in metamorphism. Overall, the fossils exhibit a marked shift towards mineralogical equilibration with the matrix (except for their pyritized cuticles which remain unaffected), obscuring primary taphonomic modes. Sequential replacement of the phosphatized soft tissues released phosphorus to form new accessory monazite (and apatite and xenotime), whose presence in other BST biotas might signal the prior, more widespread, occurrence of this primary mode of preservation. Our results provide critical context for interpreting the Sirius Passet biota and for identifying late-stage overprints in other biotas.

2.2 Introduction

Burgess Shale-type (BST) biotas provide critical insight into the function of Cambrian marine ecosystems and into the soft-part anatomy of diverse animal stem lineages (e.g., Daley and Edgecombe, 2014). Much progress has been made towards resolving the depositional controls on their occurrence (see Gaines, 2014) and the resulting biases in the view they provide. They are primarily preserved as carbonaceous cuticular compressions (Butterfield, 1990; Gaines et al., 2012), locally augmented by early diagenetic pyrite coatings (e.g., Gabbott et al., 2004). This commonality in preservation has promoted the view that BST biotas form a coherent taphonomic grouping, the consequence of a complex trade-off between decay, organic stabilization and early diagenetic mineralization (Schiffbauer et al., 2014; Anderson et al., 2020b; Saleh et al., 2021a). However, little is known about the impact of deeper burial and very low to low-grade metamorphism (i.e. anchizone to epizone; ~ 100–500 °C, 1–5 kbar) on their outcome. These processes have predictable consequences for the maturation of the carbonaceous fossils (Butterfield, 1990; Topper et al., 2018) and for the mineralogy and texture of their host sediments (Powell, 2003; Strang et al., 2016b; Lerosey-Aubril et al., 2018), but the extent to which they overprint primary taphonomic signals or introduce artefacts is unclear.

Here, we combine geochemical and petrographic analyses from scanning electron microscopy, and stable silicon isotopes (Supplementary Material), to resolve the impact of these processes on the early Cambrian (Series 2, Stage 3) Sirius Passet Lagerstätte, one of the oldest and least well understood BST biotas (Harper et al., 2019). It, like most other BST biotas, is dominated by arthropods, but is distinguished by having experienced an unusually high grade of metamorphism for a fossil Lagerstätte, reaching a peak temperature of 409 ± 50 °C (lower greenschist-grade) during the Devonian Ellesmerian Orogeny (Soper and Higgins, 1987); by comparison, the Burgess Shale reached a peak temperature of 335 ± 50 °C (Topper et al., 2018). The occurrence of silicified muscles in this biota (Fig. 2.1) has led to the hypotheses that an Ediacaran silicification window (Tarhan et al., 2016) continued into the Cambrian, resulting in a unique style of BST preservation (Strang et al., 2016b). However, we show instead that this is a consequence of the Lagerstätte's burial history, which has profoundly altered original fossil preservation. This new understanding provides both a context for interpreting this biota and for recognizing modified primary taphonomic signals in others.

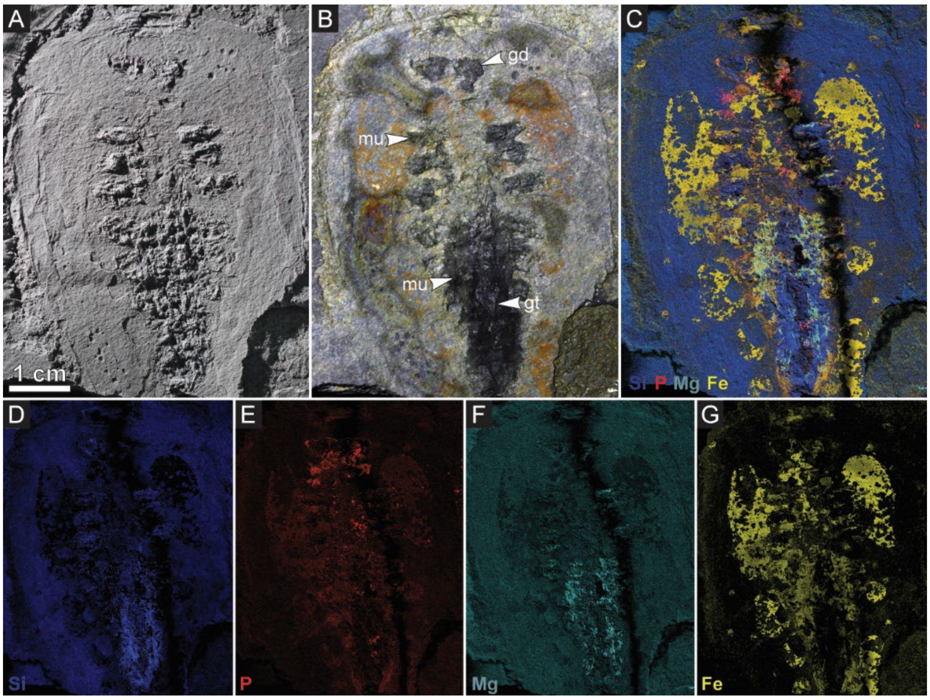

Figure 2.1. Soft-tissue preservation in *Sidneyia*? sp. MGUH 33947. (A, B) Contrasting preservation of the compressed exoskeleton and three-dimensional internal anatomy revealed by low-angle light (A) and high-angle light under water (B). (C–G) Corresponding EDS elemental maps, with brightness indicating relative abundance. (C) Composite for silicon (Si), phosphorus (P), magnesium (Mg) and iron (Fe), showing localization of mineral phases. (D) Si map indicating preferential silicification of the muscle. (E) P map indicating phosphatization of the gut tract and diverticula. (F) Mg map representing chlorite associated with the silicified muscle. (G) Fe map indicating partial pyritization of the cuticle. Abbreviations: gd, gut diverticula; gt, gut tract; mu, muscle.

2.3 Results and Interpretation

The mineralized labile soft tissues of panarthropods are preserved in a diversity of silicate and non-silicate minerals (Fig. 2.1C, 2.2A), most shared with the host sediment. Cross-cutting relationships reveal the general paragenetic sequence: apatite > quartz > chlorite+/- muscovite > chloritoid > xenotime.

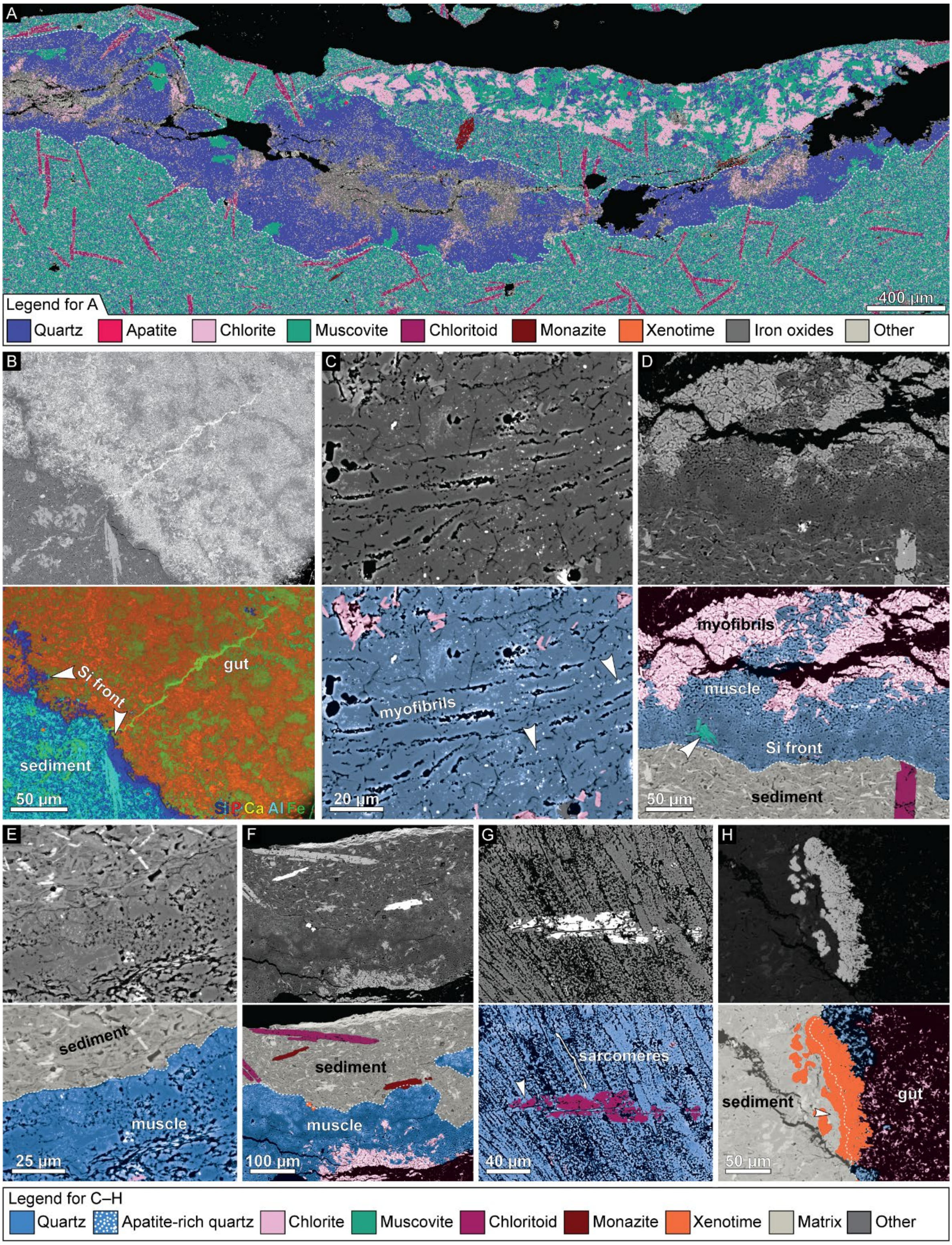

Figure 2.2. Key textural relationships of minerals in sectioned soft tissues. (A) EDS mineral map of transverse section through *Sidneyia*? sp. MGUH 33942, with extensively silicified musculature and chloritized viscera; chloritoid and monazite are mostly confined to the host sediment. (B) BSE and corresponding WDS elemental map of gut diverticula preserved in apatite (P and Ca) against Al-rich sediment with an intervening rim of quartz (Si front). *Arthroaspis bergstroemi*, MGUH 33920. (C–H) BSE images with corresponding false-color overlays. (C) Silicified muscle locally overprinted by chlorite; original preservation in apatite indicated by relict inclusions (arrowed). *Siriocaris trollae*, MGUH 33945. (D) Muscle

preserved by quartz and chlorite; silicification is densest (Si front) against the sediment (dotted white line) where patchy muscovite (arrowed) destroys the muscle's structure. *Sidneyia*? sp., MGUH33942. (E) Muscle preserved by microcrystalline quartz, except against the sediment (white dotted line) where it is replaced by prismatic inclusion-rich quartz. *Sidneyia*? sp., MGUH 33942. (F) Silicified and chloritized muscle with accessory monazite and xenotime at or near the sediment boundary (dotted line). *Sidneyia*? sp., MGUH 33942. (G) Silicified muscle cross-cut by late-stage chloritoid which destroys subcellular detail (sarcomeres) and is itself partially replaced by later quartz (arrowed). *Sidneyia*? sp., MGUH 33936. (H) Xenotime growing inwards (partially dendritic) and outwards (prismatic) at the fossil–sediment junction; the intervening cuticle (arrowed), outlined by xenotime, is now preserved by interlocking quartz and muscovite. *Kiisortoqia soperi*, MGUH-33931.

Apatite [$Ca_5(CO_3, PO_4)_3(OH, F)$] is invariably the first phase, consistent with its early preservation of soft tissues in other biotas (Briggs et al., 1993). It is extensively replaced by subsequent phases, except in the guts (Fig. 2.2B) where it frequently remains important. Quartz [SiO_2] is the dominant phase (Fig. 2.2A) and formed in multiple generations, including after late-stage chloritoid (see below; Fig. 2.2G). However, it everywhere succeeds apatite, as evidenced by abundant relict (<1 µm) apatite inclusions (Fig. 2.2C). Silicification is focused at the margins of the fossils (Fig. 2.2B, D), where interlocking crystals of quartz (~5–20 µm) growing inwards from the sediment may obliterate fine morphological detail (Fig. 2.2E; Fig. 2.4A). Elsewhere, the quartz is microcrystalline and faithfully replicates subcellular details originally captured by apatite, such as muscle myofibrils (Fig. 2.2C,G). Silicified muscle $\delta^{30}Si$ values range between −0.76 and −0.99 ‰ (Fig. 2.3, Data Table E2.1), and are notably closer to that of the matrix (−0.7 ‰) than to other potential contemporary early diagenetic and biogenic low-temperature sources (see Geilert et al., 2014), consistent with a metamorphic origin.

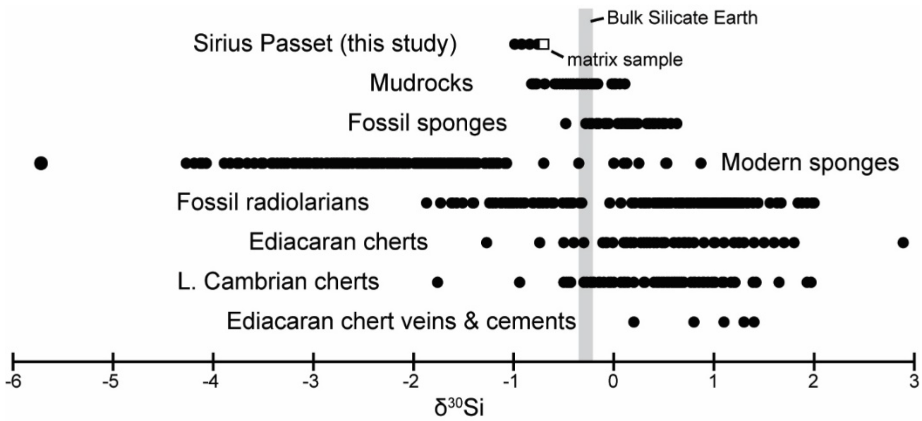

Figure 2.3. Comparison of Sirius Passet $\delta^{30}Si$ values with published values. $\delta^{30}Si$ for silicified muscle (closed circles) and matrix (open square) samples from Sirius Passet compared to published ranges for early diagenetic and biogenic silicas. Minimal variability within the Sirius Passet samples, and their distinction from alternative potential sources, suggest a matrix-derived source for soft-tissue silicification.

Chlorite [$(Mg,Fe)_6AlSi_3O_{10}(OH)_8$] and muscovite [$KAl_2(AlSi_3O_{10})(OH)_2$] typically occur as similarly-sized (<20 µm long) lath-shaped crystals; locally, they are intergrown indicating cogenesis. Whereas chlorite is widespread (Fig. 2.1F) and may faithfully pseudomorph silicified soft tissues (Fig. 2.2D; Fig. 2.4B), muscovite is generally confined to discrete domains (Fig. 2.2A,D; Fig. 2.4C) and does not replicate ultrastructural details. Chloritoid [$(Fe, Mg, Mn)_2Al_4Si_2O_{10}(OH)_4$] principally occurs in the sediment (Fig. 2A), along with pyrite [FeS_2] porphyroblasts (generally 50-90 µm), but it locally overprints silicified muscle and gut diverticula (Fig. 2.4C), particularly near the fossil margins or adjacent to sediment inclusions. The chloritoid forms large (up to 320 µm long) lath-shaped euhedra that traverse multiple muscle fibers and destroy all original morphology (Fig. 2.2G). Their long axes exhibit a degree of preferred orientation (Fig. 2.4D), implying growth under stress.

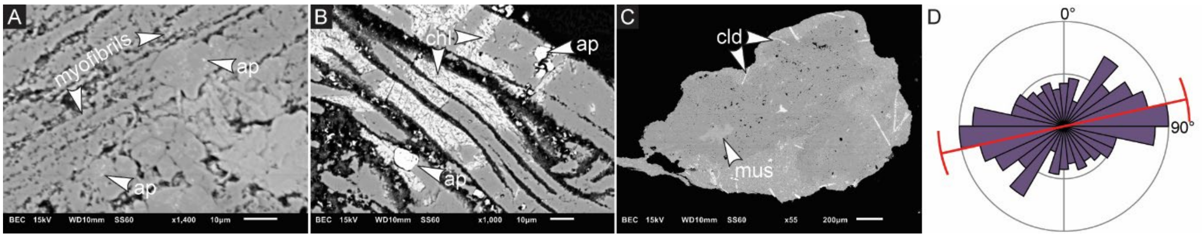

Figure 2.4. Additional textural relationships. (A) BSE image of silicified muscle preserved with subcellular fidelity by microcrystalline quartz and partially overprinted by a later prismatic (coarser) generation of quartz. Relict inclusions are arrowed. *Sidneyia*? sp., MGUH 33936. (B) BSE image of silicified muscle fibers replaced by patchy chlorite and late accessory apatite. *Campanamuta mantonae*, MGUH 33926. (C) BSE image of muscovite and chloritoid overprinting a block of silicified muscle fibers, destroying their fine morphology. *Siriocaris trollae*, MGUH 33945. (D) Long-axis orientations of chloritoid crystals suggesting formation under evolving tectonic stress; red line represents mean (78°) with 95% confidence intervals (67–88°). Abbreviations: ap, apatite; chl, chlorite; cld, chloritoid; mus, muscovite.

Cuticles typically appear as thin kerogen films (carbon compressions), often accompanied by a patchy coating of (now oxidized) pyrite (Fig. 2.1B,G; Fig. 2.5). However, they may also be preserved by interlocking muscovite and quartz, indistinguishable from the sediment (Fig. 2.2H).

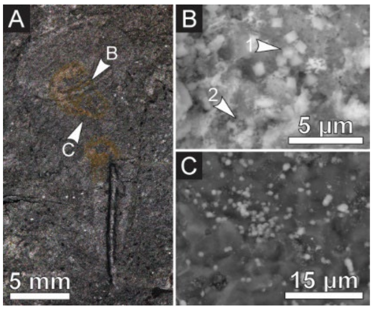

Figure 2.5. Iron oxides, after pyrite, partially preserving the cuticle of *Pauloterminus spinodorsalis*. MGUH 33946. (A) High-angle photograph of specimen with patchy orange-colored iron oxide coatings. (B) BSE image of area correspondingly arrowed in (A) comprising euhedral cubes and octahedra (arrow 1), and imprints of framboids (arrow 2), set in an amorphous groundmass. (C) BSE image of scattered micro-euhedra minerals at the periphery of the iron oxide coating.

Accessory phosphate minerals occur in close association with the fossils and overprint the mineralized soft tissues, largely destroying their fine morphology. Xenotime [YPO_4] forms rosettes within the digestive tract, may crudely preserve muscle tissue (Fig. 2.6D), and locally grows outwards (Fig. 2.6A–C) and inwards from the walls of fossils (Fig. 2.2H; Fig. 2.6B, C). Similarly, subhedral to euhedral apatite (up to ~20 µm) (Fig. 2.6G) occurs both inside and outside the fossils, in the latter case as a diffuse corona extending ~400um away (Fig. 2.6F). By contrast, monazite [$REEPO_4$] is generally confined to the adjacent sediment (Fig. 2.2F), where it may be concentrated on only one side of fossils (Fig. 2.6E,F), suggesting growth linked to fluid movement (e.g., Evans et al., 2002). In all cases, it is poikiloblastic and comparatively coarse (30–380 µm), locally replacing accessory apatite (Fig. 2.6H) and at least partially overlapping syntectonic chloritoid formation (Fig. 2.6I) (see Wilby et al., 2007).

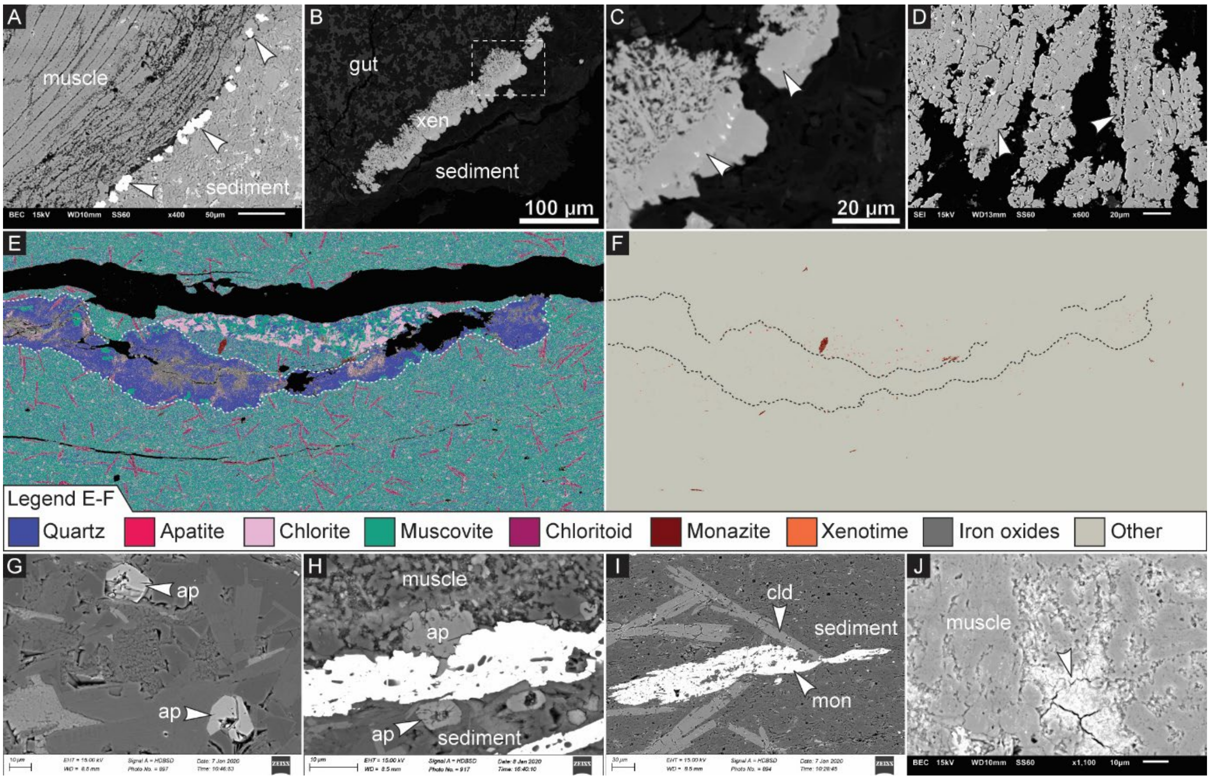

Figure 2.6. Accessory phosphate minerals in fossils and sediment. (A) BSE image of xenotime (arrowed) selectively formed along a fossil wall where outward diffusing P (released during silicification of the fossil's originally phosphatized muscle) encountered Y released by the recrystallization of the enclosing sediment. *Sidneyia*? sp., MGUH 33936. (B, C) BSE images of xenotime formed at the gut wall, showing zoned growth (arrowed). *Siriocaris trollae*, MGUH 33944. (D) SEI image of xenotime crudely preserving muscle fibers (arrowed). *Sidneyia*? sp., MGUH 33940. (E–F) EDS mineral map for all phases (E) and for apatite and monazite only (F), showing the distribution of accessory phosphates within a fossil (dashed lines) and as a diffuse halo around it. *Sidneyia*? sp., MGUH 33942. (G) BSE image of euhedral accessory apatite forming part of a halo around *Sidneyia*? sp. MGUH 33942. (H) BSE image of monazite overprinting late accessory apatite in the sediment adjacent to *Pambdelurion whittingtoni*. MGUH 33934. (I) BSE image of chloritoid crystals intersecting a monazite crystal in the sediment, suggesting at least partially coeval formation *Sidneyia*? sp., MGUH 33942. (J) BSE image of a P-, Ca-, Fe-, Al-bearing phase (arrow), likely a recent weathering product, impacting silicified muscle. *Kiisortoqia soperi*, MGUH 33932. Abbreviations: ap, apatite; cld, chloritoid; mon, monazite; xen, xenotime.

The bulk rock is enriched in aluminum and depleted in calcium compared to the Burgess Shale, but its major element composition otherwise overlaps (for details, see Supplementary Material; Data Table E2.2; Fig. 2.S1). Powell (2003) considered the Burgess Shale to be unremarkable for a pelite and, though the mineralogy of the Sirius Passet protolith cannot be ascertained with certainty (especially the starting clay composition), it likely passed through a typical prograde sequence of mineral reactions for an aluminum-rich pelite (e.g., see Bucher and Grapes, 2011), leading to the observed succession of soft-tissue replacements (Fig. 2.7).

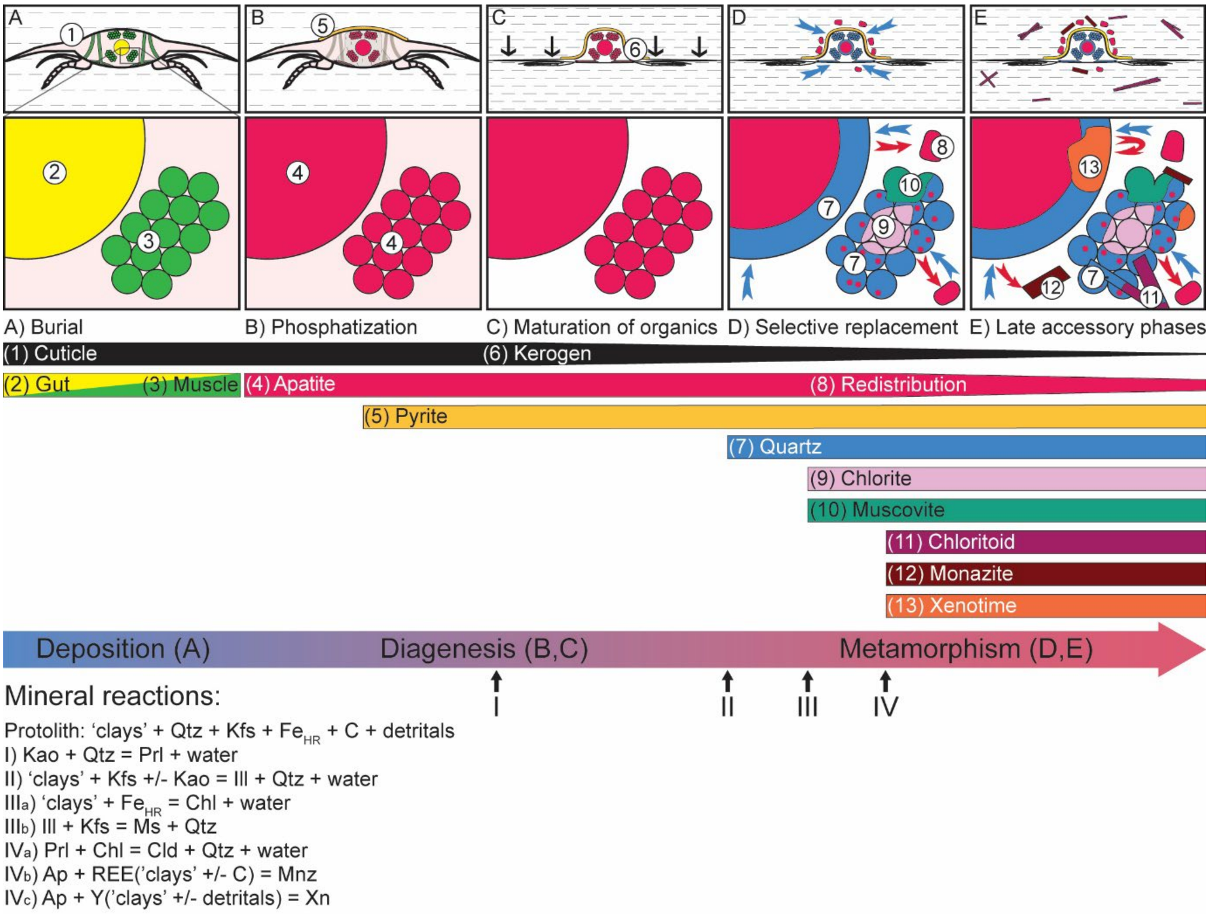

Figure 2.7. Schematic explanation of key stages (A to E) in the preservation of Sirius Passet fossils, and postulated pathways for relevant mineral transformations. (A) At burial, prior to decay of the cuticle and labile soft tissues (gut and muscle). (B) Phosphatization of labile soft tissues, and organic conservation and light pyritization of cuticle. (C) Partial compaction, start of progressive maturation of organics, and transformation of clays. (D) Selective replacement of phosphatized soft tissues by quartz, with concomitant release of P to pore fluids. Silicified soft tissues undergo progressive replacement by chlorite and muscovite during sediment recrystallization. (E) Precipitation of accessory phosphate minerals at reaction fronts, and growth of chloritoid under strain. Quartz continues to precipitate in response to ongoing mineral transformations. Abbreviations: Ap, apatite; C, organic carbon; Chl, chlorite; Cld, chloritoid; FeHR, highly reactive iron; detritals, heavy detrital minerals; Ill, illite; Kfs, K-feldspar; Kao, kaolinite; Mnz, monazite; Ms, muscovite; Prl, pyrophyllite; Qtz, quartz; REE, rare earth elements; Xn, xenotime; Y, yttrium; "clays" refers to the presumed composition of deposited clays and micas (smectite, kaolinite, chlorite and biotite).

2.4 Discussion

Silicified soft-bodied biotas are scarce in the Phanerozoic, they rarely preserve labile soft tissues (e.g. muscle) and are confined to exotic non-marine settings (e.g., Trewin et al., 2003). By contrast, early diagenetic silicification was active in diverse marine environments in the Ediacaran and has been implicated in the preservation of several of its soft-bodied biotas

(Muscente et al., 2015; Tarhan et al., 2016). This dichotomy has led to the suggestion that a silicification taphonomic window may have persisted into the Cambrian and have been responsible for silicifying soft tissues in the Sirius Passet Lagerstätte (Strang et al., 2016b, 2016a; Topper et al., 2018). Our petrographic and isotopic data refute this idea, and reveal instead that silicification was a product of very low to low-grade metamorphism, consistent with its late-stage formation in other BST Lagerstätten (e.g., Powell, 2003; Lerosey-Aubril et al., 2018). Evidence for multiple episodes of silicification in the Sirius Passet Lagerstätte (e.g., before and after chloritoid formation) is consistent with the release of silica from the host sediment during successive clay mineral transformations (Fig. 2.7).

Textural relationships indicate that preserved muscle and digestive systems were initially stabilized by early diagenetic apatite (e.g., Wilby et al., 1996b; Butterfield, 2002), prior to being progressively replaced by other minerals. Overall, the mineralogy, isotopic composition and texture of the soft tissues have converged on the host sediment, where quartz, aluminosilicate clays, and chlorite are abundant, and their primary preservation mode has been irrevocably altered. Likewise, the originally phosphatized guts have been replaced by quartz and clays, supporting an alternate explanation for apparently sediment-filled guts (Butterfield, 2002), which have been used elsewhere to invoke deposit-feeding habits in certain arthropods (Hou and Bergström, 1997; Lerosey-Aubril et al., 2012). Each new replacing mineral retains a particular level of detail and is focused in discrete anatomical regions (Fig. 2.1C, 2.2A), imposing significant biases on the ultimate survival and fidelity of preservation of different tissues. Muscovite and chloritoid growth were especially deleterious, suggesting that aluminum-rich protoliths, such as the Burgess Shale (Powell, 2003), have the least potential for conserving labile soft-tissues during very low to low-grade metamorphism. By contrast, pyrite is unaffected, meaning that this taphonomic pathway at least is reliably conserved (now weathered).

Our model offers a relatively simple taphonomic explanation for the Sirius Passet soft tissues. Phosphatization of guts, amongst a few other tissues, is elsewhere associated with BST carbonaceous compressions in e.g., Burgess Shale (Butterfield, 2002), Emu Bay Shale (Paterson et al., 2015), and Weeks Formation (Lerosey-Aubril et al., 2018). Silicified mudrocks are found associated with late diagenesis (Thyberg & Jahren, 2011; Milliken and Day-Stirrat, 2013; Dowey and Taylor, 2017) and metamorphism (e.g., Terabayashi et al., 2010). The presence of apatite inclusions within quartz in muscle and in the irregular silicification fronts interlacing the primary apatite of guts (Fig. 2.2B) strongly suggest that quartz consistently replaces a primary apatite phase. We consider this a simpler model than the unique model involving selective and coincident preservation by quartz and apatite proposed by Strang et al. (2016a and 2016b). Additionally, Strang et al.'s model does not account for the fact that tissues are not only silicified, but also, to lesser extent, aluminosilicified (Fig. 2.2A,D) and chloritized (Fig. 2.2D). Aluminosilicate and chlorite phases are predominantly euhedral phases that cross-cut both apatite (Fig. 2D) and quartz (Figs 2.2C,D and 2.4C) structures which indicates a post-silicification timing. The equilibration of tissue mineralogy with that of the matrix occurred during increasing diagenesis and metamorphism, while the replaced apatite mostly reprecipitated as a halo predominantly around the fossils (Fig. 2.7). A similar model of metamorphic equilibration of fossil mineralogies with the surround matrix has been proposed for replacement of bone apatite by bituminous materials in the metamorphosed coal deposit containing the Jarrow assemblage in Ireland (Gogáin et al., 2022).

Phosphorus released during successive mineral transformations was redistributed into new accessory phosphates. Accessory monazite is widely reported in other BST biotas (Conway Morris, 1990; Moore and Lieberman, 2009; Broce and Schiffbauer, 2017), implying that phosphatized soft tissues may have been lost from these too and have been a more important component of BST preservation than their present distribution suggests (Daley and Edgecombe, 2014; Paterson et al., 2015). The sum of evidence, including other examples of late-stage overprint (e.g., Gaines et al., 2019), demonstrates the potential for deep burial and metamorphism to modify primary taphonomic signals and biological information, and emphasizes the need for their site-specific characterization.

2.5 Conclusions

Silicified soft tissues in the Sirius Passet Lagerstätte are a product of progressive alteration of originally phosphatized soft tissues during very low to low-grade metamorphism. Contrary to previous assertions, they do not record a novel mode of primary BST preservation, but rather an extreme example of a spectrum late-stage processes that operated in other BST Lagerstätten. The mineralogy and chemistry of Sirius Passet fossils have converged on that of the host sediment, preferentially destroying certain tissues and inducing a reduction in resolution of others. Growth of muscovite and chloritoid was especially destructive, suggesting that protolith composition has a bearing on the ultimate fate of soft tissues during metamorphism. Accessory monazite formed in response to the replacement of the originally phosphatized soft tissues and may serve as a useful proxy for the former presence of such tissues elsewhere.

2.6 Supplementary Material

The Sirius Passet Lagerstätte comprises a ~12 m thick interval of finely bedded mudstones and silty mudstones within the early Cambrian (Series 2, Stage 3) Buen Formation, North Greenland (Conway Morris et al., 1987; Ineson and Peel, 2011). It has yielded a number of important stem-group fossils (e.g., Budd, 1993; Conway Morris and Peel, 1995; Peel, 2010a) and is interpreted as a series of dilute sediment gravity flows deposited under periodically low oxygen conditions on a shelf-slope break (see Harper et al., 2019). The strata are overturned and form part of a narrow, fault-bounded, structure within a thrust duplex (Harper et al., 2019). The mudstones were subjected to greenschist facies metamorphism during the Devonian Ellesmerian Orogeny (Soper and Higgins, 1987), reaching a peak temperature of 409 ± 50 °C (Topper et al., 2018).

Articulated body fossils crowd the bedding surfaces and are readily discernible as reflective, low-relief, carbonaceous compressions (Topper et al., 2018); some are additionally highlighted by a thin coating of orange-colored weathering products after pyrite (Fig. 2.1B,G; Fig. 2.5). Labile soft-tissues are widely preserved and occur in two modes: either as kerogenous compressions (e.g., nerve tissue, Park et al., 2018), or as dark grey (white-weathering), three-dimensional, secondarily mineralized masses (e.g. muscle tissue and gut diverticula; Fig. 2.1A, B). All samples are registered at the Natural History Museum of Denmark, Copenhagen, Denmark (MGUH).

Detailed petrographic and isotopic analyses were performed on 29 arthropod specimens with conspicuous mineralized labile soft tissues (Data Table E2.3). These are representative of the range of preservation observed through the full stratigraphic thickness of the Lagerstätte, and include seven taxa (*Arthroaspis bergstroemi*, *Buenellus higginsi*, *Campanamuta mantonae*, *Kiisortoqia soperi*, *Pambdelurion whittingtoni*, *Sidneyia*? sp., *Siriocaris trollae*). Samples of soft tissue were mechanically extracted, embedded in epoxy resin and polished to a 1 μ m grade using polycrystalline diamond paste. They were carbon coated prior to analysis with a JEOL JSM-6610 scanning electron microscope (SEM) equipped with an energy dispersive X-ray spectroscopy (EDS) Oxford Instruments INCA x-act detector at 15kV at Korea Polar Research Institute (Korea) and a Hitachi S3500N SEM with a backscattered electron detector at 20 kV at the University of Bristol (UK). Images were provided by backscattered electrons (BSE) or secondary electrons (SEI). Elemental maps of three polished samples were generated with a JEOL JXA-8530F field emission electron microprobe using wavelength dispersive X-ray spectroscopy (SEM-WDS) at 20kV, 200 nA probe current, 12 msec dwell time, 0.1μm probe diameter, and 0.1 μm step size. Elemental map of *Sidneyia*? sp. (MGUH 33947) (Fig. 2.1) was generated on the same machine but using the SEM-EDS at 20kV, 200 nA probe current, 12 msec dwell time, 25 μm probe diameter, and 25 μm step size. Mineral maps of polished transverse thin sections through entire fossils (*Sidneyia*? sp. and *P. whittingtoni*) and their enclosing matrix were generated with a Zeiss Sigma 300 field emission SEM-EDS fitted with twin Bruker Xflash detectors running with Brucker Esprit (v2) software and Zeiss' Mineralogic phase-mapping software (v1.6.2) at the British Geological Survey (UK). Iron oxides coating the cuticle of *Pauloterminus spinodorsalis* were analyzed uncoated at 20 kV with a Zeiss Sigma 300 field emission SEM-EDS fitted with twin Bruker Xflash detectors at the Geological Survey of Denmark and Greenland (Denmark).

Long-axis orientations of 331 chloritoid crystals were measured in two dimensions on a thin section cut perpendicular to the bedding plane (Block A [see Chapter 4], thin section 4) image using ImageJ (v1.48) (Data Table E2.4) and the accompanying rose diagram (Fig. 2.4D) was created using PAST (v3.20) (Hammer et al., 2001).

The δ^{30}Si isotope composition of one matrix and four silicified fossil muscle samples (Data Table E2.1) were determined using a Thermo-Finnigan Neptune multi collector-inductively coupled plasma-mass spectrometer (MC-ICP-MS) at the Bristol Isotope Group Laboratory (UK), following the methodology of Ng et al. (2020). Powdered samples (5–10 mg) and a solid NaOH pellet (~200 mg) were placed in an Ag crucible and fused in a muffle furnace at 720°C for 12 minutes (cf. Georg et al., 2006). Samples were then dissolved in 15 ml of Milli-Q water and ultrasonicated for 30 minutes before being weakly acidified (to about pH 2) with distilled HCl and further purified in cation exchange columns consisting of 1.8 ml Bio-Rad AG50W-X12, 200–400 mesh cation exchange resin in H+ form (see Georg et al., 2006). Replicate analyses of reference standards were carried out to monitor long-term reproducibility of the method. Measurements of Diatomite and LMG08 sponge standards yielded δ^{30}Si of +1.23 ± 0.11 ‰ (n = 18) and -3.47 ± 0.14 ‰ (n = 11) respectively, which agree with reference values within 2 SD (Reynolds et al., 2007; Hendry and Robinson, 2012). Analytical uncertainties associated with samples were evaluated based on 2 SD of sample replicate measurements (n = 2–3), which ranged from 0.03–0.18 ‰ for δ^{30}Si (Data Table E2.1). Silicon isotopes in quartz and chert are generally considered highly resistant to metamorphic resetting and are assumed to reflect the original biotic or abiotic source(s) (André et al., 2006; Marin-Carbonne et al., 2014; Stefurak et al., 2015; Ding et al., 2017; Li et al., 2020). Data from other potential sources are from Robert and Chaussidon (2006), Wille et al. (2010), Hendry et al. (2010, 2014, 2019; 2012), Savage et al. (2013), Fan et al. (2013), Ramseyer et al. (2013), Abelmann et al. (2015), Wen et al. (2016), Fontorbe et al. (2016), Tatzel et al. (2017, 2020), Cassarino et al. (2018), Zhang et al. (2020), and Gao et al. (2020).

Mineral and small area bulk sediment composition data were acquired from polished thin sections of fossiliferous (SID Mu 2, MGUH 33942; PAMB Mu 2, MGUH 33934; Int.Min.3 S11, MGUH 33943) and non-fossiliferous samples (A4 and A9) using the Zeiss Sigma 300 field emission SEM-EDS at the British Geological Survey. The bulk compositional data were acquired using two complementary approaches. In the first, average mineral compositions (derived by quantitative point microanalyses of several examples each of the major constituent minerals, including chlorite, muscovite and chloritoid) were combined with the modal area % cover of those minerals, as derived by automated quantitative mineralogy (AQM, the Zeiss' Mineralogic system). Idealized compositions (Deer et al., 2013) were used for quartz and for trace mineral constituents, and the modal area % cover values were converted to weight % using published mineral densities. The second approach averages the quantitative compositional data generated for each pixel within every particle or discrete area enclosed by macro-pores, as defined by the AQM system. The bulk sample composition was obtained by averaging all of these particles and discrete particles across the total area analyzed, with a particle size cut-off of 30 μm^2. The total area analyzed for each sample using each approach was $100 mm^2$).

The resultant bulk compositional datasets were normalized to 100% and calculated as oxides using a stoichiometric approach for oxygen content (Data Table E2.2), prior to plotting on an AFK diagram (Fig. 2.S1) together with published XRF whole-rock values for Sirius Passet (Boudec et al., 2014) and the Marble Canyon and Walcott Quarry localities of the Burgess Shale (Gaines et al., 2019), relevant idealized end-member minerals (Deer et al., 2013), and the PAAS composite shale standard (Taylor and McLennan, 1985). Average compositions for the Burgess Shale in the Raymond Quarry at the Tuzoia Beds (Powell, 2003; not shown) correspond closely to the compositional ranges given by Gaines et al. (2019). All Fe in the Sirius Passet samples is assigned to FeO in order to minimize the impact of observed oxidation, and the system is assumed to have been closed during weathering. The AFK diagram successfully separates the data along the K-axis, and was generated using the excel-based spreadsheet of Graham and Midgley (2000), using the following axis definitions (wt% values):

$A = (Al_2O_3 + Fe_2O_3 - K_2O - Na_2O - CaO)$

$F = (FeO + MgO + MnO)$

$K = K_2O$

The veracity and internal consistency of our approach to acquiring bulk sediment compositions is demonstrated by the data being confined to a field defined by the end member minerals within the assemblage (muscovite, chloritoid, pyrite), by the close correspondence between the determined compositions using the two approaches, and by the data projecting onto a linear mixing line that parallels that of the Boudec et al. (2014) XRF-generated dataset.

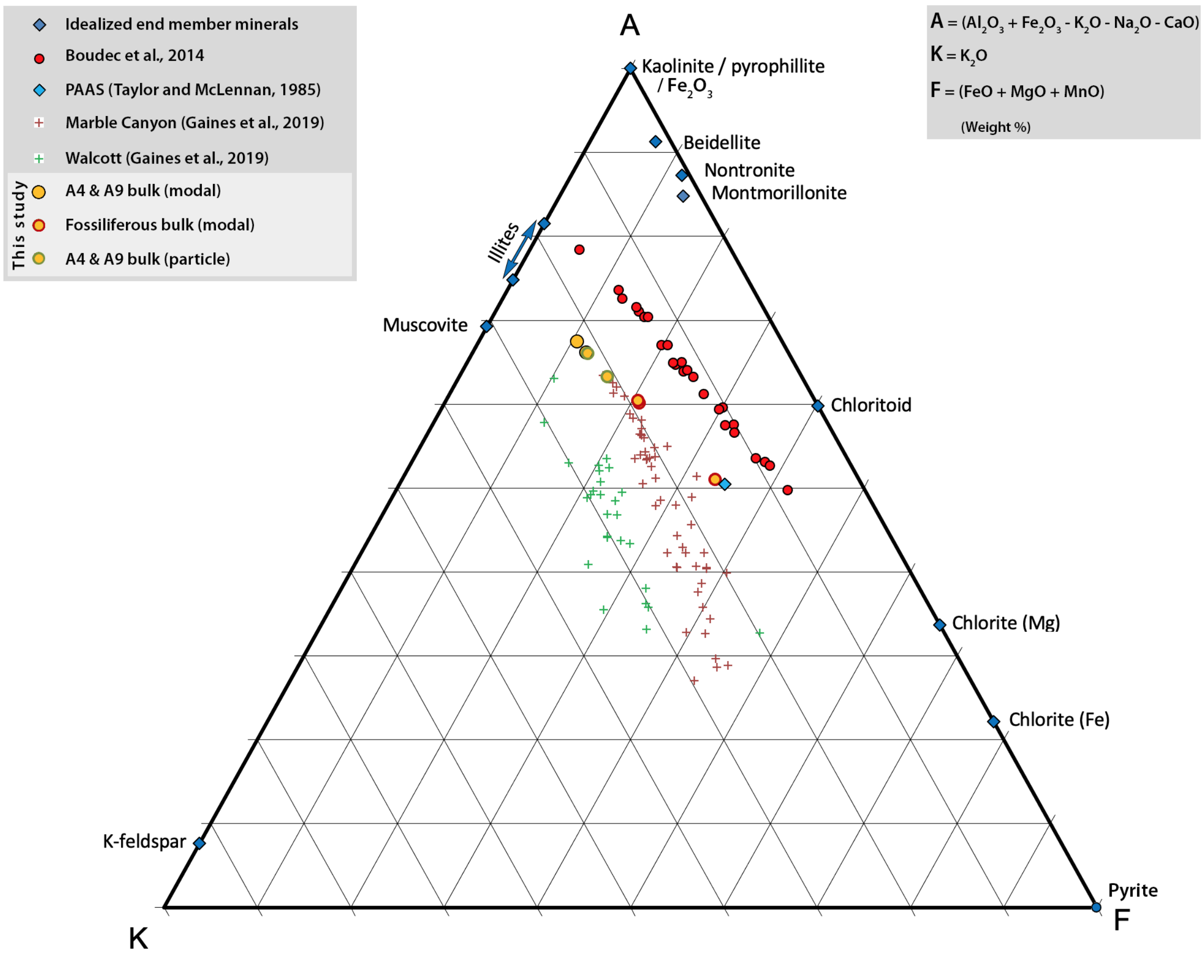

Figure 2.S1. AFK diagram for the Sirius Passet Lagerstätte and for the Marble Canyon and Walcott Quarry occurrences (crosses) of the Burgess Shale (after Gaines et al., 2019). Data for Sirius Passet derived from XRF analyses (red circles; Boudec et al., 2014) are shown separately from our own SEM-derived small area bulk analyses (orange circles). The fossiliferous Sirius Passet samples are SID Mu 2, PAMB Mu 2 and Int.Min.3 S11. Relevant idealized end-member minerals (Deer et al., 2013) and the PAAS composite shale standard (Taylor and McLennan, 1985) are shown for reference. Overall trends are similar, but the Sirius Passet Lagerstätte likely had a higher kaolinite (pyrophyllite) and lower feldspar content than the Burgess Shale. See Supplementary Material for details.

The Sirius Passet bulk rock is enriched in Al and depleted in Ca compared to the various occurrences of the Burgess Shale, but its major element composition otherwise overlaps (Data Table E2.2). In comparison to the PAAS composite shale standard (Taylor and McLennan, 1985) it is enriched in K and Al, and depleted in Na, Ca and Si. Its Si/Ti is between that of the Burgess Shale and PAAS (Data Table E2.2), consistent with an intermediate abundance of detrital minerals, and its low Ca plausibly reflects the absence of carbonate cements like those reported in the Burgess Shale (see Gaines et al., 2012). Thus, except for elevated Al, the protolith compared closely to that of the Burgess Shale, which Powell (2003) considered to be unremarkable for a pelite. Strang et al. (2016b) determined the current mineral assemblage to be dominated by chlorite, mica and quartz, with minor/trace chloritoid, albite and illite, and with at least some of the quartz being detrital. Boudec et al. (2014) considered the protolith to be derived from one source dominated by smectite or chlorite, and another by K-feldspar and quartz. Given the below-average Na and Ca (in comparison to PAAS), we do not consider albite to have constituted an appreciable fraction of the protolith, and it was not identified during our small area bulk sediment analysis. Early diagenetic pyrite is widespread in the Sirius Passet Lagerstätte, as demonstrated by the localized pyritization of arthropod cuticles, and required a source of highly reactive iron minerals (e.g., goethite, haematite, magnetite; Raiswell and Canfield, 1998) which may have also been important in subsequent reactions.

Kaolinite is believed to have played an important role in BST preservation (Anderson et al., 2018), both by inhibiting bacterial activity and by bonding to tissues and facilitating their long-term stability (Anderson et al., 2020b). Yet, despite the suggestion that complexation with organic matrices might render kaolinite resilient to metamorphism, many BST fossils are replicated by thin films of alternative aluminosilicates or lack them altogether (e.g., Anderson et al., 2011), potentially as a result of late-stage alteration (Anderson et al., 2020a). Kaolinite is absent from the Sirius Passet Lagerstätte (Boudec et al., 2014) but, based on the high Al content, it is considered to have been an important component of the protolith. Chloritoid is characteristic of Al-rich metapelites at the transition from subgreenschist to greenschist facies (very low to low-grade metamorphism) and is generally considered to form via the sequential reactions [Kln + 2Qtz = Prl + H_2O] and [Chl + 4Prl = 5Cld + 2Qtz + $3H_2O$], though see Rahn et al. (2002) for a route not involving kaolinite.

Chapter 3

Biological controls on soft tissue phosphatization in the fossil record

Author contributions

This chapter is written with the intention to submit it for publication as soon as possible.

The research for this chapter was developed by me, Jakob Vinther, and Philip R. Wilby. I did all data collection and analyses, both from a photographic catalogue (produced by Tae-Yoon Park at KOPRI) and several visits to the collection at KOPRI for hands-on scrutiny, and I photographed specimens presented herein. I wrote the manuscript and produced figures with input from Jakob Vinther and Philip R. Wilby.

3.1 Abstract

Phosphatization of labile soft tissues provides an important window on anatomical information otherwise not preserved in fossils. However, the process of phosphatization is inherently biased resulting in highly selective preservation of tissues within—as well as between—specimens, taxa, and deposits that may distort interpretations of the fossil record. Multiple controls have been hypothesized based on experimental investigations and fossil assemblages, but comprehensive hypothesis testing has been impeded by a lack of suitable quantitative datasets. Here, we exploit the abundance of phosphatization in the Lower Cambrian Sirius Passet Lagerstätte (North Greenland) to conduct a community-scale analysis of phosphatization to test the validity of current models for the underlying intrinsic controls. Sirius Passet is a natural laboratory for phosphatization: Fossils are extremely abundant, labile soft tissues are frequently preserved, and essentially occur throughout the Lagerstätte interval. Our compiled dataset records absence/presence data for 15 different tissues in 1159 specimens, across 21 taxa. Phosphatization varied substantially between taxa: it did not occur in three taxa (*Aaveqaspis*, *n*=9; *Buenaspis*, *n*=51; *Molaria*, *n*=3), had low frequencies (0.1–25%) in four taxa (*Kleptothule*, *n*=112; *Sirilorica*, *n*=63; polychaetes spp., *n*=28; vetulicolians spp., *n*=50), high frequencies (77–99.9%) in five taxa (*Campanamuta*, *n*=348; *Kiisortoqia*, *n*=69; *Sidneyia*?, *n*=62; *Kerygmachela*, *n*=22; palaeoscolecids spp., *n*=10), and consistently occurred in three taxa (*Siriocaris*, n=9; *Pambdelurion whittingtoni*, *n*=14; cf. *Pambdelurion* sp. nov., *n*=30). Phosphatization of axial musculature is regionalized in three arthropods (*Arthroaspis*, *n*=14; *Kiisortoqia*, *n*=19, *Sidneyia*?, *n*=32) and most frequently occurs in the posterior-midregion. In the model organism *Campanamuta*, phosphatization requires specimens to cross a minimum size (~20 mm width) threshold to phosphatize most tissues (e.g., muscle), and is generally more extensive in enrolled (*n*=32) vs outstretched (*n*=170) specimens The likelihood of an individual tissue being phosphatized varies between and within taxa but is not random. We recognize five intrinsic biological controls from these patterns (taxonomy, tissue, microenvironments, size, and diet), each with inherent biases, including a size-related ontogenetic bias. Each control is unable to guarantee phosphatization independently but acts in unison with others through a complex interplay. While understanding the role of the depositional environment in facilitating phosphatisation was outside the scope of this study, constraining the intrinsic controls provide a framework to predict taphonomic biases in other phosphatized deposits.

3.2 Introduction

Phosphatization can preserve labile soft tissues in the most extraordinary detail (Martill, 1990; Briggs et al., 1993; Briggs, 2003). It is relatively common through the fossil record and therefore provides a treasure trove of information on ancient diversity (Fuchs et al., 2009; Fuchs and Larson, 2011), phylogeny (Aldridge et al., 1993; Donoghue et al., 2000; Trinajstic et al., 2007, 2022; Vannier et al., 2014; Parry et al., 2015b; Young and Vinther, 2016), and ecology (Wilby and Martill, 1992; Wilby et al., 2004; Vannier et al., 2014; Hoffmann et al., 2020; Klug et al., 2021). At the same time, phosphatization distorts the fossil record by being highly selective and biased in favor of certain taxa and tissues (Wilby and Whyte, 1995; Briggs and Nedin, 1997; Wilby and Briggs, 1997; Butterfield, 2002; Klug et al., 2005, 2021; McNamara et al., 2009; Wilson et al., 2016; Clements et al., 2017). The cause of these biases and their effects remains debated, in part due to the difficulties in collecting large comprehensive datasets to test competing postulated controls. Understanding these biases (i.e., what is not preserved) is, however, crucial to correctly interpret morphological or ecological absences in fossil deposits (e.g., see Xiao et al., 1998, Donoghue et al., 2006, and Huldtgren et al., 2011 for an example on purported Ediacaran metazoan embryos).

Phosphatization has both intrinsic (biological) controls (e.g., Wilby and Briggs, 1997) and external (environmental) controls (e.g., Dornbos et al., 2006). Broadly speaking, biology controls *what* can phosphatize while environment controls *where* and *when* it can phosphatize. Here, we focus on the biological controls because they bias soft tissue distributions within a given biota (ecosystem).

Several fundamental elements have been proposed to give rise to phosphatization of soft tissues during early decay: *(1)* There has to be a source of phosphorous for calcium phosphate (apatite) to replace tissues (Wilby and Whyte, 1995). However, it is uncertain to what extent this source is restricted to internally derived tissue-bound phosphorus released by the decaying tissue itself (Briggs and Kear, 1993, 1994; Wilby and Whyte, 1995; Briggs and Nedin, 1997) or adjacent tissues (Lerosey-Aubril et al., 2018), or additional, externally derived phosphorus diffusing into the carcass from the surrounding sediment (Allison, 1988b; Martill, 1988; Briggs and Wilby, 1996; Wilby and Briggs, 1997). *(2)* It requires the right internal chemical (micro)environment for anaerobic bacterial activity to decrease pH-values below <6.38 where apatite precipitates instead of calcium carbonate (Briggs and Kear, 1994; Briggs and Wilby, 1996; Sagemann et al., 1999). However, it is uncertain how important anoxic microenvironments actually are (Gueriau et al., 2020), and whether they are consistent within a carcass (Clements et al., 2022) or localized around certain tissues (Sagemann et al., 1999; McNamara et al., 2009). *(3)* Suitable tissue substrate is necessary for nucleation of apatite microcrystals (Wilby, 1993; Wilby and Briggs, 1997; McNamara et al., 2009). However, it is uncertain whether the suitability is controlled by the primary structure of the tissue itself (McNamara et al., 2009; Dornbos, 2010) or preconditioning of the organic matrices by decay (Wilby, 1993). Other, less rigorously tested, controls have been proposed. These include: *(4)* taxonomic control where taxon-specific anatomical or morphological features either suppress or promote phosphatization (Hof and Briggs, 1997; Wilby and Briggs, 1997; Wilson et al., 2016; Clements et al., 2017). *(5)* carcass size control on ability to develop reducing microenvironments (Allison, 1988d) *(6)* invading gut microbes control phosphatization of tissues within the body cavity (Butler et al., 2015); *(7)* diet controls internal availability of phosphorus to facilitate phosphatization (Chatterton et al., 1994; Lerosey-Aubril et al., 2012). It is unlikely that these controls are (equally) important, but their true significance and relative hierarchy has so far been difficult to observe. Difficulties reconciling common controls across diverse data types emphasize the complexity of the system.

Hypothesized controls on phosphatization are based on both experimental and fossil evidence. The lines of evidence complement each other as they approach the questions from different angles with separate advantages and limitations: experiments give control over specific variables and the ability to track chemical dynamics through time, but they are simplistic and require a thorough control over numerous external and internal variables to interpret (Allison, 1988d; Briggs and Kear, 1993, 1994; Briggs et al., 1993; Kear et al., 1995; Hof and Briggs, 1997; Sagemann et al., 1999; Butler et al., 2015; Clements et al., 2017, 2022). Fossils yield actual patterns of phosphatization at the tissue- and taxon-scale, but phosphatized fossils within deposits are often scant, forcing hypotheses to be based on restricted stratigraphic (Wilby et al., 1996a, 2004) and taxonomic (Allison, 1988b; Briggs and Nedin, 1997; Butterfield, 2002; McNamara et al., 2009; Lerosey-Aubril et al., 2012; Wilson et al., 2016) data subjected to infinite variables before, during and after deposition. Both approaches have so far been limited by small sample sizes. This has constrained the ability to hypothesize general controls on phosphatization that transcend taxon-specific examples since a complex system requires large quantitative datasets.

Here, we use such a large quantitative dataset based on fossils from the lower Cambrian Sirius Passet Lagerstätte (Conway Morris et al., 1987; Harper et al., 2019) to evaluate the relative merits of popular hypotheses for intrinsic controls on phosphatization of labile soft tissues posed from experimental, qualitative and anecdotal evidence. Sirius Passet exhibits a high frequency of fossils with three-dimensionally preserved internal anatomy (e.g., Budd 2011; Young et al., 2016) that was originally phosphatized before selective replacement of certain tissues by predominantly silica occurred during metamorphism (Nielsen et al., 2022). It is a natural laboratory to study phosphatization: its high frequency within the dense fossil assemblages permits quantification; phosphatization appears to occur in most beds throughout the Lagerstätte interval, limiting the influence of external (environmental) controls; and phosphatized tissues occur within multiple organisms from different taxonomic groups (Fig. 3.1). Our focus here is to assess critical biological controls that can be gauged from such fossil deposits in which phosphatisation result in permineralization of specific tissues. Identifying important controls is key to recognize their biases. We do not address the possible controls resulting in phosphatized microfossils from winnowed deposits (e.g. Dornbos et al., 2006). The controls identified and examined here are: 1) taxonomy, 2) tissue, 3) size, 4) microenvironment; 5) diet. We show that these controls do not individually guarantee phosphatization but instead have a complex hierarchic interplay.

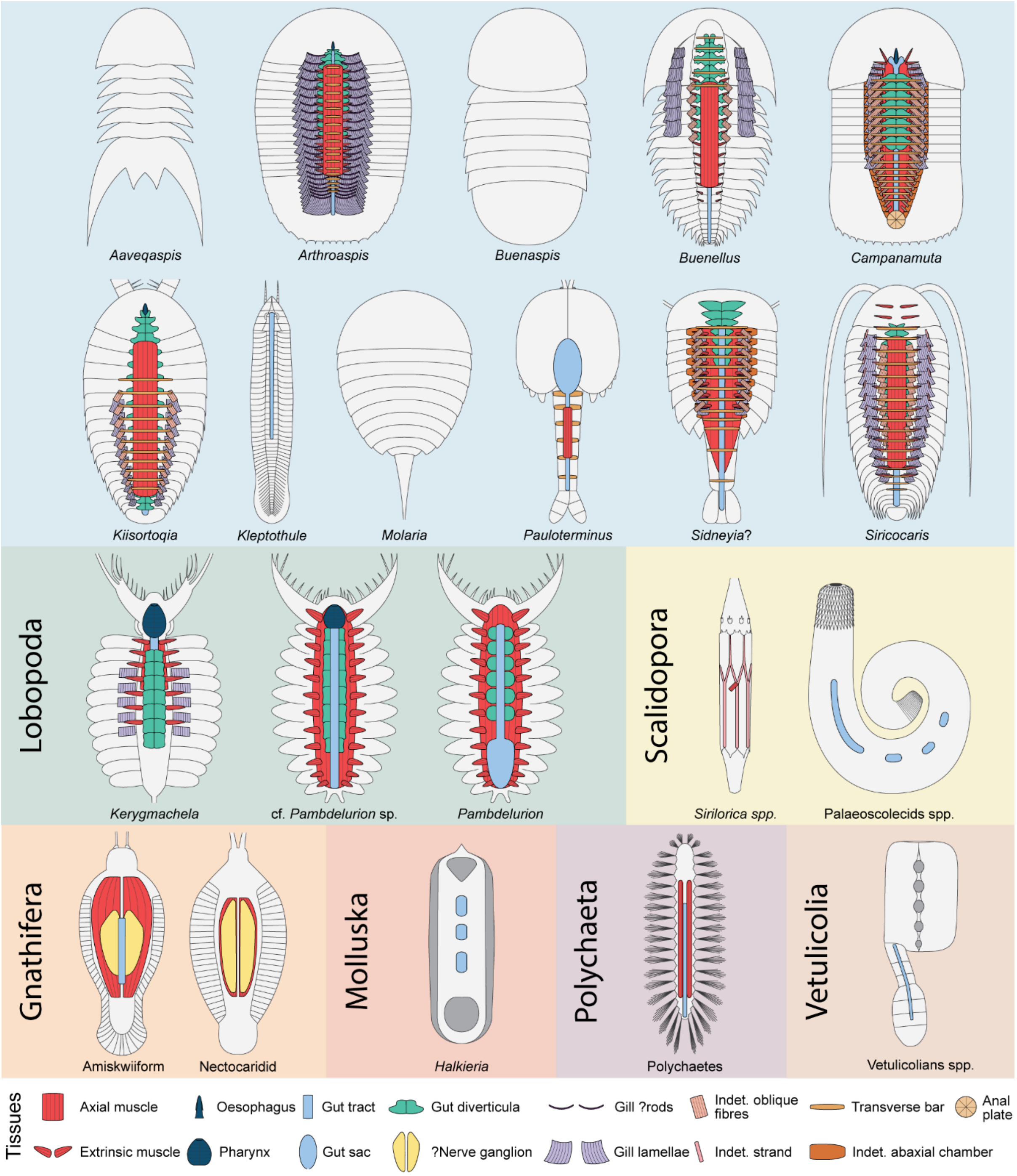

Figure 3.1. Diversity of the Sirius Passet Lagerstätte and their phosphatized tissues. Reconstructed tissues reflect their observed and not the biological extent. Their distributions therefore show clear bias against certain taxa and anatomical regions. Relative dorsoventral position of tissues does not reflect their in-life position but has been layered to visualize as many tissues as possible. Sponges are excluded.

3.3 Geological setting

3.3.1 Regional geology

The Sirius Passet Lagerstätte is part of the (likely basal) Buen Formation of the J. P. Koch Fjord area in Peary Land, North Greenland (Ineson and Peel, 2011; Harper et al., 2019). The fossiliferous intervals comprise *c.* 8 m of a *c.* 12 m thick section at the Sirius Passet main locality (cf. Peel and Ineson, 2011). The section is overturned to a 48° angle and bound by faults on both sides, likely during the Devonian Ellesmerian Orogeny (Harper et al., 2019). Regional metamorphism profoundly altered the mineralogy of the mudrocks (Strang et al., 2016b) and the fossils including the phosphatized tissues (Chapter 2). Dating the Lagerstätte is difficult due to the endemic nature of the fauna, but it has previously been assigned to the lower Cambrian *Nevadella* Zone based on the affinity of the endemic trilobite genus *Buenellus higginsi* occurring in Sirius Passet (Cambrian Series 2, Stage 3) (Blaker, 1988; Babcock and Peel, 2007).

3.3.2 Sedimentological context

The Sirius Passet Lagerstätte occur in fossiliferous fissile dark mudstones, sporadically interrupted by non-fossiliferous completely bioturbated silty mudstone to siltstone-grade beds 5–>100 cm thick (Harper et al. 2019). Beds are thin and laminated, around 2-5 mm thick deposited by dilute gravity flows (Chapter 4; Harper et al., 2019) in a predominantly very low-oxygen environment (Hammarlund et al., 2018). The Lagerstätte shows an extraordinarily high density of fossils. Fossils are preserved as low-relief BST carbonaceous compressions (Topper et al., 2018) with auxiliary pyritization and three-dimensionally preserved anatomy (Chapter 2). The majority of these fossils are found articulated, often with their internal labile soft tissues still preserved, suggesting very little disturbance after death (Chapter 4). Additionally, bedding surfaces are often covered in dense accumulations of amorphous organic detritus, putative algae, and indeterminate patches of various sizes (<1 to 20 mm). Horizontal trace fossils occur on some surfaces, especially inside fossils (Mángano et al., 2012), but do not affect three-dimensional anatomy even when they cross-cut them. Occasionally, bedding surfaces and their fossils are stained by rusty-orange iron oxide from weathering (Chapter 4; Harper et al., 2019).

3.4 Material and methods

3.4.1 Material

The material consists of 'Burgess Shale-type' fossils (i.e., carbonaceous compressions, Topper et al., 2018) from Sirius Passet with internal anatomy preserved by a distinctly different mineralogy in 'three dimensions' (Fig 3.2), meaning that they have a considerably higher relief than the surrounding compressions (Fig. 3.3). These three-dimensional tissues have a complex taphonomy that has been subjected to much speculation (e.g., Budd, 2011; Strang et al., 2016a; Young et al., 2016; Topper et al., 2018). They are currently preserved by a complex of different minerals with overall selectivity: guts are predominantly preserved by apatite (e.g., Vannier et al., 2014) while muscles are predominantly preserved by silica (e.g., Budd 2011; Young et al., 2016) with minor patches of muscovite and chlorite (Chapter 2). Tiny apatite inclusions observed within the other mineral phases (including within partially silicified rims of apatite gut structures) strongly suggest that these phases are late-stage replacements of a primary apatite phase (Chapter 2). For this study, we therefore assume the original taphonomic pathway of these distinct three-dimensional tissues to be phosphatization.

The investigated material was collected during the 2016 expedition to Sirius Passet (SP-2016). It represents a subset of 1219 slabs from the collected 1595 slabs. The investigated slabs were selected purely numerically and comprise specimens with field numbers SP-2016-1 through SP-2016-1219 that exhibit a total of 3609 registered specimens (including parts and counterparts). Material is currently housed at the Korea Polar Research Institute. Once published, material will be deposited at the Natural History Museum of Denmark, Copenhagen, Denmark (MGUH).

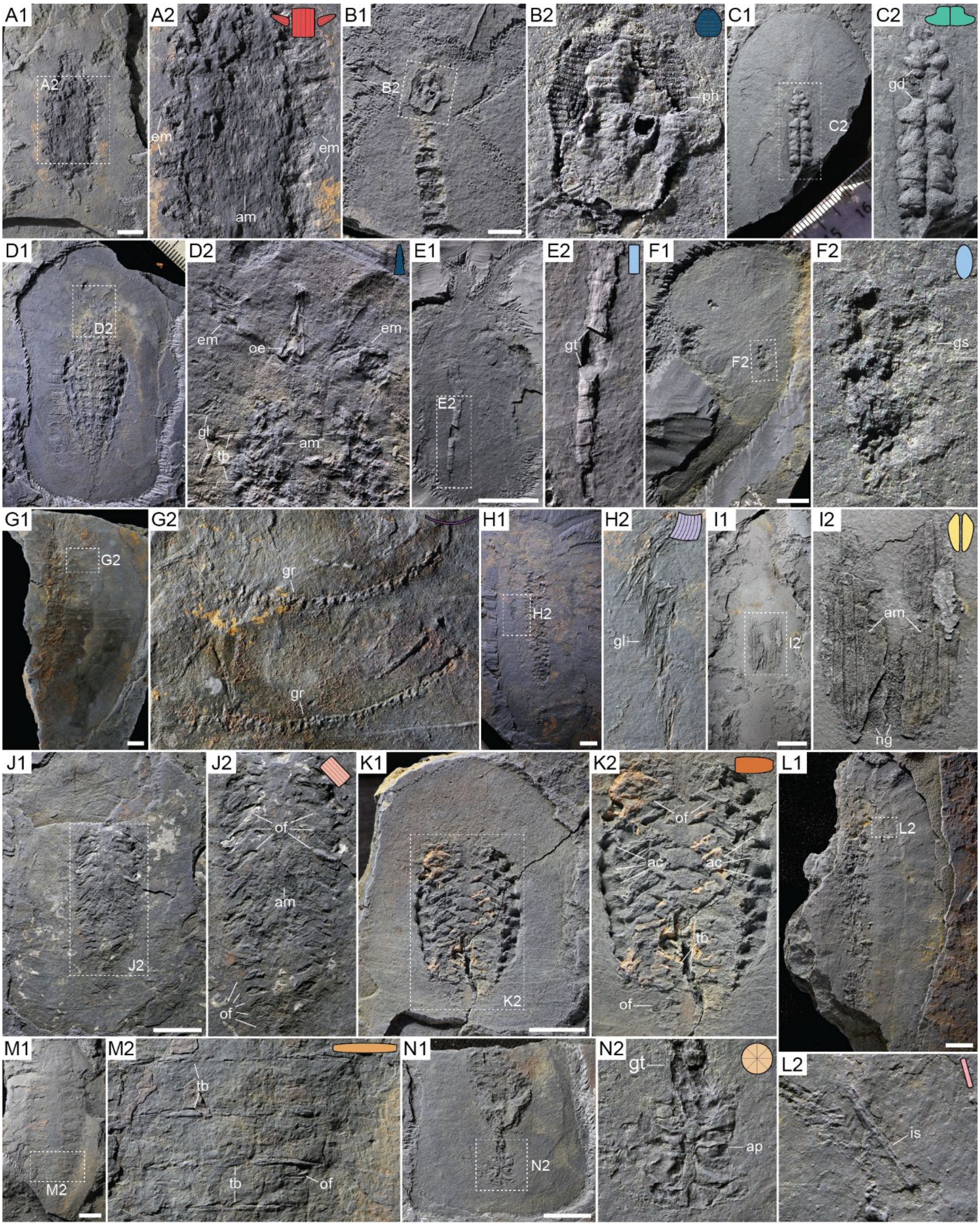

Figure 3.2. Examples of the different phosphatized tissues quantified in this study. (A) *Pambdelurion whittingtoni* showing axial and extrinsic muscles (A2). SP-2016-6. (B) *Kerygmachela kierkegaardi* showing pharynx (B2). SP-2016-195. (C) *Campanamuta mantonae* showing gut diverticula (C2). MGUH 17512. (D) *Campanamuta mantonae* showing oesophagus alongside extrinsic and axial muscles, gill lamellae, and transverse bars (D2). SP-2016-140. (E) *Kiisortoqia soperi* showing gut tract (E2). SP-2016-1027. (F) *Pauloterminus spinodorsalis* showing gut sac (F2). SP-2016-617. (G) *Arthroaspis bergstroemi* showing gill structures putatively interpreted as gill ?rods (G2). SP-2009-873. (H) *Siriocaris trollae*

showing gill lamellae (H2). SP-2017-839. (I) Amiskwiiform sp. showing structures putatively interpreted as nerve ganglia under banded axial muscle (I2). SP-2011-824. (J) *Campanamuta mantonae* showing indeterminate oblique fibres alongside axial muscle (J2). SP-2016-722. (K) *Campanamuta mantonae* showing indeterminate oblique abaxial chambers alongside indeterminate oblique fibres and transverse bars (K2). MGUH 29165. (L) *Siriocaris trollae* showing indeterminate strand (L2). (M) *Siriocaris trollae* showing transverse bars alongside indeterminate oblique fibres (M2). (N) *Campanamuta mantonae* showing anal plate (N2). SP-2016-563.Tissue reconstructions in upper-right corners are similar to those in Fig. 3.1. Abbreviations: ac, indeterminate abaxial chambers; am, axial muscle; ap, anal plate; em, extrinsic muscle; gd, gut diverticula; gl, gill laminae; gr, gill ?rods; gs, gut sac; gt, gut tract; is, indeterminate strands; ne, nerve ganglia; tr, transverse bars; oe, oesophagus; of, indeterminate oblique fibers; ph, pharynx.Scale bars are 10 mm.

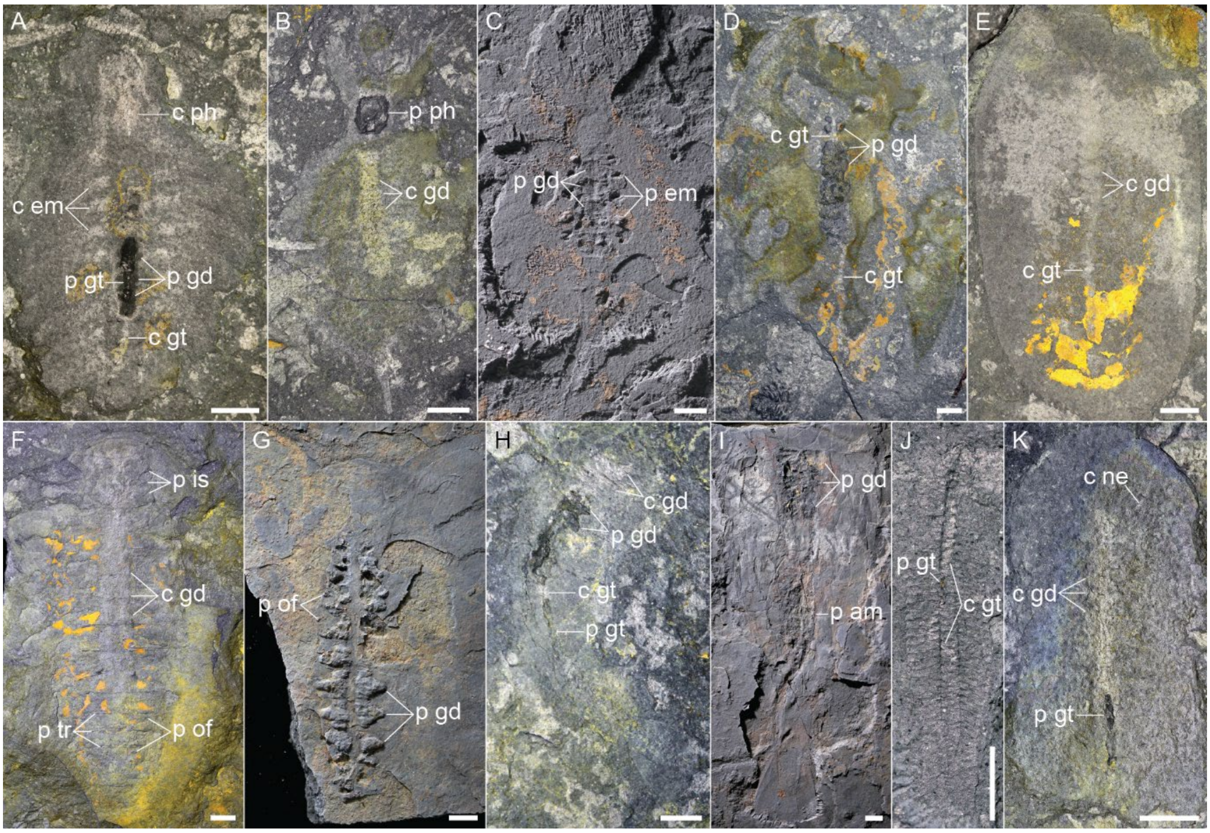

Figure 3.3. Examples of associated phosphatized (p) and carbonized (c) tissues in Sirius Passet fossils. Phosphatized tissues are high-relief black structures, while carbonized tissues are flat, silvery reflective films. (A–C) *Kerygmachela kierkegaardi*. (A) SP-2017-1 showing carbonized extrinsic muscle, partially carbonized and partially phosphatized gut tract, and phosphatized gut diverticula. Photographed submerged in water under high-angle light. (B) SP-2017-6 showing carbonized gut diverticula and phosphatized pharynx. Photographed submerged in water under high-angle light. (C) SP-2016-604 showing high-relief phosphatized gut diverticula and extrinsic muscle. Photographed coated and under low-angle light. (D–E) *Arthroaspis bergstroemi*. (D) SP-2016-1422 showing carbonized gut tract and phosphatized gut diverticula. Photographed submerged in water under high-angle light. (E) SP-2016-696 showing carbonized gut tract and gut diverticula. Photographed submerged in water under high-angle light. (F–G) *Siriocaris trollae*. (F) SP-2016-770 showing carbonized gut diverticula, and patchy phosphatized transverse bars, oblique fibers, and indeterminate strands. Photographed submerged in water under high-angle light. (G) SP-2016-288 showing high-relief phosphatized gut diverticula and oblique fibers. Photographed coated and under low-angle light. (H–I) *Sidneyia* sp. (H) SP-2016-69 showing partial carbonization and

phosphatization of both the gut tract and gut diverticula. Photographed submerged in water under high-angle light. (I) SP-2017-861 show phosphatized gut diverticula and phosphatized axial muscle. Photographed coated and under low-angle light. (J) *Kleptothule rasmusseni*. SP-2016-170 showing partially carbonized and partially phosphatized gut tract. Photographed submerged in water under high-angle light. (K) Juvenile *Campanamuta mantonae*. SP-2016-838 showing carbonized nervous tissues and gut diverticula, and phosphatized posterior gut tract. Scale bars are 5 mm. Abbreviations: c, carbonized; am, axial muscle; em, extrinsic muscle; gd, gut diverticula; gt, gut tract; is, indeterminate strands; ne, nervous tissues; tr, transverse bars; of, oblique fibers; p, phosphatized; ph, pharynx.

3.4.2 Collection bias

Non-exhaustive collections are subject to collection biases (Whitaker and Kimmig, 2020). Early expeditions to Sirius Passet were exceedingly biased as they only collected weathered material from the scree which would favor identification of high-relief fossils and conceal a significant portion of the fauna (Harper et al. 2019, box 1). During the 2016 expedition, a large portion of the material was selected for collection after exhaustive scrutiny of bulk material under water and under different light angles in the field camp. *In situ* material comprise two-thirds of the collection and mostly derives from an interval between 5.6–7.9 m with a particular focus on the 5.8–6.3 m interval. The remaining ~one-third were collected from scree. The 2016 collection is biased towards rare data. For Sirius Passet this means that rarely phosphatized taxa are likely oversampled for phosphatized specimens and *vice versa.* Extensive and well-preserved internal anatomy collected to aid anatomical reconstructions are also oversampled. Collection bias is mitigated by a considerable ‘side-catch’ of fossils that accompany target fossils on collected slabs due to the high fossil abundances (e.g., Vinther et al., 2011b). These fossils comprise a significant part of the registered collection due to the high fossil density in Sirius Passet, especially for common arthropods (e.g., *Buenellus*, *Campanamuta*) that are not specifically targeted when choosing specimens to collect.

3.4.3 Photography

Specimens were coated with magnesium and photographed under low-angle lighting except when mentioned otherwise. Images were subsequently processed in Adobe Photoshop 2022.

3.4.4 Tissue identification

Phosphatized soft tissues are identified from their location and three-dimensional morphology that mostly appear black in color. In some cases, the color is reflective or grey, especially at their border to the sediment, or yellow to white if weathered. Negative imprints remain when tissues have been lost to e.g., sampling (splitting and washing) or weathered away after natural rockfall. Metamorphic overprinting (Chapter 2) can under certain circumstances destroy microstructures (e.g., subcellular myofibrils) but it does not affect the macrostructures (e.g., muscle fibers) used to identify tissues herein. Tissues are sometimes concealed by adjacent tissues and hence any frequency should be considered a minimum value. For instance, gut diverticula for *Campanamuta* are likely grossly underestimated as the overlying axial muscle are very frequently preserved. Not all phosphatized structures could be attributed to known tissues; these are either included in the frequency analysis as tentative structures or excluded as indeterminate phosphatization if poorly preserved. Both part and counterpart were used to identify tissues when possible.

Anatomical reconstructions were based on available evidence and published records (Conway Morris and Peel, 1995, 2010; Taylor, 2002; Babcock and Peel, 2007; Lagebro et al., 2009; Stein, 2010; Budd, 2011; Peel et al., 2013; Stein et al., 2013; Young and Vinther, 2016). Extent of tissues in reconstructions reflects their observed distribution. The in-life extents of gut diverticula were verified with carbonized diverticula, except in cf. *Pambdelurion* sp. nov. and *Pambdelurion whittingtoni* where diverticula have not been found carbonized.

3.4.5 Quantitative dataset

To assess biological controls on phosphatization, we use a quantitative dataset of absence (“0”)/presence (“1”) of phosphatized tissues in 21 taxa (*n*=1159) and 15 different phosphatized tissues (Fig 3.2, Data Table E3.1). We place particular focus on arthropod taxa (12 taxa) to limit the effects of taxonomically controlled differences, since their general anatomy is broadly similar, but include ‘gilled lobopods’ (three taxa), scalidophorans (two taxa), gnathiferans (two taxa), molluscs (one taxon), vetulicolians (one taxon) and polychaetes (one taxon) to examine taxonomic biases and the complexity of the system (Fig. 3.1). Taxonomic groups with species that are difficult to separate or are very rare (palaeoscolecids spp., polychaetes spp., *Sirilorica* spp. and vetulicolians spp.) are conflated into an appropriate taxonomic group to prioritize higher-taxon preservational patterns over taxon-specific patterns for those groups. *Isoxys volucris* was omitted from the analysis since its ubiquitous presence means that it has not been catalogued properly in the collection. Incomplete specimens (e.g., broken or covered by matrix) missing regions with potentially phosphatized tissues were removed from the dataset if they had no visible phosphatization but included if they had; this is expected to slightly underestimate the frequency of (mostly large) non-phosphatized specimens. Specimens where certain tissues could not be identified or scored due to missing or obscured areas are marked as uncertain ("?"). Frequencies of soft tissues are calculated after subtracting uncertain values from the total. They are presented as heat maps on the fossil reconstructions (see Fig. 3.1) where each tissue is colored according to its frequency; their values are available in (Data Table E3.1).

To identify multivariate preservational patterns, we performed principal component analysis (PCA) on part of the quantitative dataset using Past 4.11 (Hammer et al., 2001). Only arthropods were included to limit the artefacts created by different anatomical structures. PCA collapses variance from tissue absences/presences in different specimens into as few components as possible, with each new component defined by certain tissue relationships. Tissue relationships (i.e., their relative effects) are presented as loading plots and eigenvectors on the PCA plots. Additionally, a transposed version of the dataset was subjected to PCA to visualize tissue co-occurrences. We used a variance-covariance matrix where uncertain presences ("?") were replaced with hypothetical mean values using the Iterative imputation in Past 4.11, which produced unwanted noise in analyses. To assess this noise, we performed a complementary PCA that excluded specimens with uncertainties, but this did not differ considerably from the PCA on the full dataset.

To assess the impact of body size on phosphatization, we use measured widths of *Campanamuta mantonae* (*n*=267; Data Table E3.1E) and compared the results with published records for other taxa to assess any interspecific size-biases. *Campanamuta mantonae* is an ideal model organism due to its high abundance, presence of both adults and juveniles, and high frequency of phosphatization (93,4%) of numerous different tissues.

Specimens were measured primarily from standardized images with ImageJ 1.46r (Schneider et al., 2012). Violin box plots that visualize distributions as surrounding 'violins' were used to show size distributions for tissues in *Campanamuta* and produced with Past 4.11 (Hammer et al., 2001).

To test for the importance of microenvironments within the carcasses, we scored the longitudinal extent of continuously phosphatized axial muscle areas for four taxa: the arthropods *Arthroaspis*, *Kiisortoqia*, and *Sidneyia*? and the 'gilled' lobopod cf. *Pambdelurion* sp. nov. (Data Table E3.2). Axial muscle covers longitudinal and oblique musculature that occur throughout the body axis of arthropods. However, their phosphatization varies in extent; therefore, we assume that the areas approximately reflect the extent of a phosphatizing microenvironment. Phosphatized areas were scored as absent ("0") or present ("1") for each segment (including cephalon and pygidia if present). Only specimens that could be scored for each segment are included. Patchy occurrences or other tissue types are not included here.

To test whether more closed conditions facilitate phosphatizing microenvironments we categorized enrolled vs outstretched specimens of *Campanamuta* as well as the lateral and longitudinal extent of continuous phosphatization of axial muscle on an index from 1–4 (n=329; Data Table E3.1E): *(1)* no continuously phosphatized muscle areas (but other tissues can be phosphatized), *(2)* continuously phosphatized axial muscle area is limited to parts of the trunk/pygidium, *(3)* continuously phosphatized axial muscle area extends from the cephalon to the pygidium but without phosphatization of the laterally distalmost indeterminate abaxial chambers (lateral domes cf. Budd, 2011), *(4)* continuously phosphatized axial muscle area extends from the cephalon to the pygidium and include phosphatization of the laterally distalmost indeterminate abaxial chambers. The assumption is that more laterally extensive phosphatized areas reflect more pervasive microenvironments. This is based on the observation that locally restricted phosphatized areas occur predominantly in the axis (although not exclusively). The indeterminate abaxial chambers represent the distalmost intrinsic tissue/organ recorded for *Campanamuta* (Budd, 2011). The analysis only included specimens with widths >24.1 mm, representing the minimum width for enrolled specimens in the collection.

3.5 Results and interpretation

3.5.1 Taxonomic distribution of phosphatization

Results

Phosphatization varies considerably across the community (Fig. 3.4). For example, phosphatized tissues do not occur, or very rarely occur, in the arthropods *Aaveqaspis* (0%, *n*=9), *Buenaspis* (0%, *n*=51), *Kleptothule* (3%, *n*=112) and *Molaria* (0%, *n*=3). In contrast, they almost consistently occur in *Campanamuta* (93%, *n*=348), *Sidneyia*? (98%, *n*=62), and *Siriocaris* (100%, *n*=9). Beyond arthropods, vetulicolians (4%, *n*=50) and the ecdysozoan scalidophoran *Sirilorica* spp. (5%, *n*=63) show low phosphatization frequencies, whereas the gnathiferans amiskwiiform sp. (63%, *n*=8) and nectocaridid sp. (57%, *n*=7) show comparatively high frequencies. However, the most consistently phosphatized taxonomic group is the 'gilled' lobopods with *Kerygmachela* (91%, *n*=22), cf. *Pambdelurion* sp. nov. (100%, *n*=30), and *Pambdelurion whittingtoni* (100%, *n*=14).

Tissue frequencies vary between taxa (Fig. 3.4): the trilobite *Buenellus* (*n*=168) preserves high frequencies of both gut tracts (68%) and diverticula (cephalic diverticula: 41%; thoracic diverticula: 18%) but very low frequencies of axial muscle (1%). In contrast, *Sidneyia*? (*n*=62) frequently preserve axial muscle (67%) and/or gut tracts (72%) but rarely gut diverticula (22%). Similarly, in 'gilled lobopods', *Kerygmachela* (*n*=22) frequently preserve the pharynx (59%) and/or gut diverticula (73%) but rarely axial (5%) or extrinsic (19%) muscle, or gut tracts (0%), a clear contrast to cf. *Pambdelurion* sp. nov.'s (*n*=30) ubiquitous preservation of gut tracts (96%), and extrinsic (93%) and axial (100%) muscle. Lastly, in rare cases, *Arthroaspis* (2%, *n*=63) and *Sidneyia*? (3%, *n*=62) preserve readily recognizable gill ?rods connecting the lamellae; a tissue that is otherwise not widely distributed in other taxa.

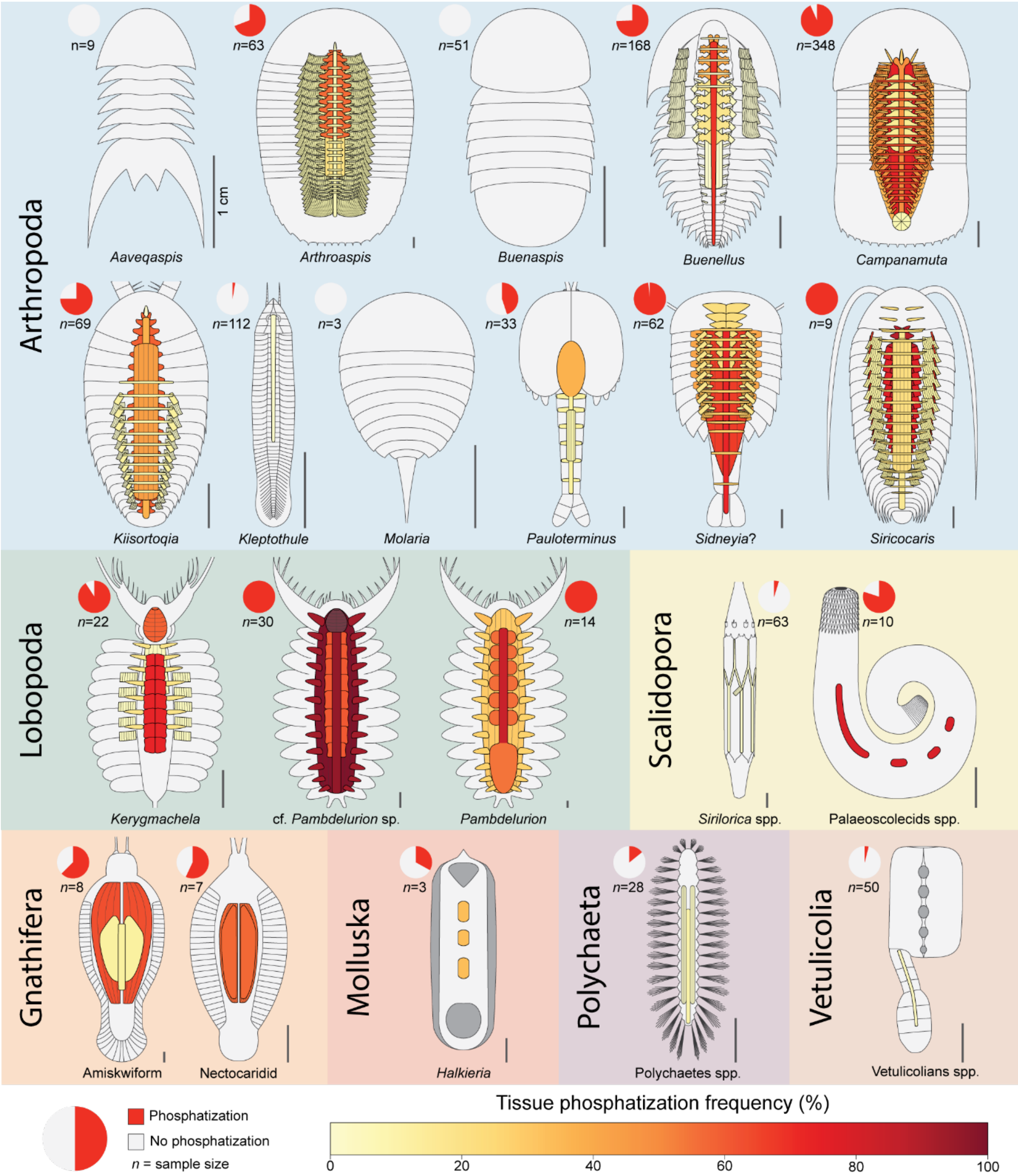

Figure 3.4. Frequencies of phosphatization. There is a clear variability in frequency between both taxa and tissues, both within and between higher taxa. Each tissue is colored after their value on the frequency-heatmap below, from low (pale yellow) to high (dark red) frequencies. Pie charts for each taxon show ratio between phosphatized (red) and non-phosphatized (light grey) specimens. Legend for tissues is shown on Fig. 3.1. Scale bar is 1 cm for all taxa.

Multivariate principal component (PC) analysis of arthropods (*n*=909 between 11 taxa) visualizes this taxonomic variation (Fig. 3.5). Taxa show different extents (convex hulls) in the plot: specimens without phosphatization plot in a cluster (including all *Aaveqaspis*, *Buenaspis*, and *Molaria*) with the lowest PC1 value, while convex hulls with increasingly higher ranges on PC1 reflect taxa with increasingly more types of tissues preserved simultaneously (e.g., *Campanamuta*: green dots; *Sidneyia*: blue dots). Only one taxon, *Siriocaris* (*n*=9), does not show any specimens without phosphatization, perhaps due to the small sample size.

Interpretation

The non-random distribution of tissue frequencies within taxa reflects taxonomic controls (Martill, 1988; Wilby and Whyte, 1995; Wilby and Briggs, 1997; Klug et al., 2005; Wilson et al., 2016). In some cases, they appear to correlate with higher taxonomic ranks: 'gilled lobopods' show consistently high frequencies across all three taxa suggesting that they are taxonomically susceptible to phosphatization. But this is not always the case as the trilobite-like artiopodan arthropods, *Campanamuta* (*n*=348) and *Sidneyia*? (*n*=62) show high frequencies of multiple tissues whereas not a single *Buenaspis* specimen (*n*=51) exhibits phosphatization (Fig. 3.4). These findings are consistent with taxonomic controls that create taphonomic biases elsewhere (e.g., Wilby and Briggs, 1997; Wilson et al., 2016). This control can be influenced by e.g., anatomical features that prohibit phosphatization by chemical buffering (Clements et al., 2017). Taxonomic controls create broadly predictable distributional patterns within a taxon but not necessarily between taxa (e.g., the disparate extents along PC1 in Fig. 3.5), even when taxa are closely related.

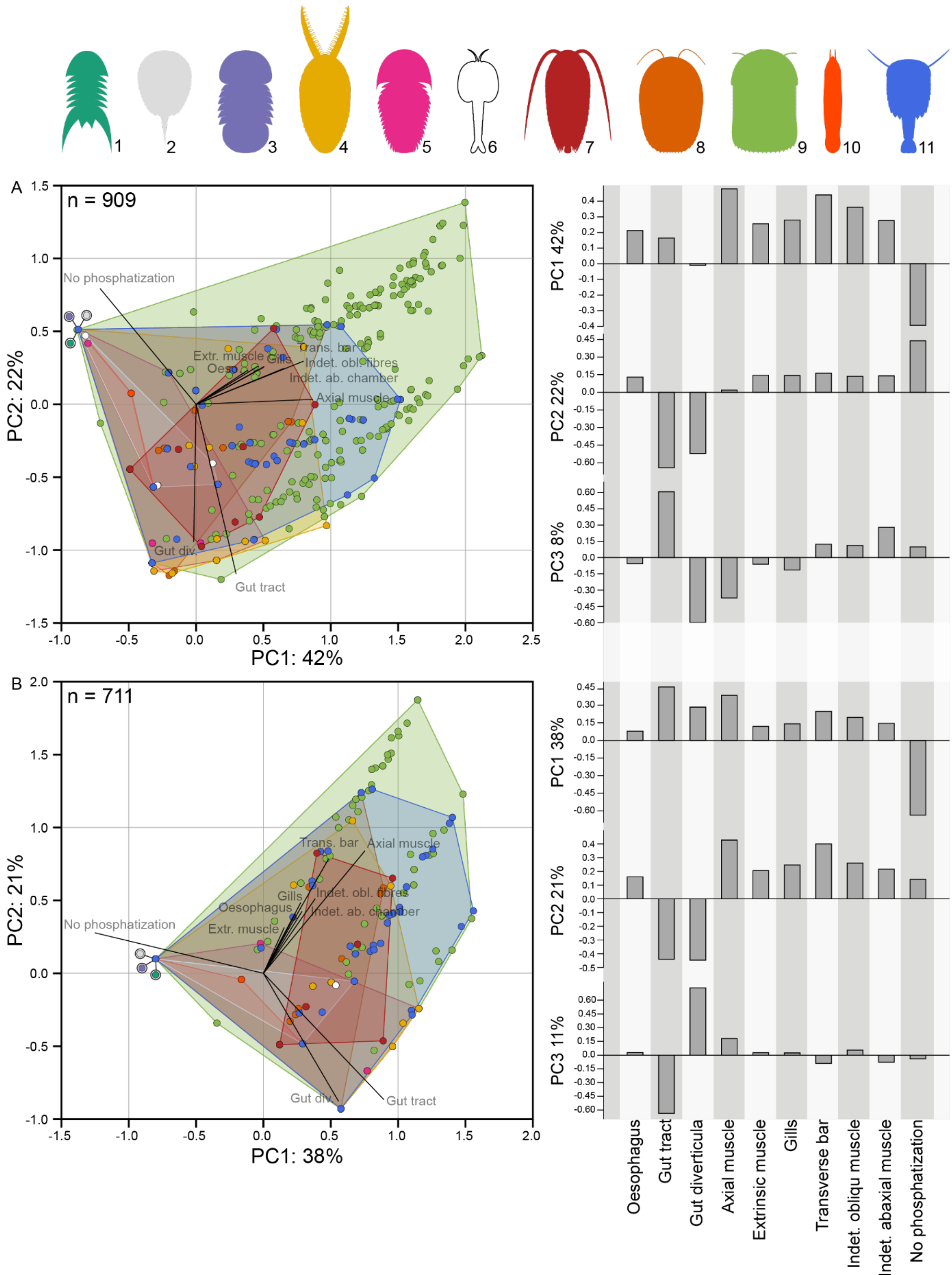

Figure 3.5. Principal component (PC) analyses of phosphatized tissues in Sirius Passet arthropods showing their taxonomic variation. Each circle represents a specimen, and convex hulls show the range of phosphatization for a given taxon. Loading plots show the relationship between phosphatized tissues for PC 1-3, and their relative effect on each PC plot

is visualised as eigenvectors. Taxa extending towards NE corner of the PC plots reflect higher number of phosphatized tissues within the specimens, while those extending towards S (A) or SE (B) reflect number of phosphatized gut tissues. Specimens without phosphatization all cluster towards W. (A) PC plot of the full data set. (B) PC plot excluding specimens with uncertainties, validating that the patterns of A are not artefacts of noise. Taxa: 1: *Aaveqaspis inesoni*, 2: *Molaria steini*, 3: *Buenaspis higginsi*, 4: *Kiisortoqia soperi*, 5: *Buenellus higginsi*, 6: *Pauloterminus spinodorsalis*, 7: *Siriocaris trollae*, 8: *Arthroaspis bergstroemi*, 9: *Campanamuta mantonae*, 10: *Kleptothule kierkegaardi*, 11: *Sidneyia*? sp.

3.5.2 Bedding plane distribution of phosphatization

Results

Within-taxon phosphatization is heterogenous on individual bedding planes. We record several bedding planes (*n*=10) with multiple co-occurring specimens of *Campanamuta* (total *n*=29) showing heterogenous levels of phosphatization (Fig. 3.6). They differ both in which tissues preserve as well as their extent. For example, one bedding plane (Fig. 3.3A) shows three specimens that all preserve muscle but differ in extent and additional tissues: one specimen shows an extensive area with phosphatized muscle spanning the entire width of the axis from the cephalon to pygidium (Fig. 3.6A1); a second specimen show muscle area around, and just posterior to, partially phosphatized gut diverticula in addition to an isolated phosphatized oesophagus in the cephalon (Fig. 3.6A2); a third specimen show a more confined muscle area posterior to fully phosphatized diverticula in addition to the gut tracts' anterior lobes (Fig. 3.6A3). Another bedding surface (Fig. 3.6B) show an enrolled specimen (see Regionalization of phosphatization) with extensive phosphatization close to a small specimen without any phosphatized tissues (see Size distribution of phosphatization). Heterogeny prevails even when specimens of broadly similar sizes are in direct contact (Fig. 3.6C): one specimen preserves partial gut diverticula and transverse bars (Fig. 3.6C1) while the other preserves partial gut diverticula, transverse bars, musculature, and anal plate (Fig. 3.6C2).

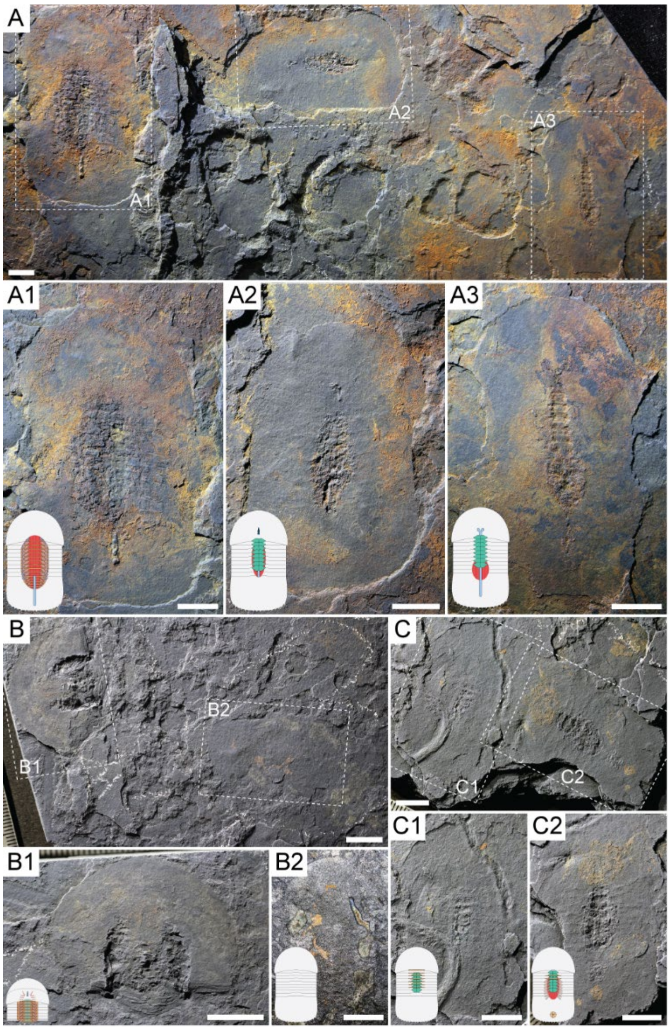

Figure 3.6. Bedding plane heterogeneity of phosphatization. Examples show co-occurring Campanamuta mantonae specimens on specific bedding planes with different phosphatized tissues and extents. Bedding plane heterogeneity highlights the importance of biological controls on phosphatization. (A) Three specimens with strongly heterogenous phosphatization: (A1) specimen preserves several different tissues within an extended axial area; (A2) specimen preserves a more restricted axial area with fewer tissues (gut tract, gut diverticula, muscle) in addition to the isolated oesophagus; (A3) specimen preserves a very localized axial area with muscle in addition to gut tracts (with gut lobes) and diverticula. SP-2016-410. (B) Two specimens with strong heterogeneity: (B1) specimen is enrolled and preserves an extended area with several tissues (note that not all tissue types could be identified); (B2) specimen is a small, outstretched specimen without any phosphatization at all. SP-2016-851. (C) Two specimens in direct contact that show heterogeneity: (C1) specimen preserves a restricted area with diverticula and transverse bars; (C2) specimen preserves a larger area that also included muscle. SP-2016-1206b. Scale bars are 1 cm.

Interpretation

Phosphatization of intimately associated specimens presumably occurs under similar external (environmental) conditions. This precludes external controls on the heterogenous phosphatization between taxa. Consequently, the heterogeneity in Sirius Passet is interpreted to reflect internal biological controls.

3.5.3 Tissue distribution of phosphatization

Results

No individual tissue phosphatizes across all taxa (Fig. 3.4). However, certain tissues are more widely distributed than others. Gut tracts are the most common and occur in 15 (of a total 21) taxa and are known from taxa with low overall phosphatization frequencies (e.g., the arthropod *Kleptothule*, or polychaetes and vetulicolians). Muscle tissue occurs in 14 taxa and is the second most common tissue. On the other hand, putative phosphatized nerve tissue is only observed in the two gnathiferan taxa (amiskwiiform sp. and nectocaridid sp.). In arthropods, where anatomy is expected to be broadly similar, distribution of phosphatized tissues also varies: out of a total of 14 taxa, gut tracts preserve in eight, musculature in seven, transverse bars in seven, gut diverticula in six, gill lamella in six, indeterminate oblique fibers in five, oesophaguses in three, indeterminate abaxial chambers in two, and gill ?rods in a single taxon (Fig. 3.4). Abaxial chambers are restricted to the two most frequently phosphatized taxa (*Campanamuta*, *Sidneyia*), suggesting that this is not simply a reflection of presence in life.

Multivariate PCA analyses show that phosphatization patterns of arthropod gut structures (tracts, diverticula) differ from other tissues. Guts show an inverse correlation with other tissues on PC2 (Fig. 3.5). Gut phosphatization divides the dataset into four distinct ‘plateaus’ (eigenvectors on Fig. 5.5b): 1) specimens without phosphatization; 2) phosphatized specimens but without guts; 3) specimens with either gut tracts or gut diverticula phosphatized; and 4) specimens with both gut tracts and diverticula phosphatized. Each plateau shows an internal variation depending on the overall number of phosphatized tissues, as represented by the eigenvectors pulling the groups in a 'north-eastern' direction. Additionally, an inverse correlation between gut tracts and diverticula defines PC3. The same overall pattern is visible on a PCA of the transposed dataset, to reveal co-occurrence patterns of tissues. Here, guts cluster differently to all other tissues on PC1 while tracts and diverticula show an inverse relationship on PC2 (Fig. 3.7).

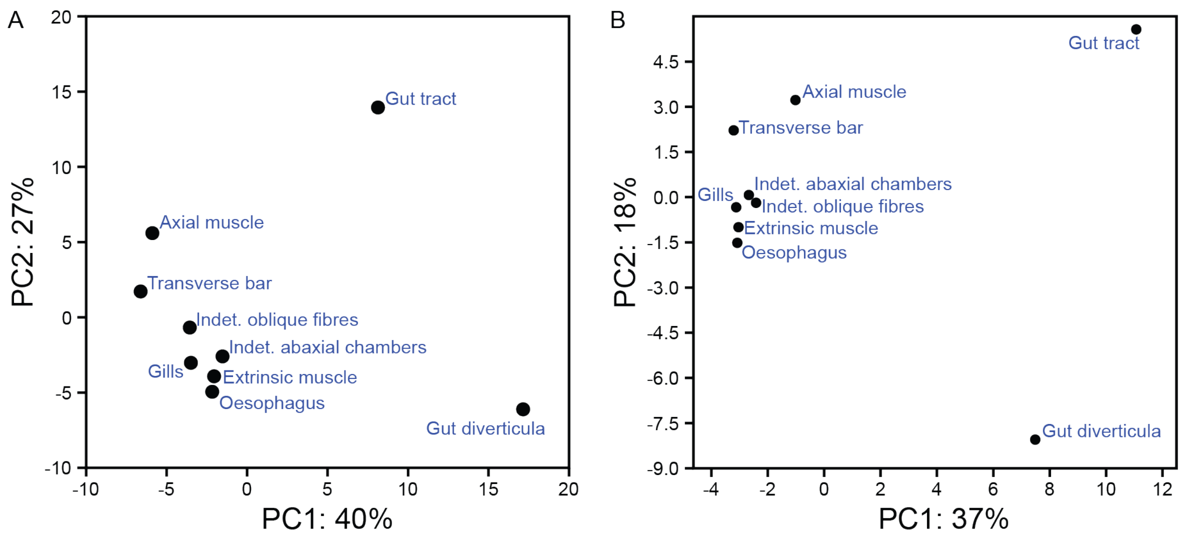

Figure 3.7. Principal component (PC) analysis on a transposed version of the dataset on Fig. 3.5, showing preservational relationships of different phosphatized tissues. Tissues with frequent co-occurrences cluster. Gut tissues (tracts and diverticula) do not cluster with other tissues, indicating a dependence on different phosphatization controls. See Fig. 3.1 for tissue reconstructions.

Interpretation

The most widely distributed phosphatized tissues, guts and musculature, were certainly present in life in all analyzed taxa. Nervous tissues were also present in life, and are preserved by reflective films in *Kerygmachela* (Park et al., 2018); however, this tissue is not phosphatized except for the tentative ganglia in the gnathiferans amiskwiiform sp. and nectocaridid sp. (Park *et al.* in prep., Vinther *et al.* in prep). Gill lamellae present another example of tissue control. They are part of a larger exopod situated next to an enlarged exopodal lobe in *Arthroaspis* (Stein et al., 2013), *Kiisortoqia* (Stein, 2010), and *Siriocaris* (Lagebro et al., 2009). While gill lamella are relatively commonly phosphatized herein, no other exopod structures (e.g., lobes) are phosphatized except for the tentative gill ?rods observed in *Arthroaspis* and *Sidneyia*?. Still, phosphatization of tissues is not always predictable between taxa even when they share similar tissues (e.g., muscle).

Gut phosphatization appears to have a separate control from other tissues, as indicated by the eigenvectors on Fig. 3.5. This is supported by phosphatization of guts (tracts and/or diverticula) in taxa with very low or low phosphatization frequencies of other tissues (i.e., *Kleptothule*, *Pauloterminus*, Vetulicolia spp.). Phosphatization of gut tracts and gut diverticula does not necessarily co-occur, which in turn suggests that they have different controls. This is likely attributed to their different functions and compositions (Butterfield, 2002).

3.5.4 Regionalization of phosphatization

Results

Phosphatized axial muscle show distinct regionalization in extent (Fig. 3.8). The arthropods *Arthroaspis* (*n*=9), *Kiisortoqia* (*n*=19), and *Sidneyia*? (*n*=32) most commonly preserve axial muscle in posterior-midregions: *Arthroaspis* show highest frequencies in segments 8–9 (78%), *Kiisortoqia* in segments 7–8 (100%), and *Sidneyia*? in segment 6 (91%). In contrast, continuous muscle areas rarely preserve in their cephala (0%) or anteriormost (11%) segments and posteriormost (2%) sclerites (segment/pygidium/telson). Other metameric tissues in the trunk show similar regionalization (Fig. 3.6C1, 8D), and in some cases their presence is only observed in those regions. For example, gill lamella and indeterminate oblique fibers are only known from the same posterior-midregion in *Kiisortoqia*. There are exceptions to the position of these regions: *Buenellus* more frequently preserves gut diverticula in the cephalon than in the trunk, the same region its gill lamellae are observed (Fig. 3.4). Regionalization of cf. *Pambdelurion* sp. nov.. of axial muscle extends from the head to segment 8 (Fig. 3.8).

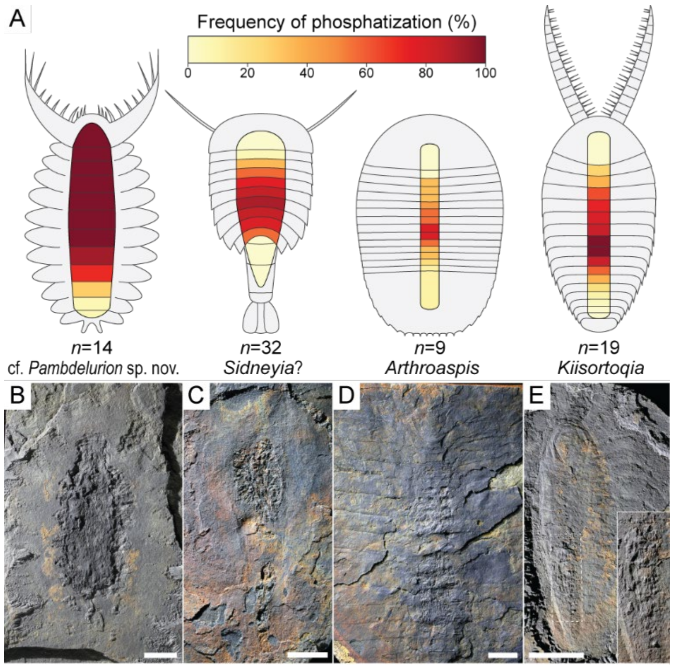

Figure 3.8. Regionalized distribution of continuously phosphatized axial muscle. (A) Heat map showing frequencies per segment of preserved axial muscle within the 'gilled lobopod' cf. *Pambdelurion* sp. nov., and the arthropods *Sidneyia*?, *Arthroaspis*, and *Kiisortoqia*. The highest frequencies are concentrated within the posterior-midregion in all three arthropods, and occurrences in the sagittally distal segments are very rare. This is different for cf. *Pambdelurion* sp. nov. where frequencies are high through the anterior half of the trunk. (B–C) Examples of regionalized continuous axial muscle in fossils. (B) cf. *Pambdelurion* sp. nov. with axial muscle from head–segment 7. Note that isolated, patchy extrinsic muscle and the gut tract extend beyond the axial muscles to segments 8–9. SP-2016-6. (C) *Sidneyia*? with axial muscle from segments 2–8, in addition to a gut tract isolated in the posterior abdomen. SP-2016-195. (D) Trunk of *Arthroaspis bergstroemi* with axial muscle from segments 2–10 superimposed on transverse bars and gut diverticula (negative imprints). SP-2016-1021. (E) *Kiisortoqia soperi* with axial muscle from segments 7–13 (dashed box), in addition to transverse bars and thick oblique bundles. SP-2016-32. Scale bars are 1 cm.

Enrolled specimens of *Campanamuta* (Fig. 3.6B1) generally show more extensive degrees of continuous phosphatization of axial muscle areas than outstretched specimens (Fig. 3.9). The most extensive index for continuous phosphatization (Index 4; Fig. 3.9A4) occur in 66% of enrolled specimens and in 15% of outstretched specimens. Likewise, the index for restricted areas (Index 2; Fig. 3.9A2) occurs in 16% in enrolled and 28% in outstretched specimens.

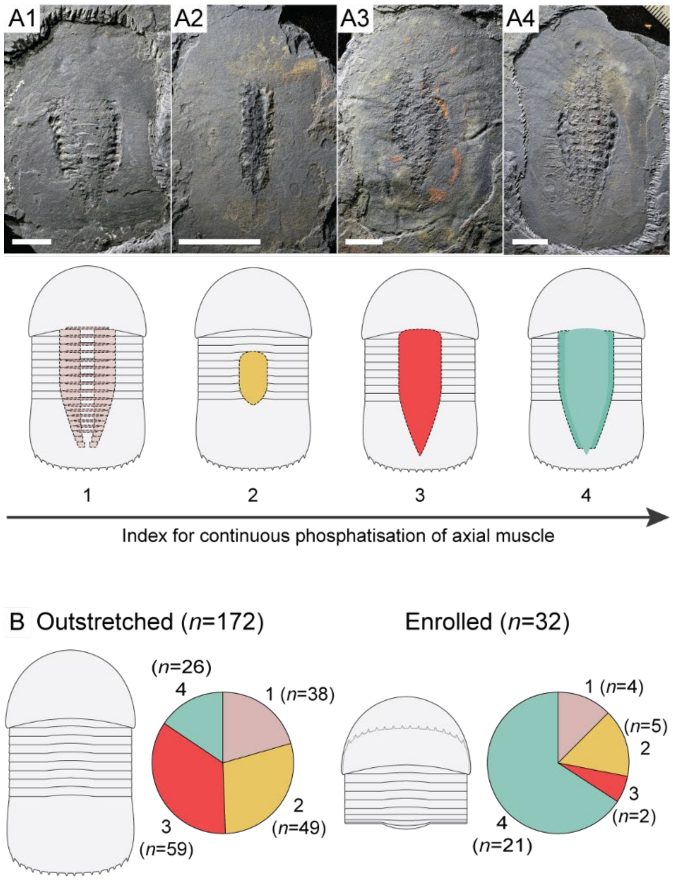

Figure 3.9. Comparison of phosphatization between outstretched and enrolled *Campanamuta mantonae* specimens. (A) Index of increasing extent of continuously phosphatized areas (Index 1–4) and representative fossil specimens (A1–A4). (A1–A4) representative fossils of the index. (A1) Index 1: No continuous axial muscle area, but other tissues may be present (here indeterminate abaxial chambers and transverse bars). SP-2016-614. (A2) Index 2: Restricted continuous axial muscle areas within the trunk/pygidium. SP-2016-22. (A3) Index 3: Extensive continuous axial muscle areas ranging from cephalon to pygidium. SP-2016-269. (A4) Index 4: Same as Index 4 but include distalmost abaxial chambers. SP-2015-140. (B) Comparison of indices between stretched and enrolled specimens. Enrolled specimens show much higher frequencies of most extensive axial muscle areas (Index 4). Numbers on pie chart refer to indices. Scale bars are 1 cm.

Interpretation

Regionalized preservation of the arthropods' axial muscle, which is presumed to have been continually present along the axis in life, might reflect: *(1)* nearby available phosphorus source, *(2)* higher tissue density, *(3)* microenvironments. *(1)* Gut diverticula could pose an obvious regionalized phosphorus source (Butterfield, 2002; Lerosey-Aubril et al., 2012) for adjacent muscle if they decay; however, they are unlikely to explain regionalization herein since they occur in the less-frequently phosphatized anterior area of *Arthroaspis* and *Sidneyia*? (compare their position in Fig. 3.1 with Fig. 3.8) and are often not decayed but phosphatized alongside the muscle (Fig. 3.6A2, 3.6A3). *(2)* Muscle densities are likely also higher in the anterior regions where legs are largest. *(3)* with the others excluded, microenvironments, a well-known control, are considered the most likely. This is consistent with enrolled specimens showing more extensive phosphatization than outstretched specimens: enrolling would have created more closed conditions, or at least more restricted conditions, that would have been more efficient in creating and sustaining a microenvironment as well as containing decay-released phosphorus (Wilby and Whyte, 1995). Departures from the general trend can probably be explained by biology: cf. *Pambdelurion* sp. nov. have a large muscular pharynx (Young and Vinther, 2016), phosphatized in all observed specimens, that may influence the formation of the microenvironment. Importantly, specific microenvironments developed regionally within carcasses (in the posterior-midregion for arthropods) and are consequently unlikely to be highly localized around tissues (cf. McNamara et al., 2009) or a pervasive environment throughout the entire carcasses (cf. Clements et al., 2022).

3.5.5 Size distribution of phosphatization

Results

There are striking correlations between size and phosphatization: the four smallest arthropod taxa (maximum known lengths of dorsal exoskeleton: *Aaveqaspis* 26 mm, *Buenaspis* 30 mm, *Kleptothule* 31 mm, *Molaria* 20 mm) do not appear to phosphatize, except for a few rare cases (Fig. 3.2). At the same time, the two largest taxa, by far, in Sirius Passet, *Arthroaspis* and *Pambdelurion*, do not show the most extensive levels of phosphatization (Fig. 3.4).

Ontogeny of *Campanamuta* shows a more obvious phosphatization sequence with three principal preservational size thresholds (Fig. 3.10): *stage 1* no phosphatization (widths <12 mm); *stage 2* only gut tracts and/or diverticula (widths 12–20 mm); *stage 3* guts, muscle and other tissues (widths >20 mm).

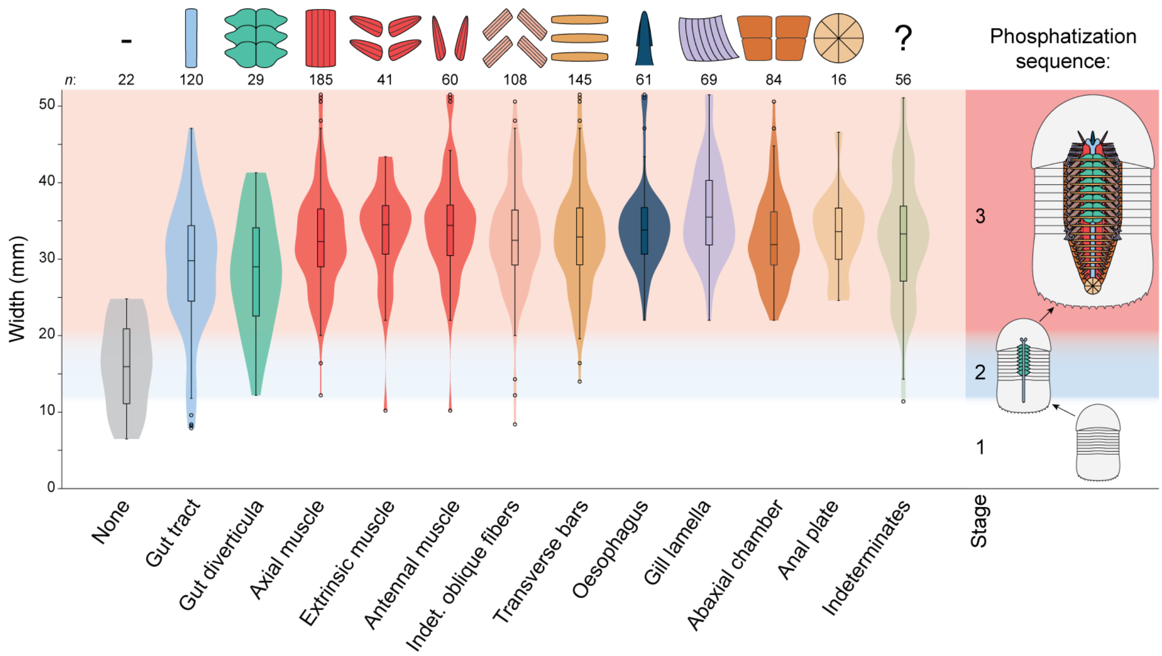

Figure 3.10. Ontogenetic distribution of phosphatized tissues in *Campanamuta mantonae*. Violin box plots show size distribution for each phosphatized tissue. Ontogeny shows a phosphatization sequence with three principal preservational stages: *stage 1* no phosphatization (widths <12 mm); *stage 2* only gut tracts and/or diverticula only (widths 12–20 mm); *stage 3* all tissues (widths >20 mm). Tissue distributions are plotted as colored kernel densities ('violins'; note that their widths are normalized separately for each tissue), size range (whiskers) excluding outliers (open circles), and 27–75 quartiles (boxes) with medians (horizontal line inside).

Interpretation

Phosphatization shows a bias against small specimens. This is likely due to an inability to create microenvironments as oxygen is constantly able to reach the decaying tissues and hence prevents formation of reducing conditions (Allison, 1988d). Other surmised explanations could be less phosphorus content, less total surface area for anaerobic bacterial metabolism, and perhaps also different ecologies (life habits and/or diets). Importantly, large size in itself does not guarantee more extensive phosphatization. Size does therefore not have a linear relationship with phosphatization, but rather a control on the minimum threshold for within-taxon phosphatization. Consequently, the size control strongly biases phosphatization against small taxa and early ontogenetic stages.

3.5.6 Dietary relationship to phosphatization

Results

Ingested organisms can be identified within the gut tracts, most commonly *Isoxys volucris* carapaces and less commonly other taxa (Peel, 2017b). The food content identified is occasionally enveloped by local phosphatized patches (Fig. 3.11). Those patches often comprise the only phosphatized regions within the specimens. For example, palaeoscolecids show a few of such patches (n=3) but phosphatization never extends to other adjacent tissues (e.g., muscle) or even full gut tracts. Panarthropod gut tracts often preserve as amorphous mineral masses (sometimes with preserved gut walls) that extend beyond phosphatized muscle areas (e.g., Fig. 3.6A1, A3; Fig. 3.8A). Their amorphous nature renders identification of ingested remains nearly impossible. Vetulicolians spp. show very low frequencies of phosphatized guts (4%, n=50).

Interpretation

Gut tracts appear to have an independent control on phosphatization to other tissues (Section 3.5.3). Mineralized patches enveloping *Isoxys volucris* imply that ingested food promotes phosphatization, at least in localized microenvironments, within the gut tract (Chatterton et al., 1994; Lerosey-Aubril et al., 2012). Therefore, diet and the nature and quality of the ingested tissues have some control on phosphatization of digestive tracts. It has not been demonstrated whether all the amorphous mineral masses represent gut contents, which may underestimate the potential importance of this control. Nonetheless, they do not always correlate with phosphatized muscle areas, and not all carnivorous taxa (e.g., palaeoscolecids) phosphatize muscle. On the other hand, vetulicolians, most likely phytoplankton herbivores (Chapter 5), show very low frequencies of gut tract phosphatization. Altogether, ingested tissue rich in phosphate (i.e., carnivory) may control phosphatization of gut tracts but are unlikely to control phosphatization beyond the gut.

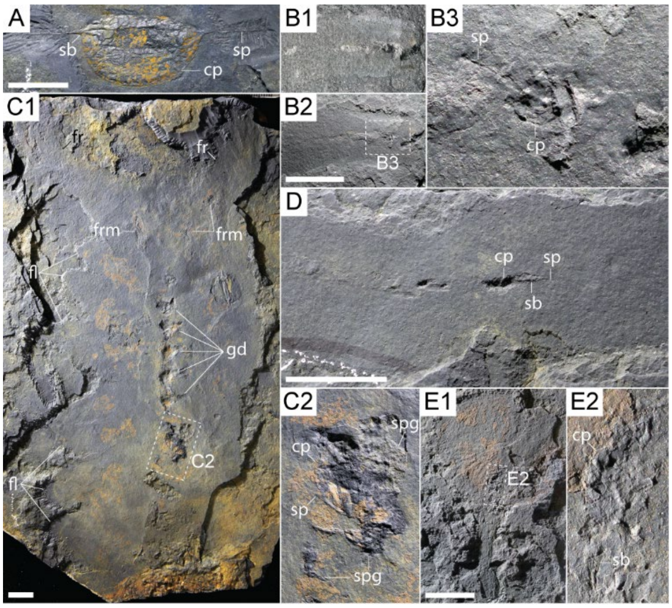

Figure 3.11. Localized gut tract phosphatization enveloping ingested *Isoxys volucris* specimens. Phosphatization does not extend significantly beyond the ingested specimens within the gut tracts. (A) Complete *Isoxys volucris* in matrix illustrating morphology. SP-2016-117. (B) Palaeoscolecid worm in high-angle (B1) and low-angle (B2) light with a phosphatized (black color) *Isoxys volucris* in the gut tract (dashed box; B3). SP-2016-1024. (C) *Pambdelurion whittingtoni* with phosphatized (black color) *Isoxys volucris* and sponges (dashed box; C2) in its guts. Other phosphatized tissues in the specimen are patchy frontal appendage muscle and gut diverticula. SP-2016-751. (D) Palaeoscolecid worm with phosphatized *Isoxys volucris* in its gut. SP-2016-1070. (E) *Pauloterminus spinodorsalis* (E1) with phosphatized *Isoxys volucris* (dashed box, E2). SP-2016-1147. Abbreviations: cp, carapace; fl, flap; fr, frontal appendage; frm, frontal appendage muscle; gd, gut diverticula; sb, spine base; sp, spine; spg, sponge. Scale bars are 1 cm.

3.6 Discussion

Our study provides the first attempt to use a quantitative dataset across multiple taxa to determine intrinsic controls on phosphatization. Such an approach is necessary to overcome the noise produced by an inherently complex, multifactorial process and begin to recognize general patterns. Our data shows that no single control alone explains the observed preservational patterns. Instead, phosphatization is a system of multiple interacting controls that can combine in several ways to cross the threshold for phosphatization of tissues.

Controls are not equally important and appear to have internal hierarchies. Here we briefly summarize our findings and compare them with proposed hypotheses. The principal controls are taxonomy, tissues, microenvironment, size, and diet.

Taxonomy is an overarching control on the distribution; it is the summation of complex interplays between other biological controls. The strong taxonomic bias herein is consistent with proposed biases from the fossil record (Wilby and Briggs, 1997; Klug et al., 2005; Wilson et al., 2016) and experiments (Hof and Briggs, 1997; Clements et al., 2017).

Tissues have been proposed to control phosphatization by providing suitable substrate (Wilby, 1993; McNamara et al., 2009), providing the necessary phosphorus content (Clements et al., 2022), and/or ability to develop proper microenvironments (Butterfield, 2002; Lerosey-Aubril et al., 2012). Patterns of tissue phosphatization herein follow general trends seen elsewhere: guts are the most commonly phosphatized tissue in panarthropods of other broadly comparable BST mudrocks with much lower phosphatization frequencies likely due to their internal microbially controlled microenvironment and high phosphorus contents (Butterfield, 2002; Lerosey-Aubril et al., 2012). Transverse bars may be internal apodemes (Budd, 2011); if so, they would likely be composed of collagen-rich connective tissues which would provide a competent substrate for phosphatization (Wilby, 1993; McNamara et al., 2009). Muscle is one of the most commonly phosphatized tissues likely due to its high contents of phosphorus-rich ATP and collagen (Clements et al., 2022). Gills relatively commonly phosphatize in arthropods (Wilby et al., 1996b), bivalves (Wilby and Whyte, 1995; Klug et al., 2005), and fish (Martill, 1988) but the underlying controls are uncertain. On the other hand, arthropod nervous systems are not observed to phosphatize. Instead, they are often preserved as reflective films (Chapter 4; Park et al., 2018), implying they are not removed by decay. Still, possible nervous systems are phosphatized in the gnathiferan stem-chaetognaths. They show huge, phosphatized structures interpreted as ventral nerve centers (Fig. 3.2). In this case, their preservation may relate to the extraordinary concentrations of phosphorus-rich cell nuclei in chaetognath nervous systems (Rieger et al., 2011; Vinther et al. in prep.). Tissues phosphatize inconsistently between taxa. Hence, tissues, each with distinct substrates and chemical compositions, may have a strong control on whether apatite can nucleate or not, but does not on its own explain the total distribution of phosphatization. Therefore, it should be cautioned to conclude on absence or presence of a tissue based on trends observed in one taxon and extrapolating to another.

Microenvironments are important controls on the internal distribution of phosphatized tissues as emphasized by regionalized and size-related data herein. They are not pervasive throughout the carcass (cf. Clements et al., 2022) but develop in specific regions of the carcass, for example the posterior-midregion in the case of the analyzed arthropod taxa herein (Fig. 3.4). This region does not correlate with the positions of gut diverticula, implying that decay-released phosphorus (Butterfield, 2002; Lerosey-Aubril et al., 2012) is not significant to their development. It is unclear whether supplies of gut microbes released during gut rupture (Butler et al., 2015) could explain such a consistent pattern. Instead, the position in the midregion may reflect the distance to the surrounding environment: the middle region of carcasses is least likely to be affected by diffusion of external chemistry (e.g., oxygen) that may prevent microenvironments from developing (Allison, 1988d).

Size is another important control: small taxa or juvenile specimens are strongly biased in Sirius Passet. Small specimens may be unable to develop the necessary microenvironments (cf. Allison, 1988d; see above). On the other end, comparatively large specimens may reach a certain size where phosphate ion concentration becomes too dilute or the resulting microenvironments could extend into the adjacent sediment that in turn releases chemicals that inhibits phosphatization (e.g., Clements et al., 2017).

Diet is primarily restricted to control only phosphatization of guts (cf. Chatterton et al., 1994; Lerosey-Aubril et al., 2012). It likely biases gut phosphatization towards carnivores that have more phosphorus-rich diets (Bradley, 1946) than herbivores. Obvious phosphatized gut contents do not control the systematic distribution of other phosphatized tissues within specimens.

The five presented principal controls (taxonomy, tissues, microenvironment, size, diet), albeit important, cannot account for all of the phosphatization heterogeneity in Sirius Passet. They are, for example, unable to explain the heterogeneous phosphatization between two similarly sized *Campanamuta* specimens in close contact (Fig. 3.6C). Therefore, there must be other currently unrecognized controls in play.

Decay can potentially impact the analysis by removing tissues prior to phosphatization. If decay was a major control on the distribution of phosphatized tissues, the resulting distribution would follow a predictable decay sequence, where decay-resistant recalcitrant tissues are more likely to remain than decay-prone labile tissues (e.g., Murdock et al., 2014). However, in Sirius Passet, decay is unlikely to be a major control on the distribution due to 1) the presence of taxa that only (or mostly) preserve carbonized labile tissues (e.g., *Buenaspis*, *Kleptothule*, and juvenile *Campanamuta* specimens), including the highly labile nervous tissues; and 2) the frequent co-occurrence of phosphatized and carbonized tissues within the same specimen (Fig. 3.3). Additionally, multivariate analyses (Figs 3.5 and 3.7) show no evidence of a specific decay-related sequence in the distribution of phosphatized tissues based on expected tissue lability.

Phosphatization of labile soft tissues biases the fossil record against small taxa and early ontogenetic stages. This will have implications for our reconstructions of ancient anatomy and evolution of taxa with ecological strategies favoring small sizes (Hanken and Wake, 1993). It may seem counterintuitive since phosphatization favors preservation of small microfossils in winnowed deposits (e.g., Dornbos, 2010). However, these two types of phosphatizing systems are different in terms of the source of phosphate and the depositional environment that produce them: phosphatization of labile soft tissues depends mainly on intrinsic biological controls and an internal source of phosphorus (Briggs, 2003) whereas phosphatized microfossils (e.g., embryos) depend more on depositional controls and an extrinsic source of phosphorus (Dornbos et al., 2006), although there specificity as to which organisms preserves (e.g., classic Orsten-type deposits is mainly ecdysozoan organisms with a chitinous cuticle that becomes impregnated, Maas et al., 2006).

Identification of certain tissues through the phosphatization window is unreliable for determining absence. Biases, such as preservation restricted to certain regions from microenvironmental controls, may lead to deduction of absence elsewhere. Apparent absences should, if possible, be verified by other preservational pathways (e.g., carbonaceous compressions) and be considered in relation to the functional role of the tissue. This potentially poses a limitation to phosphatization as a tool for e.g., phylogenetics, although it does provide a fidelity impossible to obtain by other pathways.

The present study provides a framework to understand the important biological controls for phosphatization based on a mudrock deposit. Hierarchy of controls likely varies between depositional environments. For example, phosphatization is well-known in limestone ‘plattenkalks’, such as Cerin (Wilby et al., 1996a), Osteno (Wilby and Briggs, 1997), and Solnhofen Plattenkalk (Briggs and Wilby, 1996), but their biases vary: crustaceans rarely phosphatize in Solnhofen (6%, n=865) but relatively frequently in Osteno (33%, n=155).

Likewise, BST deposits are not typical hot spots for diverse suites of phosphatized tissues. Burgess Shale commonly preserves digestive tracts and diverticula in arthropods (e.g., Butterfield, 2002) and priapulid-like worms such as *Ottoia* (Vannier, 2012). Apart from putative lateral patches along the trunk in *Anomalocaris canadensis* (Daley and Edgecombe, 2014), there are no muscle tissue preserved. Chengjiang often has digestive tracts preserved as 3D infills composed of aluminosilicates. While originally thought to reflect a deposit-feeding mode it has been argued that the aluminosilicates are weathering products from original phosphatisation (Butterfield, 2002). Apart from these, there is no muscle tissue preservation either, except some smooth muscle fibers associated with the digestive tract of some still undescribed vermiform taxa (J. Vinther pers comm. 2022). Emu Bay Shale is a significant BST locality which hosts more common occurrences of phosphatized digestive systems (e.g., Paterson et al., 2012), and, in particular, one problematic taxon, *Myoscolex* (Briggs and Nedin, 1997), is preserved almost entirely as an articulated assemblage of muscle tissue. This suggests that each deposit, even when highly comparable in depositional setting, exhibits separate extrinsic (depositional and environmental) controls on phosphatization, influencing magnitude of phosphatized taxa and their biases (i.e., the relative importance of biological controls). Extrinsic controls may include amount of pre-burial decay (Gabbott et al., 2021), abundance of microbial mats (Wilby et al., 1996), and external phosphorus availability (Sinha et al., 2021). However, extrinsic controls are outside the scope of this study, which is based on material from a single mudrock deposit. Since mudrocks are the most abundant sedimentary rocks, and host multiple important deposits with phosphatization throughout the Phanerozoic (e.g., Allison, 1988c, 1988b; Butterfield, 2002; Paterson et al., 2015), our results should be widely applicable.

The significance of external phosphorus availability in driving the extensive phosphatization in Sirius Passet can potentially be assessed by comparing calculated mass balance concentrations of phosphorus in contemporary arthropods to the phosphorus requirement of apatite in the mineralized tissues. If the arthropods can supply the necessary phosphorus internally, from its partially decaying tissues, it is less likely that external phosphorus is a primary control on phosphatization. However, it is difficult to estimate phosphate concentrations in three-dimensional apatite mineralizations that have subsequently undergone partial to extensive replacement and homogenization with sediment (Chapter 2). Alternatively, enrolled *Campanamuta* specimens may offer insights. Assuming enrolment forms an effective barrier that prevents external phosphorus from entering the carcass, phosphatization would rely almost entirely on internal phosphorus sourced from the carcass, as hypothesized for closed Jurassic bivalves in Portland Roach by Wilby and Whyte (1995). Given that enrolled specimens in Sirius Passet more frequently show extensive phosphatization (Fig. 3.9), it then suggests that internal phosphorus contents within *Campanamuta* were likely sufficient for phosphatization and therefore not a limiting factor. However, since their enrolment did likely not create a fully enclosed barrier, as the taxon's cephalic and pygidial morphology appears unable to interlock (Fig. 3.9B), there may have been at least some phosphorus diffusion between the carcass and sediment. Nevertheless, observations from enrolled specimens herein and from bivalves in Portland Roach (Wilby & Whyte, 1995) suggests that phosphorus contents within carcasses may be adequate for phosphatization, provided the appropriate microenvironment is present.

The present study also provides a framework for formulating hypotheses to be tested experimentally. By focusing here on a single locality, Sirius Passet, we have tried to eliminated as many variables as possible. Due to the large sample size, we have been able to delimit a complex plethora of controls on phosphatisation that are governed by the intrinsic conditions of the organism preserved. But several questions are left unanswered, most crucially the mechanisms of phosphatization and the roles of substrates, microbes and internal phosphorus (Wilby & Briggs, 1997). This is in part due to the altered, sometimes completely overprinted, nature of the tissues' original ultrastructures in Sirius Passet fossils. Such analyses require extensive scanning electron microscopy on, preferably, unaltered, and, most importantly, histologically well-defined tissues. It is also still uncertain why tissues in large taxa appear to phosphatize relatively less frequently. Most importantly, the data show that experiments are most informative when performed on several anatomically comparable taxa. A single taxon is unlikely to reflect the conditions needed to evaluate all general controls. Higher taxonomic groups may show different hierarchies of controls if their anatomy differs significantly.

3.7 Conclusion

Phosphatization of labile soft tissues is an inherently biased system composed of a plethora of biological controls. Its complexity is highlighted by the discrepancy in models and mechanisms proposed from either experiments and fossil assemblages. We show with a comprehensive quantitative dataset that noise, produced by the systems complexity, can be reduced to reveal generalized controls. Principal controls and their biases for soft-tissue preservation observed herein are taxonomy, tissue, microenvironments, size, and diet: Taxonomy is the summary of all controls and strongly biases certain taxa. Tissues control where phosphatization can initiate and hence biases against preservation of some tissues (e.g., nervous systems). Microenvironments control the distribution of phosphatization within a carcass with a strong bias against tissues outside these regions or in taxa unable to develop them. Size controls whether these microenvironments can form and bias against small taxa and early ontogenetic stages. Diet only controls the likelihood of preserving guts by phosphatisation and imposes limited bias beyond that. No control, albeit important, guarantees phosphatization. Instead, they constantly interact and exhibit a hierarchy that may vary between deposits. These principal controls cannot alone explain the total distribution of phosphatization, and other unrecognized controls must be present. Recognition of the controls presented herein is a step towards a better understanding of the bias imposed on biotas in deposits with phosphatization.

Chapter 4

Juvenile-rich fossil assemblages of *Isoxys* reveal high depositional frequencies in a Burgess Shale-type Lagerstätte

Author contributions

This chapter is written with intention to submit it for publication as soon as possible.

The research for this chapter was developed by me, Philip R. Wilby, and Jakob Vinther. I did the field sampling, all data collection and analyses, wrote the manuscript and produced figures with input from Philip R. Wilby and Jakob Vinther. Emily Mitchell adviced on the mixture analysis and R code, and gave input on that part of the methods section.

4.1 Abstract

'Burgess Shale-type' (BST) Lagerstätten are crucial windows into the Cambrian Explosion, providing an unprecedented view to both hard-bodied and soft-bodied diversity for a given time interval. However, oftentimes, such sites are filtered by transport and style of deposition which affects the preserved ecological information of the fossil assemblages. Ecological information is generally degraded by the combined effects of time-averaging (temporal bias), and translocation and/or mixing of discrete communities. Consequently, reconstruction of early ecosystem dynamics has concentrated on generalized large-scale macroecological trends, imposing a significant knowledge gap on within-community dynamics. Here, we integrate and analyze fossil assemblages at a microstratigraphic level in the lower Cambrian Sirius Passet Lagerstätte (North Greenland) revealing original population structures. Fossil assemblages predominantly occur on bedding planes between stacked, millimeter-thick homogenous and fine-grained beds. Since the fossil assemblages show high taphonomic qualities, with high proportions of articulation (69.7% for arthropods) and preserved labile soft tissues (e.g., muscles, nerves, and guts; 50% for arthropods, excluding *Isoxys volucris*), they are interpreted as representing a mixture of *in situ* benthic communities and nektonic components that passively died and settled from the water column with limited time-averaging. Bedding planes with high numbers of small individuals of the bivalved arthropod *Isoxys volucris* are on this basis interpreted as records of mass-spawns, comparable to seasonally controlled changes in the population structure of certain extant arthropods. The depositional setting that gave rise to the exceptional preservation with minimal temporal bias in Sirius Passet is unique amongst Burgess Shale-type Lagerstätten as a high-frequency (perhaps multiple depositional events per year) input of low-concentration muddy gravity flows possibly hyperpycnal. BST Lagerstätten each have substantially different temporal biases that present different opportunities to understand early animal ecosystems.

4.2 Introduction

Animal evolution is shaped by ecological processes, as exemplified by the Cambrian radiation where the rise of carnivory accelerated the emergence of diverse animal groups and modern-looking ecosystems (Dunne et al., 2008; Sperling et al., 2013). Much of our understanding of early animal ecology comes from a few Cambrian BST Lagerstätte, where exceptional preservation conserves soft tissues as carbonaceous compressions (Gaines, 2014). However, the information that these windows provide is distorted by processes of decay and preservation (Saleh et al., 2020b), community mixing (Bath Enright et al., 2021) and time-averaging (Caron and Jackson, 2006; Zhao et al., 2009). While the detrimental effects of taphonomic biases and the degree of allochthonous taxonomic input have received considerable attention, the impacts of time-averaging on paleoecological signals (i.e., their temporal biases) are less well resolved (cf. Kidwell and Bosence, 1991).

Time-averaging is the mixing into a single fossil assemblage of temporally successive organismal populations that did not necessarily live together at the same time (Staff et al., 1986; Fürsich and Aberhan, 1990; Kidwell and Bosence, 1991). Mixing can occur from reworking of previously buried fossils (Fürsich, 1978; Kidwell and Bosence, 1991) and condensation (Fürsich and Aberhan, 1990). Previous work has focused on shelly assemblages, and these can be divided into four categories depending on the magnitude of averaging (Kidwell and Bosence, 1991): census assemblages, within-habitat assemblages, environmentally condensed assemblages, and biostratigraphically condensed assemblages. The first three categories operate on timescales that are relevant to the decay-susceptible, soft-bodied, organisms that dominate BST Lagerstätten (Kidwell and Bosence, 1991, their figure 9). *Census assemblages* comprise recently deceased (but taphonomically filtered) individuals from a local community that have collected over intervals of days to years. These are of particular interest to paleoecologists because of their potential to record the dynamics of populations and communities, as well as to preserve true ecological processes (Haug et al., 2013). *Within-habitat assemblages* are mixes of accumulated death assemblages in a relatively stable environment. They are useful for determining the average community structure of a given environment and have a temporal span of seasons (i.e., intra-annual) to millennia (Caron and Jackson, 2008; Dunne et al., 2008; Nanglu et al., 2020). *Environmentally condensed assemblages* comprise mixes of taxa from substantially different environments (i.e., sedimentological facies) which likely never spatially co-existed; they commonly exceed the temporal span of within-habitat assemblages.

Time-averaging imposes temporal bias: a critical upper limit on the temporal resolution of BST biotas and on the paleoecological dynamics that can be determined from them (Caron and Jackson, 2006; Dunne et al., 2008; Nanglu et al., 2020). Fossiliferous event beds preserve hybrid assemblages (cf. Kidwell, 1998) of 'fresh' census components and decayed within-habitat components (Caron and Jackson, 2006; Zhao et al., 2009) of mixed/filtered environmentally condensed communities, (Bath Enright et al., 2021; Saleh et al., 2021c).

In Burgess Shale, these beds are scant and punctuated by thick intervals of poorly fossiliferous event beds (Caron and Jackson, 2008; Gabbott et al., 2008; Nanglu et al., 2020). In Chengjiang, they are separated by background sediment derived from hemipelagic fallout and dilute nepheloid plumes (Zhao et al., 2009; MacKenzie et al., 2015) (Fig. 4.1). The fossils in the latter type at Chengjiang are typically poorly preserved (Zhao et al., 2009), suggesting that they predominantly represent accumulated, within-habitat assemblages with significant temporal reworking and near-surface decay. Most BST Lagerstätte, therefore, preserves weak ecological signals where evidence of interactions is mostly confined to gut contents (e.g., Vannier, 2012) and rare slabs retaining direct associations (e.g., Hou et al., 2009; Nanglu and Caron, 2021; Yang et al., 2021b). Hints of the dynamic communities that surely existed are so far offered only by rare uncontextualized mass assemblages (e.g., Haug et al., 2013; Vannier and Martin, 2017), leaving the temporal dynamics of population and aspects of community structures poorly determined for Cambrian ecosystems.

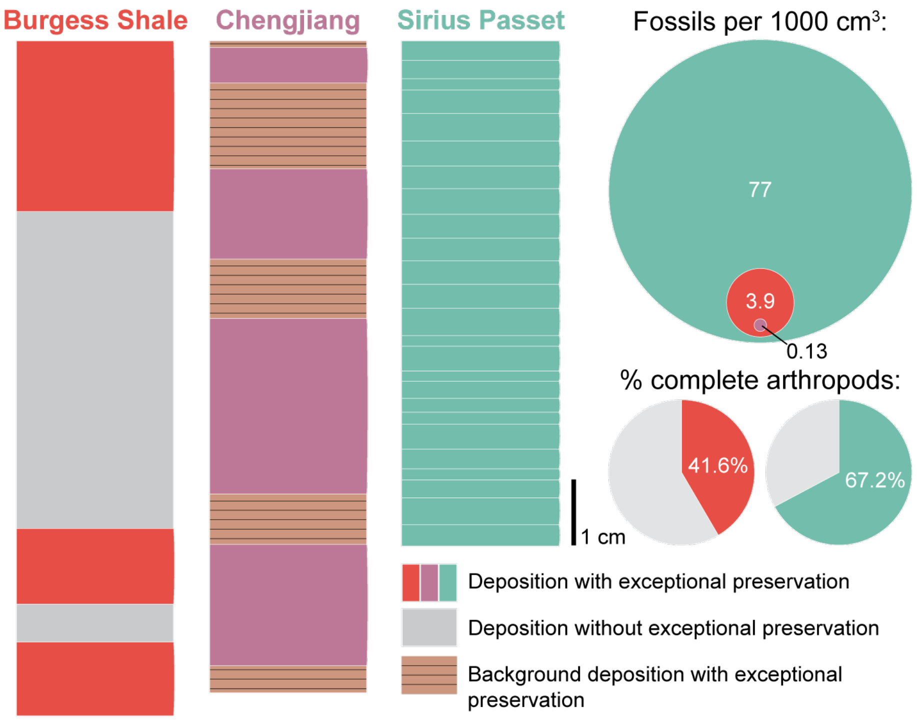

Figure 4.1. Comparative distributions and densities of exceptionally preserved fossils in Burgess Shale (Walcott Quarry section, Canada), Chengjiang (Mafang section, China) and Sirius Passet (North Greenland). Sirius Passet is an

uninterrupted sequence of beds with highly dense exceptionally preserved fossil assemblages with a high degree of complete specimens. Data for Burgess Shale and Chengjiang based on Caron & Jackson (2006), Zhao et al. (2009) and, for their standardized fossil abundances, Caron et al. (2014).

The early Cambrian Sirius Passet Lagerstätte, North Greenland (Conway Morris et al., 1987; Harper et al., 2019), differs from other BST Lagerstätten by comprising a stacked sequence of highly fossiliferous beds largely without intervening fossil-poor beds (Fig. 4.1) (Ineson and Peel, 2011). The high proportion of articulated specimens (see Babcock and Peel, 2007 and Hammarlund et al., 2018 for the trilobite *Buenellus higginsi*) (Fig. 4.1) and consistently frequent preservation of labile soft tissues, such as musculature (Budd, 1998a, 2011; Conway Morris and Peel, 2008; Stein, 2010; Young and Vinther, 2016) and nervous systems (Park et al., 2018), indicate very limited taphonomic filtering of the original biota (Fig. 4.2).

The biota includes a diverse range of benthic and nektobenthic/pelagic organisms (Fig. 4.2K–S) but is numerically dominated by the bivalved arthropod *Isoxys volucris* (66.5% of all catalogued fossils herein; Data Table E4.1). Here, we examine the degree of time-averaging in the Sirius Passet Lagerstätte using a microstratigraphical approach that combines bed-by-bed variations in the population structure of *Isoxys volucris* with sedimentological, ichnological and taphonomic data. We use this combination to show that the BST Lagerstätte captures signatures of seasonal variations in population structure comparable to those of modern ecological equivalents. Thus, Sirius Passet provides a unique opportunity to understand Cambrian population dynamics at a biologically meaningful resolution.

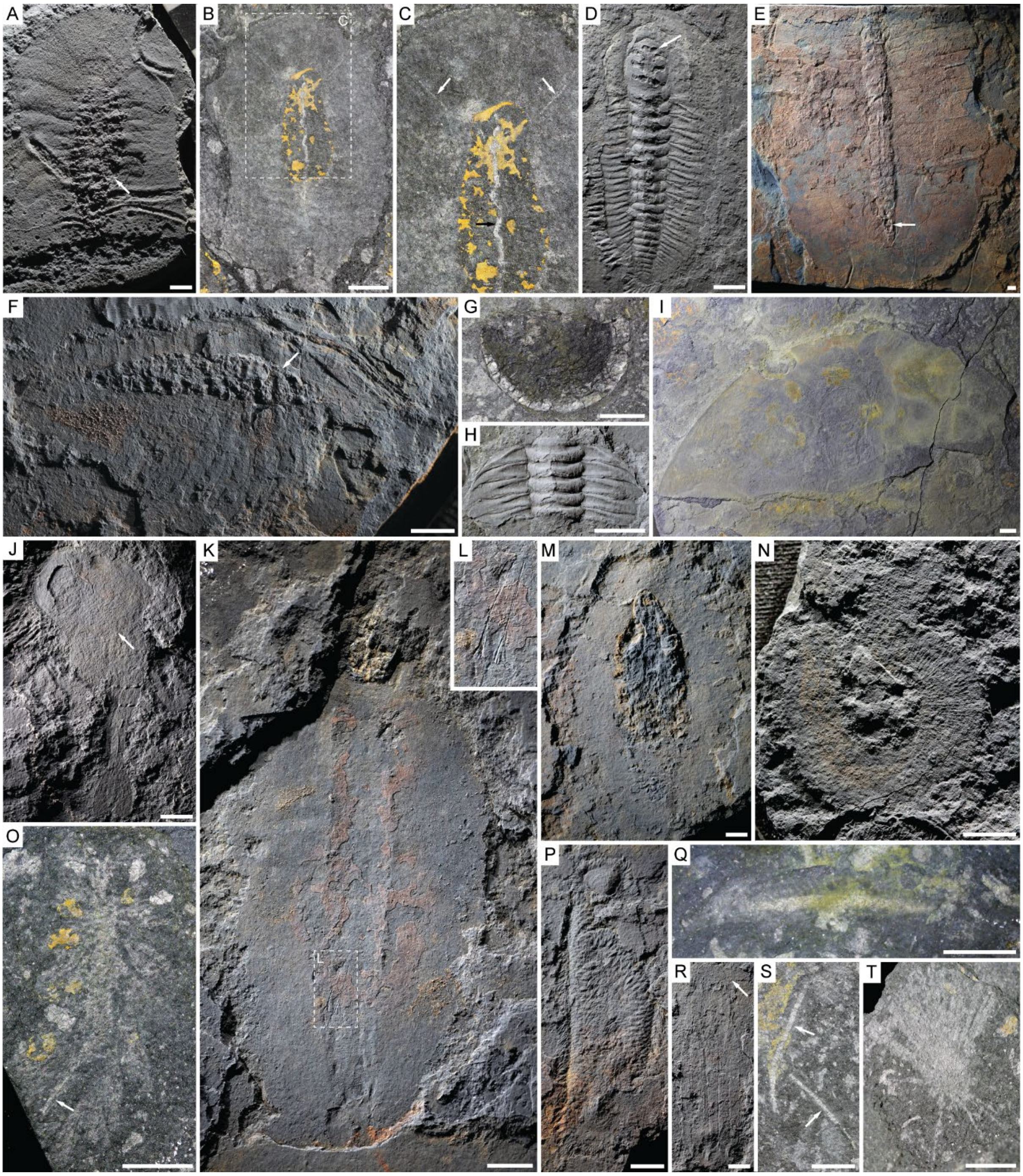

Figure 4.2. Diversity and taphonomy of fossils in investigated blocks, Sirius Passet. A–G Phosphatized and carbonized labile soft tissues (arrowed) in arthropods. (A) *Campanamuta mantonae* with phosphatized muscle (arrow). Legs are visible as shallow depressions. Block A, Bed 24. (B) *Campanamuta mantonae* with carbonized antennal nerves and gut tract (dashed box), partially coated by iron oxide axially (yellow color), photographed under water. Block B, Bed 9. (C) Close-up of B showing carbonized antennal nerves (white arrows) and gut tract (black arrow). (D) *Buenellus higginsi* with phosphatized cephalic gut diverticula (white arrow) and tract (black arrow). Block B, Bed 2. (E) *Arthroaspis bergstroemi* with phosphatized gut tract (arrow), extensively encrusted by iron oxide (rusty red color). Block A, Bed 17. (F) *Kiisortoqia soperi* preserved in lateral aspect with legs (bottom), phosphatized muscle (arrow) and gut diverticula (in below extension of muscle). Block A, Bed 27. (G) *Isoxys volucris* in lateral aspect with phosphatized indeterminate tissue (black color),

photographed under water. Block B, Bed 20. (H–J) Examples of fragmentary arthropods. (H) Isolated section of five thoracic *B. higginsi* segments. Block A, Bed 19. (I) Isolated *Arthroaspis bergstroemi* cephalon, photographed under water. Block B, Bed 2. (J) *Pauloterminus spinodorsalis* with visible (but effaced) mass of appendages and dislocated carapace (arrow). (K–T) Examples of fossil diversity. (K) 'Gilled lobopod' *Kerygmachela kierkegaardi* with phosphatized pharynx and crumpled *Isoxys volucris* in axial region (dashed box), possibly ingested. Block A, Bed 27. (L) Close-up of K showing *Isoxys volucris*. (M) 'Gilled lobopod' *Pambdelurion whittingtoni* with phosphatized muscle. Block A, Bed 27. (N) Partially enrolled palaeoscolecid worm *Xystoscolex boreogyrus*. Block B, Bed 6. (O) Indeterminate polychaete worm with chaetae flanking a medial body with carbonized gut tract (arrow), photographed under water. Block B, Bed 20. (P) Mollusk *Halkieria evangelista*, fully articulated and preserved in relatively high relief. Block A, Bed 5. (Q) Possible chordate preserving a longitudinal gut tract and at least 10 vertical myomere in the mid-region, partially obscured by weathering (yellow-green color), photographed under water. Block A, Bed 29. (R) Stem-loriciferan *Sirilorica carlsbergi* lorica preserved as carbonaceous compression in relief with smooth introvert (arrow). Block A, Bed 9. (S) Two common chaetognath-like worms most readily visible from their carbonized gut tracts (arrows), photographed under water. Block B, Bed 8. (T) Sponge *Choia* cf. *carteri* with spicules preserved as reflective films with relief, photographed under water. Block B, Bed 16. Scale bars are 5 mm.

4.3 Geological setting

The Sirius Passet Lagerstätte is part of the Buen Formation of Peary Land, North Greenland (Conway Morris et al., 1987; Ineson and Peel, 2011; Harper et al., 2019). The main locality exposes an 8 m thick succession of dark grey, fissile, organic debris-rich, siliceous, mudrocks, overturned (Hammarlund et al., 2018; but see Ineson and Peel, 2011 for a different view) and metamorphosed to greenschist-grade facies during the late Devonian to early Carboniferous Ellesmerian Orogeny (Ineson and Peel, 2011; Topper et al., 2018). It yields a diverse and exceptionally well-preserved lower Cambrian (Series 2, Stage 3) biota (Blaker, 1988; Babcock and Peel, 2007), including the mollusc *Halkieria* (Conway Morris and Peel, 1995; Vinther and Nielsen, 2005), 'gilled' lobopods (Budd, 1993, 1998a), suspension-feeding anomalocarids (Vinther et al., 2014), and large stem-loriciferans (Peel et al., 2013). The mudrocks are mostly very thinly bedded (2-5 mm) and, notably, host high densities of articulated fossils and aggregates of indeterminate organic debris (typically <1 to 20 mm) (Fig. 4.3). Most fossils occur on bedding-plane surfaces, rather than within the beds, and they may reach densities of up to 0.12 specimens/cm^2 (Data Table E4.1). They were originally preserved as carbonaceous films (Topper et al., 2018) with accessory phosphatized and pyritized labile soft tissues, subsequently altered by metamorphic overprints (Chapter 2). Arthropods, such as *Isoxys volucris*, may retain some relief. Bioturbation occurs in many, but not all, intervals as horizontal burrows that transect the fossils (Mángano et al., 2012), although thoroughly bioturbated intervals up to 45 cm thick and without fossils occur at several levels (Ineson and Peel, 2011). The depositional environment is interpreted as having been below storm-wave base on a low-gradient shelf-slope break with recurring burial by dilute, storm-generated mud and silt gravity flows (Harper et al., 2019) although Ineson and Peel (2011) originally considered the depositional setting to be adjacent to a steep carbonate platform.

4.4 Material and methods

Different primary (i.e. depositional) and secondary (i.e. preservational) processes can produce similar size-frequency patterns in fossil assemblages (Cummins et al., 1986; Kidwell and Bosence, 1991) and integrated approaches are required to distinguish between them (Olszewski and West, 1997). We systematically consider depositional environment, taphonomy (decay) and size frequency distributions of fossils in two representative blocks (A and B) of sediment from Sirius Passet that were collected *in situ* during the 2018 field expedition. Their exceptionally high fossil densities (averaging 29.1 and 35.2 specimens/1000 cm^2, respectively; Data Table E4.1) enable quantification of bed-by-bed fossil variability from relatively small surface areas (Fig. 4.3). Block A is 14 cm thick and contains 32 discrete beds, and Block B is 7.7 cm thick and contains 20 beds; these have a total surface area of 30658 cm^2 and 24369 cm^2, respectively (Data Table E4.1). Blocks A and B encapsulate nuances of the dominant depositional environment and the one in which exceptional preservation occurs in Sirius Passet.

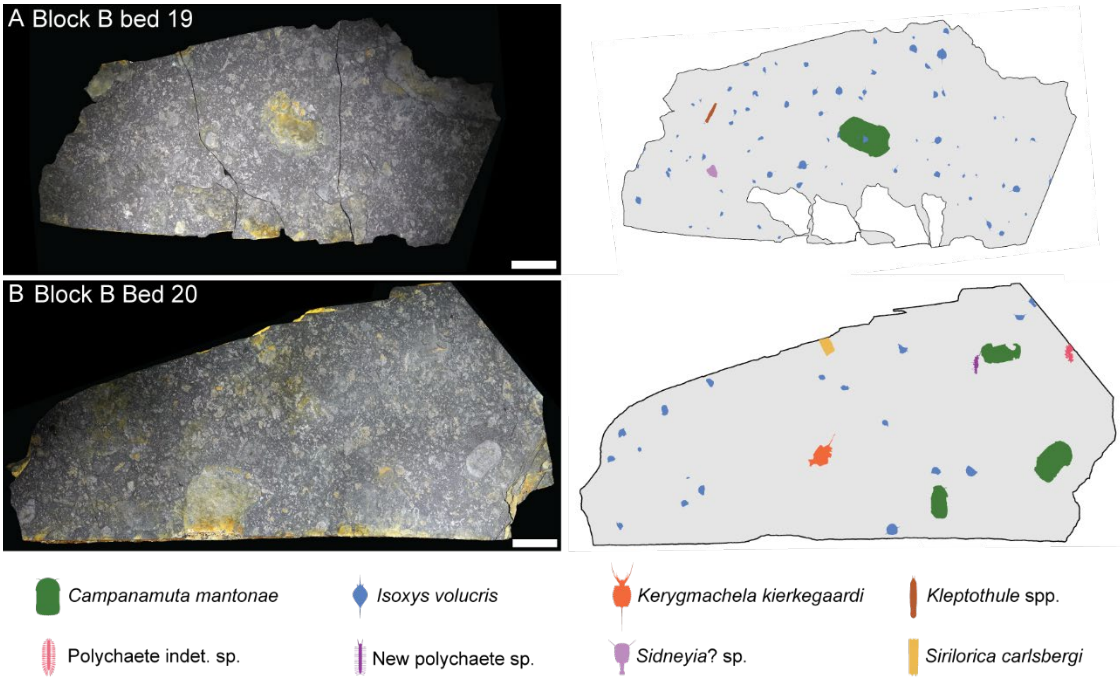

Figure 4.3. Comparison of fossil density on beds 19 and 20 of Block B. Identifiable fossils (color-coded) are distinguished from the high-density background mass of structureless organic debris (lustrous silver in images). (A) Bedding plane hosting a high-density, juvenile rich, *Isoxys volucris* assemblage. (B) Bedding plane hosting a more typical *Isoxys volucris* density. Density of structureless organic debris does not increase with *Isoxys volucris*. Note that not all juvenile fossils could be drawn in A. Scale bars are 5 cm.

4.4.1 Material and data collection

Block A contains high-diversity assemblages consisting of both benthic and nektonic organisms (Fig. 4.4; Data Table E4.2), on some bedding planes associated with horizontal trace fossils (Fig. 4.2A,F; Supplementary Material). Many of the bedding planes host carbonaceous patches on the order of several decimeters in diameter with smooth surface textures generally interpreted as microbial/algal mats (Harper et al., 2019).

Block B contains a broadly similar, but less diverse, biota, lacks bioturbation and contains notably high numbers of *Isoxys volucris* (79.3% of all specimens in Block B vs 53.5% in Block A; Fig. 4.4).

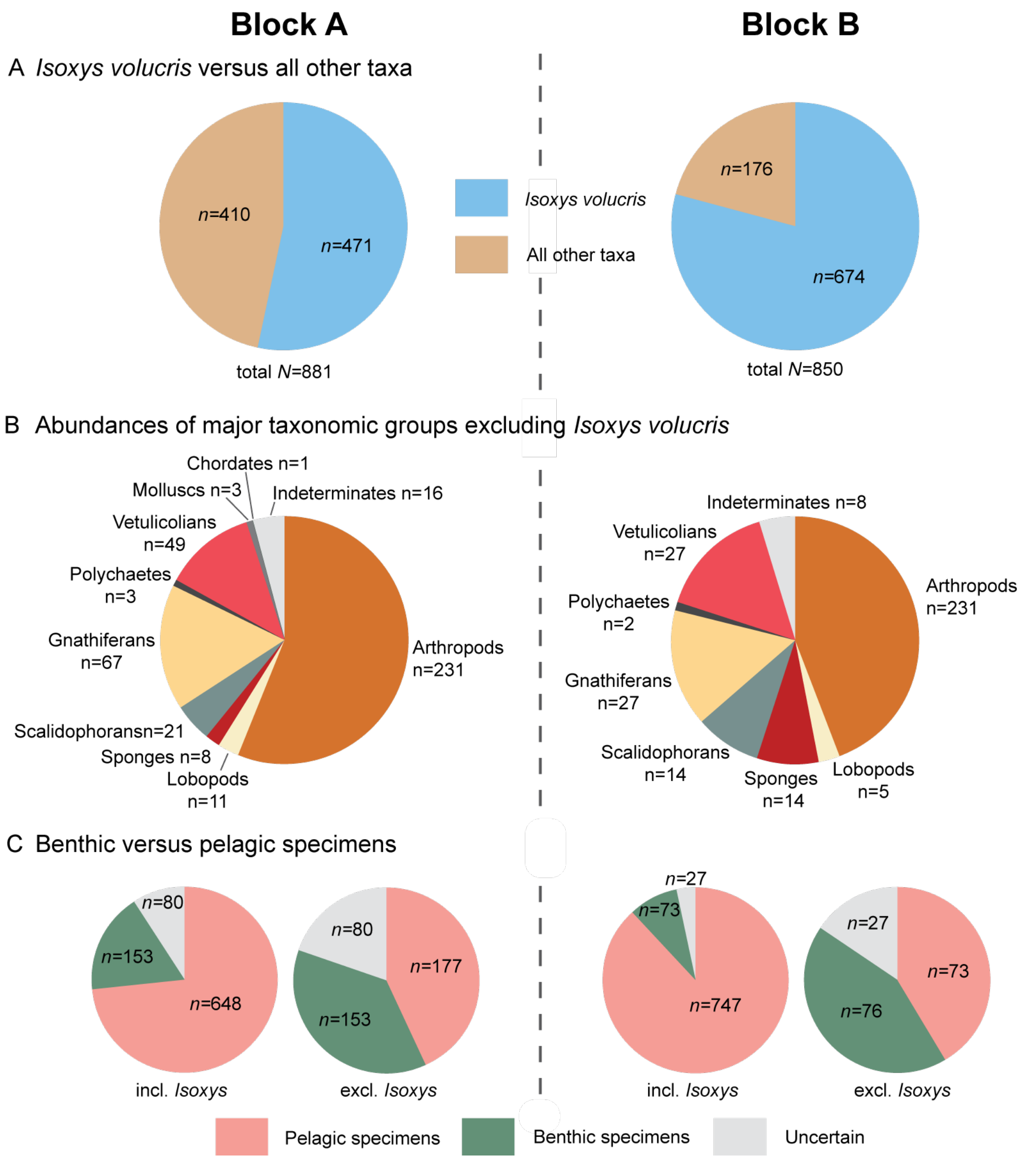

Figure 4.4. Comparisons of abundances and diversity between within-habitat communities in Block A (left) and Block B (right) in Sirius Passet. (A) *Isoxys volucris* abundances relative to all other encountered specimens. *Isoxys volucris* comprise a much larger proportion of the total community in Block B than in Block A. (B) Diversity of higher taxonomic groups and their abundances (excluding *Isoxys volucris*). Patterns are broadly comparable except for a lower overall diversity and relative arthropod abundance in Block B. (C) Benthic versus pelagic life habits of the preserved communities showing strikingly similar relative distributions when *Isoxys volucris* is excluded: Block A shows slightly higher proportions of pelagic taxa (benthic taxa: 37%; pelagic taxa: 43%), while Block B shows almost equal proportions (benthic taxa: 42%; pelagic taxa: 41%). Benthic taxa are *Halkieria, Arthroaspis bergstroemi*, *Buenellus higginsi*, *Buenaspis forteyi*, *Campanamuta mantonae*, *Molaria steini*, *Sidneyia*? sp., Lobopoda sp., *Pambdelurion whittingtoni*, polychaetes, scalidophorans, and sponges. Pelagic (or predominantly nektonic) taxa are *Isoxys volucris*, *Kiisortoqia soperi*, *Kleptothule rasmusseni*, *Kleptothule*? sp. nov., *Pauloterminus spinodorsalis*, *Siriocaris trollae*, *Kerygmachela kierkegaardi*, gnathiferan stem-chaetognaths, vetulicolians, and chordates.

Fossil data were collected by splitting the blocks bed-by-bed (*n*=32, Block A; *n*=20, Block B), exposing, on average, 958 cm^2 (Block A) and 1218 cm^2 (Block B) per parting surface (Data Table E4.1). Each surface was washed, photographed and stitched in Adobe Photoshop CS6. Surface area was calculated in ImageJ 1.48r software (Schneider et al., 2012) using the wand tracing tool. Every fossil on the parts and counterparts of each surface was identified (where possible) to species level (Data Table E4.2), and the side with the most complete record of each taxon exposed was used in the following analyses (e.g., part/counterpart records—Block B, Bed 19: 118 vs 100 counts; Block B, Bed 4: 88 vs 74 counts).

Parting surfaces vary in smoothness. Block B generally exhibit smoother parting surfaces than Block A. Fossils predominantly occur on parting surfaces, interpreted as the bedding plane, with subordinate input from occasionally few, very closely spaced, laminae (0.5-2 mm apart) (Fig. 4.5). Some fossils are clearly entombed within intrabeds evident as emerging from slanting splits (Fig. 4.6) with low overall fossil content and organic debris.

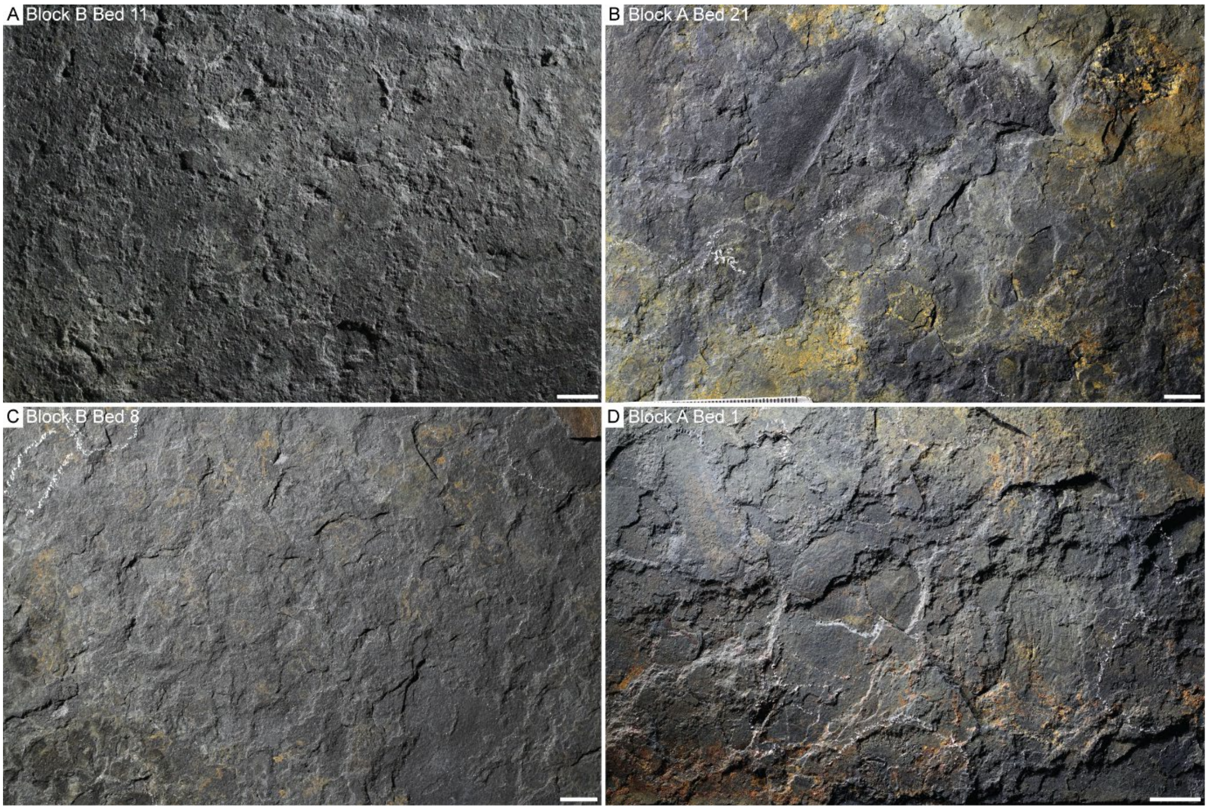

Figure 4.5. Variable bedding-plane surface irregularity and its effects on observed fossil assemblage. (A) Smooth parting, largely exposing a single lamina (the bedding plane); small windows to other levels (stratigraphically up to 0.6 mm above/beneath) are restricted to obvious hollows and ridges and the fossils in these areas are easily distinguished. (B) Moderately smooth parting exposing more laminae than the bedding plane, but none more than 0.4 mm above/beneath it. Most fossils occur on the bedding plane; a few fossils crosscut the exposed laminae at low angles indicating preservation within the beds. (C) Moderately rough parting exposing several laminae, the highest/lowest of which exposes several large

carbonaceous patches and fossils up to 0.6 mm above/below. (D) Rough parting exposing fossils at several levels, mostly <0.6 mm stratigraphically above/below the bedding plane but locally up to 2 mm. Still, most of the fossils (e.g., *Isoxys volucris*) occur on the bedding plane. White lines mark out fossils. Scale bars are 1 cm.

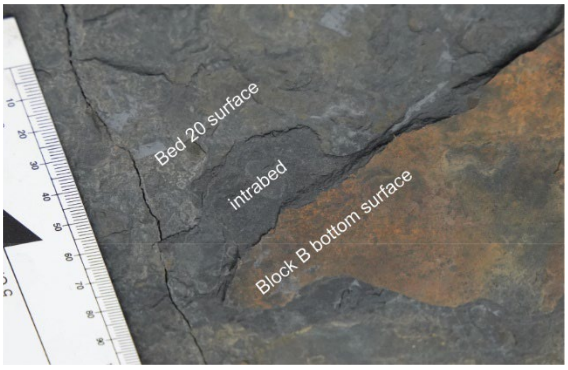

Figure 4.6. Oblique view through Bed 20, top to the right. Note the darker and slightly coarser appearance of the slanting intrabed sediment, which also contains less fossil material (lustrous silver). The base of the block is stained with iron oxides, as is the case with many partings.

Individual fossils were photographed under either low-angle lighting, coated with magnesium, or high-angle lighting, under water. The former is ideal for highlighting relief, such as sclerotized external morphology and phosphatized labile soft tissues, while the latter highlights carbonaceous structures, such as carbonized guts or nerves.

4.4.2 Taphonomic analyses

Fossils were assigned a taphonomic index based on their degree of articulation and the presence/absence of preserved internal labile soft tissues (here guts, musculature, and nervous systems; Fig. 4.2A–J) (Data Table E4.3). Inconclusive preservational states (e.g., due to partial concealment by sediment) were excluded from the analysis. Emphasis was placed on arthropods to allow comparison with published data from the Burgess Shale (see Fig. 4.1), though most organisms are generally well preserved (Fig. 4.2K–S).

Assessment of articulation was limited to the dorsal exoskeleton since legs are often concealed by the tergal skeleton Sirius Passet fossils (Fig. 4.2A). Three states are used (except for *Isoxys volucris*, see below): complete, dislocated, and disarticulated: *complete* are exoskeletons without significant disturbances; *dislocated* are ruptured or displaced elements that are otherwise still attached; *disarticulated* are fully dismembered or isolated elements.

The taphonomic index for *Isoxys volucris* (Fig. 4.7) is based on articulation of valves along the hinge-line only (Fig. 4.7E), since spines are commonly dislocated or lost even when delicate morphology is preserved (see e.g., Stein et al., 2010). Some articulated shields have been distorted by crumpling but often still articulated along the supposedly weak hinge line with unbroken but dislocated spines (Fig. 4.7F–H). This suggests that such specimens are not the result of decay and/or *post-mortem* transport (Allison, 1986; Briggs and Kear, 1994). Instead, they are interpreted tentatively as specimens that have been ingested and passed through a narrow gut (Fig. 4.2K).

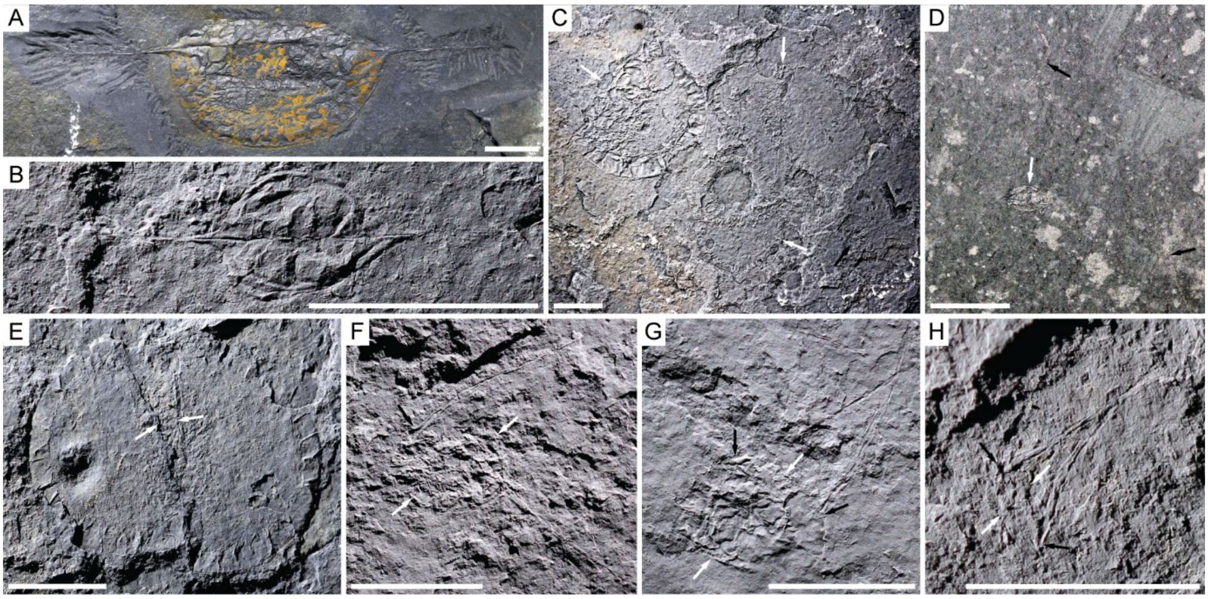

Figure 4.7. Representative taphomorphs of *Isoxys volucris*. (A) Large specimen in oblique aspect photographed under water. Specimen not from this material. (B) Small specimen in open butterfly state, exposing dorsal hinge line. Block B, Bed 19. (C, D). Clusters of specimens (arrowed) preserved on single laminae. (C) Four specimens, three comparatively large (white arrows) and one small (black arrow). Block A, Bed 1. (D) Three small specimens (arrows) photographed under water, two of them effaced (black arrows) and most readily visible from their higher-relief spines. Block B, Bed 19. (E) Specimen preserved in dorsal aspect with its valves disarticulated along the hinge line (arrows) but still closely associated, suggesting limited post-mortem transport. Block A, Bed 20. (F–H) Progressive crumpling of articulated specimens. All from Block B, Bed 19. (F) Minor crumpling of carapace (white arrows) and dislocation of only one spine (black arrow). (G) Moderate crumpling of carapace (white arrows) and dislocation of both spines (black arrows). (H) High degree of crumpling: now the carapace is almost indistinguishable (white arrows) but dislocated spines (black arrows) remain attached. Scale bars are 5 mm.

4.4.3 Sedimentological analyses

The sedimentological analysis was based on polished surfaces and vertical continuous sequences of polished thin sections from each block. Sedimentary features, such as planar lamination, grading, etc., were subtle microstructures only visible from thin sections. They could not be augmented by scanning electron microscopy and mineral mapping using the Mineralogic software, possibly due to their very fine grain size and/or metamorphic overprint. Macroscopic features recorded during splitting were very scarce and mostly limited to putative microbial mats. Bedding thicknesses were measured from the main parting surface.

Trace fossil density can, if present, reflect the sedimentation rate (Fürsich, 1978) and their distribution on bedding planes were recorded during splitting using a newly developed index (Supplementary Material).

4.4.4 Size frequencies and size class modelling

Size-frequency distributions can be used to infer time-averaging and transportation of assemblages (Fagerstrom, 1964; Olszewski and West, 1997). For *Isoxys volucris,* they are based on the maximum length of dorsal hinge line, excluding the spine. In total, 674 individuals were measured, representing 59% of the total number of *Isoxys volucris* specimens identified in both blocks (Data Table E4.4). Histograms and kernel densities were produced with PAST 4.10 (Hammer et al., 2001).

Size classes for *Isoxys volucris* size distributions in Block B were defined using the mclust R package (Scrucca et al., 2016) that uses Gaussian finite mixture models to find the most likely number of cohorts (assumed to be normally distributed) within the size-frequency dataset (e.g., Mitchell et al., 2015). The different number of cohorts within the population is assessed using BIC (Wit et al., 2012), for both cohorts with equal standard deviations and unequal standard deviations. Mixture models were both run for the total Block B dataset and then separately for each bed to compare consistency of cohorts. Robustness of modelled cohorts was bootstrapped by modelling the number of cohorts on simulated datasets resampled under three different assumptions: A) the dataset is composed of a single pre-classified cohorts (corresponding to the actual total dataset); B) the dataset is composed of two pre-classified cohorts (corresponding to size classes I and II) with resampling reflecting their observed distribution within the total Block B dataset; and C) the dataset is composed of two cohorts (size classes I and II) with resamples reflecting their actual observed distribution within each bed. In each case, the resampled *n* would equal that of the bed. The code is available in Appendix A1.

4.5 Results and interpretation

4.5.1 Arthropod taphonomy

Most arthropods in the Lagerstätte are articulated (Fig. 4.1), especially non-isoxyid arthropods where complete specimens in Block A constitute 89% of the total (*n*=149) and in Block B 81% of the total (*n*=53; Data Table E4.3). Disarticulated elements in a few cases occur together (Fig. 4.7E) and belong to taxa otherwise found articulated in the same blocks, except for a single *Arthroaspis* head shield in Block B (Fig 4.2I; Data Table E4.3). Labile soft tissues occur abundantly in taxa with both inferred benthic (4 out of 6: 67%) and pelagic (6 out of 7: 86%) life habits (Data Table E4.3). They occur in 50% (*n*=101) of all specimens (excluding *Isoxys volucris*; *n*=202) and are generally more prevalent in Block B (35 out of 53 specimens: 66%) than Block A (66 out of 149 specimens: 44%) (Data Table E4.3). Together, they are interpreted as minimally decayed autochthonous or, for pelagic taxa, parautochthonous assemblages without spatial mixing or filtration (cf. Saleh et al., 2021c).

4.5.2 Sedimentological context

The Sirius Passet protolith was a silty mudstone consisting of a mixture of "clays", quartz, K-feldspar and accessory heavy detritals, subsequently metamorphosed to a chlorite+muscovite+quartz framework with euhedral chloritoid and pyrite porphyroblasts (Chapter 2). At hand, planar (but sometimes rough) bedding-plane surfaces are separated by 2–5 mm thick, coarser-looking, unevenly splitting intrabed matrix with comparatively low contents of fossils and organic debris (Fig. 4.3). In vertical section, the bedding planes are apparent as partings (Fig. 4.8). Micro-sedimentary structures are scant and, in both blocks, limited to subtle planar lamination and normal and reverse grading (Fig. 4.8; Fig. 4.9); a single possible minor erosion scour was additionally observed in Block A (Fig. 4.9E). Both blocks lack structures suggestive of traction, such as cross-lamination and floating grains (Gabbott et al., 2008; Fu et al., 2019; Bath Enright et al., 2021), or consistent evidence of erosive bases (Gabbott et al., 2008; Bath Enright et al., 2021). Similarly, they lack dark laminated interbeds, suggesting an absence of intervening finer-grained background rain-out (cf. Zhao et al., 2009). Together, this suggests that the Sirius Passet Lagerstätte was deposited in a stable, very low energy environment that received high frequency, low magnitude inputs of fine-grained sediment and experienced negligible reworking. We interpret it as a distal prodelta environment below storm wave base influenced by constantly pulsating waxing and waning flows too dilute for significant transport of imported elements. Flows possibly derive from river discharge-driven hyperpycnal plumes due to the diffuse boundaries between continuously stacked beds that show both normal and reverse grading (Bhattacharya and MacEachern, 2009). The environment must have been highly productive to accumulate the ubiquitous organic debris.

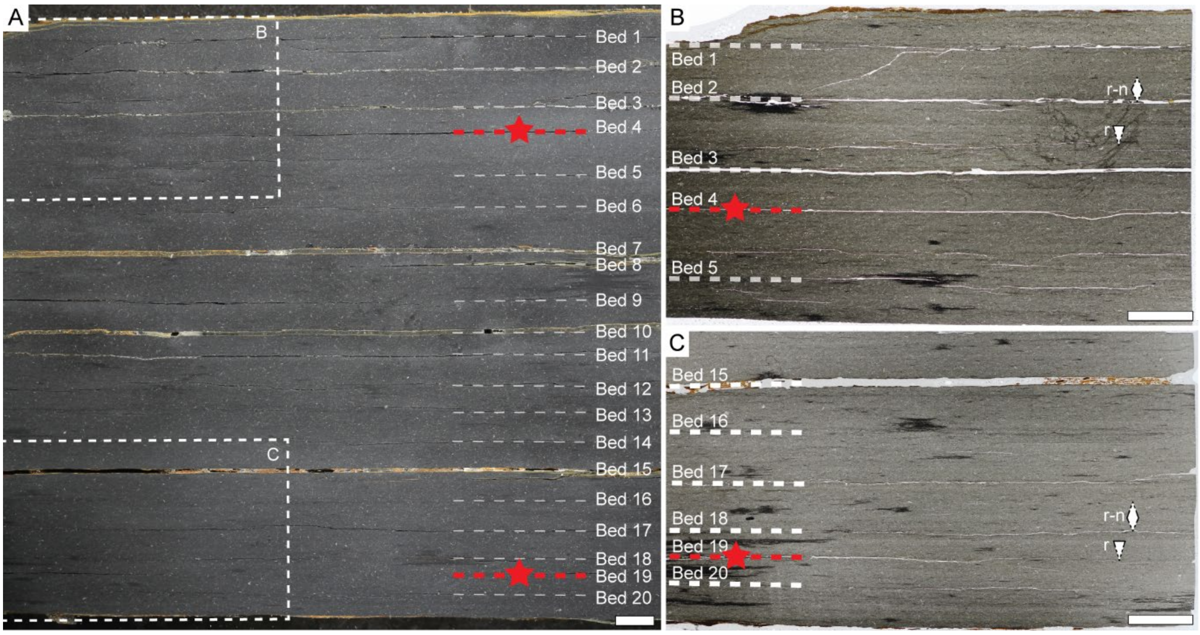

Figure 4.8. Investigated bedding planes and sedimentological structures of Block B. (A) Polished slab photographed under water showing a largely homogenous matrix. Bedding planes are visible as partings, some stained with iron oxide. Note that not all bedding planes were split during sampling; those omitted were often too thin or close to parted surfaces. (B, C) Thin sections of dashed areas shown in (A). The juvenile-rich mass-assemblage beds (4 and 19, red stars) are indistinguishable from other beds. Weak reverse (r) and reverse-to-normal (r-n) grading are locally discernible. The dark serrated, vertically tiering bodies are reflective post-metamorphic mineralizations. Scale bars are 5 mm.

Horizontal burrows remained low throughout the investigated blocks and did not exceed ichnofabric index 2 (Droser & Bottjer 1986), where less than 10% of the sediment is disturbed (Supplementary Material). They were only present in the lower half of Block A and show a pattern of gradual, upward, decreasing density (Supplementary Material), consistent with (near)continuous sedimentation during environmental improvement (e.g., Garson et al., 2012).

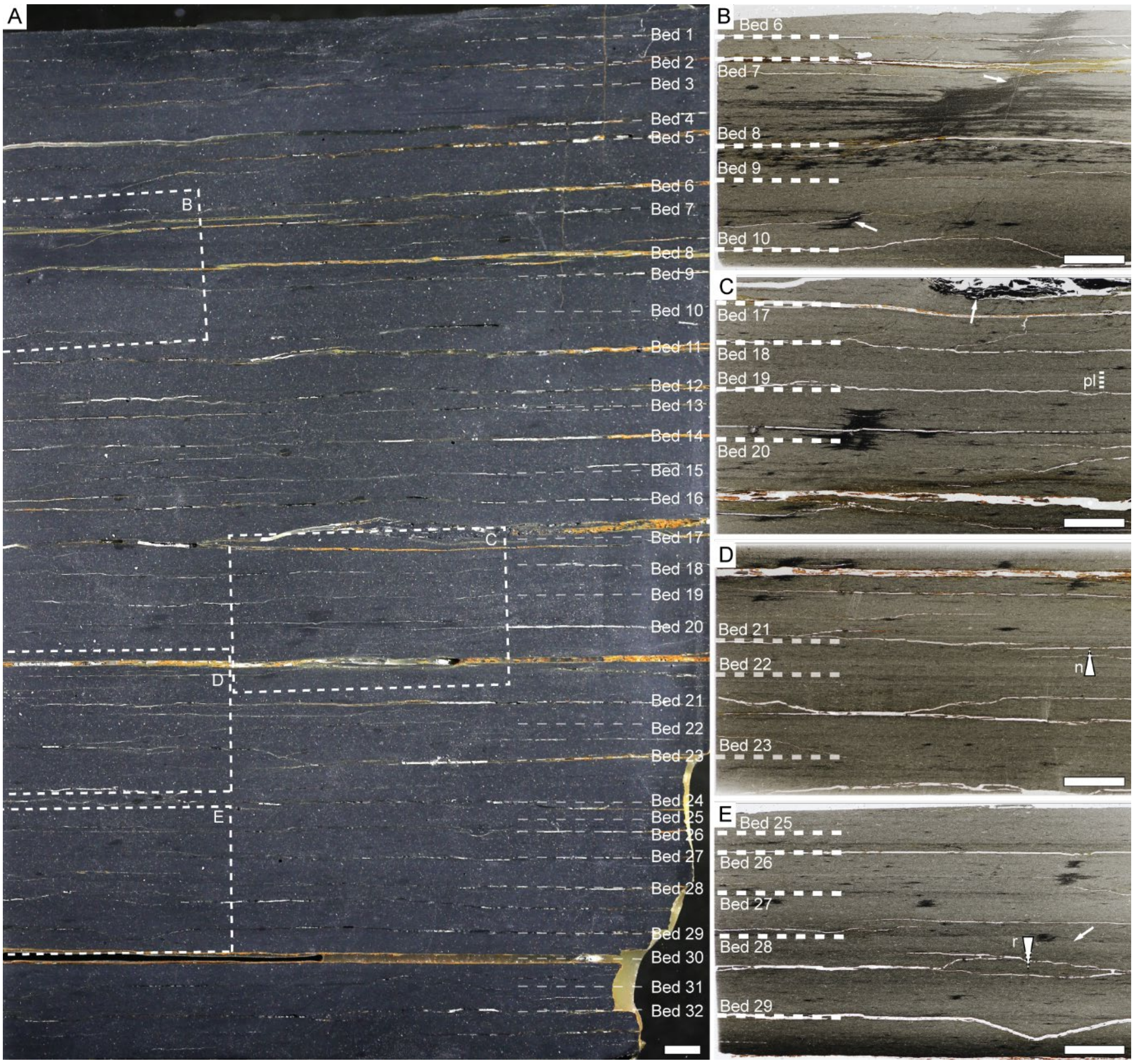

Figure 4.9. Sedimentary structures in Block A. (A) Polished slab, photographed under water. (B) Thin section illustrating the relatively uniform grain size and planar-bedding, overprinted by late-stage mineralization (black serrated bodies, arrowed). (C) Thin section showing example of subtle, laterally continuous, planar lamination (pl). Black, structured, mass (arrow) likely represents a phosphatized fossil. (D) Thin section showing weak normal grading (n). (E) Thin section showing reverse grading (r) with a sharp, slightly irregular and possibly erosive, upper surface (arrow). Scale bars are 5 mm.

4.5.3 Isoxys volucris size frequencies

Isoxys volucris show stratigraphic variability in their distribution and size frequencies. Block B is the primary focus since it shows distinct bed-by-bed variability in its relatively dense *Isoxys volucris* assemblages, whereas Block A's lower-density assemblages did not yield detectable patterns.

Block A

Isoxys volucris occur on every bedding plane in Block A with densities ranging from 2.2–37.3 individuals per 1000 cm^2 (mean 15.5; Data Table E4.1). Bedding planes show variable levels of specimen disarticulation (median=31%, range 0–75%, *n*=252; Data Table E4.3) and generally low levels of crumpling (median=6.1%, range 0–37.5%, *n*=274; Data Table E4.3). Block A shows an overall bell-shaped size distribution for carapace lengths that range between 3.5–16.9 mm (mean 9.5 mm, variance 7.3; *n*=282; Data Table E4.3; see also Fig .4.11).

Block B

Isoxys volucris occurs on every bedding plane in Block B (Fig. 4.10), achieving densities of 7.8–108.6 individuals per 1000 cm^2 (mean 28.1; Data Table E4.1). Specimens are especially abundant in two beds (Bed 4 and Bed 19), with densities of 108.6 and 62.4 individuals per 1000 cm^2, respectively. Significantly, these two beds show the lowest levels of disarticulation in *Isoxys volucris* (6.3% and 3.8%, respectively; median=21.6%, range 0–54.5%, *n*=383) in Block B, besides one bed with no disarticulated specimens (Bed 7), and they show some of the highest proportions of crumpled specimens (23.6% and 24.6%, respectively; median=12.7%, range 0–50%, *n*=390) (Fig 4.10; Data Table E4.3).

Isoxys volucris shows an overall bimodal size-frequency distribution in Block B (Fig 4.10; Data Table E4.4). Sizes range from 1.8–17.1 mm (mean 8.4, variance 11.9; *n*=392). Mixture analysis of all the specimens yields a best fit with two components (Size Class I and Size Class II), each defining a peak (Fig. 4.10B). Size Class I ranges from 1.8–5.4 mm (mean 4.13 mm, variance 1.21, *n*=97) and Size Class II from 5.5–17.1 mm (mean 9.6 mm, variance 8.39; *n*=295). Size Class I is present in the majority of beds (70%) in the block and is only absent from one when sampling *n*>10. A large proportion of all specimens of Size Class I (60%) occur in just the two high-abundance beds (Bed 4 and Bed 19; Fig. 4.10B), where they each comprise 55% of *Isoxys volucris* fossils in their respective beds. Separate mixture analyses of these beds give three (Bed 4) and two (Bed 19) cohort best-fit models, and their exclusion from the total population in Block B results in a single cohort best-fit model. Bootstrapping support the robustness of the two cohorts by consistently simulating medians of one component for beds with >20 *Isoxys volucris* specimens, except for beds 4 and 19 and only when simulated after resampling with two cohorts reflecting their actual relative distributions: this indicates that the peaks for Size Class I are not just artefacts of larger sample sizes.

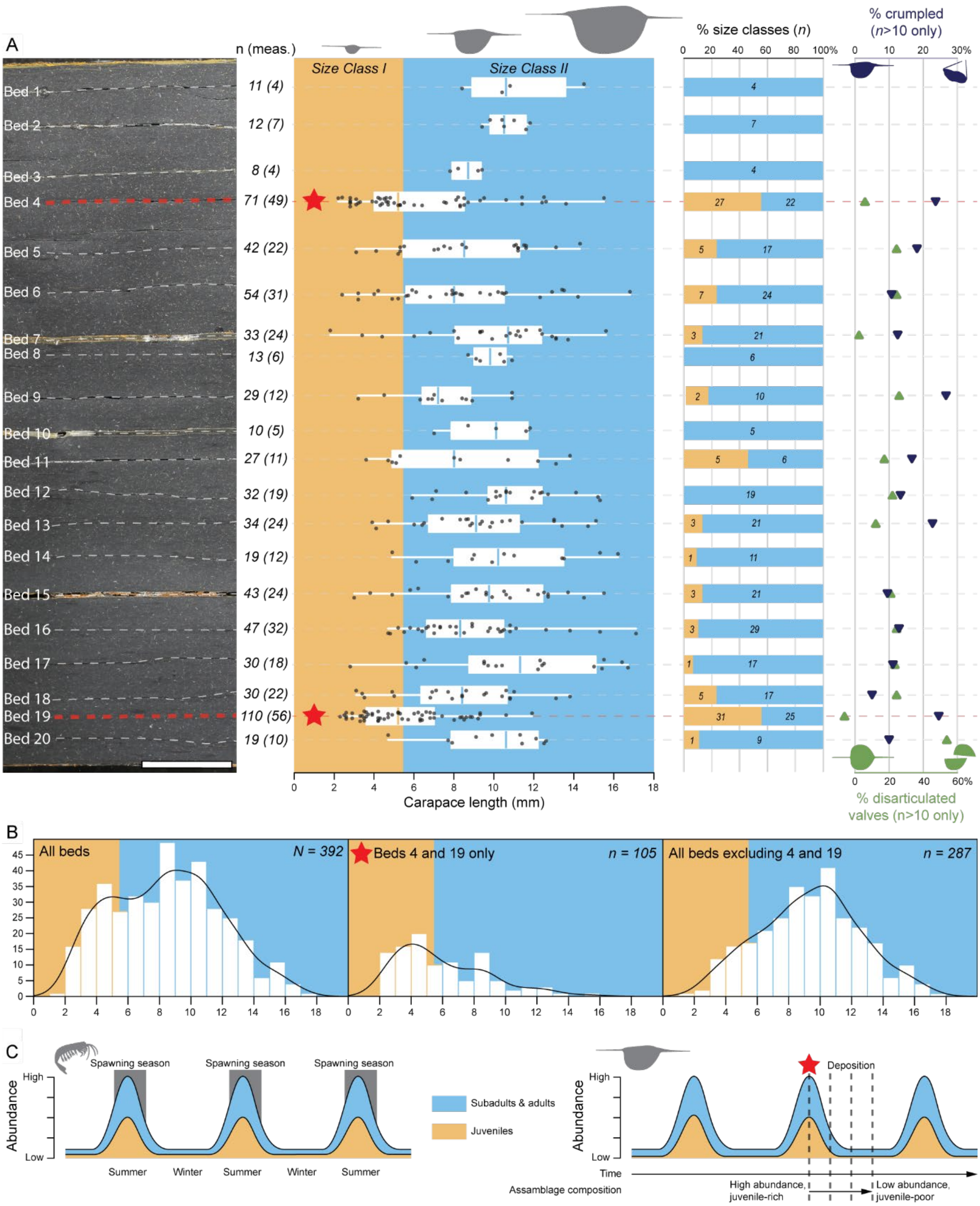

Figure 4.10. Size-frequency distributions of *Isoxys volucris* bedding-plane assemblages. (A) Sample sizes, carapace lengths and proportions of size classes I and II and of crumpled and disarticulated specimens on each sampled bedding plane. Carapace lengths for each bed are shown as jitters in box plots along their full size range (whiskers) and 25–75 quartiles (white boxes) with medians (vertical line inside). Juvenile-rich assemblages (beds 4 and 19, red stars) show higher numbers of individuals, relatively low ratios of disarticulated specimens and relatively high ratios of crumpled specimens. Size-class designations are based on a mixture analysis (see text). (B) Size-frequency histograms with kernel densities (black line) for the all the beds, both including and excluding the juvenile-rich horizons; most of the Size Class I peak derives from

beds 4 and 19. (C) Conceptualization of seasonal population dynamics for Antarctic krill (modified after Siegel, 2005) and for *Isoxys volucris* based on the former. Deposition (dashed vertical lines) captures different views (juvenile-to-adult assemblage compositions) of cohorts depending on their timing. Scale bar is 1 cm.

4.5.4 Interpretation

Monospecific mass assemblages of fossils, such as those of small *Isoxys volucris* specimens from Sirius Passet presented herein, may be a product of intrinsic (biotic) or extrinsic (i.e., depositional and preservational) factors. Depositional factors include condensation of death assemblages during slow deposition, reworking of accumulated remains, and hydrodynamic sorting (Fürsich, 1978; Fürsich and Aberhan, 1990; Kidwell and Bosence, 1991) and can generally be distinguished by their taphonomic impacts, including disarticulation, abrasion, and breakage (Plotnick, 1986; Brett and Baird, 1986). Such processes typically favor preservation of large, robust adults over small, delicate juveniles (Cummins et al., 1986; Staff et al., 1986). Condensation and reworking promote lithologically discrete bedding surfaces and disarticulation of fossils (from decay/scavenging), inconsistent with these beds' simple sedimentological boundaries and their higher ratios of articulated specimens. Furthermore, such processes would be expected to capture higher densities of all present fossils instead of the confined size distributions and absences of abnormally high densities of other (robust) fossils herein. Hydrodynamic sorting during transportation filters the size range of fossil assemblages (Shimoyama, 1985; Westrop, 1986) but is here dismissed by the unsorted associated organic debris (Fig. 4.3), right-skewed size-distributions of small specimens co-occurring with large specimens which contradict transportation (Olszewski and West, 1997), and presence of fossils mainly on bed junctions indicative of buried assemblages (Gaines, 2014; Bath Enright et al., 2021; Saleh et al., 2021a). Lastly, a bathymetric size control (Saleh et al., 2018, 2021b) is precluded by the homogenous sedimentology. Preservational factors include bed-by-bed variation in preservational potential, such as chemical (diagenetic) events or predation. Since *Isoxys volucris* is the only organism influenced, a chemical explanation is unlikely. Predation may shield prey items from the taphonomically active zone in the water column and create an effective transport mechanism to the sea floor (Petro et al., 2018). This corresponds with the increased ratio of crumpled (predated) *I. volucris* specimens. However, the crumpled specimens alone cannot account for the mass assemblages.

Instead, the two mass assemblages of small *Isoxys volucris* specimens have the hallmarks of intrinsic factors (e.g., Olszewski and West, 1997; Boomer et al., 2003). Populations of small individuals are commonly explained by mass-molting, morphological plasticity (dwarfism) to tolerate stressed environments, and population dynamics (spawning events). Mass-molting has been proposed to explain monospecific mass assemblages in Burgess Shale (Haug et al., 2013), but the high degree of articulated specimens in the *Isoxys volucris* mass-assemblages excludes this. Dwarfism can occur in response to stressed environments (Price, 1982), but is unlikely here given the concurrent four-fold increase in *Isoxys volucris* abundance and apparent monotony in depositional environment. Instead, the populations are most consistent with snapshots of juvenile cohorts during periodic spawning events (e.g., Tarling, 2010), comparable to those also seen in juvenile-rich size-frequency patterns of trilobites (Paterson et al., 2007; Hughes et al., 2014; Pauly and Holmes, 2022). Mass (or synchronized) spawning behavior is common in modern secondary consumers such as krill (e.g. Tarling and Cuzin-Roudy, 2003; Fig. 4.10C), and produces large cohorts with subsequently high mortality rates. For instance, in an initial cohort of Northern Krill where 57% of the spawned eggs reach the final larval furcilia stage, only 10% reach adolescence and 3% sexual maturity after a year (Tarling, 2010). This is consistent with the low proportions of large *Isoxys volucris* specimens and possibly also the high ratios of predation-induced crumpling of carapaces in the juvenile-rich beds (Fig. 4.10A).

Recurring mass-spawns in a depositional setting seemingly without sedimentological gaps prompts the question: what was their temporal frequency? This depends on the time-averaging that can be assessed using the taphonomic quality, i.e., the ratio of pristine soft-bodied specimens (with internal anatomy preserved) to degraded specimens (decayed and disarticulated, i.e., without internal anatomy preserved, including shed exuviae) of especially recalcitrant (biomineralized) taxa. The temporal spectrum for a soft-bodied assemblage spans the annual, decadal, and, more unlikely, centennial scale (Kidwell & Bosence, 1991). An annual scale implies that each successive bed represents about a month and that the two mass-spawn beds represent yearly spawning seasons. Taphonomic expectations for an annual scale are high quality: very low degrees of degradation and exuviae, resulting in well-preserved assemblages with high frequencies of internal soft tissues. A decadal scale implies that each successive bed generally represents a single or a few years and that mass-spawn beds most likely reflect years with extremely successful spawning events that greatly surpass normal ‘background’ spawns in cohort size (see Brinton, 1976; Tanasichuk, 1998 for krill examples). Taphonomic expectations for a decadal scale are a higher ratio of degraded specimens and exuviae, and biomineralized trilobites. A centurial scale would imply that each bed represents around a decade. Accumulated carcasses and exuviae would greatly outnumber recently deceased or freshly killed animals. Taphonomic expectations are low quality: a dominance of degraded, disarticulated material, mostly from trilobites, in combination with low ratios of soft-tissue preservation. In Sirius Passet, the low ratio of disarticulated material discards the centennial scale. In fact, for trilobites, preservation of internal anatomy is much more common than disarticulation (44% vs 22%, respectively, in Block B; n=27). Distinction between annual and decadal scale is more difficult. However, the high taphonomic quality (with limited degradation and exuviae) and preservation of fragile juveniles, in combination with high bed-by-bed fossil variability, strongly suggest minimal time-averaging between depositional events, most likely preserving seasonal variation at the annual scale.

4.6 Discussion

The population and community scale dynamics of Early Phanerozoic animal ecosystems remain poorly understood (Haug et al., 2013). Preservation of within-community dynamics in the fossil record is rare (Cummins et al., 1986) since they require continuously stacked beds with minimal time-averaging in depositional environments with high sedimentation rates (Fürsich, 1978). Fairly high fossil densities (or large sampling areas) are helpful as sample intervals straddling multiple beds effectively conceal dynamics (Fig. 4.11). In Lagerstätten, they also require persistent conditions facilitating BST preservation. These conditions are rarely achieved: ‘normal’ shelly assemblages provide highly biased records and the depositional styles of most BST Lagerstätten generate allochthonous, time-averaged and temporally punctuated records (Fig. 4.12). Sirius Passet is conspicuously different. Multiple lines of evidence point to a continuous record with minimal time-averaging, where stacked beds with continuous BST preservation preserve successive census assemblages (snapshots) of the (par-) autochthonous populations and communities (Fig. 4.12).

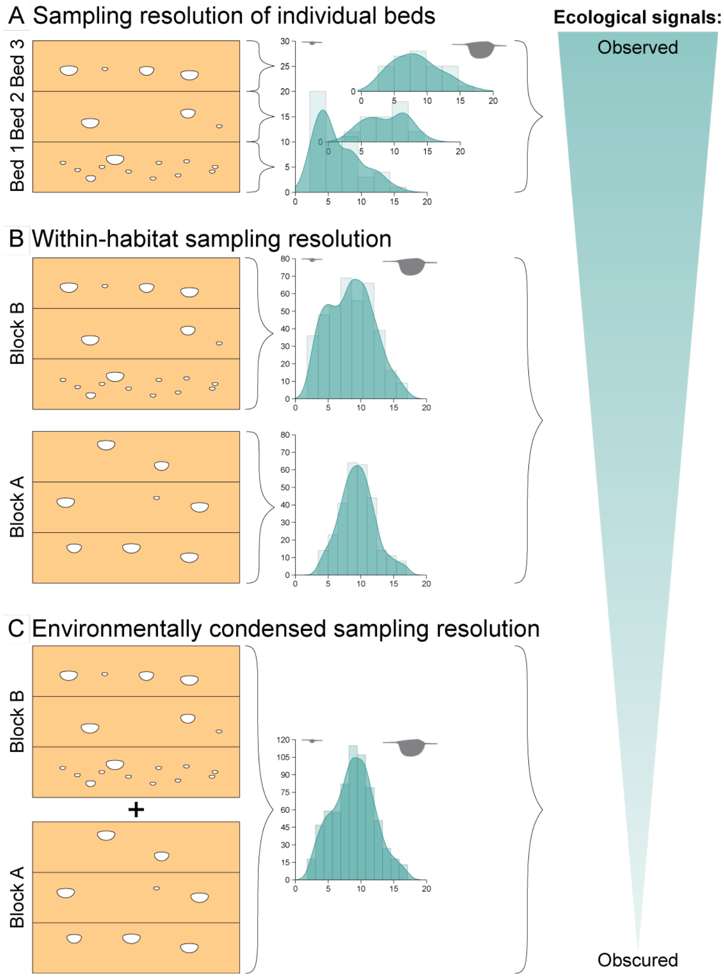

Figure 4.11. Effects of different sampling resolutions on how apparent (i.e., temporally biased) ecological signals are in *Isoxys volucris* size-frequency distributions. This type of time-averaging differs from depositional time averaging but the overall effects are broadly the same. (A) Individually sampled beds from Block B, each with census assemblages, showing markedly different size-frequency distributions; temporal population dynamics can be interpreted from e.g. juvenile-rich beds. (B) Beds compounded into within-habitat samples (Block A and B), each comprised of several beds from a similar depositional environment. The juvenile-rich beds are only present in Block B where their signal is still observable as a peak in the bimodal distribution. (C) Environmentally condensed sampling combining Block A and B; the juvenile-rich temporal signal is suppressed and barely resolvable.

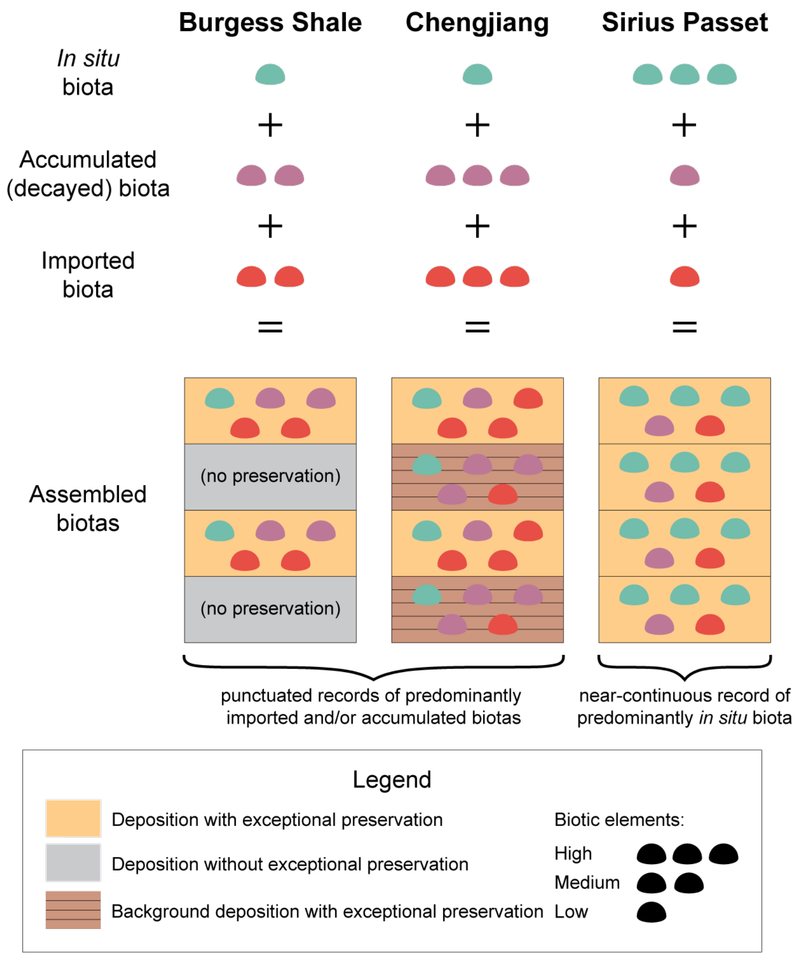

Figure 4.12. Conceptual model for the observed differences in the composition of exceptionally preserved fossils assemblages in Burgess Shale, Chengjiang and Sirius Passet. *In situ* census (i.e., living) biotas are mixed to varying degrees with accumulated (i.e., time-averaged) and allochthonous (i.e., imported) elements which act to dilute their respective primary ecological signals; punctuated records limit temporal context. Preservation of temporal dynamics and primary ecological signals requires near-continuous, low-energy, deposition, as seen in Sirius Passet.

Sirius Passet provides a novel opportunity to reconstruct the complex life strategy of an organism from a BST Lagerstätte. Mass spawnings are adaptations to maximize reproduction success during optimal conditions (Ims, 1990) and are often related to temporally recurring environmental fluctuations (Cury and Roy, 1989). Optimal conditions for spawning seasons are complex but overall related to food availability (e.g. Cushing 1990). Given that generation time in arthropods is proposed to be proportional to size (Escribano and Riquelme-Bugueño, 2015), we can estimate 1-2 years between generations for *Isoxys volucris* (maximum size ~20 mm). This makes it likely that they spawned annually, and therefore, by extension, that the optimal environmental conditions in Sirius Passet fluctuated in annual cycles (i.e., seasons). *Isoxys volucris* mass spawns imply that strategies to exploit seasonalities had already evolved in early Cambrian panarthropods. Increased *I. volucris* prey items may suggest that mass spawns in turn offered a plentiful (seasonal) food source for predators.

It was not possible to track the growth of a given cohort bed-by-bed in the dataset. This could be explained by high mortality rates if the surviving cohort does not exceed the background spawning 'noise'. Alternatively, spatial ontogenetic segregation could result in lack of mid-sized specimens if the environment represents a nursery or juvenile habitat (Gillanders et al., 2003; Yang et al., 2021a). In that case, it would still reflect population dynamics with minimal time-averaging.

The collected dataset is limited by spatially and stratigraphically restricted sample areas and (in case of taphonomy) small sample sizes. For example, uneven seafloors could potentially form accumulation traps for small elements (although broadly regular bedding thicknesses oppose this). These limitations are due to difficulties obtaining material from the remote Arctic. We have tried to mitigate them with a holistic approach. Our hypotheses could be tested by similar analyses of additional intervals which would also give a fuller picture of the temporal depositional and ecological nuances of Sirius Passet.

The stacked, highly fossiliferous beds of Sirius Passet record a significantly different depositional environment to other BST Lagerstätten. Beds were deposited under higher-frequency, lower-energy gravity flows than in Burgess Shale, Chengjiang or Fezouata Shale . The sedimentological analysis shows that a plausible depositional mechanism for the stacked beds is hyperpycnal flows developed by discharge from sediment-rich rivers (Mulder et al., 2003) at a frequency (>1 per year?) able to capture the biotas fluctuating seasonal signatures. This contrasts the mostly storm-related deposition of fossiliferous beds in Burgess Shale, Chengjiang or Fezouata Shale (Gabbott et al., 2008; Saleh et al., 2020; Saleh et al., 2022). In Sirius Passet, dense fossil accumulations occur mainly on bedding planes, i.e., between beds, rather than within them, suggesting that they were buried *in situ*, instead of having been entrained and translocated by the flows (see Gaines, 2014; Bath Enright et al., 2021). This supports recent advances proposing that BST biotas were not confined to a single type of depositional environment (Saleh et al., 2022b).

4.7 Conclusions

Temporal dynamics and behavior of early animals are rarely preserved in BST Lagerstätten. However, they are recorded at high fidelity in Sirius Passet by near-continuous low-energy deposition that minimizes temporal biases. The dense (par)autochthonous fossil assemblages in thin, stacked beds enable a combination of microstratigraphical and paleoecological approaches to uncover ecological dynamics at a high temporal resolution. Here we have shown that mass assemblages of juvenile *Isoxys volucris* specimens, can be robustly interpreted as mass spawnings, reflecting their population dynamics. Our analyses reveal that synchronized spawning behavior had already evolved in panarthropods by the early Cambrian.

Sirius Passet adds to the different windows provided by Cambrian Lagerstätten. These windows complement each other and provide different opportunities to understand early animal ecosystems. Examples include the pristine morphological information and broad-scale spatial distribution of (heavily filtered) ancient communities provided by Burgess Shale and Chengjiang (Zhao et al., 2009; Nanglu et al., 2020; Saleh et al., 2020b) while Hiyan provides a window to evolution of larvae and ontogeny (Yang et al., 2021a). Sirius Passet provides, amongst other things, a new minimally-filtered window into temporal community variation at an unprecedented resolution, offering a unique opportunity to investigate early animal ecosystem dynamics.

4.8 Supplementary Material

Trace fossils in Sirius Passet predominately comprise *Alcyonidiopsis*-, *Multina*- and *Pilichnus*-like horizontal burrows (Mángano et al., 2012, 2019). Locally, these intersect fossils, including ones with preserved labile soft tissues (e.g., muscle), but there is minimal evidence of them having disrupted the carcasses or sediment lamination.

We assessed bed-by-bed changes in bioturbation intensity of horizontal burrows at a scale relevant to this study using the following index:

1) Absent: No observed burrows.
2) Rare: Very few (often only one or two) burrows are present.

3) Few: Several burrows, but too few to regularly intersect or occur in proximity (within 5 cm) to one another.
4) Common: Scattered burrows, occasionally in proximity (within 5 cm). Local areas showing high density of burrows of varying sizes.
5) Abundant: Burrows regularly occur in proximity (within 5 cm) to one another and often intersect.

Horizontal burrows are present in the lower half of Block A (Table 4.S1) and are almost completely absent from Block B (except for rare occurrences in beds 11 and 16). Most of them are simple, isolated and relatively wide (1–2.5 mm) burrows. Their distribution is not controlled by taphonomic shielding within fossils (Mángano et al., 2019) since they may occur in both fossils and sediment; however, larger concentrations of burrows tend to occur in fossils and putative mats.

Horizontal burrows in Block A show an overall pattern of decreasing density with height from the base (Table 4.S1). This pattern can be divided into three relatively stable general phases showing stepwise increases in burrow intensity: Predominantly absent occurrences in beds 1–14; predominantly few occurrences in beds 15–26; and predominantly common occurrences in beds 27–32 (peaking in intensity at Bed 30).

The broadly gradual transition in burrowing intensity is interpreted to reflect that Block A records a gradual change in the sediment's chemical environment from relatively benign to hostile for infauna, with a fairly steep main transition around Bed 15. Altogether, this record is consistent with frequent deposition since significant breaks in sedimentation and/or sediment loss would generate sudden bed-by-bed variability in intensity by their prolonged accumulation window.

Table 4.S1. Densities of horizontal burrows on investigated bedding planes in Block A.

Bed	Trace fossil density				
	Absent	Rare	Few	Common	Abundant
1	x				
2	x				
3	x				
4	x				
5	x				
6	x				

7	x	x			
8	x				
9	x				
10	x				
11	x				
12	x				
13	x				
14	x				
15	x	x	x		
16	x				
17	x	x	x	x	
18	x	x	x	x	
19	x	x			
20	x	x	x		
21	x	x	x	x	
22	x	x	x		
23	x	x	x		
24	x	x	x		
25	x	x	x		
26	x	x	x		
27	x	x	x	x	
28	x	x	x	x	
29	x	x			
30	x	x	x	x	x
31	x	x	x		
32	x	x	x	x	

Chapter 5

Pelagic food web structure of the Cambrian Sirius Passet biota

Author contributions

This chapter was written as a preliminary manuscript with intention to submit it for publication at a later stage.

The research for this chapter was developed by me and Jakob Vinther. I did all data collection and analyses, and all photography besides the photos on Figs 5.5, 5.6, and 5.7A–C that was photographed by Tae-Yoon Park. “In-life” drawings of Sirius Passet fossils on Fig. 5.14 were made by Mike Cawthorne with my input. I wrote the manuscript and produced figures with input from Jakob Vinther.

5.1 Abstract

The Ediacaran–Cambrian transition (~540 million years ago) was marked by an exceptionally large expansion in animal diversity and disparity that included colonization of pelagic ecospace. Many modern pelagic niches were exploited already by the early Cambrian, probably fueled by predator-prey arms races that established a complex food web with multiple trophic levels. Little is known about the earliest Cambrian food webs and what controls their shape and how they compare to modern ecosystems. Here, we review and infer life habits and trophic roles for pelagic taxa from Sirius Passet to reconstruct the trophic food web. Higher trophic levels were dominated by large panarthropods, such as the anomalocarid *Amplectobelua*? sp., and a giant stem-chaetognath amiskwiiform. In contrast, chordates were small, low-level primary consumers. These positions contrast modern ecosystems where vertebrates are the dominant pelagic predators and chaetognaths are tiny planktivorous carnivores. Mid-trophic levels show low diversity dominated by a single taxon, *Isoxys volucris*. This, together with evidence that suggests it was a frequent food source, is characteristic of modern 'wasp-waist' ecosystems of high-productivity ecosystems. Wasp-waist taxa both enforce top-down and bottom-up control on their food webs and are the primary channel for energy transfer to higher trophic levels. Sea floors below high primary productivity zones usually experience high levels of hypoxia and anoxia. Sirius Passet is unique amongst Burgess Shale-type Lagerstätten in its density and quality of fossil preservation and hence its unique ecological setting may have been an important contributing factor in having made Sirius Passet both a Konservat and Konzentrat Lagerstätte.

5.2 Introduction

The Ediacaran–Cambrian transition (~540 million years ago) marked the appearance of highly diverse and disparate animal ecosystems (Marshall, 2006; Na and Kiessling, 2015). Cambrian animal diversity expanded in concert with dynamic ecological innovations that outcompeted more passive Ediacaran strategies (Butterfield, 2007, 2009; Liu et al., 2015; Darroch et al., 2018). Ecological innovations were likely driven by the rise of heterotrophy (Stanley, 1973; Butterfield, 2009, 2011) initiating carnivory and escalating predator-prey arms races (Sperling et al., 2013) that developed complex food webs where energy transferred through multiple trophic levels (Bengtson, 2002; Butterfield, 2007; Dunne et al., 2008; Bush and Bambach, 2011). Predation forced exploration of vacant ecospace, leading to colonization of infaunal space (Mangano and Buatois, 2017) as well as the water column (Vannier and Chen, 2000). Colonization of the water column by pelagic animals caused significant oxygenation and de-stratification of oceans by effectively transferring biomass from pelagic phytoplankton to the benthos through a biological pump driven by sinking fecal matter and vertical migration (Logan et al., 1995; Butterfield, 2011, 2018). Pelagic food webs rapidly attained a diverse, modern-like structure (Hu, 2005; Vannier et al., 2007; Dunne et al., 2008) and mirrored niches with large (~1 m long) predators (Whittington and Briggs, 1985; Paterson et al., 2011; De Vivo et al., 2021), small vertically-migrating arthropod (Vannier and Chen, 2000; Pates et al., 2021) and chaetognath (Vannier et al., 2007) predators, and large, nektonic sweep-net filter-feeders (Vinther et al., 2014). Large predators require energy that has to pass from the bottom to the top of the food web: from primary producing phytoplankton to apex predators (see Antell and Saupe, 2021 for a deep-time perspective). Unfortunately, pelagic species-interactions remain poorly understood due to the biased nature of most Lagerstätten (Butterfield, 2003) and only few efforts have tried to estimate Cambrian food web structures (Debrenne and Zhuravlev, 1997; Hu et al., 2007; Dunne et al., 2008). BST Lagerstätten offers some of the best windows to Cambrian macrofossil biotas (eg., Holmes et al., 2018), but actual species interactions are difficult to assess since fossil assemblages are often taphonomically biased or spatially filtered/mixed (Saleh et al., 2020b, 2021c; Bath Enright et al., 2021), despite suggestions that these uncertainties do not exceed those for modern food web analyses (Dunne et al., 2008). Cambrian food webs were non-actualistic in the sense that modern top-tier pelagic predators such as jawed vertebrates or large cephalopods had not yet evolved (Brett and Walker, 2002). So, in their absence, were the trophic levels of early Cambrian food webs structured similarly to modern ones?

Here, we aim to reconstruct the pelagic food web of the early Cambrian Sirius Passet biota by evaluating taxa's probable life habits and trophic roles based on indirect (functional morphology) and direct (gut contents) evidence. Sirius Passet is suitable for such reconstructions due to the frequent preservation of pelagic taxa, without significant spatial mixing or taphonomic filtering (Chapter 4), and sheer abundance of fossils that appear to show little broad-scale vertical (temporal) variation. Gut contents, the most reliable evidence for predator-prey relationships, are not uncommon (Peel, 2017b). We use this reconstruction to argue that, while the food web has characteristics of a specific modern-like trophic structure, organisms exploiting different trophic levels have shifted markedly since the Cambrian.

5.3 Methods for establishing food web

5.3.1 Adaptive function of spines in Isoxys

To assess the biological function of the spines in *Isoxys volucris*, we measured the spine lengths (as a sum of the posterior and anterior spine length combined) and carapace lengths (excluding spines) of 97 articulated specimens. The specimens were measured digitally from photographic material using ImageJ software, except for 22 specimens which were measured by hand with a digital caliper. Measurements were plotted in R (R Core Team, 2013). The specimens are currently part of the research collection at Korea Polar Research Institute (KOPRI), Incheon, South Korea but will be accessioned to the Natural History Museum of Denmark, Copenhagen, Denmark. Specimen numbers refer to the collection of Natural History Museum of Denmark (MGUH) or field collection at KOPRI (SP-numbers).

5.3.2 Food network analysis

The goal is to explore the complexity of the food web structure in the newly colonized pelagic realm to better understand how rapidly ecosystem structures evolved. Pelagic taxa are defined as nektonic/nektobenthic taxa, i.e., animals that likely spend most of their time swimming in the water column. The food web is oversimplified since it is based on fossils accumulated and deposited on the sea floor. In reality, some pelagic taxa will likely have been separated vertically within the water column. The biotas pelagic component is here investigated in isolation from the benthic component. Nektobenthic taxa, living close to the sea floor, will undoubtedly have connected the pelagic and benthic food webs, and benthic taxa likely had cascading effects on the pelagic food web (and vice versa). However, a full analysis of the entire food web within the Sirius Passet biota is outside the scope of this chapter.

The pelagic food web for the Sirius Passet biota was based on qualitative assessments of each taxon's likely life habits and trophic roles, and estimations of possible predator-prey relationships from sizes. Qualitative assessments were based on published images from collections at the Natural History Museum of Denmark and the collection at Korea Polar Research Institute, South Korea. It was not possible to standardize data due to a lack of complete specimen cataloguing within these collections. The food web was then constructed by assigning 'certain prey' and 'estimated prey' to each pelagic taxon. Certain prey is direct evidence from gut contents. Estimated prey is unconfirmed inference based on probable maximum prey size estimations. Size is a good indicator of trophic position within a food web since most predators are larger than their prey (Brose et al., 2006). In this analysis, any taxon with the shortest axis (longitudinal or transverse) below the maximum prey size estimation is estimated prey. Prey size estimations for each taxon derive from indirect evidence of functional morphology (measurements of width between e.g., mouthparts or manipulating appendages) or ingested prey scaled to maximum body size. Prey sizes relate to adults only since ontogeny is not properly known for these taxa. Prey size estimates contain uncertainties, for example, due lack of contemporary analogues for certain fossil morphologies, but nevertheless represents a falsifiable attempt to estimate potential species interactions. Food web tiers are based on these estimated and certain relationships and are here hierarchical as taxa on a given tier must only be able to feed on the tiers below. Only the nektonic/nektobenthic taxa were included in this analysis (Fig. 5.1). Sirius Passet is biased against microfossils (phytoplankton and/or zooplankton) from metamorphic alteration (Slater et al., 2018). Their presence in the food web is here assumed.

Measurements derived from collected material currently housed at KOPRI or published records when noted. Mesozooplankton and phytoplankton widths are based on Sieburth et al. (1978).

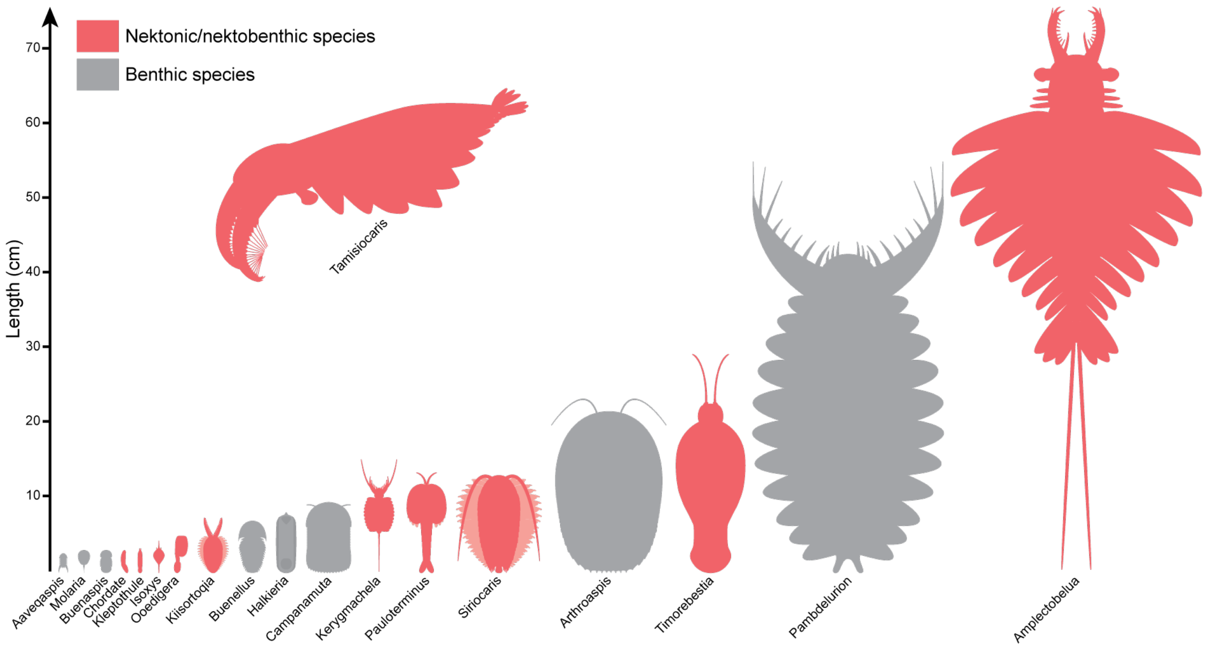

Figure 5.1. Size chart for benthic and pelagic Sirius Passet fossils (excluding sponges). Sizes are from the collection housed at Korea Polar Research Institute (KOPRI) and Budd (1999a, 2011), Conway Morris and Peel (1995), Lagebro et al. (2009), Peel and Stein (2009), Peel (2017), Stein (2010), Stein et al. (2013), Taylor (2002) and Vinther et al. (2011, 2016). Maximum size for *Pambdelurion* is based on an extrapolation of isolated mouth parts (Vinther et al., 2016). *Amplectobelua* and *Tamisiocaris* are only known from frontal appendages; the maximum size of the former is based on a comparison with *Amplectobelua symbrachiata* (Chen et al., 1994).

5.3.3 Notes on functional morphology

Many panarthropod taxa display similar functional traits that inform their autecological lifestyle. They are briefly treated here.

Predatory adaptations

Gnathobases

Gnathobasic spines are common in modern and Cambrian panarthropods (Manton, 1964; Cong et al., 2018; Bicknell et al., 2021). They support a carnivorous lifestyle as they suggest the taxon was able to masticate its prey prior to ingestion. Proximally situated spines are often associated with manipulating and tearing or crushing prey and have been reported from Cambrian arthropods (Bruton, 1981; Fortey and Owens, 1999; Jago et al., 2016; Bicknell et al., 2018, 2021) and radiodonts (Cong et al., 2018). Their presence is here interpreted as a carnivorous trait.

Gut diverticula

Many Cambrian panarthropods have pouches on their gut tracts that have been interpreted as analogous to digestive glands (herein termed gut diverticula) (Butterfield, 2002; Vannier et al., 2014). These have been interpreted as supporting carnivorous lifestyles through food storage or aiding the digestion of prey through enzyme production (Vannier et al., 2014). They are frequently phosphatized in Cambrian BST Lagerstätten. Their high preservational potential may have been enhanced by phosphate-rich food storage from a carnivorous diet (Bradley, 1946; see also Chapter 3). Their presence is here interpreted as a carnivorous trait.

Nektonic adaptations

Paddle-shaped exopods

Cambrian arthropods have biramous legs that are divided into a robust often leg-like endopod and a flat flap- or lamella-like exopod. In some cases, exopods are wide and almost as long as the endopods. In those cases, their function has been interpreted as paddles used to generate propulsion by power strokes (Briggs and Whittington, 1985) in a range of other proposed nektobenthic Cambrian arthropods such as e.g. *Leanchoilia* (Haug et al., 2012), *Alalcomenaeus* (Briggs and Collins, 1999), and the upside-down swimming *Balhuticaris voltae* (Izquierdo-López and Caron, 2022). Their presence is here interpreted as a functional trait supporting a nektonic or nektobenthic life habit.

5.4 Results

5.4.1 Likely life habits and trophic roles

Stem-chaetognath

Amiskwiiform sp.

Taxonomic notes.

This taxon is currently under description by Vinther et al. It resembles *Amiskwia* and its position as a stem-chaetognath (cf. Vinther and Parry, 2019) is supported by the presence of lateral and caudal fins (Fig. 5.2) with fin rays, and large paired axial structures interpreted as ventral ganglia (Fig. 3.1).

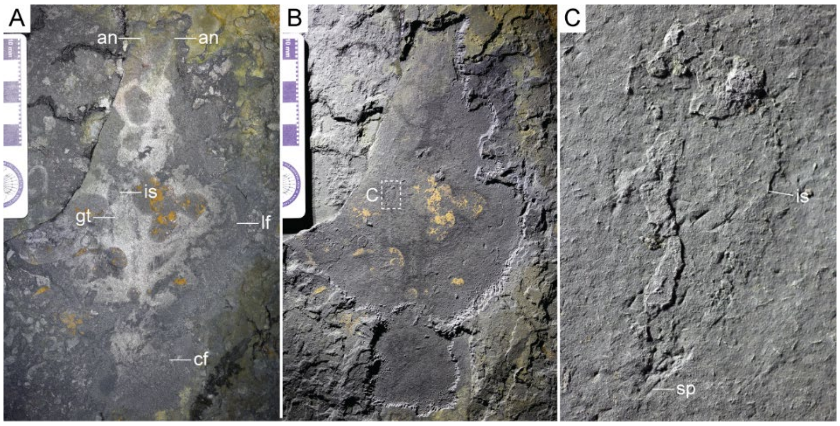

Figure 5.2. Amiskwiiform sp. (A–C) large amiskwiiform showing overall morphology and an *Isoxys volucris* specimen (C) within the gut. SP-2011-MS0039. a Specimen photographed at high-angle lighting submerged in water. (B) Specimen photographed at low-angle lighting. (C) Dashed box of (B) showing close-up of ingested *Isoxys* specimen with readily visible spine and effaced body outline. Abbreviations: an, antennae; cf, caudal fan, is, *Isoxys volucris*; gt, gut tract, lf, lateral fan.

Life habit.

Nektonic. The presence of tail and lateral fins (Fig. 5.2A) suggests that amiskwiiform sp. was able to swim by rapid dorsoventral undulations as in most extant chaetognaths (Jordan, 1992).

Trophic role.

Carnivorous predator. All extant chaetognaths are predators. Predatory behavior in amiskwiiform sp. is supported by gut contents that commonly include ingested *Isoxys volucris* specimens. One specimen shows an *Isoxys volucris* oriented longitudinally within the gut tract of amiskwiiform sp. (Fig. 5.2C) as expected for swallowed prey and we consider it unlikely to be externally superimposed by chance.

Prey size estimation.

Maximum width at least 19.3 mm. One specimen shows an ingested *Isoxys volucris* (width 2.2 mm) that is about 22.9% of the ingesting width of amiskwiiform sp. (9.6 mm). This gives an estimated maximum prey size of at least 18.8 mm when extrapolated to the largest known specimen (82 mm; Table 5.1).

Certain prey (gut content).

Isoxys volucris.

Estimated prey.

Chordata sp., *Kleptothule rasmusseni*, *Ooedigera peeli*.**Table 5.1. Estimated maximum body sizes and maximum prey sizes for nektonic taxa in the Sirius Passet Lagerstätte.** Height is used for taxa where width is unknown (Chordata sp., *Isoxys volucris*, *Ooedigera peeli*, *Pauloterminus spinodorsalis*).

Taxon	Maximum body width/height (mm)	Maximum prey width/height (mm)	Notes
Amiskwiiform sp.	82	18.8	
Kerygmachela kierkegaardi	39*	18	*Body flaps included
Amplectobelua sp.	N/A	37	
Tamisiocaris borealis	N/A	2	
Isoxys volucris	11	1	
Kiisortoqia soperi	25	17.6	
Kleptothule rasmusseni	6	N/A	
Pauloterminus spinodorsalis	31	7.4	
Siriocaris trollae	47	31	
Chordata sp.	5	0.2	
Ooedigera peeli	14	0.02	
Mesozooplankton	1	0.02	
Phytoplankton	0.02	N/A	

Stem-Euarthropods

Kerygmachela kierkegaardi

Life habit.

Nektonic. *Kerygmachela* is a gilled lobopod with 11 pairs of lateral flaps (Fig. 5.3) and small poorly-known lobopodous legs. Despite the possible presence of legs, it is generally believed to have been an active swimmer, evidenced by the imbricating flap morphology (Budd, 1998b; Delle Cave et al., 1998; Hou and Bergström, 2006; Liu and Dunlop, 2014). However, putative legs would suggest that it could have spent some time on the sea floor as well.

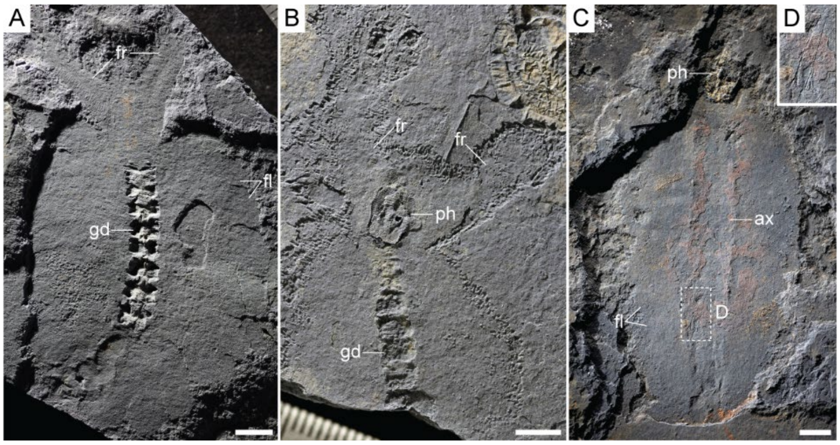

Figure 5.3. *Kerygmachela kierkegaardi*. (A) Specimen showing wrinkled frontal appendages, lateral flaps, and gut diverticula. MGUH 22084. (B) Specimen showing mineralized pharynx, frontal appendages, and gut diverticula. SP-2016-195. (C) Specimen showing *Isoxys volucris* within the axis (dashed box), possibly an ingested specimen. SP-[Block A, Bed 27]. (D) Dashed box of (C) showing close-up of aligned *Isoxys volucris* spines within the axis. Scale bars are 5 mm. Abbreviations: ax, axis; fl, lateral flaps; gd, gut diverticula; ph, pharynx.

Trophic role.

Carnivorous predator. *Kerygmachela* has large frontal appendages carrying several processes (Fig. 5.3A). Anterolaterally there are four considerably elongated processes, the longest of which comprise more than 20% of the total body length. The processes were likely sensory (Hou and Bergström, 2006) and used to catch and manipulate prey, while hunting would be aided by its compound eyes (Park et al., 2018). Wrinkles on the frontal appendages suggest that they were likely flexible (Chen et al., 1994), perhaps motile enough to move prey to the mouth. The mouth itself is poorly known but recent evidence suggests that it is anteriorly facing and ventrally situated (Park et al., 2018), and not terminally situated (cf. Budd, 1998b). There is nothing that suggests a mouth apparatus consisting of large circumoral mouth plates as seen in, for example, *Pambdelurion whittingtoni* (Vinther et al., 2016), but rather a cone composed of a series of denticles sitting rostrally in the pharynx between two rostral spines (Park et al., 2018). The pharynx is very muscular and often phosphatized (Fig. 5.3B,C). A muscular pharynx is often a specialization for a swallowing or sucking strategy (Manton and Heatley, 1937; Nielsen, 2013), and the lack of several series of mouth plates in *Kerygmachela* is consistent with these feeding strategies, as previously surmised by Budd (1998b). *Kerygmachela* also has gut diverticula. Gut contents have not been decisively shown, but a single specimen shows a longitudinally aligned *Isoxys volucris* specimen within its axis that may have been ingested (Fig. 5.3D).

Prey size estimation.

Maximally *c.* 18 mm wide. We hypothesize that the maximum caught prey size would correspond to the space between the two sets of anterolateral processes (Fig. 5.4A). This would suggest maximum size of *c.* 18 mm for captured prey based on the largest specimen at hand (fig. 1a in Park et al., 2018). The mouth opening in that specimen is 2.1 mm wide, corresponding to *c.* 21% of the maximum head width measured between the eyes. The width is highly variable but the widest pharynx corresponds to *c.* 60% of the maximum head width (see suppl. fig. 7j in Park et al., 2018). This could be extrapolated to a potential width of 6 mm for the largest specimen. If *Kerygmachela* swallowed its prey, the mouth could likely expand and perhaps ingest prey up to about the same size as the width of the pharynx. On the other hand, if *Kerygmachela* employed a sucking strategy, the appendages would be the main constraint on prey size. A sucking strategy may need some mechanism for puncturing the prey to access the fluids after the initial suction, as seen in other edysozoans, like jaws in onychophorans (Manton and Heatley, 1937) or stylets in tardigrades (Guidetti et al., 2012). This could have been attained by rasping with the denticles and/or pharyngeal teeth or puncturing the prey with the two rostral spines.

Certain prey (gut content).

Isoxys volucris.

Estimated prey.

Chordata sp., *Kleptothule rasmusseni*, *Ooedigera peeli*.

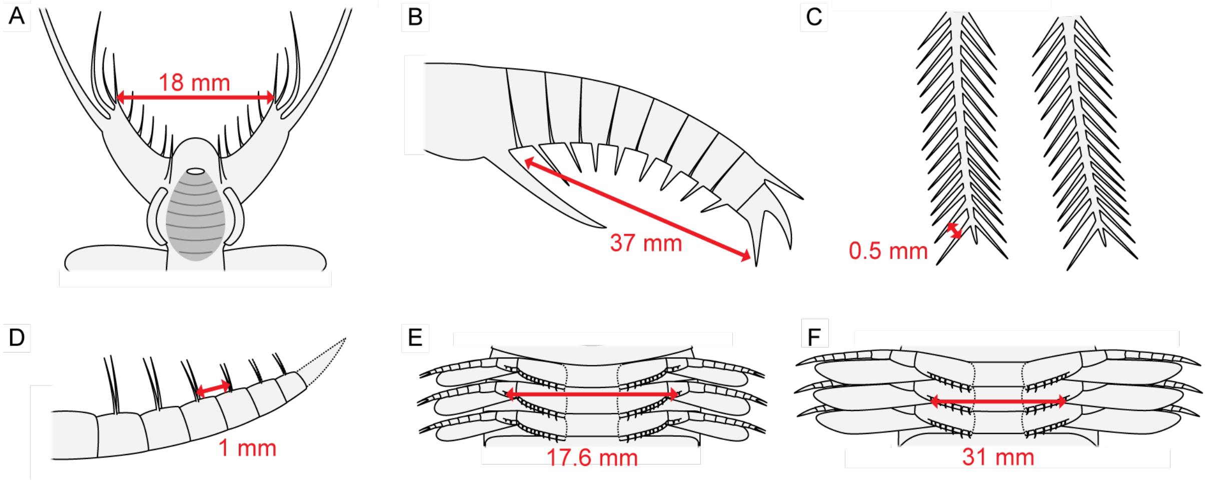

Figure 5.4. Schematic drawings of morphological constraints for maximum prey size interpretations (red arrows, see text for details). (A) Ventral view of *Kerygmachela kierkegaardi* with visible pharynx (dark grey area) posterior to the mouth. (B) Frontal appendage of *Amplectobelua* sp. (C) Auxiliary spines of *Tamisiocaris borealis*. (D) Frontal appendage of *Isoxys volucris*. (E, F) Ventral views of arthropods showing lateral extent of prominent ventral gnathobasic spines on surmised protopodites/endopods. (E) *Kiisortoqia soperi*. (F) *Siriocaris trollae*.

Amplectobelua sp.

Life habit.

Nektonic. A pair of frontal appendages (Fig. 5.5) comprises the only material currently assigned to *Amplectobelua* sp. From Sirius Passet. Trunk appendages are known from a single *Amplectobelua* taxon which resembles the swimming flaps of *Anomalocaris* (Chen et al., 1994; Cong et al., 2017). There are no endopods associated with them.

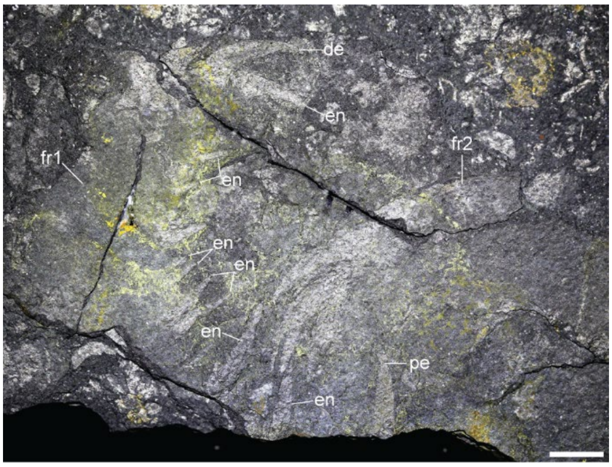

Figure 5.5. ***Amplectobelua*** **sp.** Pair of frontal appendages (fr1, fr2) with fr1 showing a prominent proximal endite, a series of ventral endites, and large distal endites. SP-2016-1170. Scale bar is 5 mm. Abbreviations : de, distalmost endite ; en, endite ; fr, frontal appendage ; pe, proximal endite ;

Trophic role.

Carnivorous predator. *Amplectobelua* is characterized by frontal appendages where serially arranged endites are opposed by a long forwards-facing proximal endite creating an apparatus able to make a pincer-like movement to grasp and/or tear prey (Chen et al., 1994; Hou et al., 1995; Cong et al., 2017). This morphology is also present in *Amplectobelua* sp. (Fig. 5) indicating a predatory trophic role.

Prey size estimation.

Maximally *c.* 37 mm wide. We assume that *Amplectobelua* sp. Caught its prey using the frontal appendages as pincers (see Trophic role) much like chelae in extant crabs and lobsters. The long proximal endite spine would be immobile while podomeres of the frontal appendage would bend down closing the gap between the proximal endite and the rest of the podomere endites (Chen et al., 1994; De Vivo et al., 2021). Thus, we hypothesize that the space between the distalmost endites and the base of the proximal endite represents the maximum width of caught prey, which is 37 mm in the most well-preserved appendage (Fig. 5.4B; Fig. 5.5). However, as the frontal appendage has a dorsal bend, which lowers the measured value, the maximum prey size may have been slightly larger.

Estimated prey.

Chordata sp., *Isoxys volucris*, *Kerygmachela kierkegaardi*, *Kiisortoqia soperi*, *Kleptothule rasmusseni*, *Ooedigera peeli*, *Pauloterminus spinodorsalis*.

Tamisiocaris borealis

Life habit.

Nektonic. The life habit is solely based on phylogenetic bracketing (Vinther et al., 2014) as only the frontal appendages have been described for *Tamisiocaris borealis* (Fig. 5.6).

Figure 5.6. ***Tamisiocaris borealis*.** Frontal appendage showing paired spines with tiny auxiliary spines. Scale bar is 5 mm. Abbreviations: as, auxiliary spines; fr, frontal appendage; sp, spines.

Trophic role.

Suspension-feeder. The frontal appendages of *Tamisiocaris borealis* carry long thin ventral spines equipped with small auxiliary spines (Fig. 5.6) interpreted to function as a mesh for filtering particles while swimming (Vinther et al., 2014).

Prey size estimation.

0.5–2 mm. Vinther *et al.*(2014) compared the mesh of the auxiliary spines to extant taxa and their known prey sizes, giving an estimated prey size range between 0.5–2 mm for *Tamisiocaris borealis* (Fig. 5.4C). This is within the range of smaller mesozooplankton (0.2–20 mm).

Estimated prey.

Small mesozooplankton.

Isoxys volucris

Life habit.

Nektonic. The nektonic life habit of *Isoxys volucris* (Fig. 5.7) has been inferred from comparisons of carapace morphology to extant crustaceans (Williams et al., 1996; Vannier and Chen, 2000) and paddle-like exopods from a single specimen (fig. 2 in Stein et al., 2010). The latter suggests that *Isoxys volucris* used them for swimming as proposed for other *Isoxys* taxa (Vannier et al., 2009). Well-developed spines have been proposed to be anti-predator adaptations (Vannier and Chen, 2000) or aid vertical swimming as has been proposed for other *Isoxys* taxa (Pates et al., 2021). Measurements for *Isoxys volucris* show that the relative spine length decreases with size (ontogeny): they are longest in juveniles and become progressively smaller with size (Fig. 5.7A–D). They are interpreted to have a primarily defensive structure: as spines increase the total sizes of juveniles, they also increase the necessary gape size of predators to ingest them. Whether or not spines had a secondary hydrodynamic role (cf. Pates et al., 2021) is uncertain.

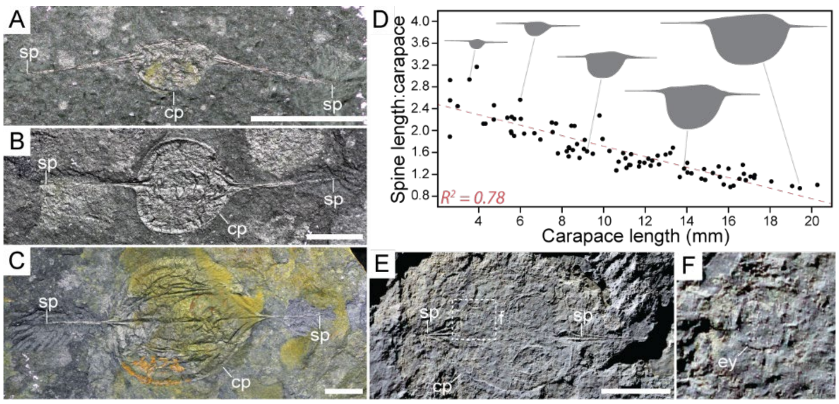

Figure 5.7. ***Isoxys volucris.*** (A–C) Ontogenetic reduction of relative spine length. Note that the white 'sp' lines mark the distal ends of the spines. (A) Juvenile specimen with long spines relative to carapace size (preserved in lateral view). SP-[Block B, Bed 4]. (B) Mid-size specimen (preserved in open 'butterfly' position). SP-2016-546. (C) Large specimen showing relatively short spines relative to carapace size (preserved in open 'butterfly' position). SP-2016-407. (D) Ratios of spine length to carapace length plotted against carapace length showing that relative spine lengths decrease with size illustrated by the red regression line (R^2=0.78). (E) Specimen showing a small, round anterior structure interpreted as an eye (dashed box). SP-[Block A, Bed 23]. (F) Dashed box of c showing close-up of round eye. Scale bars are 5 mm. Abbreviations: cp, carapace; ey, eye; sp, spine.

Trophic role.

Carnivorous predator. The long frontal appendages with presumably well-developed article spines (setae) indicate that it was used as a raptorial appendage (see 'antennula' in Stein et al., 2010). Several *Isoxys* taxa preserve raptorial appendages as well as eyes used to capture prey (Vannier et al., 2009). We find a round structure near the anterior margin (Fig. 5.7E,F) which is consistent with the structure putatively suggested to be an eye (fig. 4C,E in Stein et al., 2010), supporting that *Isoxys volucris*, like other taxa of the genus, was a visual predator.

Prey size estimation.

The prey size was likely dependent on the raptorial appendage used to capture prey (Fig. 5.4D). In the extant red king crab zoea, the minimum prey size is limited by the distance between setae on the maxillipedial endopodite used to catch food whereas maximum prey size can reach that of the zoea itself (Epelbaum and Borisov, 2006). The spines (setae) of *Isoxys volucris* are putatively known from a single specimen where each podomere has a set (fig. 2 in Stein et al., 2010). The minimum distance between the two distalmost preserved sets is 0.5 mm. However, these do not include setae on the shorter distal articles which would give a lower minimum prey size. The carapace of this specimen is *c.* 10 mm long and as the taxon often attains lengths up to 20 mm, the setal distance is extrapolated up to a calculated minimum prey size of 1 mm in large specimens. This corresponds to the size range of mesozooplankton (0.2–20 mm).

Estimated prey.

Small mesozooplankton.

Euarthropoda

Kiisortoqia soperi

Life habit.

Nektobenthic. *Kiisortoqia* has paddle-like exopods reaching more than two-thirds of the exposed endopod length (Fig. 5.8) and lined with setae at its adaxial border (Stein, 2010).

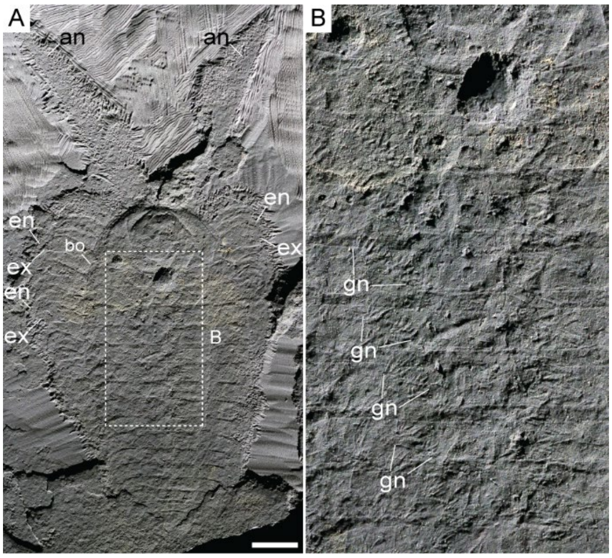

Figure 5.8. ***Kiisortoqia soperi*****.** (A) specimen showing long, thick antennae, paddle-shaped exopods flanking the endopods protruding well beyond the dorsal exoskeleton, and gnathobasic spines (dashed box). SP-2017-1601. (B) Dashed box of (A) showing close-up of gnathobases. Area between the white lines marks their transverse extent; note that it decreases posteriorly, suggesting a food processing function. Scale bar is 5 mm. Abbreviations: bo, distal border of dorsal exoskeleton; en, endopod; ex, exopod; gn, gnathobases.

Trophic role.

Carnivorous predator. The large robust antennae with long spines on each article have been surmised to catch prey (see Stein, 2010 for further discussion). *Kiisortoqia* has 'basipod spines' (cf. Stein, 2010) that may have functioned like gnathobasic spines in masticating prey, supported by the fact that the number of spines on the endopods increases anteriorly towards the mouth (Fig. 5.8B). Additionally, *Kiisortoqia* frequently preserves gut diverticula.

Prey size estimation.

Maximally *c.* 17.6 mm wide. Even though the antennae could potentially have been used to catch prey, the well-developed gnathobasic spines suggest that the legs had an important control on the prey size it could manipulate. We surmise that the maximum prey size corresponds to the width between the distalmost gnathobasic spines on two opposing endopods (Fig. 5.4E). The specimen (fig. 4 in Stein, 2010, 42.7 mm long) shows gnathobasic spines on the left appendages 7.5 mm from the axis, giving a calculated 15 mm breadth between two opposing legs. This suggests a prey size of 17.6 mm when extrapolated to the largest known specimen (50 mm long in fig. 3B in Stein, 2010, excluding one extreme outlier).

Estimated prey.

Chordata sp., *Isoxys volucris*, *Kleptothule rasmusseni*, *Ooedigera peeli*.

Kleptothule rasmusseni

Life habit.

Nektonic. Inferences on the ecology of *Kleptothule* are limited to indirect evidence from its carapace (Fig. 5.9) as only the two inflexible anterior appendages are known (anterior spikes *sensu* Budd, 1995). We surmise that the strongly elongated carapace reflects a nektonic life habit. Elongation of the carapace is an adaptation for nektonic life habits in extant swimming crabs (Hartnoll, 1971) and extinct trilobites (Fortey, 1974) but is probably best exemplified by the extremely specialized hyper-elongated pelagic shrimps of the family Luciferidae (Vereshchaka et al., 2016). On the other hand, hyper-elongation may also be an adaptation to an infaunal life habit as seen in some isopods (Menzies and Barnard, 1959). It is, however, unlikely that *Kleptothule* was infaunal since infaunal arthropods would be expected to have a more laterally compressed body and robustly sclerotized legs to move sediment while digging and the lack of exposure to the epifaunal environment would likely have enhanced its preservational potential. This does not accord with the lack of preserved appendages. Lack of preservation may suggest that the appendages were delicate as seen in, for example, the pelagic fairy shrimp which preserves poorly in the fossil record (Gueriau et al., 2016) and could have been susceptible to decay or disarticulation or effaced during secondary alteration at Sirius Passet through high-grade metamorphosis (Topper et al., 2018).

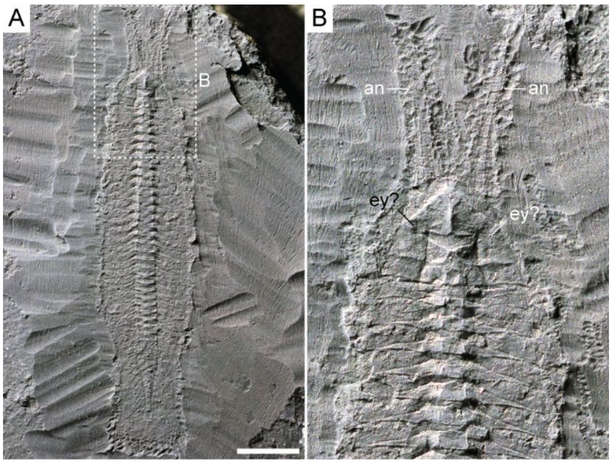

Figure 5.9. ***Kleptothule rasmusseni.*** (A) Representative specimen showing the broadly inflexible antennae (dashed box). SP-2017-903. (B) Dashed box of (A) showing close-up of cephalon and anterior thoracic region. Eyes are rarely obvious in *Kleptothule* but are here tentatively interpreted from effaced structures. Scale bar is 5 mm. Abbreviations: an, antennae; ey?, putative eye.

Trophic role.

Carnivorous predator or suspension-feeder. No post-antennal appendages are preserved to provide evidence for its trophic role. However, a nektonic life habit would imply either a predatory or filter-feeding behavior, and active hunting is perhaps preferred due to the presence of eyes (Vannier et al., 2009).

Prey size estimation.

No evidence hints at the size of its prey. The 'anterior spikes' *sensu* Budd (1995) (Fig. 5.9) were inflexible and probably not used for sensory or manipulating purposes. Many crustacean macrozooplankton taxa show filter-feeding behavior (e.g., krill, mysids, copepods). The lack of preserved appendages could indicate that they were very delicate features that acted as filter-feeding instruments (Reeve, 1963; Hamner et al., 1983) and/or raptorial appendages (Lee et al., 1992). Given the relatively small size of *Kleptothule*, *c.* 30 mm long but only 5–6 mm wide (Budd, 1995; see also Fig. 5.1), it is unlikely that it fed on anything larger than mesozooplankton (0.2–20 mm).

Estimated prey.

Small mesozooplankton.

Pauloterminus spinodorsalis

Life habit.

Nektobenthic. *Pauloterminus spinodorsalis* is a waptiid with long paddle-shaped exopods (Taylor, 2002; Fig. 5.10). Paddle-shaped exopods are also found in another waptiid, *Waptia fieldensis* (Vannier et al., 2018). Although previously believed to have been mostly benthic due to the four anterior pairs of uniramous appendages (Briggs and Whittington, 1985), recent analyses suggest that it was an effective swimmer using its six paddle-shaped appendages for propulsion and large abdomen with a caudal fan for vertical movement and stability (Vannier et al., 2018). *Pauloterminus* does not preserve the same morphological details and the overall number of appendages, and their exact shapes is poorly known. However, the presence of paddle-shaped exopods and a similarly long abdomen with a caudal fan (Fig. 5.10) is consistent with evidence from *Waptia fieldensis* and a similar life habit is inferred here.

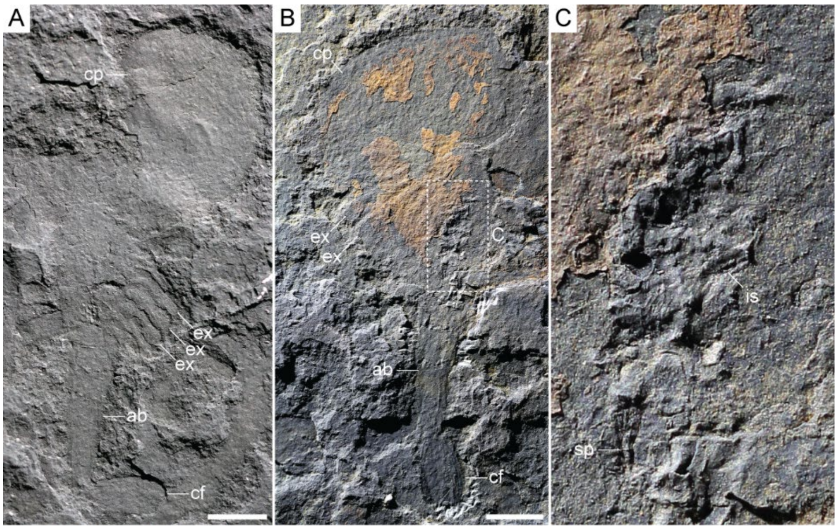

Figure 5.10. *Pauloterminus spinodorsalis*. (A) Specimen showing long, partially broken, paddle-shaped exopods and long abdomen with caudal fan. SP-2016-802. (B) Specimen with *Isoxys volucris* gut contents (dashed box). SP-2016-1147. (C) Dashed box of (B) showing close-up of ingested *Isoxys volucris* specimen with a well-defined spine and crumpled carapace. Scale bars are 5 mm. Abbreviations: ab, abdomen; cp, carapace; cf, caudal fan; ex, exopod; is, *Isoxys volucris*; sp, spine.

Trophic role.

Carnivorous predator. The morphology of head appendages in *Pauloterminus* is currently not properly described, except for the antennae However, *Waptia fieldensis* had head appendages specialized for manipulating and eating food (Vannier et al., 2018). Nonetheless, predation is supported by several examples of gut contents showing an *Isoxys volucris* carapace, in some cases with the reflective film representing the gut.

Prey size estimation.

Maximum width at least 7.4 mm. While *Waptia fieldensis* fed by moving the prey towards its mouth with four, clawed post-maxillular cephalothoracic appendages and using its spiny endites for mastication (Vannier et al., 2018), gut contents shows that *Pauloterminus* was able to ingest relatively large prey without significant mastication (Fig. 5.10C). The presence of an broadly undisturbed *Isoxys volucris* valve (2 mm high, Fig. 5.10C) within the gut of a *Pauloterminus* specimen (carapace 13.4 mm long, Fig. 10B) suggests a prey size of 7.4 mm (shortest axis) when extrapolated to the largest known *Pauloterminus* (maximum carapace length 49.5 mm *sensu* Taylor 2002).

Certain prey (gut content).

Isoxys volucris.

Estimated prey.

Chordata sp., *Kleptothule rasmusseni*.

Siriocaris trollae

Life habit.

Nektobenthic. *Siriocaris* has long paddle-shaped exopods, almost as long as the legs (Lagebro et al., 2009; Fig. 5.11).

Figure 5.11. ***Siriocaris trollae.*** (A) Specimen showing very long antennae and almost equally long exopods and endopods. SP-2017-839. (B) Specimen showing wide, paddle-shaped exopods protruding substantially beyond the dorsal exoskeleton. SP-2016-288. Scale bars are 5 mm. Abbreviations: an, antennae; bo, distal border of dorsal exoskeleton; en, endopod; ex, exopod; gd, gut diverticula.

Trophic role.

Carnivorous predator. *Siriocaris* preserves gnathobasic spines proximally on its legs (Lagebro et al., 2009). The most proximal parts of the legs are not preserved in *Siriocaris*, but the gnathobasic spines suggest it masticated prey. Frequent preservation of gut diverticula also supports carnivory. Antennal setae could have been chemoreceptive, mechanoreceptive, and/or tactile (Boxshall and Jaume, 2015). Long mechanoreceptive antennae, able to sense vibrations in the water, are present in some predatory pelagic decapods (Foxton, 1969; Denton and Gray, 1985) and copepods (Légier-Visser et al., 1986). In the former, the antennae bend backwards to act like the lateral line organ in fish (Denton and Gray, 1985). Antennal mechanoreceptive sensors are able to detect movement before the chemical signals reach the chemoreceptive sensors (Légier-Visser et al., 1986). The large size of *Siriocaris*' dorsal exoskeleton (largest known specimen is 129.4 mm long and 47.4 mm wide, see Fig. 5.11A) exceeds the maximum prey size estimation of other known predators at Sirius Passet which makes it unlikely that the antennae functioned solely as predator detection (Boxshall and Jaume, 2015). We envisage that *Siriocaris* used mainly mechanoreceptors on its long antennae to detect and hunt prey in the water column.

Prey size estimation.

Maximally *c.* 31 mm wide. The comparatively thin antennae do not suggest it functioned like a raptorial appendage. Instead, *Siriocaris* probably caught its prey with its long endopods. The space between the gnathobasic spines may serve as an indication of the maximum prey size that *Siriocaris* was able to manipulate while eating. We therefore surmise that the prey size corresponds to the maximum width between the distalmost gnathobasic spines on two opposing endopods. The distalmost visible spine on fig. 4.1 in Lagebro et al. (2009) is set 13.6 mm from the axis, resulting in a width of 27.2 mm between two such spines on opposing endopods on that specimen (trunk width 41.1 mm). This is likely to give a conservative estimate as the endopods become obscured abaxially by superimposed exopods. When extrapolated to the largest known specimen (trunk width 47.4 mm), it gives an estimated maximum prey size of 31 mm (Fig. 5.4F).

Estimated prey.

Chordata sp., *Isoxys volucris*, *Kiisortoqia soperi*, *Kleptothule rasmusseni*, *Ooedigera peeli*, *Pauloterminus spinodorsalis*.

Deuterostomia

Chordata sp.

Life habit.

Nektobenthic. This chordate, represented by only few specimens, preserves the chevron-shaped segmented muscle blocks, myomeres (Fig. 5.12) and putative dorso-posterior fin. Cephalochordates, cyclostomes, and fish create propulsion to swim by oscillating sideways movement of myomeres (Nursall, 2009). Presence of myomeres in the Cambrian chordate *Pikaia gracilens*, from Burgess Shale, led to its interpretation as a swimmer, probably with a nektobenthic life habit due to its restriction to specific stratigraphic beds (Conway Morris & Caron, 2012). Cambrian chordates resemble modern lancelets that have predominantly benthic life habits, often partly infaunal. While Cambrian chordates are normally regarded as nektonic or nektobenthic (e.g., Conway Morris & Caron, 2012), it is uncertain how much time they actually spent swimming in the water column. The consistent lateral aspect of preservation in the chordates from Sirius Passet does not imply a transversely broad body, which would have suggested it had spent long periods resting on the sea floor.

Figure 5.12. Chordata sp. Specimen showing preserved vertical myomeres characteristic of early chordate fossils. SP-[Block B, Bed 20]. Scale bar is 5 mm. Abbreviations: gt, gut tract; my, myomere.

Trophic role.

Suspension feeder. The trophic role is implied by phylogenetic bracketing. Cephalochordates and tunicates feed by excreting a mucous net from the endostyle in the pharynx which traps particles suspended in the passing water (Godeaux, 1989). A homologous endostyle is also retained in larval lampreys (Ogasawara et al., 2001; Swalla, 2007) although it is lost during metamorphosis. A similar feeding behavior has been surmised for Cambrian non-conodont chordates (Holland and Chen, 2001).

Prey size estimation.

No direct evidence is present to estimate the size of consumed particles. However, most of the particles trapped in the mucous net of larval lampreys are in the size-range 10–30 µm although particles smaller than 5 µm and as large as 200 µm also occur (Mallatt, 1981). This is within the range of nanoplankton to microplankton (2–200µm).

Estimated prey.

Nanoplankton to microplankton.

Ooedigera peeli

Life habit.

Nektonic. The lack of limbs and presence of a laterally compressed tail suggests a nektonic life habit for vetulicolians where the latter would generate propulsion while swimming (Chen and Zhou, 1997; Aldridge et al., 2007; Shu et al., 2010; Vinther et al., 2011b). *Ooedigera peeli* conforms to this general morphology (Vinther et al., 2011; Fig. 5.13) and the lack of specimens showing a dorso-ventrally wide body suggest it was nektonic and not benthic (see Caron, 2005).

Figure 5.13. *Ooedigera peeli*. Specimen displaying (from left to right) tail, large body compartment, and large mouth opening. SP-[unnumbered]. Scale bar is 5 mm. Abbreviations: tl, tail; mo, mouth.

Trophic role.

Suspension feeder. Vetulicolians are generally believed to have fed by actively pumping water currents into the main chamber through the pharynx and expelling the currents through the lateral gill slits (Ou et al., 2012). A similar mode of feeding is seen in extant tunicates (salps) where water is actively pumped through a tightly meshed net of mucous, produced by an endostyle (see also Chordata above), that traps particles suspended in the passing water (Alldredge and Madin, 1982; Sutherland et al., 2010). It is surmised that vetulicolians had a similar filter within the pharynx which would allow them to effectively filter the water currents while swimming (Vinther et al., 2011b; Ou et al., 2012).

Prey size estimation.

No direct evidence is present to estimate the size of consumed particles. However, salps, at the centimetre-scale, get the majority of nutrients from pico- and nanopolankton but can filter even smaller particles from the water current, such as viruses smaller than 0.05 µm (Sutherland et al., 2010). *Ooedigera peeli* is within the size range of these salps and we propose that it was able to filter the same particle range, which is within the size range of picoplankton to nanoplankton (0.2–20 µm).

Estimated prey.

Picoplankton to nanoplankton.

5.5 Food web

The resulting pelagic food web from these estimated predator-prey relationships has four trophic tiers (Fig. 5.14). These tiers contain two taxa as quaternary consumers (*Amplectobelua* sp. *Siriocaris*), four taxa as tertiary consumers (amiskwiiform sp., *Kerygmachela*, *Kiisortoqia*, *Pauloterminus*), three taxa as secondary consumers (*Isoxys volucris*, *Kleptothule*, *Tamisiocaris*), and two taxa as primary consumers (Chordata sp., *Ooedigera*).

Panarthropods dominate the pelagic fauna, especially the upper trophic levels, while deuterostome vetulicolians and chordates comprise the only estimated lower trophic (macrofossil) primary consumers. Remarkably, the large amiskwiiform is an estimated tertiary consumer and one of the largest pelagic taxa in the Sirius Passet biota (Fig. 5.1).

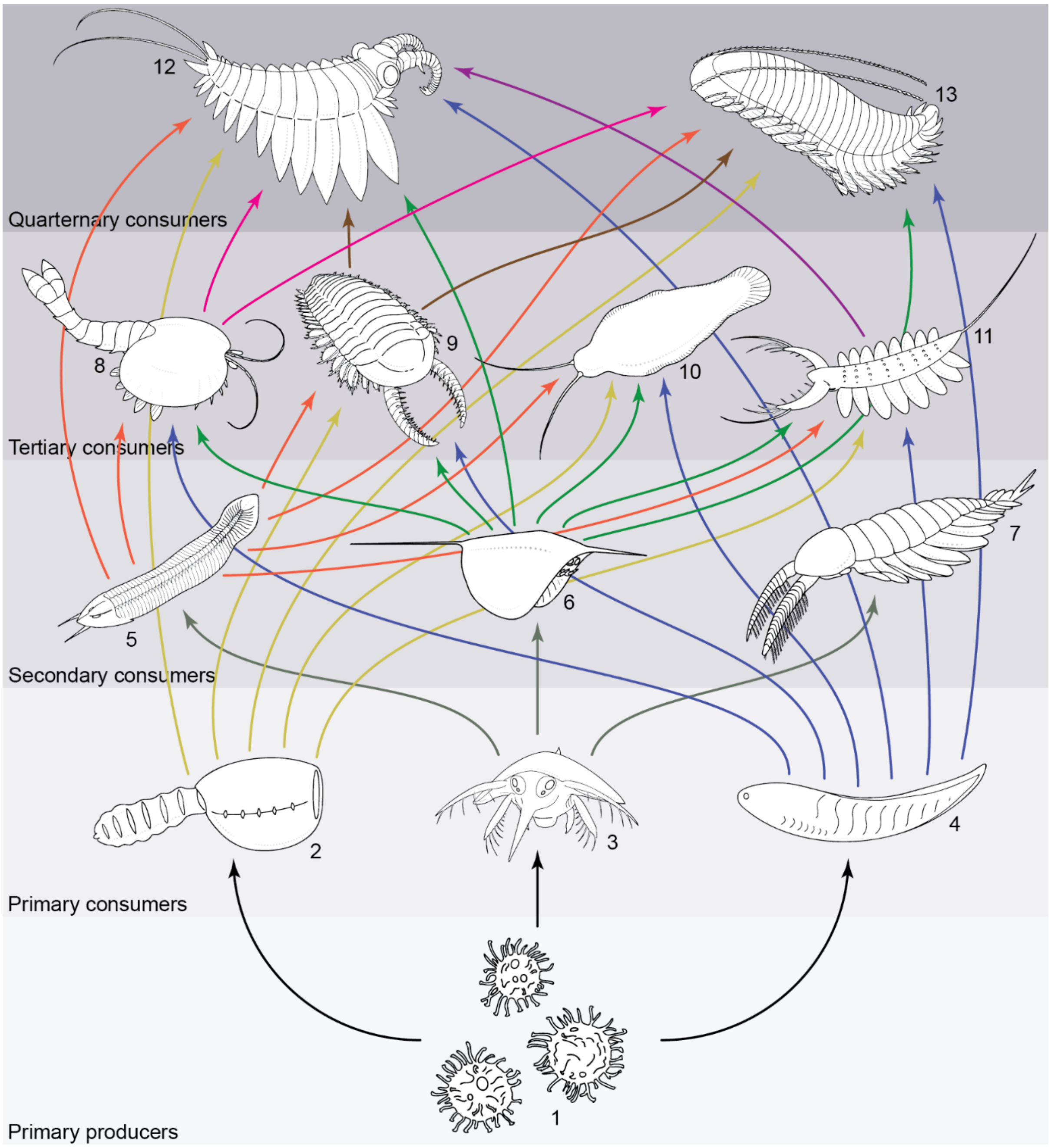

Figure 5.14. Nektonic food web reconstruction for the pelagic Sirius Passet fauna. Key: 1 Phytoplankton, 2 *Ooedigera peeli*, 3 mesozooplankton, 4 Chordata sp., 5 *Kleptothule rasmusseni*, 6 *Isoxys volucris*, 7 *Tamisiocaris borealis*, 8 *Pauloterminus spinodorsalis*, 9 *Kiisortoqia soperi*, 10 Amiskwiiform sp., 11 *Kerygmachela kierkegaardi*, 12 *Amplectobelua* sp., 13 *Siriocaris trollae*. Arrows point to predator taxa; each prey-taxon has a distinctive color.

5.6 Discussion

In this study, we estimate that the trophic structure of pelagic animals in Sirius Passet had four trophic tiers (Fig. 5.14). Upper-trophic levels had higher diversities than lower trophic levels, such as mid-trophic secondary consumers. Lower trophic levels include deuterostome primary consumers such as small chordates. Our results show that apex predators not only consisted of panarthropods, but also a stem-chaetognath. Panarthropod anomalocaridids have long been regarded as the Cambrian apex predators (Whittington and Briggs, 1985; Chen et al., 1994; Paterson et al., 2011; De Vivo et al., 2021) that could possibly feed on prey up to 10 cm in diameter (De Vivo et al., 2021) while Cambrian chaetognaths so far been recognized as small likely-secondary consumers (Vannier et al., 2007; Briggs and Caron, 2017). In Sirius Passet, amiskwiiform sp. was a tertiary consumer feeding on *Isoxys volucris* that had evolved defensive spines most likely as a response to the predation pressure.

These Cambrian top-tier predators differ markedly from modern marine ecosystems which are dominated by chordates. These include fish, sharks, and secondarily aquatic tetrapods, such as whales, which can reach body sizes by far exceeding those of Cambrian predators. By contrast, modern chaetognaths are generally small (1-2 cm long), with a single taxon reaching lengths of ~10 cm (David, 1955). This implies that there has been a marked reorganization of the pelagic food web since the Cambrian: chordates shifted from predominantly small filter-feeding primary consumers (excluding conodonts, Murdock and Smith, 2021) to apex predators. They eventually outcompeted large pelagic panarthropods and stem-chaetognaths that now prevail as small secondary consumers. This shift was likely accelerated by the Devonian radiation of jawed gnathostome fish (Klug et al., 2010).

Sirius Passet's low diversity of mid-trophic secondary consumers shows characteristics of 'wasp-waist' food web structures from (especially) modern upwelling ecosystems (Cury et al., 2000; Bakun, 2006; Kämpf and Chapman, 2016). Wasp-waist ecosystems are characterized by being dominated by a single (or few) small but highly abundant opportunistic mid-trophic taxa serving as a plentiful food source for predators (Rice, 1995; Cury et al., 2000; Griffiths et al., 2013). This taxon will, in theory, singlehandedly transfer all the energy flow from lower to higher trophic levels since it is the sole link between its (zooplankton) prey and its predators (Rice, 1995; but see Griffiths et al., 2013 for a more complex view). Consequently, this crucial taxon has potential to control other populations within the ecosystem by both top-down control of its prey and bottom-up control of its predators (Hunt and McKinnell, 2006): high abundances of the wasp-waist taxon decreases abundances of its prey by consuming them (top-down control) while simultaneously increasing abundance of predators by offering an ample food source (bottom-up control) (Fauchald et al., 2011). This contrasts the classical food web notion that bottom-up controls are most important for ecosystems (e.g., Frederiksen et al., 2006; Antell and Saupe, 2021; but see Baum and Worm, 2009 and Butterfield, 2011 for top-down perspectives). In modern ecosystems, wasp-waist taxa are often small pelagic planktivorous fish, such as anchovies sardines, or krill (Atkinson et al., 2014). They share common traits that include: very high biomass often concentrated in dense swarms, specific synchronized spawning behavior, and ecological bottom-up and top-down control (Atkinson et al., 2014). In Sirius Passet, *Isoxys volucris* fits several of the criteria of a wasp-waist taxon: it is one of only two small-sized secondary consumers (alongside *Kleptothule*, which is also relatively abundant, Harper et al., 2019); by far outnumbers any other taxa (Chapter 4), show temporally restricted synchronized spawning (Chapter 4); and is commonly found within guts of other taxa (see Results; Peel, 2017b). Despite uncertainties about the actual prey of *Isoxys volucris*, and potential biases against other (less sclerotized?) types of gut contents in its predators, the similarities are compelling. Additionally, abundant organic debris on bedding surfaces (Chapter 4) and large filter-feeding nekton (Vinther et al., 2014) are consistent with high-productivity environments such as upwelling zones. If *Isoxys volucris* was a wasp-waist taxon within a Cambrian high-productivity ecosystem in Sirius Passet, it had a major control on the food web and biomass distribution through trophic energy transfer to numerous predators exploiting it as a main food source, as well as on drawing down nutrients to the seabed through the biological pump (Pates et al., 2021). A modern analogue could be krill swarms: they have extraordinarily high abundances and biomass, sustain their ecosystem as a plentiful food source, and contributes substantially to the biological pump by vertical migration and fecal production (Cavan et al., 2019). This would further strengthen that diverse and complex modern-style ecosystems evolved rapidly in the early Cambrian (Dunne et al., 2008). Perhaps mid-trophic taxa with complex behavior were important drivers for this ecological innovation.

Could pelagic wasp-waist ecosystems have existed elsewhere in the Cambrian? Broadly similar bivalved arthropods are also the most common taxa in Burgess Shale (Caron and Jackson, 2008) and Chengjiang (Zhao et al., 2009). In Burgess Shale, the bradoriid *Liangshanella* sp. comprise 12% of the assemblages in the allochthonous event beds (Caron and Jackson, 2008). In Chengjiang, *Kunmingella douvillei* comprise 19.2% in the allochthonous event beds but 61.9% in the temporally biased (par)autochthonous background beds (Zhao et al., 2009), a ratio closely similar to *Isoxys volucris* in Sirius Passet (Chapter 4). *Kunmingella douvillei* likely had an important ecological role since it frequently occurs densely in coprolites, but its appendage morphology suggests a benthic, rather than nektonic, life habit (Shu et al., 1999). Direct comparisons of ecologic roles with *Isoxys volucris* are, however, difficult since the fossil assemblages in Burgess Shale and Chengjiang have different taphonomic biases (Chapter 4).

Broader comparisons between pelagic food web structures in Burgess Shale and Chengjiang to investigate variability in Cambrian pelagic realms require consistent methods with similar assumptions. For example, the quantitative food web analysis for Burgess Shale and Chengjiang (Dunne et al., 2008), interpreted to show organizational similarities between Cambrian and modern food webs, mostly uses total size relationships to estimate predator-prey relationships instead of size estimations from functional morphology analyses. Moreover, they combine benthic and pelagic faunas in a single, undistinguished, network. Comparisons with the pelagic food web from Sirius Passet would therefore require extensive re-analysis of the Burgess Shale and Chengjiang material, which is outside the scope of this study that focus solely on Sirius Passet.

5.7 Conclusions

Reconstructing Cambrian ecosystem structures is challenging due to the biased nature of most Lagerstätten and has consequently focused mostly on autecological niches with multiple examples mirroring those of modern ecosystems. Hence Cambrian ecosystem's broader-scale ecological structures (i.e., food web) and its evolution remain poorly understood.

However, our results from the Sirius Passet biota indicate potential for a four-tier trophic macrofaunal structure with a relatively high diversity of upper trophic predators notably occupied by comparatively large panarthropods and stem-chaetognaths. These predators fed on a low-diversity assemblage of mid-trophic taxa, most likely the hyperabundant *Isoxys volucris*. *Isoxys volucris*, and the ecosystem structure in general, share characteristics with modern krill-based 'wasp-waist' ecosystems (Atkinson et al., 2014). If so, *Isoxys volucris* may have had immense importance in shaping the ecosystem at both small scale, by controlling the food web and energy transfer, and large scale, by fuelling the biological pump (cf. Pates et al., 2021). In that case, abundant mid-trophic taxa should be considered, at least, equally to top-tier predators when analyzing drivers of early evolution of pelagic ecosystems. These pelagic ecosystem structures evolved rapidly in the early Cambrian and have since been resilient to major taxonomic reorganizations.

Chapter 6

Summary & perspectives

Author contributions

This chapter is not intended for publication. I wrote it with minor input from Jakob Vinther.

6.1 Thesis summary

This thesis aims to explore the ecosystem of a Cambrian biota by determining the interplay between taphonomic biases, depositional environment, and ecosystem of a given paleoenvironment through detailed case studies from a geologically complex and poorly understood Lagerstätte. To do this, I used a multidisciplinary approach involving metamorphic petrology (Chapter 2), quantitative taphonomy (Chapter 3), integrated microstratigraphic analyses (Chapter 4), as well as qualitative autecology (Chapter 5). I show that properly contextualizing Lagerstätte can both improve our understanding of the secondary/tertiary biases and their effects on biotas (chapters 2–4) and reveal new primary ecosystem information (chapters 4–5). Here, I first summarize these findings and highlight potential implications for other biotas, and then how they present a new context for the Sirius Passet Lagerstätte.

In Chapter 2, I show that late-stage metamorphism can almost completely overprint primary taphonomic pathways and bias the fossil record. Primarily phosphatized muscles are replaced by predominantly silica with the matrix-related paragenetic sequence: apatite > quarts > chlorite +/- muscovite ('clays') > chloritoid > xenotime +/- monazite. Replacement is selective since phosphatized guts retain their apatite (but recrystallized). Metamorphic replacement is a double-edged sword: silica appears to be more stable than apatite during progressive metamorphism and weathering, and silicified tissues thus preserve most detailed ultrastructures in Sirius Passet. At the same time, muscovite completely overprints and removes ultrastructure. This, in addition to the selective nature of replacements, creates a bias on biotas in similar metapelites. Another metamorphic bias in Sirius Passet is the complete volatilization of small carbonaceous fossils into unidentifiable kerogen structures that entirely removes an ecological window present elsewhere in the Buen Formation (Slater et al., 2018). I reject a hypothesized taphonomic pathway for exceptional preservation (by silicification) unique to Sirius Passet (Strang et al., 2016a, 2016b) and replaced it with a much more common pathway; phosphatization (Dornbos, 2010). If late-stage processes (e.g., metamorphism) in Sirius Passet can obscure taphonomic pathways in Sirius Passet, it may obscure pathways elsewhere too. 'Clays' (i.e., aluminosilicates), a late-stage mineral in Sirius Passet, have been proposed to be a unique taphonomic pathway for three-dimensional muscle in Soom Shale (Gabbott et al., 2001), and have been used to infer ingested sediment in three-dimensional guts in some arthropods (Hou and Bergström, 1997; Bergström et al., 2007). However, both preservational styles are consistent with late-stage overprints (Butterfield, 2002; Butterfield et al., 2007a; Gabbott et al., 2017) of primarily phosphatized tissues (Butterfield, 2002). My work supports that recognizing late-stage overprints gives fewer, more consistent pathways for exceptional preservation of labile soft tissues (Butterfield, 2002; Butterfield et al., 2007b), consequently with more predictable bias on the fossil record.

In Chapter 3, I build on Chapter 2 to determine important controls and their biases on phosphatisation. I show that a large quantitative dataset of taxonomically variable phosphatized tissues in Sirius Passet reveals preservational patterns. Using these, I identify five controls: taxonomy, tissue, microenvironments, size, and diet. Taxonomical control is the sum of all controls within a given taxon (Wilby and Briggs, 1997; Wilson et al., 2016). Tissues control where phosphatization can nucleate and what it can replace by primarily their substrates and phosphate content (Wilby, 1993). Microenvironmental control is crucial and their development dictates in which region phosphatization-prone tissues preserve (Sagemann et al., 1999). Size controls the minimum (ontogenetic) threshold for a specimen to phosphatize and is likely dependent on the microenvironmental control (Allison, 1988d). Diet is a minor control on mainly the phosphatization of gut tracts (Lerosey-Aubril et al., 2012). None of these controls guarantees phosphatization individually and they cannot explain the total distribution of phosphatization in Sirius Passet. I then assess each of their biases on the fossil assemblages. Phosphatization appears unlikely to initiate in some tissues, such as most nervous systems (except under extraordinary biological circumstances, such as in gnathiferan stem-chaetognaths). Overall, the most prevalent tissues to phosphatize in Sirius Passet are certain groups of muscle tissue in each taxon while digestive tracts are more common elsewhere in BST sites with less common occurrences of phosphatized soft tissue. Microenvironments may be restricted to specific regions of carcasses, and may not develop at all in small taxa/juveniles or taxa with anatomical features that inhibit phosphatization (e.g., Clements et al., 2017). Differences in taxonomic distribution of phosphatized tissues between deposits suggest that the hierarchy of these controls varies depending on external, environmental controls. My work gives a framework to identify biased in other deposits and show that laboratory experiments should be based on multiple taxa/sizes given the highly biased nature of phosphatization.

In Chapter 4, I show that the temporal bias in Sirius Passet is low enough to preserve population dynamics. Fossil assemblages with high proportions of articulated specimens and preserved labile soft tissues present on bedding surfaces are interpreted to reflect (par-)autochthonous census assemblages with limited time averaging and transportation. Two (of 20) bedding surfaces in an 8 cm thick interval show mass assemblages of juvenile *Isoxys volucris* specimens interpreted as synchronized mass spawnings. Together, these two beds comprise a juvenile peak in the overall bimodal distribution. I argue that similar patterns are poorly preserved in more temporally biased Lagerstätten, due to punctuated deposition or higher time-averaging with BST preservation, such as Burgess Shale and Chengjiang. I also demonstrate how progressive time-averaging suppresses temporal patterns until multimodal distributions are effectively absorbed by the major mode. This presents a possible interpretation for bimodal distributions reported from other Lagerstätte: *Marrella splendens* (García-Bellido and Collins, 2006), *Canadaspis perfecta* (Briggs, 1978), and *Naraoia magna* (Mayers et al., 2019) in Burgess Shale, and *Misszhouia longicaudata* (Mayers et al., 2019) in Chengjiang. While these distributions may hint at population dynamics, such as mass spawnings, they remain unresolvable without a continuous high-resolution temporal record as in Sirius Passet. My finding implies that synchronized mass spawning behavior had evolved already by the early Cambrian. Mass spawning is a highly successful, widely applied reproductive strategy (Ims, 1990). It is well-known in one of the most successful modern animals in terms of biomass, the krill (Bar-On et al., 2018; Meyer et al., 2020). I argue that *Isoxys volucris* population dynamics support rapid establishment of marine ecosystems with similarities in reproductive behavior and niches that resemble modern systems in several respects (e.g., Vannier et al., 2007). Since mass spawnings in modern animals are temporally synchronized with recurring environmental cues (Ims, 1990), I conclude that Sirius Passet can capture seasonal dynamics within the preserved biota.

Finally, in Chapter 5, I build on the parautochthonous interpretation of Sirius Passet in Chapter 4 to reconstruct the trophic structure of the within-habitat pelagic fauna. I show that panarthropods and stem-chaetognaths were apex predators while chordates were small primary consumers, a contrast to the vertebrate-dominated pelagic faunas in modern marine ecosystems. I also show that the food web structure has characteristics of a modern wasp-waist ecosystem (Cury et al., 2000). Higher trophic levels were comparatively diverse while lower levels were less so. One particular secondary consumer, *Isoxys volucris*, numerically dominates the biota. I interpret this as the wasp-waist taxon, again comparable to modern krill (cf. Atkinson et al., 2014): it likely occurred in very dense, large swarms, had synchronized spawning behavior (Chapter 4), and exploited the abundant food (zooplankton) in a high-productivity epipelagic environment. As the dominant mid-trophic link between lower levels (i.e., zooplankton and phytoplankton) and higher-level predators (i.e., tertiary and quaternary consumers), *Isoxys volucris* would have had a strong control on energy transfer through the food web and therefore both top-down control on its prey and bottom-up control on its predators (Hunt and McKinnell, 2006). Likewise, its sheer abundance would have had an immense impact on the biological pump (e.g., Pates et al., 2021), like modern krill (Cavan et al., 2019).

6.2 A new depositional context for the Sirius Passet biota

A full revision of the depositional environment for Sirius Passet is beyond the scope of this thesis. However, my thesis does provide a new contextual framework for future work. In Chapter 4, I argue that the Sirius Passet biota was deposited in a high-productivity prodelta environment by dilute, low-energy gravity flows, possibly hyperpycnal. Deposition was highly frequent, without evidence for significant sedimentation gaps or reworking, resulting in minimal temporal bias. Flows may have been able to encapsulate and transport organisms, but most of the benthic and pelagic fauna was buried *in situ* on the seafloor. In Chapter 5, I show that the pelagic ecosystem structure is consistent with a high productivity paleoenvironment that may have created benthic hypoxic or anoxic conditions. Perhaps the high productivity was sustained by inorganic nutrients from a river discharge plume (Smith and Demaster, 1996; Macias et al., 2018). River plumes may build up sediment at their mouth to trigger occasional hyperpycnal gravity flows (Mulder et al., 2003) that can be highly frequent (>1 per year for sediment-rich rivers; Mulder and Syvitski, 1995) and flow up to 700 km away from the river mouth (Nakajima, 2006). Altogether, river plumes may represent a viable explanation for both the high-productivity ecosystem and apparently frequent deposition of stacked, dilute beds with diffuse boundaries (Bhattacharya and MacEachern, 2009).

6.3 Did a high-productivity palaeoenvironment create Sirius Passet's uniquely dense, exceptionally preserved fossil assemblages?

The Sirius Passet ecosystem may have controlled exceptional preservation. High surface-water productivity is often associated with bottom-water hypoxia or anoxia in modern (Naqvi et al., 2000; Grantham et al., 2004) and Cambrian (Liu et al., 2018) environments. Large volumes of organic matter (e.g., phytoplankton) settle on the sea floor and its decay consumes the available oxygen and creates an oxygen minimum zone (OMZ) within a stratified water column (Levin, 2003). Benthic communities of low-oxygen tolerant taxa in OMZ's show low diversities but high abundances (Levin, 2003), and do not preclude considerable biomass despite the low oxygen concentrations (Levin et al., 2002; Gallardo et al., 2004; Zettler et al., 2009), possibly because the high food availability outweighs the disadvantages of low oxygen (Levin, 2003). Sirius Passet has been surmised to inhabit the OMZ (Hammarlund et al., 2018) which may explain the remarkably high densities of (par)autochthonous fossils compared to other Lagerstätten (Chapter 4): high primary productivity sustained a densely populated (e.g., high biomass) pelagic wasp-waist ecosystem (Chapter 5) that would eventually settle on the seafloor after their death alongside high volumes of organic debris, in turn creating an OMZ at the seafloor exploited by dense aggregations of low-oxygen tolerant taxa.

Since anoxia is a prerequisite for 'Burgess Shale'-type preservation (Gaines et al., 2012) and phosphatization (Briggs & Kear, 1993), the benthic low-oxygen environment, produced by a high-productivity ecosystem, likely facilitated the exceptional preservation of dense assemblages once buried. Initial decay of these dense assemblages of organic matter ensured an ample phosphorus source enabling the highly frequent anatomical preservation by phosphatization (Chapter 3). Consequently, the epipelagic ecosystem may have been a major control on the paleoenvironment to make Sirius Passet both a Konservat and Konzentrat Lagerstätte.

6.4 Resolved questions and avenues of future research on Sirius Passet

One of the goals of this thesis is to test the merits of several previously proposed hypotheses for Sirius Passet and its taphonomic pathways. Here, I provide a brief overview of the main hypotheses and whether my thesis confirms, support, or rejects them.

- *Sirius Passet was deposited by dilute gravity flows rather than hemipelagic fallout* (Strang et al., 2016b). Confirmed: The stacked, millimeter-thick beds with occasional vague grading confirm low-energy gravity flows (Chapter 4).
- *Sirius Passet shows a unique taphonomic pathway for labile soft tissues by silicification* (Strang et al., 2016b). Rejected: Silica in preserved tissues is a late-stage metamorphic replacement of primarily phosphatized tissues. Instead, Sirius Passet shares its taphonomic pathways with Burgess Shale and other Cambrian BST Lagerstätten (Chapter 2).
- *Phosphatization is taxonomically biased* (Wilby & Briggs, 1997). Confirmed: The taxonomic bias is dependent on multiple controls, such as ability to create the proper microenvironment, tissue composition and structure, organismal size, and, to a lesser degree, diet (Chapter 3).
- *The Sirius Passet fauna lived in or near an oxygen minimum zone* (Hammarlund, et al., 2018): Unconfirmed, but supported: Highly dense, exceptionally preserved, *in situ* fossil assemblages with low diversity suggest an oxygen minimum zone with high food input, possibly from highly productive surface waters (Chapters 4, 5, and 6.3)
- *Microbial mats are responsible for high-relief preservation of autochthonous, benthic, mat-dwelling communities on bedding surfaces contra flattened, kerogenous films of allochthonous, mixed nektonic and infaunal communities within beds* (Harper et al., 2019). Rejected: Both benthic and nektonic fossils co-occur in assemblages preserved on bedding surfaces. The vast majority of these fossils, including high-relief arthropods, are not associated with the occasional and patchy microbial mats (Chapter 4), suggesting that their taphonomic pathways is carbonaceous preservation with taxonomically dependent relief.

Sirius Passet offers a natural laboratory with immense potential to understand Cambrian ecosystems. The new context for Sirius Passet opens new avenues of research with many questions still unanswered. Some of these research questions are outlined below.

- Microstratigraphic analyses of other intervals will give us a better understanding of the full depositional spectrum of Sirius Passet and its relationship to possible ecological variation, including the role of microbial mats.
- A quantitative community analysis through the entire section (the original aim of my thesis) may open a window to the stability of Cambrian communities and their responses (regime shifts?) to short-term (decadal?) environmental changes, such as e.g., oxygen levels reflected by the horizontal trace fossils or, if preserved post-metamorphism, geochemical proxies.
- A full, detailed survey of gut contents may reveal true ecological predator-prey relationships to establish more robust food webs, also for the benthos. Methods using gut contents are also used by marine biologists to explore modern food webs, which offers an opportunity to directly compare results.
- Weathering destroys mineralized tissues and forms iron oxide crusts on specific bedding surfaces that obscure low-relief fossil assemblages and bias ecosystem reconstructions. The depositional control and impact on bed-by-bed community analyses of this particular aspect is uncertain. Any bias would be relevant for community analyses of other pyritized and weathered Lagerstätten.

References

Abelmann, A. et al., 2015, The seasonal sea-ice zone in the glacial Southern Ocean as a carbon sink: Nature Communications, p. 6:8136, doi:10.1038/ncomms9136.

Aldridge, R.J., Briggs, D.E.G., Smith, M.P., Clarkson, E.N.K., and Clark, N.D.L., 1993, The anatomy of conodonts: Philosophical Transactions of the Royal Society of London. Series B: Biological Sciences, v. 340, p. 405–421, doi:10.1098/rstb.1993.0082.

Aldridge, R.J., Hou, X.-G., Siveter, D.J., Siveter, D.J., and Gabbott, S.E., 2007, The systematics and phylogenetic relationships of vetulicolians: Palaeontology, v. 50, p. 131–168, doi:10.1111/j.1475-4983.2006.00606.x.

Alldredge, A.L., and Madin, L.P., 1982, Pelagic tunicates: Unique herbivores in the marine plankton: BioScience, v. 32, p. 655–663, doi:10.2307/1308815.

Allison, P.A., 1988a, Konservat-Lagerstätten: Cause and Classification: Paleobiology, v. 14, p. 331–344.

Allison, P.A., 1988b, Phosphatized soft-bodied squids from the Jurassic Oxford Clay: Lethaia, v. 21, p. 403–410, doi:10.1111/j.1502-3931.1988.tb01769.x.

Allison, P.A., 1986, Soft-bodied animals in the fossil record: the role of decay in fragmentation during transport.: Geology, v. 14, p. 979–981, doi:10.1130/0091-7613(1986)14<979:SAITFR>2.0.CO;2.

Allison, P.A., 1988c, Taphonomy of the Eocene London clay biota: Palaeontology, v. 31, p. 1079–1100.

Allison, P.A., 1988d, The Role of Anoxia in the Decay and Mineralization of Proteinaceous Macro-Fossils: Paleobiology, v. 14, p. 139–154.

Anderson, E.P., Schiffbauer, J.D., and Xiao, S., 2011, Taphonomic study of Ediacaran organic-walled fossils confirms the importance of clay minerals and pyrite in Burgess Shale-type preservation: Geology, v. 39, p. 643–646, doi:10.1130/G31969.1.

Anderson, R.P., Tosca, N.J., Cinque, G., Frogley, M.D., Lekkas, I., Akey, A., Hughes, G.M., Bergmann, K.D., Knoll, A.H., and Briggs, D.E.G., 2020a, Aluminosilicate haloes preserve complex life approximately 800 million years ago: Interface Focus, v. 10, doi:10.1098/rsfs.2020.0011rsfs20200011.

Anderson, R.P., Tosca, N.J., Gaines, R.R., Koch, N.M., and Briggs, D.E.G., 2018, A mineralogical signature for Burgess Shale-type fossilization: Geology, v. 46, p. 347–

350, doi:10.1130/G39941.1.

Anderson, R.P., Tosca, N.J., Saupe, E.E., Wade, J., and Briggs, D.E.G., 2020b, Early formation and taphonomic significance of kaolinite associated with Burgess Shale fossils: Geology, v. 49, p. 1–5, doi:10.1130/G48067.1.

André, L., Cardinal, D., Alleman, L.Y., and Moorbath, S., 2006, Silicon isotopes in ~3.8 Ga West Greenland rocks as clues to the Eoarchaean supracrustal Si cycle: Earth and Planetary Science Letters, v. 245, p. 162–173, doi:10.1016/j.epsl.2006.02.046.

Antell, G.S., and Saupe, E.E., 2021, Bottom-up controls, ecological revolutions and diversification in the oceans through time: Current Biology, v. 31, p. R1237–R1251, doi:10.1016/j.cub.2021.08.069.

Atkinson, A., Hill, S.L., Barange, M., Pakhomov, E.A., Raubenheimer, D., Schmidt, K., Simpson, S.J., and Reiss, C., 2014, Sardine cycles, krill declines, and locust plagues: Revisiting "wasp-waist" food webs: Trends in Ecology and Evolution, v. 29, p. 309–316, doi:10.1016/j.tree.2014.03.011.

Babcock, L.E., and Peel, J.S., 2007, Palaeobiology, taphonomy and stratigraphic significance of the trilobite *Buenellus* from the Sirius Passet Biota, Cambrian of North Greenland: Memoirs of the Association of Australiasian Palaeontologists, v. 34, p. 401–418.

Bakun, A., 2006, Wasp-waist populations and marine ecosystem dynamics: Navigating the "predator pit" topographies: Progress in Oceanography, v. 68, p. 271–288, doi:10.1016/j.pocean.2006.02.004.

Bar-On, Y.M., Phillips, R., and Milo, R., 2018, The biomass distribution on Earth: Proceedings of the National Academy of Sciences of the United States of America, v. 115, p. 6506–6511, doi:10.1073/pnas.1711842115.

Bath Enright, O.G., Minter, N.J., and Sumner, E.J., 2017, Palaeoecological implications of the preservation potential of soft-bodied organisms in sediment-density flows: Testing turbulent waters: Royal Society Open Science, v. 4, doi:10.1098/rsos.170212.

Bath Enright, O.G., Minter, N.J., Sumner, E.J., Mángano, M.G., and Buatois, L.A., 2021, Flume experiments reveal flows in the Burgess Shale can sample and transport organisms across substantial distances: Communications Earth & Environment, v. 2, p. 1–7, doi:10.1038/s43247-021-00176-w.

Baum, J.K., and Worm, B., 2009, Cascading top-down effects of changing oceanic predator abundances: Journal of Animal Ecology, v. 78, p. 699–714, doi:10.1111/j.1365-

2656.2009.01531.x.

Bengtson, S., 2002, Origins and Early Evolution of Predation: The Paleontological Society Papers, v. 8, p. 289–318, doi:10.1017/s1089332600001133.

Bergström, J., Hou, X.G., and Hålenius, U., 2007, Gut contents and feeding in the cambrian arthropod *Naraoia*: Gff, v. 129, p. 71–76, doi:10.1080/11035890701292071.

Bhattacharya, J.P., and MacEachern, J.A., 2009, Hyperpycnal rivers and prodeltaic shelves in the cretaceous seaway of North America: Journal of Sedimentary Research, v. 79, p. 184–209, doi:10.2110/jsr.2009.026.

Bicknell, R.D.C., Holmes, J.D., Edgecombe, G.D., Losso, S.R., Ortega-Hernández, J., Wroe, S., and Paterson, J.R., 2021, Biomechanical analyses of Cambrian euarthropod limbs reveal their effectiveness in mastication and durophagy: Proceedings of the Royal Society B: Biological Sciences, v. 288, doi:10.1098/rspb.2020.2075.

Bicknell, R.D.C., Paterson, J.R., Caron, J.B., and Skovsted, C.B., 2018, The gnathobasic spine microstructure of recent and Silurian chelicerates and the Cambrian artiopodan Sidneyia: Functional and evolutionary implications: Arthropod Structure and Development, v. 47, p. 12–24, doi:10.1016/j.asd.2017.12.001.

Blaker, M.., 1988, A new genus of nevadiid trilobite from the Buen Formation (Early Cambrian) of Peary Land, central North Greenland: Rapport Grønlands Geologiske Undersøgelse, v. 137, p. 33–41, doi:10.34194/rapggu.v137.8011.

Boomer, I., Horne, D.J., and Slipper, I.J., 2003, The Use of Ostracods in Palaeoenvironmental Studies, or What can you do with an Ostracod Shell? The Paleontological Society Papers, v. 9, p. 153–180, doi:10.1017/s1089332600002199.

Botting, J., Cárdenas, P., and Peel, J.S., 2014, A crown-group demosponge from the early Cambrian Sirius Passet Biota, North Greenland: Palaeontology, doi:10.1111/pala.12133.

Botting, J.P., and Peel, J.S., 2016, Early Cambrian sponges of the Sirius Passet Biota, North Greenland: Papers in Palaeontology, v. 2, p. 463–487, doi:10.1002/spp2.1048.

Boudec, A. Le, Ineson, J., Rosing, M., Døssing, L., Martineau, F., Lécuyer, C., and Albarède, F., 2014, Geochemistry of the Cambrian Sirius Passet Lagerstätte, Northern Greenland: Geochemistry, Geophysics, Geosystems, v. 15, p. 886–904, doi:10.1002/2013GC005068.

Boxshall, G., and Jaume, D., 2015, Antennules and Antennae in the Crustacea, *in* Watling, L. and Thiel, M. eds., Functional Morphology and Diversity, Oxford, UK, Oxford

University Press, p. 199–236, doi:10.1093/acprof:osobl/9780195398038.003.0007.

Bradley, W.H., 1946, Coprolites from the Bridger Formation of Wyoming, their composition and microorganisms: American Journal of Science, v. 244, p. 215–239, doi:10.2475/ajs.244.3.215.

Brett, C.E., and Baird, G.C., 1986, Comparative taphonomy: a key to paleoenvironmental interpretation based on fossil preservation.: Palaios, v. 1, p. 207–227, doi:10.2307/3514686.

Brett, C.E., and Walker, S.E., 2002, Predators and Predation in Paleozoic Marine Environments: The Paleontological Society Papers, v. 8, p. 93–118, doi:10.1017/s1089332600001078.

Briggs, D.E.G., 1978, The morphology, mode of life, and affinities of *Canadaspis perfecta* (Crustacea: Phyllocarida), Middle Cambrian, Burgess Shale, British Columbia: Philosophical Transactions of the Royal Society of London. Series B, v. 281, p. 439–487.

Briggs, D.E.G., 2003, The role of decay and mineralization in the preservation of soft-bodied fossils: Annual Review of Earth and Planetary Sciences, v. 31, p. 275–301, doi:10.1146/annurev.earth.31.100901.144746.

Briggs, D.E.G., and Caron, J.B., 2017, A Large Cambrian Chaetognath with Supernumerary Grasping Spines: Current Biology, v. 27, p. 2536- 2543.e1, doi:10.1016/j.cub.2017.07.003.

Briggs, D.E.G., and Collins, D., 1999, The arthropod *Alalcomenaeus cambricus* Simonetta, from the Middle Cambrian Burgess Shale of British Columbia: Palaeontology, v. 42, p. 953–977, doi:10.1111/1475-4983.00104.

Briggs, D.E.G., and Fortey, R.A., 2005, Wonderful strife: systematics, stem groups, and the phylogenetic signal of the Cambrian radiation: Paleobiology, v. 31, p. 94–112, doi:10.1666/0094-8373(2005)031[0094:wsssga]2.0.co;2.

Briggs, D.E.G., and Kear, A.J., 1994, Decay and mineralization of shrimps: Palaios, v. 9, p. 431–456, doi:10.2307/3515135.

Briggs, D.E.G., and Kear, A.J., 1993, Fossilization of soft-tissues in the laboratory: Science, v. 259, p. 1439–14424.

Briggs, D.E.G., Kear, A.J., Martill, D.M., and Wilby, P.R., 1993, Phosphatization of soft-tissues in experiments and fossils: Journal of the Geological Society, v. 150, p. 1035–

1038, doi:10.1144/gsjgs.150.6.1035.
Briggs, D.E.G., and Nedin, C., 1997, The taphonomy and affinities of the problematic fossil *Myoscolex* from the Lower Cambrian Emu Bay Shale of South Australia: Journal of Paleontology, v. 71, p. 22–32.
Briggs, D.E.G., Raiswell, R., Bottrell, S.H., Hatfield, D., and Bartels, C., 1996, Controls on the pyritization of exceptionally preserved fossils: an analysis of the Lower Devonian Hunsrück Slate of Germany: American Journal of Science, v. 296, p. 633–663.
Briggs, D.E.G., and Whittington, H.B., 1985, Modes of life of arthropods from the Burgess Shale, British Columbia: Earth and Environmental Science Transactions of The Royal Society of Edinburgh, v. 76, p. 149–160, doi:10.1017/S0263593300010415.
Briggs, D.E.G., and Wilby, P.R., 1996, The role of the calcium carbonate-calcium phosphate switch in the mineralization of soft-bodied fossils: Journal of the Geological Society, v. 153, p. 665–668, doi:10.1144/gsjgs.153.5.0665.
Brinton, E., 1976, Population biology of *Euphausia pacifica* off Southern California: Fishery Bulletin, v. 74, p. 733–762.
Broce, J.S., and Schiffbauer, J.D., 2017, Taphonomic analysis of Cambrian vermiform fossils of Utah and Nevada, and implications for the chemistry of Burgess Shale-type preservation: Palaios, v. 32, p. 600–619, doi:10.2110/palo.2017.011.
Brose, U., Jonsson, T., Berlow, E.L., Warren, P., Banasek-Richter, C., Bersier, L.F., Blanchard, J.L., Brey, T., Carpenter, S.R., Blandenier, M.F.C., and Cushing, L., 2006, Consumer–resource body-size relationships in natural food webs: Ecology, v. 87, p. 2411-2417, doi: 10.1890/0012-9658(2006)87[2411:CBRINF]2.0.CO;2.
Bruton, D.L., 1981, The arthropod *Sidneyia inexpectans*, Middle Cambrian, Burgess Shale, British Columbia: Philosophical Transactions of the Royal Society of London B: Biological Sciences, v. 295, p. 619–653, doi:10.1098/rstb.1981.0164.
Bucher, K., and Grapes, R., 2011, Petrogenesis of metamorphic rocks: Dordrecht London New York, Springer-Verlag, 428 p.
Budd, G.E., 1993, A Cambrian gilled lobopod from Greenland: Nature, v. 364, p. 709–711, doi:10.1038/364709a0.
Budd, G.E., 1999, A Nektaspid arthropod from the Early Cambrian Sirius Passet fauna, with a description of retrodeformation based on functional morphology: Palaeontology, v. 42, p. 99–122, doi:10.1111/1475-4983.00064.

Budd, G.E., 1998a, Arthropod body-plan evolution in the Cambrian with an example from anomalocaridid muscle: Lethaia, v. 31, p. 197–210, doi:10.1111/j.1502-3931.1998.tb00508.x.

Budd, G.E., 2011, *Campanamuta mantonae* gen. et. sp. nov., an exceptionally preserved arthropod from the Sirius Passet Fauna (Buen Formation, lower Cambrian, North Greenland): Journal of Systematic Palaeontology, v. 9, p. 217–260, doi:10.1080/14772019.2010.492644.

Budd, G.E., 1995, *Kleptothule rasmusseni* gen. et sp. nov.: An ?olenellinid-like trilobite from the Sirius Passet fauna (Buen Formation, Lower Cambrian, North Greenland): Transactions of the Royal Society of Edinburgh: Earth Sciences, v. 86, p. 1–12, doi:10.1017/S0263593300002121.

Budd, G.E., 1997, Stem group arthropods from the Lower Cambrian Sirius Passet fauna of North Greenland, *in* Fortey, R.A. and Thomas, R.H. eds., Arthropod Relationships, Dordrecht, Springer, p. 125–138, doi:https://doi.org/10.1007/978-94-011-4904-4_11.

Budd, G.E., 1998b, The morphology and phylogenetic significance of *Kerygmachela kierkegaardi* Budd (Buen Formation, Lower Cambrian, N Greenland): Transactions of the Royal Society of Edinburgh: Earth Sciences, v. 89, p. 249–290, doi:10.1017/S0263593300002418.

Budd, G.E., and Peel, J.S., 1998, A new Xenusiid lobopod from the early Cambrian Sirius Passet fauna of North Greenland: Palaeontology, v. 41, p. 1201–1213.

Bush, A.M., and Bambach, R.K., 2011, Paleoecologic megatrends in marine metazoa: v. 39, 241–269 p., doi:10.1146/annurev-earth-040809-152556.

Butler, D., Cunningham, J.A., Budd, G.E., and Donoghue, P.C.J., 2015, Experimental taphonomy of Artemia reveals the role of endogenous microbes in mediating decay and fossilization:

Butterfield, N.J., 2011, Animals and the invention of the Phanerozoic Earth system: Trends in Ecology and Evolution, v. 26, p. 81–87, doi:10.1016/j.tree.2010.11.012.

Butterfield, N.J., 2003, Exceptional fossil preservation and the Cambrian explosion: Integrative and Comparative Biology, v. 43, p. 166–177, doi:10.1093/icb/43.1.166.

Butterfield, N.J., 2002, *Leanchoilia* guts and the interpretation of three-dimensional structures in Burgess Shale-type fossils: Paleobiology, v. 28, p. 155–171, doi:10.1666/0094-8373(2002)028<0155:LGATIO>2.0.CO;2.

Butterfield, N.J., 2007, Macroevolution and macroecology through deep time: Palaeontology, v. 50, p. 41–55, doi:10.1111/j.1475-4983.2006.00613.x.

Butterfield, N.J., 2009, Macroevolutionary turnover through the Ediacaran transition: Ecological and biogeochemical implications: Geological Society Special Publication, v. 326, p. 55–66, doi:10.1144/SP326.3.

Butterfield, N.J., 1990, Organic preservation of non-mineralizing organisms and the taphonomy of the Burgess Shale: Paleobiology, v. 16, p. 272–286, doi:10.1017/S0094837300009994.

Butterfield, N.J., 2018, Oxygen, animals and aquatic bioturbation: An updated account: Geobiology, v. 16, p. 3–16, doi:10.1111/gbi.12267.

Butterfield, N.J., 1995, Secular distribution of Burgess-Shale-type preservation: Lethaia, v. 28, p. 1–13, doi:10.1111/j.1502-3931.1995.tb01587.x.

Butterfield, N.J., Balthasar, U., and Wilson, L.A., 2007a, Fossil diagenesis in the Burgess Shale: Palaeontology, v. 50, p. 537–543, doi:10.1111/j.1475-4983.2007.00656.x.

Butterfield, N.J., Balthasar, U., and Wilson, L.A., 2007b, Fossil diagenesis in the Burgess Shale: Palaeontology, v. 50, p. 537–543, doi:10.1111/j.1475-4983.2007.00656.x.

Caron, J.-B., 2005, *Banffia constricta*, a putative vetulicolid from the Middle Cambrian Burgess Shale: Transactions of the Royal Society of Edinburgh: Earth Sciences, v. 96, p. 95–111, doi:10.1017/s0263593300001255.

Caron, J.B., and Cheung, B., 2019, Amiskwia is a large Cambrian gnathiferan with complex gnathostomulid-like jaws: Communications Biology, v. 2, p. 1–9, doi:10.1038/s42003-019-0388-4.

Caron, J.B., Gaines, R.R., Aria, C., Mángano, M.G., and Streng, M., 2014, A new phyllopod bed-like assemblage from the Burgess Shale of the Canadian Rockies: Nature communications, v. 5, p. 3210, doi:10.1038/ncomms4210.

Caron, J.B., and Jackson, D.A., 2008, Paleoecology of the Greater Phyllopod Bed community, Burgess Shale: Palaeogeography, Palaeoclimatology, Palaeoecology, v. 258, p. 222–256, doi:10.1016/j.palaeo.2007.05.023.

Caron, J.B., and Jackson, D.A., 2006, Taphonomy of the greater phyllopod bed community, Burgess Shale: Palaios, v. 21, p. 451–465, doi:10.2110/palo.2003.P05-070R.

Cassarino, L., Coath, C.D., Xavier, J.R., and Hendry, K.R., 2018, Silicon isotopes of deep sea sponges: New insights into biomineralisation and skeletal structure: Biogeosciences, v.

15, p. 6959–6977, doi:10.5194/bg-15-6959-2018.

Cavan, E.L. et al., 2019, The importance of Antarctic krill in biogeochemical cycles: Nature Communications, v. 10, p. 1–13, doi:10.1038/s41467-019-12668-7.

Chandrasekharan Nair, K.K., and Anger, K., 1980, Seasonal variation in population structure and biochemical composition of *Jassa falcata* (Crustacea, Amphipoda) off the island of Helgoland (North Sea): Estuarine and Coastal Marine Science, v. 11, p. 505–513, doi:10.1016/S0302-3524(80)80003-X.

Chatterton, B.D.E., Johanson, Z., and Sutherland, G., 1994, Form of the Trilobite Digestive System: Alimentary Structures in Pterocephalia: Journal of Paleontology, v. 68, p. 294–305.

Chen, J.Y., Ramsköld, L., and Zhou, G.Q., 1994, Evidence for monophyly and arthropod affinity of Cambrian giant predators: Science, v. 264, p. 1304–1308, doi:10.1126/science.264.5163.1304.

Chen, J.-Y., and Zhou, G.-Q., 1997, Biology of the Chengjiang fauna: Bulletin of the National Museum of Natural Science, v. 10, p. 11–105.

Clements, T., Colleary, C., De Baets, K., and Vinther, J., 2017, Buoyancy mechanisms limit preservation of coleoid cephalopod soft tissues in Mesozoic Lagerstätten: Palaeontology, v. 60, p. 1–14, doi:10.1111/pala.12267.

Clements, T., Purnell, M.A., and Gabbott, S., 2022, Experimental analysis of organ decay and pH gradients within a carcass and the implications for phosphatization of soft tissues: Palaeontology, v. e12617, p. 1–13, doi:10.1111/pala.12617.

Cong, P., Daley, A.C., Edgecombe, G.D., and Hou, X., 2017, The functional head of the Cambrian radiodontan (stem-group Euarthropoda) *Amplectobelua symbrachiata*: BMC Evolutionary Biology, v. 17, p. 208, doi:10.1186/s12862-017-1049-1.

Cong, P.-Y., Edgecombe, G.D., Daley, A.C., Guo, J., Pates, S., and Hou, X.-G., 2018, New radiodonts with gnathobase-like structures from the Cambrian Chengjiang biota and implications for the systematics of Radiodonta: Palaeontology, v. 4, p. 605–621, doi:10.1002/spp2.1219.

Conway Morris, S., 1990, Burgess Shale, *in* Briggs, D.E.G. and Crowther, P.R. eds., Paleobiology: a synthesis, Oxford Blackwell Scientific Publications, p. 270–274.

Conway Morris, S., 1989, Burgess Shale faunas and the Cambrian explosion: Science, v. 246, p. 339–346.

Conway Morris, S., and Caron, J.B., 2012, *Pikaia gracilens* Walcott, a stem-group chordate from the Middle Cambrian of British Columbia: Biological Reviews, v. 87, p. 480-512, doi.org/10.1111/j.1469-185X.2012.00220.x.

Conway Morris, S., and Peel, J., 1990, Articulated halkieriids from the Lower Cambrian of north Greenland: Nature, v. 345, p. 802–805.

Conway Morris, S., and Peel, J.S., 1995, Articulated halkieriids from the Lower Cambrian of North Greenland and their role in early protostome evolution: Philosophical Transactions of the Royal Society of London. Series B: Biological Sciences, v. 347, p. 305–358, doi:10.1098/rstb.1995.0029.

Conway Morris, S., and Peel, J.S., 2010, New Palaeoscolecidan Worms from the Lower Cambrian: Sirius Passet, Latham Shale and Kinzers Shale: Acta Palaeontologica Polonica, v. 55, p. 141–156, doi:10.4202/app.2009.0058.

Conway Morris, S., and Peel, J.S., 2008, The earliest annelids: Lower Cambrian polychaetes from the Sirius Passet Lagerstätte, Peary Land, North Greenland: Acta Palaeontologica Polonica, v. 53, p. 137–148, doi:10.4202/app.2008.0110.

Conway Morris, S., Peel, J.S., Higgins, A.K., Soper, N.J., and Davis, N.C., 1987, A Burgess Shale-like fauna from the Lower Cambrian of North Greenland: Nature, v. 326, p. 181–183, doi:10.1038/326181a0.

Cummins, H., Powell, E., Stanton Jr., R., and Staff, G., 1986, The size-frequency distribution in palaeoecology: effects of taphonomic processes during formation of molluscan death assemblages in Texas Bays: Palaeontology, v. 29, p. 495–518.

Cushing, D.H. 1990. Plankton production and year-class strength in fish populations: an update of the match/mismatch hypothesis: Advances in marine biology, v. 26, 249-293, doi:10.1016/S0065-2881(08)60202-3

Cury, P., Bakun, A., Crawford, R.J.M., Jarre, A., Quiñones, R.A., Shannon, L.J., and Verheye, H.M., 2000, Small pelagics in upwelling systems: Patterns of interaction and structural changes in “wasp-waist” ecosystems: ICES Journal of Marine Science, v. 57, p. 603–618, doi:10.1006/jmsc.2000.0712.

Cury, P., and Roy, C., 1989, Window and Pelagic fish Recruitment Success in Upwelling region: Canadian Journal of Fisheries and Aquatic Sciences, v. 46, p. 670–680.

Daley, A.C., Antcliffe, J.B., Drage, H.B., and Pates, S., 2018, Early fossil record of Euarthropoda and the Cambrian Explosion: Proceedings of the National Academy of

Sciences of the United States of America, v. 115, p. 5323–5331, doi:10.1073/pnas.1719962115.

Daley, A.C., and Edgecombe, G.D., 2014, Morphology of Anomalocaris canadensis from the Burgess Shale: Journal of Paleontology, v. 88, p. 68–91, doi:10.1666/13-067.

Daley, A.C., and Peel, J.S., 2010, A Possible Anomalocaridid from the Cambrian Sirius Passet Lagerstätte, North Greenland: Journal of Paleontology, v. 84, p. 352–355.

Darroch, S.A.F., Smith, E.F., Laflamme, M., and Erwin, D.H., 2018, Ediacaran Extinction and Cambrian Explosion: Trends in Ecology and Evolution, v. 33, p. 653–663, doi:10.1016/j.tree.2018.06.003.

David, P.M., 1955, The distribution of *Sagitta gazellae* Ritter-Záhony: Discovery Reports, v. 27, p. 235–278.

Debrenne, F., and Zhuravlev, A.Y., 1997, Cambrian food web: A brief review: Geobios, v. 30, p. 181–188.

Deer, W.A., Howie, R.A., and Zussman, J., 2013, An Introduction to the Rock-Forming Minerals:, doi:10.1180/DHZ.

Delle Cave, L., Insom, E., and Simonetta, A.M., 1998, Advances, diversions, possible relapses and additional problems in understanding the early evolution of the Articulata: Italian Journal of Zoology, v. 65, p. 19–38, doi:10.1080/11250009809386724.

Denton, E.J., and Gray, J., 1985, Lateral-line-like antennae of certain of the Penaeidea (Crustacea, Decapoda, Natantia): Proceedings of the Royal Society of London. Series B. Biological Sciences, v. 226, p. 249–261, doi:10.1098/rspb.1985.0094.

Ding, T., Jiang, S., Li, Y., Gao, J., and Hu, B., 2017, Geochemistry of Silicon Isotopes: Berlin/Boston, Walter de Gruyter GmbH, 1–279 p., doi:10.1515/9783110402452.

Donoghue, P.C.J., Forey, P.L., and Aldridge, R.J., 2000, Conodont affinity and chordate phylogeny: Biological Reviews, v. 75, p. 191–251, doi:10.1111/j.1469-185X.1999.tb00045.x.

Donoghue, P.C.J., Kouchinsky, A., Waloszek, D., Bengtson, S., Dong, X.P., Val'kov, A.K., Cunningham, J.A., and Repetski, J.E., 2006, Fossilized embryos are widespread but the record is temporally and taxonomically biased: Evolution and Development, v. 8, p. 232–238, doi:10.1111/j.1525-142X.2006.00093.x.

Dornbos, S.Q., 2010, Phosphatization Through the Phanerozoic, *in* Allison, P.A. and Bottjer, D.J. eds., Taphonomy: Process and Bias Through Time, Dordrecht, Springer, p. 435–

456, doi:10.1007/978-90-481-8643-3.

Dornbos, S.Q., Bottjer, D.J., Chen, J.-Y., Geo, F., Oliveri, P., and Li, C.-W., 2006, Environmental Controls on the Taphonomy of Phosphatized Animals and Animal Embryos from the Neoproterozoic Doushantuo Formation, Southwest China: Palaios, v. 21, p. 3–14, doi:10.2110/palo.2004.p04-37.

Dowey, P.J., and Taylor, K.G., Extensive authigenic quartz overgrowths in the gas-bearing Haynesville-Bossier Shale, USA: Sedimentary Geology, v. 356, 15–25, doi:10.1016/j.sedgeo.2017.05.001

Dunne, J.A., Williams, R.J., Martinez, N.D., Wood, R.A., and Erwin, D.H., 2008, Compilation and network analyses of Cambrian food webs: PLoS Biology, v. 6, p. 693–708, doi:10.1371/journal.pbio.0060102.

Epelbaum, A., and Borisov, R., 2006, Feeding behaviour and functional morphology of the feeding appendages of red king crab *Paralithodes camtschaticus* larvae: Marine Biology Research, v. 2, p. 77–88, doi:10.1080/17451000600672529.

Escribano, R., and Riquelme-Bugueño, R., 2015, Planktonic crustaceans: Lifestyles in the water column, *in* Thiel, M. and Watling, L. eds., The Natural History of Crustaceans Volume 2. Life Styles and Feeding Biology, Oxford University Press, p. 262–279.

Evans, J.A., Zalasiewicz, J.A., Fletcher, I., Rasmussen, B., and Pearce, N.J.G., 2002, Dating diagenetic monazite in mudrocks: Constraining the oil window? Journal of the Geological Society, London, v. 159, p. 619–622, doi:10.1144/0016-764902-066.

Fagerstrom, J.A., 1964, Fossil Communities in Paleoecology: Their Recognition and Significance: Geological Society of America Bulletin, v. 75, p. 1197–1216, doi:10.1130/0016-7606(1964)75.

Fan, H., Wen, H., Zhu, X., Hu, R., and Tian, S., 2013, Hydrothermal activity during Ediacaran-Cambrian transition: Silicon isotopic evidence: Precambrian Research, v. 224, p. 23–35, doi:10.1016/j.precamres.2012.09.004.

Fauchald, P., Skov, H., Skern-mauritzen, M., Johns, D., and Tveraa, T., 2011, Wasp-Waist Interactions in the North Sea Ecosystem: PLoS ONE, v. 6, p. e22729, doi:10.1371/journal.pone.0022729.

Fontorbe, G., Frings, P.J., De La Rocha, C.L., Hendry, K.R., and Conley, D.J., 2016, A silicon depleted North Atlantic since the Palaeogene: Evidence from sponge and radiolarian silicon isotopes: Earth and Planetary Science Letters, v. 453, p. 67–77, doi:10.1016/j.epsl.2016.08.006.

Forchielli, A., Steiner, M., Kasbohm, J., Hu, S., and Keupp, H., 2014, Taphonomic traits of clay-hosted early Cambrian Burgess Shale-type fossil Lagerstätten in South China: Palaeogeography, Palaeoclimatology, Palaeoecology, v. 398, p. 59–85, doi:10.1016/j.palaeo.2013.08.001.

Fortey, R., 1974, A new pelagic trilobite from the Ordovician of Spitsbergen, Ireland, and Utah: Palaeontology., v. 17, p. 111–124.

Fortey, R.A., and Owens, R.M., 1999, Feeding habits in trilobites: Palaeontology, v. 42, p. 429–465, doi:10.1111/1475-4983.00080.

Foxton, P., 1969, The morphology of the antennal flagellum of certain of the Penaeidea (Decapoda, Natantia): Crustaceana, v. 16, p. 33–42.

Frederiksen, M., Edwards, M., Anthony, J., Halliday, N.C., and Wanless, S., 2006, From plankton to top predators: bottom-up control of a marine food web across four trophic levels: Journal of Animal Ecology, v. 75, p. 1259–1268, doi:10.1111/j.1365-2656.2006.01148.x.

Fu, D. et al., 2019, The Qingjiang biota—a Burgess Shale–type fossil Lagerstätte from the early Cambrian of South China: Science, v. 363, p. 1338–1342, doi:10.1126/science.aau8800.

Fuchs, D., Bracchi, G., and Weis, R., 2009, New octopods (cephalopoda: Coleoidea) from the late cretaceous (upper cenomanian) of Hâkel and Hâdjoula, Lebanon: Palaeontology, v. 52, p. 65–81, doi:10.1111/j.1475-4983.2008.00828.x.

Fuchs, D., and Larson, N., 2011, Diversity, Morphology, and Phylogeny of Coleoid Cephalopods from the Upper Cretaceous Plattenkalks of Lebanon–Part I: Prototeuthidina: Journal of Paleontology, v. 85, p. 815–834, doi:10.1666/10-089.1.

Fürsich, F.T., 1978, The influence of faunal condensation and mixing on the preservation of fossil benthic communities: Lethaia, v. 11, p. 243–250, doi:10.1111/j.1502-3931.1978.tb01231.x.

Fürsich, F.T., and Aberhan, M., 1990, Significance of time-averaging for palaeocommunity analysis: Lethaia, v. 23, p. 143–152, doi:10.1111/j.1502-3931.1990.tb01355.x.

Gabbott, S.E., 1998, Taphonomy of the Ordovician Soom Shale Lagerstätte: an example of soft tissue preservation in clay minerals: Palaeontology, v. 41, p. 631–668.

Gabbott, S.E., Browning, C., Theron, J.N., and Whittle, R.J., 2017, The late Ordovician

Soom Shale Lagerstätte: An extraordinary post-glacial fossil and sedimentary record: Journal of the Geological Society, v. 174, p. 1–9, doi:10.1144/jgs2016-076.

Gabbott, S.E., Hou, X.G., Norry, M.J., and Siveter, D.J., 2004, Preservation of Early Cambrian animals of the Chengjiang biota: Geology, v. 32, p. 901–904, doi:10.1130/G20640.1.

Gabbott, S.E., Norry, M.J., Aldridge, R.J., and Theron, J.N., 2001, Preservation of fossils in clay minerals; A unique example from the upper ordovician soom shale, South Africa: Proceedings of the Yorkshire Geological Society, v. 53, p. 237–244, doi:10.1144/pygs.53.3.237.

Gabbott, S.E., Zalasiewicz, J., and Collins, D., 2008, Sedimentation of the phyllopod bed within the Cambrian Burgess Shale Formation of British Columbia: Journal of the Geological Society, v. 165, p. 307–318, doi:10.1144/0016-76492007-023.

Gabbott, S.E., Sansom, R.S., Purnell, M.A., 2021, Systematic analysis of exceptionally preserved fossils: correlated patterns of decay and preservation: Palaeontology, v. 64, 789–803, doi.org/10.1111/pala.12571.

Gaines, R.R., 2014, Burgess Shale-type Preservation and its Distribution in Space and Time, *in* Laflamme, M., Schiffbauer, J.D., and Darroch, S.A.F. eds., Reading and Writing of the Fossil Record: Preservational Pathways to Exceptional Fossilization. The Paleontological Society Papers, Volume 20, The Paleontological Society, p. 123–146, doi:10.1017/s1089332600002837.

Gaines, R.R., Briggs, D.E.G., and Zhao, Y., 2008, Cambrian Burgess Shale-type deposits share a common mode of fossilization: Geology, v. 36, p. 755–758, doi:10.1130/G24961A.1.

Gaines, R.R., Hammarlund, E.U., Hou, X., Qi, C., Gabbott, S.E., Zhao, Y., Peng, J., and Canfield, D.E., 2012, Mechanism for Burgess Shale-type preservation: Proceedings of the National Academy of Sciences of the United States of America, v. 109, p. 5180–5184, doi:10.1073/pnas.1111784109.

Gaines, R.R., Lombardo, A.J., Holzer, I.O., and Caron, J.B., 2019, The limits of Burgess Shale-type preservation: Assessing the evidence for preservation of the blood protein hemocyanin in the Burgess Shale: Palaios, v. 34, p. 291–299, doi:10.2110/palo.2019.026.

Gallardo, V.A., Palma, M., Carrasco, F.D., Gutiérrez, D., Levin, L.A., and Cañete, J.I., 2004, Macrobenthic zonation caused by the oxygen minimum zone on the shelf and slope off central Chile: Deep-Sea Research Part II: Topical Studies in Oceanography, v. 51, p. 2475–2490, doi:10.1016/j.dsr2.2004.07.028.

Gao, P., Li, S., Lash, G.G., He, Z., Xiao, X., Zhang, D., and Hao, Y., 2020, Silicification and Si cycling in a silica-rich ocean during the Ediacaran-Cambrian transition: Chemical Geology, v. 552, p. 119787, doi:10.1016/j.chemgeo.2020.119787.

García-Bellido, D.C., and Collins, D.H., 2006, A new study of Marrella splendens (Arthropoda, Marrellomorpha) from the Middle Cambrian Burgess Shale, British Columbia, Canada: Canadian Journal of Earth Sciences, v. 43, p. 721–742, doi:10.1139/E06-012.

Garson, D.E., Gaines, R.R., Droser, M.L., Liddell, W.D., and Sappenfield, A., 2012, Dynamic palaeoredox and exceptional preservation in the Cambrian Spence Shale of Utah: Lethaia, v. 45, p. 164–177, doi:10.1111/j.1502-3931.2011.00266.x.

Geilert, S., Vroon, P.Z., Roerdink, D.L., Van Cappellen, P., and van Bergen, M.J., 2014, Silicon isotope fractionation during abiotic silica precipitation at low temperatures: Inferences from flow-through experiments: Geochimica et Cosmochimica Acta, v. 142, p. 95–114, doi:10.1016/j.gca.2014.07.003.

Georg, R.B., Reynolds, B.C., Frank, M., and Halliday, A.N., 2006, New sample preparation techniques for the determination of Si isotopic compositions using MC-ICPMS: Chemical Geology, v. 235, p. 95–104, doi:10.1016/j.chemgeo.2006.06.006.

Gillanders, B.M., Able, K.W., Brown, J.A., Eggleston, D.B., and Sheridan, P.F., 2003, Evidence of connectivity between juvenile and adult habitats for mobile marine fauna: an important component of nurseries: Marine Ecology Progress Series, v. 247, p. 281–295.

Godeaux, J.E., 1989, Functions of the Endostyle in the Tunicates: Bulletin of Marine Science, v. 45, p. 228–242.

Gogáin, A.Ó., O'Sullivan, G., Clements, T., Hoare, B.C., Murray, J., Jackson, P.W., 2022, Metamorphism as the cause of bone alteration in the Jarrow assemblage (Langsettian, Pennsylvanian) of Ireland: Palaeontology, v. 65, e12628, doi.org/10.1111/pala.12628.

Gould, S.J., 1989, Wonderful Life. The Burgess Shale and the nature of history: New York, W.W. Norton, 347 p.

Graham, D.J., and Midgley, N.G., 2000, Graphical representation of particle shape using triangular diagrams: An excel spreadsheet method: Earth Surface Processes and Landforms, v. 25, p. 1473–1477, doi:10.1002/1096-9837(200012)25:13<1473::AID-ESP158>3.0.CO;2-C.

Grantham, B.A., Chan, F., Nielsen, K.J., Fox, D.S., Barth, J.A., Huyer, A., Lubchenco, J., and Menge, B.A., 2004, Upwelling-driven nearshore hypoxia signals ecosystem and oceanographic changes in the northeast Pacific: Nature, v. 429, p. 749–754, doi:10.1038/nature02605.

Griffiths, S.P., Olson, R.J., and Watters, G.M., 2013, Complex wasp-waist regulation of pelagic ecosystems in the Pacific Ocean: Reviews in Fish Biology and Fisheries, v. 23, p. 459–475, doi:10.1007/s11160-012-9301-7.

Gueriau, P. et al., 2020, Oxidative conditions can lead to exceptional preservation through phosphatization: Geology, v. 48, p. 1164–1168, doi:10.1130/G45924.1.

Gueriau, P., Rabet, N., Clément, G., Lagebro, L., Vannier, J., Briggs, D.E.G., Charbonnier, S., Olive, S., and Béthoux, O., 2016, A 365-million-year-old freshwater community reveals morphological and ecological stasis in branchiopod crustaceans: Current Biology, v. 26, p. 383–390, doi:10.1016/j.cub.2015.12.039.

Guidetti, R., Altiero, T., Marchioro, T., Amade, L.S., Avdonina, A.M., Bertolani, R., and Rebecchi, L., 2012, Form and function of the feeding apparatus in *Eutardigrada* (Tardigrada): Zoomorphology, v. 131, p. 127–148, doi:10.1007/s00435-012-0149-0.

Hammarlund, E.U., Smith, M.P., Rasmussen, J.A., Nielsen, A.T., Canfield, D.E., and Harper, D.A.T., 2018, The Sirius Passet Lagerstätte of North Greenland — A geochemical window on early Cambrian low- - oxygen environments and ecosystems: Geobiology, p. 1–15, doi:10.1111/gbi.12315.

Hammer, Ø., Harper, D.A.T., and Ryan, P.D., 2001, Past: Paleontological statistics software package for education and data analysis: Palaeontologia Electronica, v. 4.

Hamner, W.M., Hamner, P.P., Strand, S.W., and Gilmer, R.W., 1983, Behavior of Antarctic Krill, *Euphausia superba*: Chemoreception, Feeding, Schooling, and Molting: Science, v. 220, p. 433–435, doi:10.1126/science.220.4595.433.

Hanken, J., and Wake, D.B., 1993, Miniaturization of body size: Organismal consequences and evolutionary significance: Annual Review of Ecology and Systematics, v. 24, p. 501–519, doi:10.1146/annurev.es.24.110193.002441.

Harper, D.A.T., Hammarlund, E.U., Topper, T.P., Nielsen, A.T., Rasmussen, J.A., Park, T.Y.S., and Smith, M.P., 2019, The Sirius Passet Lagerstätte of North Greenland: A remote window on the Cambrian Explosion: Journal of the Geological Society, v. 176, p. 1023–1037, doi:10.1144/jgs2019-043.

Hartnoll, R.G., 1971, The occurrence, methods and significance of swimming in the Brachyura: Animal Behaviour, v. 19, p. 34–50, doi:10.1016/S0003-3472(71)80132-X.

Haug, J.T., Briggs, D.E., and Haug, C., 2012, Morphology and function in the Cambrian Burgess Shale megacheiran arthropod *Leanchoilia superlata* and the application of a descriptive matrix: BMC Evolutionary Biology, v. 12, p. 162, doi:10.1186/1471-2148-12-162.

Haug, J.T., Caron, J.B., and Haug, C., 2013, Demecology in the Cambrian: Synchronized molting in arthropods from the Burgess Shale: BMC Biology, v. 11, p. 64, doi:10.1186/1741-7007-11-64.

Hendry, K.R., Cassarino, L., Bates, S.L., Culwick, T., Frost, M., Goodwin, C., and Howell, K.L., 2019, Silicon isotopic systematics of deep-sea sponge grounds in the North Atlantic: Quaternary Science Reviews, v. 210, p. 1–14, doi:10.1016/j.quascirev.2019.02.017.

Hendry, K.R., Georg, R.B., Rickaby, R.E.M., Robinson, L.F., and Halliday, A.N., 2010, Deep ocean nutrients during the Last Glacial Maximum deduced from sponge silicon isotopic compositions: Earth and Planetary Science Letters, v. 292, p. 290–300, doi:10.1016/j.epsl.2010.02.005.

Hendry, K.R., and Robinson, L.F., 2012, The relationship between silicon isotope fractionation in sponges and silicic acid concentration: Modern and core-top studies of biogenic opal: Geochimica et Cosmochimica Acta, v. 81, p. 1–12, doi:10.1016/j.gca.2011.12.010.

Hendry, K.R., Robinson, L.F., McManus, J.F., and Hays, J.D., 2014, Silicon isotopes indicate enhanced carbon export efficiency in the North Atlantic during deglaciation: Nature Communications, v. 5, doi:10.1038/ncomms4107.

Higgins, A.., Ineson, J.., Peel, J.., Surlyk, F., and Sønderholm, M., 1991, Lower Palaeozoic Franklinian Basin of North Greenland: Bulletin Grønlands Geologiske Undersøgelse, v. 160, p. 71–139, doi:10.34194/bullggu.v160.6714.

Higgins, A.K., Soper, N.J., and Leslie, A.G., 2000, The Ellesmerian and Caledonian orogenic belts of Greenland: Polarforschung, v. 68, p. 141–151.

Hof, C.H.J., and Briggs, D.E.G., 1997, Decay and mineralization of mantis shrimps (Stomatopoda; Crustacea); a key to their fossil record: PALAIOS, v. 12, p. 420–438.

Hoffmann, R., Bestwick, J., Berndt, G., Berndt, R., Fuchs, D., and Klug, C., 2020, Pterosaurs ate soft-bodied cephalopods (Coleoidea): Scientific Reports, v. 10, p. 1–7, doi:10.1038/s41598-020-57731-2.

Holland, N.D., and Chen, J., 2001, Origin and early evolution of the vertebrates: New insights from advances in molecular biology, anatomy, and palaeontology: BioEssays, v. 23, p. 142–151, doi:10.1002/1521-1878(200102)23:2<142::AID-BIES1021>3.0.CO;2-5.

Holmes, J.D., García-Bellido, D.C., and Lee, M.S.Y., 2018, Comparisons between Cambrian Lagerstätten assemblages using multivariate, parsimony and Bayesian methods: Gondwana Research, v. 55, p. 30–41, doi:10.1016/j.gr.2017.10.007.

Hou, X., and Bergström, J., 1997, Arthropods of the Lower Cambrian Chengjiang fauna, southwest China: Fossils and Strata, v. 45, p. 1–116.

Hou, X.-G., and Bergström, J., 2006, Dinocaridids: anomalous arthropods or arthropod-like worms?, *in* Rong, J., Fang, Z., Zhou, Z., Zhan, R., Wang, X.-D., and Yuan, X. eds., Originations, Radiations and Biodiversity Changes – evidences from the Chinese fossil record, Science Press, Beijing, p. 139–158.

Hou, X.-G., Bergström, J., and Ahlberg, P., 1995, Anomalocaris and other large animals in the Lower Cambrian Chengjiang fauna of southwest China: GFF, v. 117, p. 163–183, doi:10.1080/11035899509546213.

Hou, X.-G., Siveter, D.J., Aldridge, R.J., and Siveter, D.J., 2009, A new arthropod in chain-like associations from the Chengjiang lagerstätte (Lower Cambrian), Yunnan, China: Palaeontology, v. 52, p. 951–961, doi:10.1111/j.1475-4983.2009.00889.x.

Hu, S., 2005, Taphonomy and Palaeoecology of the Early Cambrian Chengjiang: Berliner Paläobiologische Abhandlungen, v. 7, p. 1–197.

Hu, S., Steiner, M., Zhu, M., Erdtmann, B.D., Luo, H., Chen, L., and Weber, B., 2007, Diverse pelagic predators from the Chengjiang Lagerstätte and the establishment of modern-style pelagic ecosystems in the early Cambrian: Palaeogeography, Palaeoclimatology, Palaeoecology, v. 254, p. 307–316, doi:10.1016/j.palaeo.2007.03.044.

Hughes, N.C., Kříž, J., Macquaker, J.H.S., and Huff, W.D., 2014, The depositional environment and taphonomy of the Homerian "Aulacopleura shales" fossil assemblage near Loděnice, Czech Republic (Prague Basin, Perunican microcontinent): Bulletin of Geosciences, p. 219–238, doi:10.3140/bull.geosci.1414.

Huldtgren, T., Cunningham, J.A., Yin, C., Stampanoni, M., Marone, F., Donoghue, P.C.J., and Bengtson, S., 2011, Fossilized nuclei and germination structures identify ediacaran "animal embryos" as encysting protists: Science, v. 334, p. 1696–1699, doi:10.1126/science.1209537.

Hunt, G.L., and McKinnell, S., 2006, Interplay between top-down, bottom-up, and wasp-waist control in marine ecosystems: Progress in Oceanography, v. 68, p. 115–124, doi:10.1016/j.pocean.2006.02.008.

Ims, R.A., 1990, The ecology and evolution of reproductive synchrony: Trends in Ecology and Evolution, v. 5, p. 135–140, doi:10.1016/0169-5347(90)90218-3.

Ineson, J.R., and Peel, J.S., 1997, Cambrian shelf stratigraphy of North Greenland: v. 173, doi:10.34194/ggub.v173.5024.

Ineson, J.R., and Peel, J.S., 2011, Geological and depositional setting of the Sirius Passet Lagerstätte (Early Cambrian), North Greenland: Canadian Journal of Earth Sciences, v. 48, p. 1259–1281, doi:10.1139/e11-018.

Izquierdo-López, A., and Caron, J.B., 2022, Extreme multisegmentation in a giant bivalved arthropod from the Cambrian Burgess Shale arthropod from the Cambrian Burgess Shale: iScience, v. 25, p. 104675, doi:10.1016/j.isci.2022.104675.

Jago, J.B., García-Bellido, D.C., and Gehling, J.G., 2016, An early Cambrian chelicerate from the Emu Bay Shale, South Australia: Palaeontology, v. 59, p. 549–562, doi:10.1111/pala.12243.

Jordan, C.E., 1992, A model of rapid-start swimming at intermediate Reynolds number: undulatory locomotion in the chaetognath Sagitta elegans: Journal of Experimental Biology, v. 163, p. 119–137, doi:10.1242/jeb.163.1.119.

Kämpf, J., and Chapman, P., 2016, Upwelling Systems of the World:, doi:10.1007/978-3-319-42524-5.

Kear, A.J., Briggs, D.E.G., and Donovan, D., 1995, Decay and fossilization of non-mineralized tissue in coleoid cephalopods: Palaeontology, v. 38, p. 105–131.

Kidwell, S.M., 1998, Time-averaging in the marine fossil record: Overview of strategies and uncertainties: Geobios, v. 30, p. 977–995.

Kidwell, S.M., and Bosence, D.W.J., 1991, Taphonomy and Time-Averaging of Marine

Shelly Faunas, *in* Allison, P.A. and Briggs, D.E.G. eds., Taphonomy: Releasing the Data Locked in the Fossil Record, New York, Plenum Press, p. 115–209, doi:10.1007/978-1-4899-5034-5_4.

Kidwell, S.M., and Holland, S.M., 2002, The quality of the fossil record: Implications for evolutionary analyses: Annual Review of Ecology and Systematics, v. 33, p. 561–588, doi:10.1146/annurev.ecolsys.33.030602.152151.

Klug, C., Hagdorn, H., and Montenari, M., 2005, Phosphatized soft-tissue in Triassic Bivalves: Palaeontology, v. 48, p. 833–852, doi:10.1111/j.1475-4983.2005.00485.x.

Klug, C., Kröger, B., Kiessling, W., Mullins, G.L., Servais, T., Klug, C., Fryda, J., Korn, D., and Turner, S., 2010, The Devonian nekton revolution: Lethaia, v. 43, p. 465–477, doi:10.1111/j.1502-3931.2009.00206.x.

Klug, C., Schweigert, G., Fuchs, D., and De Baets, K., 2021, Distraction sinking and fossilized coleoid predatory behaviour from the German Early Jurassic: Swiss Journal of Palaeontology, v. 140, doi:10.1186/s13358-021-00218-y.

Lagebro, L., Stein, M., and Peel, J.S., 2009, A new ?lamellipedian arthropod from the early Cambrian Sirius Passet fauna of North Greenland: Journal of Paleontology, v. 83, p. 820–825, doi:10.1666/09-011.1.

Lee, W.Y., Omori, M., and Peck, R.W., 1992, Growth, reproduction and feeding behavior of the planktonic shrimp, Lucifer faxoni Borradaile, off the Texas coast: Journal of Plankton Research, v. 14, p. 61–69, doi:https://doi.org/10.1093/plankt/14.1.61.

Légier-Visser, M.F., Mitchell, J.G., Okubo, A., and Fuhrman, J.A., 1986, Mechanoreception in calanoid copepods: Marine Biology, v. 90, p. 529–535, doi:10.1007/BF00409273.

Lerosey-Aubril, R., Gaines, R.R., Hegna, T.A., Ortega-Hernández, J., Van Roy, P., Kier, C., and Bonino, E., 2018, The Weeks Formation Konservat-Lagerstätte and the evolutionary transition of Cambrian marine life: Journal of the Geological Society, v. 175, p. 705–715, doi:10.1144/jgs2018-042.

Lerosey-Aubril, R., Hegna, T.A., Kier, C., Bonino, E., Habersetzer, J., and Carré, M., 2012, Controls on gut phosphatisation: The trilobites from the Weeks formation Lagerstätte (Cambrian; Utah): PLoS ONE, v. 7, p. e32934, doi:10.1371/journal.pone.0032934.

Levin, L.A., 2003, Oxygen Minimum Zone Benthos: Adaptation and Community Response To Hypoxia: Oceanography and Marine Biology, An Annual Review, Volume 41, v. 41, p. 1–45, doi:10.1201/9780203180570-3.

Levin, L., Gutiérrez, D., Rathburn, A., Neira, C., Sellanes, J., Muñoz, P., Gallardo, V., and Salamanca, M., 2002, Benthic processes on the Peru margin: A transect across the oxygen minimum zone during the 1997-98 El Niño: Progress in Oceanography, v. 53, p. 1–27, doi:10.1016/S0079-6611(02)00022-8.

Li, Y., Yu, H., Gu, X., Guo, S., and Huang, F., 2020, Silicon isotopic fractionation during metamorphic fluid activities: constraints from eclogites and ultrahigh-pressure veins in the Dabie orogen, China: Chemical Geology, v. 540, p. 119550, doi:10.1016/j.chemgeo.2020.119550.

Liu, J., and Dunlop, J.A., 2014, Cambrian lobopodians: A review of recent progress in our understanding of their morphology and evolution: Palaeogeography, Palaeoclimatology, Palaeoecology, v. 398, p. 4–15, doi:10.1016/j.palaeo.2013.06.008.

Liu, K., Feng, Q., Shen, J., Khan, M., and Planavsky, N.J., 2018, Increased productivity as a primary driver of marine anoxia in the Lower Cambrian: Palaeogeography, Palaeoclimatology, Palaeoecology, v. 491, p. 1–9, doi:10.1016/j.palaeo.2017.11.007.

Liu, A.G., Kenchington, C.G., and Mitchell, E.G., 2015, Remarkable insights into the paleoecology of the Avalonian Ediacaran macrobiota: Gondwana Research, v. 27, p. 1355–1380, doi:10.1016/j.gr.2014.11.002.

Logan, G.A., Hayes, J.M., Hieshima, G.B., and Summons, R.E., 1995, Terminal Proterozoic reorganization of biogeochemical cycles: Nature, v. 376, p. 53–56.

Maas, A., Braun, A., Dong, X.P., Donoghue, P.C.J., Müller, K.J., Olempska, E., Repetski, J.E., Siveter, D.J., Stein, M., and Waloszek, D., 2006, The 'Orsten'-More than a Cambrian Konservat-Lagerstätte yielding exceptional preservation: Palaeoworld, v. 15, p. 266–282, doi:10.1016/j.palwor.2006.10.005.

Macias, D., Garcia-Gorriz, E., and Stips, A., 2018, Major fertilization sources and mechanisms for Mediterranean Sea coastal ecosystems: Limnology and Oceanography, v. 63, p. 897–914, doi:10.1002/lno.10677.

MacKenzie, L.A., Hofmann, M.H., Junyuan, C., and Hinman, N.W., 2015, Stratigraphic controls of soft-bodied fossil occurrences in the Cambrian Chengjiang Biota Lagerstätte, Maotianshan Shale, Yunnan Province, China: Palaeogeography, Palaeoclimatology, Palaeoecology, v. 420, p. 96–115, doi:10.1016/j.palaeo.2014.11.006.

Mallatt, J., 1981, The suspension feeding mechanism of the larval lamprey *Petromyzon marinus*: Journal of Zoology, v. 194, p. 103–142, doi:10.1111/j.1469-

7998.1981.tb04581.x.
Mángano, M.G., Bromley, R.G., Harper, D.A.T., Nielsen, A.T., Smith, M.P., and Vinther, J., 2012, Nonbiomineralized carapaces in Cambrian seafloor landscapes (Sirius Passet, Greenland): Opening a new window into early Phanerozoic benthic ecology: Geology, v. 40, p. 519–522, doi:10.1130/G32853.1.
Mangano, M.G., and Buatois, L.A., 2017, The Cambrian Explosion, *in* Buatois, L.A. and Mangano, M.G. eds., The Trace-Fossil Record of Major Evolutionary Events Volume 1: Precambrian and Paleozoic, p. 73–126.
Mángano, M.G., Hawkes, C.D., and Caron, J.B., 2019, Trace fossils associated with Burgess Shale non-biomineralized carapaces: Bringing taphonomic and ecological controls into focus: Royal Society Open Science, v. 6, doi:10.1098/rsos.172074.
Manton, S.M., 1964, Mandibular mechanisms and evolution of arthropods: Philosophical Transactions of the Royal Society of London. Series B: Biological Sciences, v. 247, p. 1–183, doi:doi.org/10.1098/rstb.1964.0001.
Manton, S.M., and Heatley, N.G., 1937, Studies on the Onychophora. II. The Feeding, Digestion, Excretion, and Food Storage of Peripatopsis with Biochemical Estimations and Analyses: Philosophical Transactions of the Royal Society B: Biological Sciences, v. 227, p. 411–464, http://rstb.royalsocietypublishing.org/cgi/doi/10.1098/rstb.1937.0006.
Marin-Carbonne, J., Robert, F., and Chaussidon, M., 2014, The silicon and oxygen isotope compositions of Precambrian cherts: A record of oceanic paleo-temperatures? Precambrian Research, v. 247, p. 223–234, doi:10.1016/j.precamres.2014.03.016.
Marshall, C.R., 2006, Explaining the Cambrian “explosion” of animals: Annual Review of Earth and Planetary Sciences, v. 34, p. 355–384.
Martill, D.M., 1990, Macromolecular resolution of fossilized muscle tissue from an elopomorph fish: Nature, v. 346, p. 171–172, doi:10.1038/346171a0.
Martill, D.M., 1988, Preservation of fish in the Cretaceous Santana Formation: Palaeontology, v. 31, p. 1–18.
Mayers, B., Aria, C., and Caron, J.B., 2019, Three new naraoiid species from the Burgess Shale, with a morphometric and phylogenetic reinvestigation of Naraoiidae: Palaeontology, v. 62, p. 19–50, doi:10.1111/pala.12383.
McMahon, S., Anderson, R.P., Saupe, E.E., and Briggs, D.E.G., 2016, Experimental evidence

that clay inhibits bacterial decomposers: Implications for preservation of organic fossils: Geology, v. 44, p. 867–870, doi:10.1130/G38454.1.

McNamara, M.E., Orr, P.J., Kearns, S.L., Alcalá, L., Anadón, P., and Molla, E.P., 2009, Soft-tissue preservation in miocene frogs from Libros, Spain: Insights into the genesis of decay microenvironments: Palaios, v. 24, p. 104–117, doi:10.2110/palo.2008.p08-017r.

Menzies, R.J., and Barnard, J.L., 1959, Marine Isopoda on coastal shelf bottoms of Southern California: Systematics and Ecology: Pacific Naturalist, v. 1, p. 4–35.

Meyer, B. et al., 2020, Successful ecosystem-based management of Antarctic krill should address uncertainties in krill recruitment, behaviour and ecological adaptation: Communications Earth and Environment, v. 1, p. 1–12, doi:10.1038/s43247-020-00026-1.

Milliken, K.L., Day-Stirrat, R.J., 2013, Cementation in mudrocks: Brief review with examples from cratonic basin mudrocks *in* Chatellier, J.-Y. and Jarvie, D.M. eds., Critical Assessment of Shale Resource Plays, p. 133–150, doi.org/10.1306/13401729H55252

Mitchell, E.G., Kenchington, C.G., Liu, A.G., Matthews, J.J., and Butterfield, N.J., 2015, Reconstructing the reproductive mode of an Ediacaran macro-organism: Nature, v. 524, p. 343–346, doi:10.1038/nature14646.

Moore, R.A., and Lieberman, B.S., 2009, Preservation of early and Middle Cambrian soft-bodied arthropods from the Pioche Shale, Nevada, USA: Palaeogeography, Palaeoclimatology, Palaeoecology, v. 277, p. 57–62, doi:10.1016/j.palaeo.2009.02.014.

Mulder, T., and Syvitski, J.P.M., 1995, Turbidity currents generated at river mouths during exceptional discharges to the world oceans: Journal of Geology, v. 103, p. 285–299, doi:10.1086/629747.

Mulder, T., Syvitski, J.P.M., Migeon, S., Faugères, J.C., and Savoye, B., 2003, Marine hyperpycnal flows: Initiation, behavior and related deposits. A review: Marine and Petroleum Geology, v. 20, p. 861–882, doi:10.1016/j.marpetgeo.2003.01.003.

Murdock, D.J.E., Gabbott, S.E., Mayer, G., and Purnell, M.A., 2014, Decay of velvet worms (onychopora), and bias in the fossil record of lobopodians: BMC Evolutionary Biology, v. 14, 222, doi: 10.1186/s12862-014-0222-z

Murdock, D.J.E., and Smith, M.P., 2021, Panderodus from the Waukesha Lagerstätte of Wisconsin, USA: a primitive macrophagous vertebrate predator: Papers in

Palaeontology, v. 7, p. 1977–1993, doi:10.1002/spp2.1389.

Muscente, A.D., Hawkins, A.D., and Xiao, S., 2015, Fossil preservation through phosphatization and silicification in the Ediacaran Doushantuo Formation (South China): A comparative synthesis: Palaeogeography, Palaeoclimatology, Palaeoecology, v. 434, p. 46–62, doi:10.1016/j.palaeo.2014.10.013.

Na, L., and Kiessling, W., 2015, Diversity partitioning during the Cambrian radiation: Proceedings of the National Academy of Sciences of the United States of America, v. 112, p. 4702–4706, doi:10.1073/pnas.1424985112.

Nakajima, T., 2006, Hyperpycnites deposited 700 km away from river mouths in the central Japan Sea: Journal of Sedimentary Research, v. 76, p. 60–73, doi:10.2110/jsr.2006.13.

Nanglu, K., and Caron, J.B., 2021, Symbiosis in the Cambrian: Enteropneust tubes from the Burgess Shale co-inhabited by commensal polychaetes: Proceedings of the Royal Society B: Biological Sciences, v. 288, doi:10.1098/rspb.2021.0061.

Nanglu, K., Caron, J.B., and Gaines, R.R., 2020, The Burgess Shale paleocommunity with new insights from Marble Canyon, British Columbia: Paleobiology, v. 46, p. 58–81, doi:10.1017/pab.2019.42.

Naqvi, S.W.A., Jayakumar, D.A., Narvekar, P. V., Naik, H., Sarma, V.V.S.S., D'Souza, W., Joseph, S., and George, W.D., 2000, Increased marine production of N2O due to intensifying anoxia on the Indian continental shelf: Nature, v. 408, p. 1998–2001.

Ng, H.C., Cassarino, L., Pickering, R.A., Woodward, E.M.S., Hammond, S.J., and Hendry, K.R., 2020, Sediment efflux of silicon on the Greenland margin and implications for the marine silicon cycle: Earth and Planetary Science Letters, v. 529, p. 115877, doi:10.1016/j.epsl.2019.115877.

Nielsen, C., 2013, The triradiate sucking pharynx in animal phylogeny: Invertebrate Biology, v. 132, p. 1–13, doi:10.1111/ivb.12010.

Nielsen, M.L., Lee, M., Ng, H.C., Rushton, J.C., Hendry, K.R., Kihm, J.H., Nielsen, A.T., Park, T.Y.S., Vinther, J., and Wilby, P.R., 2022, Metamorphism obscures primary taphonomic pathways in the early Cambrian Sirius Passet Lagerstätte, North Greenland: Geology, v. 50, p. 4–9, doi:10.1130/G48906.1.

Nielsen, M.L., Rasmussen, J.A., and Harper, D.A.T., 2017, Sexual dimorphism within the stem-group arthropod *Isoxys volucris* from the Sirius Passet Lagerstätte, North Greenland: Bulletin of the Geological Society of Denmark, v. 65, p. 47–58, doi:10.37570/bgsd-2017-65-04.

Nursall, J.R., 2009, The lateral musculature and the swimming of fish: Proceedings of the Zoological Society of London, v. 126, p. 127–144, doi:10.1111/j.1096-3642.1956.tb00429.x.

Ogasawara, M., Shigetani, Y., Suzuki, S., Kuratani, S., and Satoh, N., 2001, Expression of Thyroid transcription factor-1 (TTF-1) gene in the ventral forebrain and endostyle of the agnathan vertebrate, Lampetra japonica: Genesis, v. 30, p. 51–58, doi:10.1002/gene.1032.

Olszewski, T.D., and West, R.R., 1997, Influence of transportation and time-averaging in fossil assemblages from the Pennsylvanian of Oklahoma: Lethaia, v. 30, p. 315–329, doi:10.1111/j.1502-3931.1997.tb00475.x.

Orr, P.J., Briggs, D.E.G., and Kearns, S.L., 1998, Cambrian Burgess Shale Animals Replicated in Clay Minerals: Science, v. 281, p. 1173–1176, doi:10.1126/science.281.5380.1173.

Ou, Q., Conway Morris, S., Han, J., Zhang, Z., Liu, J., Chen, A., and Zhang, X.-L., 2012, Evidence for gill slits and a pharynx in Cambrian vetulicolians: implications for the early evolution of deuterostomes: BMC Biology, v. 10, p. 81, doi:10.1186/1741-7007-10-81.

Page, A., Gabbott, S.E., Wilby, P.R., and Zalasiewicz, J.A., 2008, Ubiquitous Burgess Shale–style “clay templates” in low-grade metamorphic mudrocks: Geology, v. 36, p. 855–858, doi:10.1130/G24991A.1.

Park, T.Y.S., Kihm, J.H., Woo, J., Park, C., Lee, W.Y., Smith, M.P., Harper, D.A.T., Young, F., Nielsen, A.T., and Vinther, J., 2018, Brain and eyes of *Kerygmachela* reveal protocerebral ancestry of the panarthropod head: Nature Communications, v. 9, p. 1–7, doi:10.1038/s41467-018-03464-w.

Parry, L.A., Smithwick, F., Nordén, K.K., Saitta, E.T., Lozano-Fernandez, J., Tanner, A.R., Caron, J.B., Edgecombe, G.D., Briggs, D.E.G., and Vinther, J., 2018, Soft-Bodied Fossils Are Not Simply Rotten Carcasses – Toward a Holistic Understanding of Exceptional Fossil Preservation: Exceptional Fossil Preservation Is Complex and Involves the Interplay of Numerous Biological and Geological Processes: BioEssays, v. 40, p. 1–11, doi:10.1002/bies.201700167.

Parry, L., Vinther, J., and Edgecombe, G.D., 2015a, Cambrian stem-group annelids and a metameric origin of the annelid head: Biology Letters, v. 11, p. 20150763, doi:10.1098/rsbl.2015.0763.

Parry, L.A., Wilson, P., Sykes, D., Edgecombe, G.D., and Vinther, J., 2015b, A new fireworm (Amphinomidae) from the Cretaceous of Lebanon identified from three-dimensionally preserved myoanatomy: BMC Evolutionary Biology, v. 15, p. 1–10, doi:10.1186/s12862-015-0541-8.

Paterson, J.R., García-Bellido, D.C., and Edgecombe, G.D., 2012, New artiopodan arthropods from the early Cambrian Emu Bay Shale Konservat-Lagerstätte of South Australia: Journal of Paleontology, v. 86, p. 340–357, doi:10.1666/11-077.1.

Paterson, J.R., García-bellido, D.C., Jago, J.B., Gehling, J.G., Lee, M.S.Y., and Edgecombe, G.D., 2015, The Emu Bay Shale Konservat-Lagerstätte: a view of Cambrian life from East Gondwana: Journal of the Geological Society, v. 173, p. 1–11, doi:10.1144/jgs2015-083.

Paterson, J.R., García-Bellido, D.C., Lee, M.S.Y., Brock, G.A., Jago, J.B., and Edgecombe, G.D., 2011, Acute vision in the giant Cambrian predator *Anomalocaris* and the origin of compound eyes: Nature, v. 480, p. 237–240, doi:10.1038/nature10689.

Paterson, J.R., Jago, J.B., Brock, G.A., and Gehling, J.G., 2007, Taphonomy and palaeoecology of the emuellid trilobite *Balcoracania dailyi* (early Cambrian, South Australia): Palaeogeography, Palaeoclimatology, Palaeoecology, v. 249, p. 302–321, doi:10.1016/j.palaeo.2007.02.004.

Pates, S., Daley, A.C., Legg, D.A., and Rahman, I.A., 2021, Vertically migrating *Isoxys* and the early Cambrian biological pump: Proceedings of the Royal Society B: Biological Sciences, v. 288, doi:10.1098/rspb.2021.0464.

Pauly, D., and Holmes, J.D., 2022, Reassessing growth and mortality estimates for the Ordovician trilobite *Triarthrus eatoni*: Paleobiology, p. 1–11, doi:10.1017/pab.2022.22.

Peel, J.S., 2010a, A corset-like fossil from the Cambrian Sirius Passet Lagerstätte of North Greenland and its implications for cycloneuralian evolution: Journal of Paleontology, v. 84, p. 332–340, doi:10.1666/09-102r.1.

Peel, J.S., 2010b, Articulated hyoliths and other fossils from the Sirius Passet Lagerstätte (early cambrian) of North Greenland: Bulletin of Geosciences, v. 85, p. 385–394, doi:10.3140/bull.geosci.1207.

Peel, J.S., 2017a, Feeding behaviour of a new worm (Priapulida) from the Sirius Passet

Lagerstätte (Cambrian Series 2, Stage 3) of North Greenland (Laurentia): Palaeontology, v. 60, p. 795–805, doi:10.1111/pala.12316.
Peel, J.S., 2017b, Mineralized gutfills from the Sirius Passet Lagerstätte (Cambrian Series 2) of North Greenland: GFF, v. 139, p. 83–91, doi:10.1080/11035897.2016.1260051.
Peel, J.S., 2017c, Molaria (Euarthropoda) from the Sirius Passet Lagerstätte (Cambrian series 2, stage 3) of North Greenland: Bulletin of Geosciences, v. 92, p. 133–142, doi:10.3140/bull.geosci.1658.
Peel, J.., 1990, Studying the early history of life in Greenland: Rapport Grønlands Geologiske Undersøgelse, v. 148, p. 54–56, doi:10.34194/rapggu.v148.8121.
Peel, J.S., and Ineson, J.R., 2011, The extent of the Sirius Passet Lagerstätte (early Cambrian) of North Greenland: Bulletin of Geosciences, v. 86, p. 535–543, doi:10.3140/bull.geosci.1269.
Peel, J.S., and Stein, M., 2009, A new arthropod from the lower Cambrian Sirius Passet Fossil-Lagerstätte of North Greenland: Bulletin of Geosciences, v. 84, p. 625–630, doi:10.3140/bull.geosci.1158.
Peel, J.S., Stein, M., and Kristensen, R.M., 2013, Life Cycle and Morphology of a Cambrian Stem-Lineage Loriciferan: PLoS ONE, v. 8, p. 1–12, doi:10.1371/journal.pone.0073583.
Petro, Sandro Monticelli, Matias do Nascimento Ritter, María Alejandra Gómez Pivel, and Joao Carlos Coimbra, 2018, Surviving in the water column: defining the taphonomically active zone in pelagic systems: Palaios v. 33, p. 85–93, doi:10.2110/palo.2017.032
Powell, W., 2003, Greenschist-facies metamorphism of the Burgess Shale and its implications for models of fossil: Canadian Journal of Earth Sciences, v. 40, p. 13–25, doi:10.1139/E02-103.
Price, A.R.G., 1982, Western arabian gulf echinoderms in high salinity waters and the occurrence of dwarfism: Journal of Natural History, v. 16, p. 519–527, doi:10.1080/00222938200770421.
Pushie, M.J., Pratt, B.R., Macdonald, T.C., George, G.N., and Pickering, I.J., 2014, Evidence for biogenic copper (hemocyanin) in the Middle Cambrian arthropod marrella from the Burgess Shale: Palaios, v. 29, p. 512–524, doi:10.2110/palo.2014.073.
R Core Team, 2013, R: A language and environment for statistical computing:
Rahn, M.K., Steinmann, M., and Frey, M., 2002, Chloritoid composition and formation in the eastern Central Alps: A comparison between Penninic and Helvetic occurrences:

Schweizerische Mineralogische und Petrographische Mitteilungen, v. 82, p. 409–426.
Raiswell, R., and Canfield, D.E., 1998, Sources of iron for pyrite formation in marine sediments: American Journal of Science, v. 298, p. 219–245, doi:10.2475/ajs.298.3.219.
Ramseyer, K., Amthor, J.E., Matter, A., Pettke, T., Wille, M., and Fallick, A.E., 2013, Primary silica precipitate at the Precambrian/Cambrian boundary in the South Oman Salt Basin, Sultanate of Oman: Marine and Petroleum Geology, v. 39, p. 187–197, doi:10.1016/j.marpetgeo.2012.08.006.
Reeve, M.R., 1963, The Filter-Feeding of Artemia: Journal of Experimental Biology, v. 40, p. 195–205, doi:10.1242/jeb.40.1.195.
Reynolds, B.C. et al., 2007, An inter-laboratory comparison of Si isotope reference materials: Journal of Analytical Atomic Spectrometry, v. 22, p. 561–658, doi:10.1039/b616755a.
Rice, J., 1995, Food web theory, marine food webs, and what climate change may do to northern marine fish populations: Canadian Special Publication of Fisheries and Aquatic Sciences,.
Rieger, V., Perez, Y., Müller, C.H.G., Lacalli, T., Hansson, B.S., and Harzsch, S., 2011, Development of the nervous system in hatchlings of *Spadella cephaloptera* (Chaetognatha), and implications for nervous system evolution in Bilateria: Development Growth and Differentiation, v. 53, p. 740–759, doi:10.1111/j.1440-169X.2011.01283.x.
Rigby, J., 1986, Cambrian and Silurian sponges from North Greenland: Rapport Grønlands Geologiske Undersøgelse, v. 132, p. 51–63, doi:10.34194/rapggu.v132.7964.
Robert, F., and Chaussidon, M., 2006, A palaeotemperature curve for the Precambrian oceans based on silicon isotopes in cherts: Nature, v. 443, p. 969–972, doi:10.1038/nature05239.
Sagemann, J., Bale, S.J., Briggs, D.E.G., and Parkes, R.J., 1999, Controls on the formation of authigenic minerals in association with decaying organic matter: An experimental approach: Geochimica et Cosmochimica Acta, v. 63, p. 1083–1095, doi:10.1016/S0016-7037(99)00087-3.
Saleh, F. et al., 2021a, Insights into soft-part preservation from the Early Ordovician Fezouata Biota: Earth-Science Reviews, v. 213, p. 103464, doi:10.1016/j.earscirev.2020.103464.
Saleh, F. et al., 2021b, Large trilobites in a stress-free Early Ordovician environment:

Geological Magazine, v. 158, p. 261–270, doi:10.1017/S0016756820000448.

Saleh, F. et al., 2020a, Taphonomic pathway of exceptionally preserved fossils in the Lower Ordovician of Morocco: Geobios, v. 60, p. 99–115, doi:10.1016/j.geobios.2020.04.001.

Saleh, F., Antcliffe, J.B., Lefebvre, B., Pittet, B., Laibl, L., Perez Peris, F., Lustri, L., Gueriau, P., and Daley, A.C., 2020b, Taphonomic bias in exceptionally preserved biotas: Earth and Planetary Science Letters, v. 529, p. 115873, doi:10.1016/j.epsl.2019.115873.

Saleh, F., Bath-Enright, O.G., Daley, A.C., Lefebvre, B., Pittet, B., Vite, A., Ma, X., Mángano, M.G., Buatois, L.A., and Antcliffe, J.B., 2021c, A novel tool to untangle the ecology and fossil preservation knot in exceptionally preserved biotas: Earth and Planetary Science Letters, v. 569, p. 117061, doi:10.1016/j.epsl.2021.117061.

Saleh, F., Candela, Y., Harper, D.A.T., Polechová, M., Lefebvre, B., and Pittet, B., 2018, Storm-induced community dynamics in the fezouata biota (Lower Ordovician, Morocco): Palaios, v. 33, p. 535–541, doi:10.2110/palo.2018.055.

Saleh, F., Lefebvre, B., Hunter, A.W., and Nohejlová, M., 2020c, Fossil Weathering and Preparation Mimic Soft Tissues in Eocrinoid and Somasteroid Echinoderms from the Lower Ordovician of Morocco: Microscopy Today, v. 28, p. 24–28, doi:10.1017/s1551929519001238.

Saleh, F., Ma, X., Guenser, P., Mángano, M.G., Buatois, L.A., and Antcliffe, J.B., 2022a, Probability-based preservational variations within the early Cambrian Chengjiang biota (China): PeerJ, v. 10, p. e13869, doi:10.7717/peerj.13869.

Saleh, F., Qi, C., Buatois, L.A., Mángano, M.G., Paz, M., Vaucher, R., Zheng, Q., Hou, X.G., Gabbott, S.E., and Ma, X., 2022b, The Chengjiang Biota inhabited a deltaic environment: Nature Communications, v. 13, p. 1–9, doi:10.1038/s41467-022-29246-z.

Sansom, R.S., Gabbott, S.E., and Purnell, M.A., 2010, Non-random decay of chordate characters causes bias in fossil interpretation: Nature, v. 463, p. 797–800, doi:10.1038/nature08745.

Savage, P.S., Georg, R.B., Williams, H.M., and Halliday, A.N., 2013, The silicon isotope composition of the upper continental crust: Geochimica et Cosmochimica Acta, v. 109, p. 384–399, doi:10.1016/j.gca.2013.02.004.

Schiffbauer, J.D., Xiao, S., Cai, Y., Wallace, A.F., Hua, H., Hunter, J., Xu, H., Peng, Y., and Kaufman, A.J., 2014, A unifying model for Neoproterozoic–Palaeozoic exceptional fossil preservation through pyritization and carbonaceous compression: Nature Communications, v. 5, p. 1–12, doi:10.1038/ncomms6754.

Schneider, C.A., Rasband, W.S., and Eliceiri, K.W., 2012, NIH Image to ImageJ: 25 years of image analysis: Nature Methods, v. 9, p. 671–675, doi:10.1038/nmeth.2089.

Scrucca, L., Fop, M., Murphy, T.B., and Raftery, A.E., 2016, mclust 5: Clustering, Classification and Density Estimation Using Gaussian Finite Mixture Models: R Journal, v. 8, p. 289–317.

Seilacher, A., Reif, W.-E., and Westphal, F., 1985, Sedimentological, ecological and temporal patterns of fossil Lagerstatten: Philosophical Transactions of the Royal Society of London. B, Biological Sciences, v. 311, p. 5–24, doi:https://doi.org/10.1098/rstb.1985.0134.

Shimoyama, S., 1985, Size-frequency distribution of living populations and dead shell assemblages in a marine intertidal sand snail, Umbonium (Suchium) moniliferum (Lamarck), and their palaeoecological significance: Palaeogeography, Palaeoclimatology, Palaeoecology, v. 49, p. 327–353.

Shu, D., Vannier, J., Luo, H., Chen, L., Zhang, X., Hu, S., 1999, Anatomy and lifestyle of *Kunmingella* (Arthropoda, Bradoriida) from the Chengjiang fossil Lagerstätte (Lower Cambrian; Southwest China): Lethaia, v. 32, p. 279-298, doi.org/10.1111/j.1502-3931.1999.tb00547.x

Shu, D., Conway Morris, S., Zhang, Z., and Han, J., 2010, The earliest history of the deuterostomes: the importance of the Chengjiang Fossil-Lagerstätte: Proceedings of the Royal Society B: Biological Sciences, v. 277, p. 165–174, doi:10.1098/rspb.2009.0646.

Sieburth, J.M., Smetacek, V., and Lenz, J., 1978, Pelagic ecosystem structure: Heterotrophic compartments of the plankton and their relationship to plankton size fractions: Limnology and oceanography, v. 23, p. 1256–1263.

Sinha, S., Muscente, A.D., Schiffbauer, J.D., Williams, M., Schweigert, G., Martindale, R.C., 2021, Global controls on phosphatization of fossils during the Toarcian Oceanic Anoxic Event: Scientific Reports, v. 11, 24087, doi.org/10.1038/s41598-021-03482-7

Slater, B.J., Willman, S., Budd, G.E., and Peel, J.S., 2018, Widespread preservation of small carbonaceous fossils (SCFs) in the early Cambrian of North Greenland: Geology, v. 46, p. 107–110, doi:10.1130/G39788.1.

Smith, W.O., and Demaster, D.J., 1996, Phytoplankton biomass and productivity in the

Amazon River plume: Correlation with seasonal river discharge: Continental Shelf Research, v. 16, p. 291–319, doi:10.1016/0278-4343(95)00007-N.

Soper, N.J., and Higgins, A.K., 1987, A shallow detachment beneath the North Greenland fold belt: Implications for sedimentation and tectonics: Geological Magazine, v. 124, p. 441–450, doi:10.1017/S0016756800017027.

Sperling, E.A., Frieder, C.A., Raman, A. V., Girguis, P.R., Levin, L.A., and Knoll, A.H., 2013, Oxygen, ecology, and the Cambrian radiation of animals: Proceedings of the National Academy of Sciences of the United States of America, v. 110, p. 13446–13451, doi:10.1073/pnas.1312778110.

Staff, G.M., Stanton, R.J., Powell, E.N., and Cummins, H., 1986, Time-averaging, taphonomy, and their impact on paleocommunity reconstruction: death assemblages in Texas bays (USA).: Geological Society of America Bulletin, v. 97, p. 428–443, doi:10.1130/0016-7606(1986)97<428:TTATIO>2.0.CO;2.

Stanley, S.M., 1973, An Ecological Theory for the Sudden Origin of Multicellular Life in the Late Precambrian: Proceedings of the National Academy of Sciences, v. 70, p. 1486–1489, doi:10.1073/pnas.70.5.1486.

Stefurak, E.J.T., Fischer, W.W., and Lowe, D.R., 2015, Texture-specific Si isotope variations in Barberton Greenstone Belt cherts record low temperature fractionations in early Archean seawater: Geochimica et Cosmochimica Acta, v. 150, p. 26–52, doi:10.1016/j.gca.2014.11.014.

Stein, M., 2010, A new arthropod from the Early Cambrian of North Greenland , with a ‘great appendage’-like antennula: Zoological Journal of the Linnean Society, v. 158, p. 477–500, doi:10.1111/j.1096-3642.2009.00562.x.

Stein, M., Budd, G.E., Peel, J.S., and Harper, D.A.T., 2013, Arthroaspis n. gen., a common element of the Sirius Passet Lagerstätte (Cambrian , North Greenland), sheds light on trilobite ancestry: BMC Evolutionary Biology, v. 13, p. 99.

Stein, M., Peel, J.S., Siveter, D.J., and Williams, M., 2010, *Isoxys* (Arthropoda) with preserved soft anatomy from the Sirius Passet Lagerstätte, lower Cambrian of North Greenland: Lethaia, v. 43, p. 258–265, doi:10.1111/j.1502-3931.2009.00189.x.

Strang, K.M., Armstrong, H.A., and Harper, D.A.T., 2016a, Minerals in the gut: scoping a Cambrian digestive system: Royal Society Open Science, v. 3, p. 160420, doi:10.1080/14772019.2010.492644.

Strang, K.M., Armstrong, H.A., Harper, D.A.T., and Trabucho-Alexandre, J.P., 2016b, The Sirius Passet Lagerstätte: silica death masking opens the window on the earliest matground community of the Cambrian explosion: Lethaia, v. 49, p. 631–643, doi:10.1111/let.12174.

Sutherland, K.R., Madin, L.P., and Stocker, R., 2010, Filtration of submicrometer particles by pelagic tunicates: Proceedings of the National Academy of Sciences, v. 107, p. 15129–15134, doi:10.1073/pnas.1003599107.

Swalla, B.J., 2007, New insights into vertebrate origins, *in* Moody, S.A. ed., Principles of Developemental Genetics, London, UK, Academic Press, p. 114–128.

Tanasichuk, R.W., 1998, Interannual variations in the population biology and productivity of Thysanoessa spinifera in Barkley Sound, Canada, with special reference to the 1992 and 1993 warm ocean years: Marine Ecology Progress Series, v. 173, p. 181–195, doi:10.3354/meps173181.

Tarhan, L.G., Hood, A.V.S., Droser, M.L., Gehling, J.G., and Briggs, D.E.G., 2016, Exceptional preservation of soft-bodied Ediacara Biota promoted by silica-rich oceans: Geology, v. 44, p. 951–954, doi:10.1130/G38542.1.

Tarhan, L.G., Planavsky, N.J., Wang, X., Bellefroid, E.J., Droser, M.L., and Gehling, J.G., 2018, The late-stage "ferruginization" of the Ediacara Member (Rawnsley Quartzite, South Australia): Insights from uranium isotopes: Geobiology, v. 16, p. 35–48, doi:10.1111/gbi.12262.

Tarling, G.A., 2010, Population Dynamics of Northern Krill (*Meganyctiphanes norvegica* Sars): Advances in Marine Biology, v. 57, p. 59–90, doi:10.1016/B978-0-12-381308-4.00003-0.

Tarling, G.A., and Cuzin-Roudy, J., 2003, Synchronization in the molting and spawning activity of northern krill (*Meganyctiphanes norvegica*) and its effect on recruitment: Limnology and Oceanography, v. 48, p. 2020–2033, doi:10.4319/lo.2003.48.5.2020.

Tatzel, M., Von Blanckenburg, F., Oelze, M., Bouchez, J., and Hippler, D., 2017, Late Neoproterozoic seawater oxygenation by siliceous sponges: Nature Communications, v. 8, p. 1–9, doi:10.1038/s41467-017-00586-5.

Tatzel, M., Stuff, M., Franz, G., Hippler, D., Wiechert, U., and von Blanckenburg, F., 2020, Siliceous sponge expansion and phosphogenesis in a shallow water environment in the Malyi Karatau Range (Kazakhstan) during the Precambrian-Cambrian transition:

Precambrian Research, v. 347, doi:10.1016/j.precamres.2020.105830.

Taylor, R.S., 2002, A new bivalved arthropod from the Early Cambrian Sirius Passet fauna, North Greenland: Palaeontology, v. 45, p. 97–123, doi:10.1111/1475-4983.00229.

Taylor, S.R., and McLennan, S.M., 1985, The continental crust: Its composition and evolution: Blackwell, Oxford.

Terabayashi, M., Yamamoto, H., Hiwatashi, E., Kitajima, K., 2010, Silicification of pelitic schist in the Ryoke low-pressure/temperature metamorphic belt, Southwest Japan: Origin of competent layers in the middle crust: Island Arc, v. 19, 17–29, doi.org/10.1111/j.1440-1738.2009.00701.x.

Thyberg, B., Jahren, J., 2011, Quartz cementation in mudstones: sheet-like quartz cement from clay mineral reactions during burial: Petroleum Geoscience, p. 53–63, doi:10.1144/1354-079310-028.

Topper, T.P., Greco, F., Hofmann, A., Beeby, A., and Harper, D.A.T., 2018, Characterization of kerogenous films and taphonomic modes of the Sirius Passet Lagerstätte, Greenland: Geology, v. 46, p. 359–362, doi:10.1130/G39930.1.

Trewin, N.H., Fayers, S.R., and Kelman, R., 2003, Subaqueous silicification of the contents of small ponds in an Early Devonian hot-spring complex, Rhynie, Scotland: Canadian Journal of Earth Sciences, v. 40, p. 1697–1712, doi:10.1139/e03-065.

Trinajstic, K. et al., 2022, Exceptional preservation of organs in Devonian placoderms from the Gogo Lagerstätte: Science (New York, N.Y.), v. 377, p. 1311–1314, doi:10.1126/science.abf3289.

Trinajstic, K., Marshall, C., Long, J., and Bifield, K., 2007, Exceptional preservation of nerve and muscle tissues in Late Devonian placoderm fish and their evolutionary implications: Biology Letters, v. 3, p. 197–200, doi:10.1098/rsbl.2006.0604.

Vannier, J., 2012, Gut contents as direct indicators for trophic relationships in the Cambrian marine ecosystem: PLoS ONE, v. 7, doi:10.1371/journal.pone.0052200.

Vannier, J., Aria, C., Taylor, R.S., and Caron, J., 2018, Waptia fieldensis Walcott, a mandibulate arthropod from the middle Cambrian Burgess Shale: Royal Society Open Science, v. 5, p. 172206, doi:10.1098/rsos.172206.

Vannier, J., and Chen, J.Y., 2000, The early Cambrian colonization of pelagic niches exemplified by Isoxys (Arthropoda): Lethaia, v. 33, p. 295–311, doi:10.1080/002411600750053862.

Vannier, J., García-Bellido, D.C., Hu, S.X., and Chen, A.L., 2009, Arthropod visual predators in the early pelagic ecosystem: Evidence from the Burgess Shale and Chengjiang biotas: Proceedings of the Royal Society B: Biological Sciences, v. 276, p. 2567–2574, doi:10.1098/rspb.2009.0361.

Vannier, J., Liu, J., Lerosey-Aubril, R., Vinther, J., and Daley, A.C., 2014, Sophisticated digestive systems in early arthropods: Nature Communications, v. 5, p. 1–9, doi:10.1038/ncomms4641.

Vannier, J., and Martin, E.L.O., 2017, Worm-lobopodian assemblages from the Early Cambrian Chengjiang biota: Insight into the "pre-arthropodan ecology"? Palaeogeography, Palaeoclimatology, Palaeoecology, v. 468, p. 373–387, doi:10.1016/j.palaeo.2016.12.002.

Vannier, J., Steiner, M., Renvoisé, E., Hu, S.X., and Casanova, J.P., 2007, Early Cambrian origin of modern food webs: Evidence from predator arrow worms: Proceedings of the Royal Society B: Biological Sciences, v. 274, p. 627–633, doi:10.1098/rspb.2006.3761.

Vereshchaka, A.L., Olesen, J., and Lunina, A.A., 2016, A phylogeny-based revision of the family Luciferidae (Crustacea: Decapoda): Zoological Journal of the Linnean Society, v. 178, p. 15–32, doi:10.1111/zoj.12398.

Vinther, J., Eibye-Jacobsen, D., and Harper, D.A.T., 2011a, An Early Cambrian stem polychaete with pygidial cirri: Biological Letters, p. 1–5, doi:10.1098/rsbl.2011.0592.

Vinther, J., and Nielsen, C., 2005, The early Cambrian *Halkieria* is a mollusc: Zoologica scripta, v. 34, p. 81–89, doi:10.1111/j.1463-6409.2005.00177.x.

Vinther, J., and Parry, L.A., 2019, Bilateral Jaw Elements in *Amiskwia sagittiformis* Bridge the Morphological Gap between Gnathiferans and Chaetognaths: Current Biology, v. 29, p. 881- 888.e1, doi:10.1016/j.cub.2019.01.052.

Vinther, J., Porras, L., Young, F.J., Budd, G.E., and Edgecombe, G.D., 2016, The mouth apparatus of the Cambrian gilled lobopodian Pambdelurion whittingtoni: Palaeontology, v. 59, p. 841–849, doi:10.1111/pala.12256.

Vinther, J., Smith, M.P., and Harper, D.A.T., 2011b, Vetulicolians from the Lower Cambrian Sirius Passet Lagerstätte, North Greenland, and the polarity of morphological characters in basal deuterostomes: Palaeontology, v. 54, p. 711–719, doi:10.1111/j.1475-4983.2011.01034.x.

Vinther, J., Stein, M., Longrich, N.R., and Harper, D.A.T., 2014, A suspension-feeding anomalocarid from the Early Cambrian: Nature, v. 507, p. 496–499, doi:10.1038/nature13010.

De Vivo, G., Lautenschlager, S., and Vinther, J., 2021, Three-dimensional modelling, disparity and ecology of the first Cambrian apex predators: Proceedings of the Royal Society B: Biological Sciences, v. 288, p. 20–22, doi:10.1098/rspb.2021.1176.

Wen, H., Fan, H., Tian, S., Wang, Q., and Hu, R., 2016, The formation conditions of the early Ediacaran cherts, South China: Chemical Geology, v. 430, p. 45–69, doi:10.1016/j.chemgeo.2016.03.005.

Westrop, S.R., 1986, Taphonomic versus ecologic controls on taxonomic relative abundance patterns in tempestites: Lethaia, v. 19, p. 123–132, doi:10.1111/j.1502-3931.1986.tb00722.x.

Whitaker, A.F., and Kimmig, J., 2020, Anthropologically introduced biases in natural history collections, with a case study on the invertebrate paleontology collections from the middle cambrian spence shale lagerstätte: Palaeontologia Electronica, v. 23, p. 1–26, doi:10.26879/1106.

Whittington, H.B., and Briggs, D.E.G., 1985, The largest Cambrian animal, *Anomalocaris*, Burgess Shale, British-Columbia: Philosophical Transactions of the Royal Society of London B: Biological Sciences, v. 309, p. 569–609, doi:doi:10.1098/rstb.1996.0087.

Wilby, P.R., 1993, The role of organic matrices in post-mortem phosphatization of soft tissues: Kaupia, v. 2, p. 99–113.

Wilby, P.R., and Briggs, D.E.G., 1997, Taxonomic trends in the resolution of detail preserved in fossil phosphatized soft tissues: Geobios, v. 30, p. 493–502, doi:10.1016/S0016-6995(97)80056-3.

Wilby, P.R., Briggs, D.E.G., Bernier, P., and Gaillard, C., 1996a, Role of microbial mats in the fossilization of soft tissues: Geology, v. 24, p. 787–790.

Wilby, P.R., Briggs, D.E.G., and Riou, B., 1996b, Mineralization of soft-bodied invertebrates in a Jurassic metalliferous deposit: Geology, v. 24, p. 847–850, doi:10.1130/0091-7613(1996)024<0847:MOSBII>2.3.CO;2.

Wilby, P.R., Hudson, J.D., Clements, R.G., and Hollingworth, N.T.J., 2004, Taphonomy and origin of an accumulate of soft-bodied cephalopods in the Oxford Clay Formation (Jurassic, England): Palaeontology, v. 47, p. 1159–1180, doi:10.1111/j.0031-0239.2004.00405.x.

Wilby, P.R., and Martill, D.M., 1992, Fossil Fish Stomachs: A Microenvironment for Exceptional Preservation: Historical Biology, v. 6, p. 25–36, doi:10.1080/10292389209380416.

Wilby, P.R., Page, A.A., Zalasiewicz, J.A., Milodowski, A.E., Williams, M., and Evans, J.A., 2007, Syntectonic monazite in low-grade mudrocks: A potential geochronometer for cleavage formation? Journal of the Geological Society, London, v. 164, p. 53–56, doi:10.1144/0016-76492006-035.

Wilby, P.R., and Whyte, M.A., 1995, Phosphatized soft tissues in bivalves from the Portland Roach of Dorset (Upper Jurassic): Geological Magazine, v. 132, p. 117–120, doi:10.1017/S001675680001147X.

Wille, M., Sutton, J., Ellwood, M.J., Sambridge, M., Maher, W., Eggins, S., and Kelly, M., 2010, Silicon isotopic fractionation in marine sponges: A new model for understanding silicon isotopic variations in sponges: Earth and Planetary Science Letters, v. 292, p. 281–289, doi:10.1016/j.epsl.2010.01.036.

Williams, M., Siveter, D.J., and Peel, J.S., 1996, *Isoxys* (Arthropoda) from the Early Cambrian Sirius Passet Lagerstätte, North Greenland: Journal of Paleontology, v. 70, p. 947–954, doi:10.1017/S0022336000038646.

Wilson, L.A., and Butterfield, N.J., 2014, Sediment effects on the preservation of Burgess Shale-type compression fossils: Palaios, v. 29, p. 145–153, doi:10.2110/palo.2013.075.

Wilson, P., Parry, L.A., Vinther, J., and Edgecombe, G.D., 2016, Unveiling biases in soft-tissue phosphatization: Extensive preservation of musculature in the Cretaceous (Cenomanian) polychaete *Rollinschaeta myoplena* (Annelida: Amphinomidae): Palaeontology, v. 59, p. 463–479, doi:10.1111/pala.12237.

Wit, E., van den Heuvel, E., and Romeijn, J.W., 2012, 'All models are wrong. ': An introduction to model uncertainty: Statistica Neerlandica, v. 66, p. 217–236, doi:10.1111/j.1467-9574.2012.00530.x.

Xiao, S., Zhang, Y., and Knoll, A.H., 1998, Three-dimensional preservation of algae and animal embryos in a Neoproterozoic phosphorite: Nature, v. 391, p. 553–558.

Yang, X., Kimmig, J., Zhai, D., Liu, Y., Kimmig, S.R., and Peng, S., 2021a, A juvenile-rich palaeocommunity of the lower Cambrian Chengjiang biota sheds light on palaeo-boom or palaeo-bust environments: Nature Ecology and Evolution, v. 5, p. 1082–1090, doi:10.1038/s41559-021-01490-4.

Yang, X. yu, Smith, M.R., Yang, J., Li, W., Guo, Q. hao, Li, C. li, Wang, Y., and Zhang, X. guang, 2021b, A 'hermit' shell-dwelling lifestyle in a Cambrian priapulan worm: Current Biology, v. 31, p. R1420–R1421, doi:10.1016/j.cub.2021.10.003.

Young, F.J., and Vinther, J., 2016, Onychophoran-like myanatomy of the Cambrian gilled lobopodian *Pambdelurion whittingtoni*: Palaeontology, v. 60, p. 27–54, doi:10.1111/pala.12269.

Zettler, M.L., Bochert, R., and Pollehne, F., 2009, Macrozoobenthos diversity in an oxygen minimum zone off northern Namibia: Marine Biology, v. 156, p. 1949–1961, doi:10.1007/s00227-009-1227-9.

Zhang, H., Fan, H., Wen, H., Zhu, X., and Tian, S., 2020, Oceanic chemistry recorded by cherts during the early Cambrian Explosion, South China: Palaeogeography, Palaeoclimatology, Palaeoecology, v. 558, p. 109961, doi:10.1016/j.palaeo.2020.109961.

Zhao, F., Caron, J.-B., Hu, S., and Zhu, M., 2009, Quantitative analysis of taphofacies and paleocommunities in the Early Cambrian Chengjiang Lagerstätte: Palaios, v. 24, p. 826–839.

Appendix

A1 R code for mclust mixture analysis in Chapter 4

```
#install.packages("mclust")
library(mclust)
#IsoxysR <- read.csv([file based on Data Table E4.4])
IsoxysR <- read.csv(file.choose())
#mclust simulation to determine simulated components (populations) for each bed
individually
mc.bed1<-Mclust(IsoxysR$Size[1:4])
mc.bed2<-Mclust(IsoxysR$Size[5:11])
mc.bed3<-Mclust(IsoxysR$Size[12:15])
mc.bed4<-Mclust(IsoxysR$Size[16:64])
mc.bed5<-Mclust(IsoxysR$Size[65:86])
mc.bed6<-Mclust(IsoxysR$Size[87:117])
mc.bed7<-Mclust(IsoxysR$Size[118:141])
mc.bed8<-Mclust(IsoxysR$Size[142:147])
mc.bed9<-Mclust(IsoxysR$Size[148:159])
mc.bed10<-Mclust(IsoxysR$Size[160:164])
mc.bed11<-Mclust(IsoxysR$Size[165:175])
mc.bed12<-Mclust(IsoxysR$Size[176:194])
mc.bed13<-Mclust(IsoxysR$Size[195:218])
mc.bed14<-Mclust(IsoxysR$Size[219:230])
mc.bed15<-Mclust(IsoxysR$Size[231:254])
mc.bed16<-Mclust(IsoxysR$Size[255:286])
mc.bed17<-Mclust(IsoxysR$Size[287:304])
mc.bed18<-Mclust(IsoxysR$Size[305:326])
mc.bed19<-Mclust(IsoxysR$Size[327:382])
mc.bed20<-Mclust(IsoxysR$Size[383:392])

#mclust simulation of the entire dataset.
mc.2comp <- Mclust(IsoxysR[,2])
summary(mc.2comp, parameters = TRUE)
means.mc.2comp<-mc.2comp$parameters$mean
std.mc.2comp<-sqrt(mc.2comp$parameters$variance$sigmasq)
#mclust simulation of the entire dataset forced to one single component.
mc.1comp <- Mclust(IsoxysR[,2],G=1)
summary(mc.1comp, parameters = TRUE)
means.mc.1comp<-mc.1comp$parameters$mean
std.mc.1comp<-sqrt(mc.1comp$parameters$variance$sigmasq)
```

#the below simulations multiple different distributions based on the above data, and then returns what the result of mclust would be. Sample 1 is a simulation where the dataset is composed of a single pre-classified component corresponding to the actual total dataset. Sample2 is a simulation of the expected distribution (n) of Component 1 and 2 based on their relative distribution in the total dataset. Sample3 is a simulation where the distribution (n) of Component 1 and 2 reflects the actual distribution in a given bed. The simulations return the number of components present in each bed as calculated by mclust. Sample1 simulates the number of components if the sampled distributions are explained by random samples of a homogenous size population throughout the section (null hypothesis). Sample2 simulates the number of components if the sampled distributions are explained by two components with consistent distribution throughout the sampled beds. Sample3 simulates the number of components if the sampled distributions are explained by two components with distributions reflecting the sampled distribution for each bed.

```
bed1<-matrix(NA,100,3)
colnames(bed1)<-c("1 comp", "2 comp tot", "2 comp act")

for(i in 1:100)
{
    sample1<-c(rnorm(4,means.mc.1comp[1],std.mc.1comp[1]))
    sample2<-
c(rnorm(1,means.mc.2comp[1],std.mc.2comp[1]),rnorm(3,means.mc.2comp[2],std.mc.2com
p[2]))
    sample3<-
c(rnorm(0,means.mc.2comp[1],std.mc.2comp[1]),rnorm(4,means.mc.2comp[2],std.mc.2com
p[2]))
    bed1[i,1]<-summary(Mclust(sample1))$G
    bed1[i,2]<-summary(Mclust(sample2))$G
    bed1[i,3]<-summary(Mclust(sample3))$G
}

bed2<-matrix(NA,100,3)
colnames(bed2)<-c("1 comp", "2 comp tot", "2 comp act")

for(i in 1:100)
{
  sample1<-c(rnorm(7,means.mc.1comp[1],std.mc.1comp[1]))
  sample2<-
c(rnorm(2,means.mc.2comp[1],std.mc.2comp[1]),rnorm(5,means.mc.2comp[2],std.mc.2com
p[2]))
```

```
    sample3<-
c(rnorm(0,means.mc.2comp[1],std.mc.2comp[1]),rnorm(7,means.mc.2comp[2],std.mc.2com
p[2]))
    bed2[i,1]<-summary(Mclust(sample1))$G
    bed2[i,2]<-summary(Mclust(sample2))$G
    bed2[i,3]<-summary(Mclust(sample3))$G
  }

  bed3<-matrix(NA,100,3)
  colnames(bed3)<-c("1 comp", "2 comp tot", "2 comp act")

  for(i in 1:100)
  {
    sample1<-c(rnorm(4,means.mc.1comp[1],std.mc.1comp[1]))
    sample2<-
c(rnorm(1,means.mc.2comp[1],std.mc.2comp[1]),rnorm(3,means.mc.2comp[2],std.mc.2com
p[2]))
    sample3<-
c(rnorm(0,means.mc.2comp[1],std.mc.2comp[1]),rnorm(4,means.mc.2comp[2],std.mc.2com
p[2]))
    bed3[i,1]<-summary(Mclust(sample1))$G
    bed3[i,2]<-summary(Mclust(sample2))$G
    bed3[i,3]<-summary(Mclust(sample3))$G
    }

  bed4<-matrix(NA,100,3)
  colnames(bed4)<-c("1 comp", "2 comp tot", "2 comp act")

  for(i in 1:100)
  {
    sample1<-c(rnorm(49,means.mc.1comp[1],std.mc.1comp[1]))
    sample2<-
c(rnorm(12,means.mc.2comp[1],std.mc.2comp[1]),rnorm(37,means.mc.2comp[2],std.mc.2co
mp[2]))
    sample3<-
c(rnorm(27,means.mc.2comp[1],std.mc.2comp[1]),rnorm(22,means.mc.2comp[2],std.mc.2co
mp[2]))
    bed4[i,1]<-summary(Mclust(sample1))$G
    bed4[i,2]<-summary(Mclust(sample2))$G
    bed4[i,3]<-summary(Mclust(sample3))$G
  }
```

```
bed5<-matrix(NA,100,3)
colnames(bed5)<-c("1 comp", "2 comp tot", "2 comp act")

for(i in 1:100)
{
   sample1<-c(rnorm(22,means.mc.1comp[1],std.mc.1comp[1]))
   sample2<-
c(rnorm(5,means.mc.2comp[1],std.mc.2comp[1]),rnorm(17,means.mc.2comp[2],std.mc.2co
mp[2]))
   sample3<-
c(rnorm(5,means.mc.2comp[1],std.mc.2comp[1]),rnorm(17,means.mc.2comp[2],std.mc.2co
mp[2]))
   bed5[i,1]<-summary(Mclust(sample1))$G
   bed5[i,2]<-summary(Mclust(sample2))$G
   bed5[i,3]<-summary(Mclust(sample3))$G
}

bed6<-matrix(NA,100,3)
colnames(bed6)<-c("1 comp", "2 comp tot", "2 comp act")

for(i in 1:100)
{
   sample1<-c(rnorm(31,means.mc.1comp[1],std.mc.1comp[1]))
   sample2<-
c(rnorm(8,means.mc.2comp[1],std.mc.2comp[1]),rnorm(23,means.mc.2comp[2],std.mc.2co
mp[2]))
   sample3<-
c(rnorm(7,means.mc.2comp[1],std.mc.2comp[1]),rnorm(24,means.mc.2comp[2],std.mc.2co
mp[2]))
   bed6[i,1]<-summary(Mclust(sample1))$G
   bed6[i,2]<-summary(Mclust(sample2))$G
   bed6[i,3]<-summary(Mclust(sample3))$G
}

bed7<-matrix(NA,100,3)
colnames(bed7)<-c("1 comp", "2 comp tot", "2 comp act")

for(i in 1:100)
{
   sample1<-c(rnorm(24,means.mc.1comp[1],std.mc.1comp[1]))
```

```
      sample2<-
c(rnorm(6,means.mc.2comp[1],std.mc.2comp[1]),rnorm(18,means.mc.2comp[2],std.mc.2co
mp[2]))
      sample3<-
c(rnorm(3,means.mc.2comp[1],std.mc.2comp[1]),rnorm(21,means.mc.2comp[2],std.mc.2co
mp[2]))
      bed7[i,1]<-summary(Mclust(sample1))$G
      bed7[i,2]<-summary(Mclust(sample2))$G
      bed7[i,3]<-summary(Mclust(sample3))$G
   }

   bed8<-matrix(NA,100,3)
   colnames(bed8)<-c("1 comp", "2 comp tot", "2 comp act")

   for(i in 1:100)
   {
      sample1<-c(rnorm(6,means.mc.1comp[1],std.mc.1comp[1]))
      sample2<-
c(rnorm(1,means.mc.2comp[1],std.mc.2comp[1]),rnorm(5,means.mc.2comp[2],std.mc.2com
p[2]))
      sample3<-
c(rnorm(0,means.mc.2comp[1],std.mc.2comp[1]),rnorm(6,means.mc.2comp[2],std.mc.2com
p[2]))
      bed8[i,1]<-summary(Mclust(sample1))$G
      bed8[i,2]<-summary(Mclust(sample2))$G
      bed8[i,3]<-summary(Mclust(sample3))$G
   }

   bed9<-matrix(NA,100,3)
   colnames(bed9)<-c("1 comp", "2 comp tot", "2 comp act")

   for(i in 1:100)
   {
      sample1<-c(rnorm(12,means.mc.1comp[1],std.mc.1comp[1]))
      sample2<-
c(rnorm(3,means.mc.2comp[1],std.mc.2comp[1]),rnorm(9,means.mc.2comp[2],std.mc.2com
p[2]))
      sample3<-
c(rnorm(2,means.mc.2comp[1],std.mc.2comp[1]),rnorm(10,means.mc.2comp[2],std.mc.2co
mp[2]))
      bed9[i,1]<-summary(Mclust(sample1))$G
      bed9[i,2]<-summary(Mclust(sample2))$G
```

```
    bed9[i,3]<-summary(Mclust(sample3))$G
  }

  bed10<-matrix(NA,100,3)
  colnames(bed10)<-c("1 comp", "2 comp tot", "2 comp act")

  for(i in 1:100)
  {
    sample1<-c(rnorm(5,means.mc.1comp[1],std.mc.1comp[1]))
    sample2<-
c(rnorm(1,means.mc.2comp[1],std.mc.2comp[1]),rnorm(4,means.mc.2comp[2],std.mc.2com
p[2]))
    sample3<-
c(rnorm(0,means.mc.2comp[1],std.mc.2comp[1]),rnorm(5,means.mc.2comp[2],std.mc.2com
p[2]))
    bed10[i,1]<-summary(Mclust(sample1))$G
    bed10[i,2]<-summary(Mclust(sample2))$G
    bed10[i,3]<-summary(Mclust(sample3))$G
  }

  bed11<-matrix(NA,100,3)
  colnames(bed11)<-c("1 comp", "2 comp tot", "2 comp act")

    for(i in 1:100)
  {
    sample1<-c(rnorm(11,means.mc.1comp[1],std.mc.1comp[1]))
    sample2<-
c(rnorm(3,means.mc.2comp[1],std.mc.2comp[1]),rnorm(8,means.mc.2comp[2],std.mc.2com
p[2]))
    sample3<-
c(rnorm(5,means.mc.2comp[1],std.mc.2comp[1]),rnorm(6,means.mc.2comp[2],std.mc.2com
p[2]))
    bed11[i,1]<-summary(Mclust(sample1))$G
    bed11[i,2]<-summary(Mclust(sample2))$G
    bed11[i,3]<-summary(Mclust(sample3))$G
  }

  bed12<-matrix(NA,100,3)
  colnames(bed12)<-c("1 comp", "2 comp tot", "2 comp act")

    for(i in 1:100)
  {
```

```
      sample1<-c(rnorm(19,means.mc.1comp[1],std.mc.1comp[1]))
      sample2<-
c(rnorm(5,means.mc.2comp[1],std.mc.2comp[1]),rnorm(14,means.mc.2comp[2],std.mc.2co
mp[2]))
      sample3<-
c(rnorm(0,means.mc.2comp[1],std.mc.2comp[1]),rnorm(19,means.mc.2comp[2],std.mc.2co
mp[2]))
      bed12[i,1]<-summary(Mclust(sample1))$G
      bed12[i,2]<-summary(Mclust(sample2))$G
      bed12[i,3]<-summary(Mclust(sample3))$G
   }

   bed13<-matrix(NA,100,3)
   colnames(bed13)<-c("1 comp", "2 comp tot", "2 comp act")

      for(i in 1:100)
   {
      sample1<-c(rnorm(24,means.mc.1comp[1],std.mc.1comp[1]))
      sample2<-
c(rnorm(6,means.mc.2comp[1],std.mc.2comp[1]),rnorm(18,means.mc.2comp[2],std.mc.2co
mp[2]))
      sample3<-
c(rnorm(3,means.mc.2comp[1],std.mc.2comp[1]),rnorm(21,means.mc.2comp[2],std.mc.2co
mp[2]))
      bed13[i,1]<-summary(Mclust(sample1))$G
      bed13[i,2]<-summary(Mclust(sample2))$G
      bed13[i,3]<-summary(Mclust(sample3))$G
   }

   bed14<-matrix(NA,100,3)
   colnames(bed14)<-c("1 comp", "2 comp tot", "2 comp act")

      for(i in 1:100)
   {
      sample1<-c(rnorm(12,means.mc.1comp[1],std.mc.1comp[1]))
      sample2<-
c(rnorm(3,means.mc.2comp[1],std.mc.2comp[1]),rnorm(8,means.mc.2comp[2],std.mc.2com
p[2]))
      sample3<-
c(rnorm(1,means.mc.2comp[1],std.mc.2comp[1]),rnorm(11,means.mc.2comp[2],std.mc.2co
mp[2]))
      bed14[i,1]<-summary(Mclust(sample1))$G
```

```
    bed14[i,2]<-summary(Mclust(sample2))$G
    bed14[i,3]<-summary(Mclust(sample3))$G
  }

  bed15<-matrix(NA,100,3)
  colnames(bed15)<-c("1 comp", "2 comp tot", "2 comp act")

    for(i in 1:100)
  {
    sample1<-c(rnorm(24,means.mc.1comp[1],std.mc.1comp[1]))
    sample2<-
c(rnorm(6,means.mc.2comp[1],std.mc.2comp[1]),rnorm(18,means.mc.2comp[2],std.mc.2co
mp[2]))
    sample3<-
c(rnorm(3,means.mc.2comp[1],std.mc.2comp[1]),rnorm(24,means.mc.2comp[2],std.mc.2co
mp[2]))
    bed15[i,1]<-summary(Mclust(sample1))$G
    bed15[i,2]<-summary(Mclust(sample2))$G
    bed15[i,3]<-summary(Mclust(sample3))$G
  }

  bed16<-matrix(NA,100,3)
  colnames(bed16)<-c("1 comp", "2 comp tot", "2 comp act")

    for(i in 1:100)
  {
    sample1<-c(rnorm(32,means.mc.1comp[1],std.mc.1comp[1]))
    sample2<-
c(rnorm(8,means.mc.2comp[1],std.mc.2comp[1]),rnorm(24,means.mc.2comp[2],std.mc.2co
mp[2]))
    sample3<-
c(rnorm(3,means.mc.2comp[1],std.mc.2comp[1]),rnorm(29,means.mc.2comp[2],std.mc.2co
mp[2]))
    bed16[i,1]<-summary(Mclust(sample1))$G
    bed16[i,2]<-summary(Mclust(sample2))$G
    bed16[i,3]<-summary(Mclust(sample3))$G
  }

  bed17<-matrix(NA,100,3)
  colnames(bed17)<-c("1 comp", "2 comp tot", "2 comp act")

    for(i in 1:100)
```

```
{
    sample1<-c(rnorm(18,means.mc.1comp[1],std.mc.1comp[1]))
    sample2<-
c(rnorm(4,means.mc.2comp[1],std.mc.2comp[1]),rnorm(13,means.mc.2comp[2],std.mc.2co
mp[2]))
    sample3<-
c(rnorm(1,means.mc.2comp[1],std.mc.2comp[1]),rnorm(17,means.mc.2comp[2],std.mc.2co
mp[2]))
    bed17[i,1]<-summary(Mclust(sample1))$G
    bed17[i,2]<-summary(Mclust(sample2))$G
    bed17[i,3]<-summary(Mclust(sample3))$G
}

bed18<-matrix(NA,100,3)
colnames(bed18)<-c("1 comp", "2 comp tot", "2 comp act")

    for(i in 1:100)
{
    sample1<-c(rnorm(22,means.mc.1comp[1],std.mc.1comp[1]))
    sample2<-
c(rnorm(5,means.mc.2comp[1],std.mc.2comp[1]),rnorm(17,means.mc.2comp[2],std.mc.2co
mp[2]))
    sample3<-
c(rnorm(5,means.mc.2comp[1],std.mc.2comp[1]),rnorm(17,means.mc.2comp[2],std.mc.2co
mp[2]))
    bed18[i,1]<-summary(Mclust(sample1))$G
    bed18[i,2]<-summary(Mclust(sample2))$G
    bed18[i,3]<-summary(Mclust(sample3))$G
}

bed19<-matrix(NA,100,3)
colnames(bed19)<-c("1 comp", "2 comp tot", "2 comp act")

    for(i in 1:100)
{
    sample1<-c(rnorm(56,means.mc.1comp[1],std.mc.1comp[1]))
    sample2<-
c(rnorm(14,means.mc.2comp[1],std.mc.2comp[1]),rnorm(42,means.mc.2comp[2],std.mc.2co
mp[2]))
    sample3<-
c(rnorm(31,means.mc.2comp[1],std.mc.2comp[1]),rnorm(25,means.mc.2comp[2],std.mc.2co
mp[2]))
```

```
    bed19[i,1]<-summary(Mclust(sample1))$G
    bed19[i,2]<-summary(Mclust(sample2))$G
    bed19[i,3]<-summary(Mclust(sample3))$G
  }

  bed20<-matrix(NA,100,3)
  colnames(bed20)<-c("1 comp", "2 comp tot", "2 comp act")

    for(i in 1:100)
  {
    sample1<-c(rnorm(10,means.mc.1comp[1],std.mc.1comp[1]))
    sample2<-
c(rnorm(3,means.mc.2comp[1],std.mc.2comp[1]),rnorm(8,means.mc.2comp[2],std.mc.2com
p[2]))
    sample3<-
c(rnorm(1,means.mc.2comp[1],std.mc.2comp[1]),rnorm(9,means.mc.2comp[2],std.mc.2com
p[2]))
    bed20[i,1]<-summary(Mclust(sample1))$G
    bed20[i,2]<-summary(Mclust(sample2))$G
    bed20[i,3]<-summary(Mclust(sample3))$G
  }
```

Electronic Data tables

Data Table E2.1. Silicon isotope values from Sirius Passet (‰). All samples represent mineralized muscle tissues except for 'SP-2011-0591a sediment matrix'.

	$\delta^{29}Si$					$\delta^{30}Si$				
Sample	**Replicate 1**	**Replicate 2**	**Replicate 3**	**Mean**	**2 SD**	**Replicate 1**	**Replicate 2**	**Replicate 3**	**Mean**	**2 SD**
SP-2009-0964	-0.46	-0.52		-0.49	0.09	-1.01	-0.98		-0.99	0.03
SP-2011-0591a Campa	-0.36	-0.36	-0.32	-0.35	0.04	-0.68	-0.80	-0.81	-0.76	0.14
SP-2011-0591a sedime	-0.37	-0.38	-0.34	-0.37	0.04	-0.75	-0.76	-0.60	-0.7	0.18
SP-2011-0648	-0.42	-0.45		-0.44	0.04	-0.87	-0.96		-0.92	0.13
SP-2011-0591a Pambd	-0.41	-0.42		-0.42	0.02	-0.81	-0.88		-0.84	0.10

Data Table E2.2. Bulk rock chemistry for Sirius Passet and Burgess Shale.

(A) Bulk rock chemistry for Sirius Passet for relevant oxides. Values are oxide weight %, oxygen by stoichiometry, normalised to 100%

Sample / map area	Bulk composition method	SiO2	Al2O3	K2O	FeO	Fe2O3	MgO	MnO	CaO	Na2O	Ti2O	P2O5	SO3	REEO
A4	**Modal**	56.19	30.93	7.49	3.93	0.00	0.28	0.02	0.00	0.57	0.57	0.01	0.00	0.02
A9	**Modal**	56.75	30.99	7.49	3.31	0.00	0.29	0.02	0.00	0.57	0.57	0.01	0.00	0.02
Sid Mu 2	**Modal**	61.50	25.30	5.96	6.11	0.00	0.44	0.02	0.00	0.47	0.00	0.06	0.00	0.14
PAMB Mu 2/1	**Modal**	57.64	22.50	4.93	10.47	0.00	0.24	0.01	0.87	0.39	0.34	2.54	0.05	0.02
PAMB Mu 2/2	**Modal**	59.51	25.33	5.74	5.90	0.00	0.30	0.01	0.90	0.45	0.42	1.30	0.00	0.14
A4	**Particle**	56.00	30.07	7.42	5.39	0.00	0.26	0.00	0.00	0.13	0.46	0.01	0.25	0.02
A9	**Particle**	56.86	30.59	7.50	4.06	0.00	0.27	0.00	0.00	0.12	0.46	0.01	0.11	0.02

A	**F**	**K**
66.13	12.23	21.64
67.39	10.63	21.99
60.11	20.89	19.00
51.02	33.54	15.43
60.42	20.58	19.00
63.27	15.89	20.84
66.01	12.44	21.55

$A = (Al_2O_3 + Fe_2O_3 - K_2O - Na_2O - CaO)$ *$F = (FeO + MgO + MnO)$* *$K = K_2O$*

(B) Sirius Passet data from Boudec et al. (2014) Values are element weight %, data.

Sample	SiO2	Al2O3	K2O	FeO	MgO	MnO	CaO	Na2O	TiO2	P2O5	S	SO3	REEO
3	6.428571	30.92111	4.760256	6.184286	1.55893	0.064545	0.014	0.606522	0.8	0.114516	0.14	N/A	N/A
3.3	7.071429	31.77111	4.953077	4.692857	1.29358	0.051636	0.154	0.606522	0.783333	0.160323	0.02	N/A	N/A
3.4	7.285714	25.68889	3.711795	8.537143	2.20572	0.090364	0.07	0.458261	0.8	0.091613	0.09	N/A	N/A
4	8.571429	31.26111	5.194103	1.324286	0.38144	0.012909	0.266	0.741304	0.816667	0	0.55	N/A	N/A
4.2	9	25.00889	3.494872	11.88	3.482716	0.090364	0.084	0.377391	0.816667	0.091613	0.04	N/A	N/A
4.4	9.428571	26.48222	4.013077	8.717143	2.20572	0.090364	0.042	0.525652	0.8	0.091613	0.12	N/A	N/A
5	10.71429	30.73222	4.79641	4.255714	0.928724	0.051636	0.084	0.660435	0.8	0.022903	0.08	N/A	N/A
5.3	11.35714	30.69444	4.651795	4.885714	1.077984	0.051636	0.07	0.62	0.783333	0.06871	0.07	N/A	N/A
5.7	12.21429	28.33333	4.350513	7.045714	1.675021	0.077455	0.028	0.566087	0.8	0.06871	0.15	N/A	N/A
6.7	14.35714	29.99556	4.832564	3.304286	0.630206	0.038727	0.014	0.660435	0.8	0	0.16	N/A	N/A

(C) Burgess Shale data for the Marble Canyon and Walcott Quarry localities from Gaines et al. 2019. Values are oxide weight %.

Sample	SiO2	Al2O3	K2O	FeO	Fe2O3	MgO	MnO	CaO	Na2O	Ti2O	P2O5	SO3	REEO
Marble Canyon FP 41.29	50.38	22.85	5.37	N/A	3.67	2.86	0.04	3.34	0.9	0.64	0.11	N/A	N/A
Marble Canyon FP 41.31	52.82	23.92	5.5	N/A	3.53	2.42	0.02	1.9	0.99	0.67	0.13	N/A	N/A
Marble Canyon FP 41.33	51.66	23.51	5.17	N/A	4.8	3	0.02	2.19	0.88	0.62	0.15	N/A	N/A
Marble Canyon FP 41.35	48.83	22.37	4.68	N/A	5.7	3.35	0.02	2.97	0.81	0.59	0.12	N/A	N/A
Marble Canyon FP 41.41	54.6	22.85	5.36	N/A	2.9	1.79	0.01	1.14	0.87	0.69	0.11	N/A	N/A
Marble Canyon FP 41.42	47.91	19.99	4.23	N/A	4.93	2.69	0.02	4.16	0.72	0.59	0.14	N/A	N/A
Marble Canyon FP 41.47	51.77	22.12	4.99	N/A	3.83	2.11	0.01	2.33	0.78	0.65	0.11	N/A	N/A
Marble Canyon FP 41.48	52.5	22.39	5.11	N/A	3.45	1.97	0.01	1.91	0.8	0.66	0.12	N/A	N/A
Marble Canyon FP 41.49	52.54	21.97	5.01	N/A	3.9	2.02	0.01	2.53	0.79	0.67	0.12	N/A	N/A
Marble Canyon FP 41.52	47.96	21.22	4.64	N/A	4.81	2.4	0.02	5.42	0.66	0.52	0.08	N/A	N/A
Marble Canyon FP 41.54	52.19	21.37	4.86	N/A	3.9	2.04	0.01	3.37	0.75	0.66	0.1	N/A	N/A
Marble Canyon FP 41.55	51.9	21.2	4.81	N/A	4.06	2.07	0.01	3.51	0.72	0.65	0.1	N/A	N/A
Marble Canyon FP 41 61	44.36	18.87	4.15	N/A	4.73	2.43	0.03	8.87	0.6	0.53	0.12	N/A	N/A
Marble Canyon FP 41 62	44.88	19.08	3.92	N/A	5.71	2.82	0.02	6.66	0.62	0.54	0.11	N/A	N/A
Marble Canyon FP 41 64	51.66	23.19	5.41	N/A	3.53	1.87	0	0.74	0.74	0.58	0.08	N/A	N/A
Marble Canyon FP 41 65	53.77	23.95	5.61	N/A	3.27	1.84	0	0.6	0.75	0.6	0.09	N/A	N/A
Marble Canyon FP 41.65B	52.35	24.19	5.72	N/A	3.19	1.77	0	0.38	0.79	0.62	0.08	N/A	N/A
Marble Canyon FP 41.72	46.7	19.59	4.36	N/A	4.24	2.25	0.03	7.45	0.65	0.56	0.1	N/A	N/A
Marble Canyon FP 41.73	46.48	19.21	4.29	N/A	4.24	2.18	0.02	7.3	0.61	0.57	0.1	N/A	N/A
Marble Canyon FP 41.75	52.04	20.04	4.66	N/A	3.66	1.85	0.02	4.77	0.6	0.62	0.14	N/A	N/A
Marble Canyon FP 41.77	43.78	18.43	4.14	N/A	4.26	2.17	0.03	9.98	0.55	0.56	0.18	N/A	N/A
Marble Canyon FP 41.79	55.23	23.73	5.67	N/A	2.84	1.54	0	0.39	0.76	0.6	0.08	N/A	N/A
Marble Canyon FP 41.795	51.9	22.57	5.16	N/A	4.09	2.07	0.01	1.62	0.67	0.54	0.1	N/A	N/A
Marble Canyon FP 41.80	50.4	21.93	4.98	N/A	4.15	2.51	0.01	2.66	0.68	0.56	0.1	N/A	N/A
Marble Canyon FP 41.81	50.73	22.25	5.09	N/A	4.07	2.13	0.01	2.61	0.7	0.57	0.09	N/A	N/A
Marble Canyon FP 41.82	51.37	22.26	5.09	N/A	3.81	2.11	0.01	2.69	0.71	0.57	0.09	N/A	N/A
Marble Canyon FP 41.83	50.92	21.24	4.84	N/A	3.94	2.06	0.01	3.68	0.7	0.58	0.1	N/A	N/A
Marble Canyon FP 41.87	46.35	19.73	4.24	N/A	5.41	2.52	0.02	7.04	0.57	0.53	0.11	N/A	N/A
Marble Canyon FP 41.90	51.47	21.24	4.81	N/A	4.32	2.13	0.01	3.18	0.68	0.61	0.12	N/A	N/A
Marble Canyon FP 41.91	52.51	21.41	4.9	N/A	3.87	1.95	0.01	2.55	0.66	0.62	0.11	N/A	N/A
Marble Canyon FP 41.92	46.94	20.62	4.38	N/A	5.11	2.52	0.02	5.97	0.6	0.56	0.12	N/A	N/A
Marble Canyon FP 41.87	46.29	19.73	4.23	N/A	5.41	2.52	0.02	7.03	0.56	0.52	0.11	N/A	N/A
Marble Canyon FP 42.01	46.58	18.94	4.14	N/A	5	2.34	0.03	7.28	0.61	0.56	0.1	N/A	N/A
Marble Canyon FP 42.07	50.87	21.75	5.11	N/A	3.73	1.94	0.01	4.06	0.6	0.59	0.1	N/A	N/A
Marble Canyon FP 42.09	46.77	20.52	4.58	N/A	4.73	2.3	0.02	6.53	0.55	0.55	0.11	N/A	N/A
Marble Canyon FP 42.10	42.86	18.86	4.01	N/A	5.27	2.57	0.03	9.71	0.55	0.52	0.11	N/A	N/A
Marble Canyon FP 42.13	50.02	21.41	4.9	N/A	4.36	2.16	0.02	4.44	0.55	0.55	0.12	N/A	N/A
Marble Canyon FP 42.14	44.03	20.75	4.51	N/A	5.18	2.6	0.03	7.56	0.59	0.5	0.11	N/A	N/A
Marble Canyon FP 42.15	50.02	22	5.07	N/A	3.89	2.05	0.01	3.86	0.62	0.57	0.11	N/A	N/A
Marble Canyon FP 42.16	46.16	19.88	4.37	N/A	4.7	2.36	0.02	6.96	0.52	0.51	0.12	N/A	N/A
Marble Canyon FP 42.25	50.33	19.37	4.3	N/A	4.59	2.23	0.02	6.49	0.55	0.63	0.12	N/A	N/A
Marble Canyon FP 42.32	44.92	17.83	3.86	N/A	4.75	2.26	0.03	9.3	0.5	0.56	0.11	N/A	N/A
Marble Canyon FP 42.35	46	19	4.08	N/A	5.19	2.44	0.02	6.25	0.48	0.56	0.12	N/A	N/A
Marble Canyon FP 42.52	45.54	19.45	4.26	N/A	4.79	2.48	0.03	7.99	0.54	0.55	0.1	N/A	N/A
Marble Canyon FP 42.54	47.25	20.28	4.64	N/A	4.3	2.2	0.02	7.23	0.57	0.57	0.1	N/A	N/A
Marble Canyon FP 42.56	45.89	19.48	4.28	N/A	4.97	2.48	0.03	8.38	0.56	0.55	0.1	N/A	N/A
Marble Canyon FP 42.58	44.57	18.76	4.08	N/A	4.92	2.48	0.03	9.5	0.55	0.54	0.1	N/A	N/A
Marble Canyon FP 42.62	48.75	20.99	4.83	N/A	4.21	2.13	0.02	5.67	0.59	0.58	0.12	N/A	N/A
Marble Canyon FP 42.66	44.91	19.44	4.24	N/A	5.11	2.58	0.03	8.61	0.6	0.54	0.1	N/A	N/A
Marble Canyon FP 42.68	45.43	18.94	4.28	N/A	4.3	2.22	0.03	8.99	0.6	0.54	0.1	N/A	N/A
Marble Canyon FP 42.69	50.81	21.93	5.04	N/A	4.27	2.21	0.02	3.93	0.65	0.6	0.11	N/A	N/A
Marble Canyon FP 42.94	51.15	20.22	4.61	N/A	3.97	2.32	0.02	5.08	0.62	0.63	0.11	N/A	N/A
Walcott Quarry FR 1.0	53.6	25.35	7.15	N/A	1.89	1.04	0	1.16	0.17	0.74	0.1	N/A	N/A
Walcott Quarry FR 2.0M	45.49	21.27	6.01	N/A	3.5	1.24	0.02	7.94	0.13	0.65	0.23	N/A	N/A
Walcott Quarry FR 3.41	47	21.63	5.84	N/A	3.87	1.74	0.01	5.87	0.18	0.65	0.13	N/A	N/A
Walcott Quarry FR 3.42	50.24	23.29	6.29	N/A	3.46	1.56	0.01	4.6	0.18	0.69	0.13	N/A	N/A
Walcott Quarry FR 3.43	47.69	22.25	6.09	N/A	3.46	1.47	0.01	4.48	0.11	0.65	0.12	N/A	N/A
Walcott Quarry FR 3.44	47.93	21.91	6.03	N/A	3.46	1.54	0.01	5.34	0.2	0.66	0.16	N/A	N/A
Walcott Quarry FR 5.78	49.07	22.73	6.21	N/A	3.76	1.37	0.01	5.08	0.16	0.64	0.09	N/A	N/A
Walcott Quarry FR 5.80	50.25	23.39	6.31	N/A	3.99	1.46	0.01	3.94	0.08	0.66	0.09	N/A	N/A
Walcott Quarry FR 5.81	49.26	22.86	6.23	N/A	4.08	1.44	0.01	3.96	0.18	0.65	0.09	N/A	N/A
Walcott Quarry FR 5.82	46.03	20.74	5.65	N/A	4.31	1.72	0.02	6.39	0.07	0.62	0.12	N/A	N/A
Walcott Quarry FR 5.83	47.63	21.74	5.91	N/A	3.96	1.63	0.01	5.25	0.15	0.64	0.1	N/A	N/A
Walcott Quarry FR 5.85	48.05	22.11	6.04	N/A	4.52	1.52	0.01	4.46	0.2	0.64	0.1	N/A	N/A
Walcott Quarry FR 5.86	46.42	20.66	5.49	N/A	4.56	1.97	0.02	7.93	0.13	0.62	0.16	N/A	N/A
Walcott Quarry FR 5.87	43.85	19.52	5.31	N/A	4.5	1.8	0.03	8.5	0.17	0.59	0.17	N/A	N/A
Walcott Quarry FR 6.6	46.93	21.55	5.87	N/A	4.18	1.66	0.02	6.8	0.1	0.64	0.17	N/A	N/A
Walcott Quarry FR 7.0	45.46	20.65	5.51	N/A	4.71	1.93	0.02	8.57	0.07	0.61	0.17	N/A	N/A
Walcott Quarry FR 7.5	49.01	22.44	6.23	N/A	3.25	1.37	0.01	6.08	0.1	0.65	0.1	N/A	N/A
Walcott Quarry FR 8.1	47.77	22.05	6.03	N/A	3.77	1.58	0.02	6.21	0.09	0.6	0.1	N/A	N/A
Walcott Quarry FR 8.7	47.2	21.81	6.03	N/A	3.91	1.5	0.02	6.9	0.1	0.62	0.12	N/A	N/A
Walcott Quarry FR 9.2	44.77	20.27	5.56	N/A	4.55	2.03	0.03	7.96	0.1	0.58	0.14	N/A	N/A
Walcott Quarry FR 9.7	43.85	19.36	4.73	N/A	6.37	5.54	0.05	6.67	0.16	0.68	0.1	N/A	N/A
Walcott Quarry FR 10.4	45.08	20.69	5.78	N/A	3.85	1.32	0.03	9	0.09	0.58	0.13	N/A	N/A
Walcott Quarry FR 10.75M	47.55	22.75	6.33	N/A	3.42	1.49	0.02	5.53	0.14	0.68	0.11	N/A	N/A
Walcott Quarry FR 11.75	50.27	25.37	7.19	N/A	2.1	0.9	0.01	4.32	0.18	0.66	0.1	N/A	N/A
Walcott Quarry FR 12.75	46.1	21.93	5.96	N/A	3.91	1.42	0.03	7.22	0.13	0.6	0.15	N/A	N/A
Walcott Quarry FR 13.4	47.88	22.84	6.36	N/A	3.18	1.64	0.02	5.79	0.15	0.64	0.12	N/A	N/A
Walcott Quarry FR 15.6	49.02	23.59	6.63	N/A	2.81	1.17	0.01	5.19	0.13	0.61	0.1	N/A	N/A

Data Table E2.3. List of analyzed fossil-tissues and analytical method. The full dataset is available at the University of Bristol Data Repository (data.bris) at https://doi.org/10.5523/bris.1imwjxezxgu332uqzlna2lugud.

Specimen				Secondarily mineralized labile soft-tissue				Analyses performed			
Species	**MGUH-number**	**SP-number**	**Sample stub number**	**Gut tract**	**Gut diverticulum**	**Muscle**	**Other**	**EDS**	**EDS elemental map**	**EDS mineral map**	**WDS elemental map**
Arthroaspis	33917	SP-2016-1130	Int.Min. 3		1			X			
Arthroaspis	33918	SP-2016-1023	Int.Min. 3		1			X			
Arthroaspis	33919	SP-2016-45	Int.Min. 1			1		X			
Arthroaspis	33920	SP-2016-1085	Int.Min. 2		1			X			X
Buenellus	33921	SP-2016-293	Int.Min. 2	1				X			
Campanamuta	33922	SP-2016-1206	Int.Min. 5		1			X			
Campanamuta	33923	SP-2016-669	Int.Min. 5		1			X			
Campanamuta	33924	SP-2016-1076	A,C: Int.Min. 4; B: Int.Min 5			1 (A)	2 (B,C)	X			
Campanamuta	33925	SP-2016-180	Int.Min. 4			1		X			
Campanamuta	33926	SP-2016-22	Int.Min. 5			1		X			
Campanamuta	33927	SP-2016-88	A: Int.Min.5; B: Int.Min. 4	1 (B)		1 (A)		X			
Campanamuta	33928	SP-2016-569	Int.Min. 4				1	X			
Campanamuta	33929	SP-2016-264	Int.Min. 5	1				X			
Kiisortoqia	33930	SP-2016-199	Int.Min. 3		1			X			
Kiisortoqia	33931	SP-2016-1255	Int.Min. 2		1			X			
Kiisortoqia	33932	SP-2016-1259	Int.Min. 3			1		X			
Kiisortoqia	33933	SP-2016-884	Int.Min. 1	1				X			
Pambdelurion	33934	SP-2017-2592	PAMB-Mu 1-4	1		1		X	X	X	
?*Sidneyia*	33935	SP-2016-1015	Int.Min. 1		1			X			
?*Sidneyia*	33936	SP-2016-567	A,B: Int.Min. 2			2		X			X
?*Sidneyia*	33937	SP-2016-675	Int.Min. 1		1			X			
?*Sidneyia*	33938	SP-2016-373	Int.Min. 2				1	X			
?*Sidneyia*	33939	SP-2016-390	Int.Min. 3			1		X			
?*Sidneyia*	33940	SP-2016-1022	A,B: Int.Min. 3	1 (B)		1 (A)		X		X	
?*Sidneyia*	33941	SP-2016-119	A,B: Int.Min. 3	1 (B)	1 (A)			X			
?*Sidneyia*	33942	SP-2017-2591	SID-Mu 1-4	?		1		X	X	X	
Siriocaris	33943	SP-2016-411	Int.Min. 3		?1			X		X	
Siriocaris	33944	SP-2016-288	Int.Min. 2		1			X			X
Siriocaris	33945	SP-2016-218	Int.Min. 2			1		X			

Data Table E2.4. Chloritoid angle measurements.

Angle (°)
130
70
93
144
46
36
127
97
115
83
142
138
57
32
53
127
8
134
57
91
21
120
135
30
59
101
94
92
97
107
72
137
124
53
130
8
87
139
92
101
122
123
120
95
31
174
125
104
87

87
178
170
34
102
58
168
137
13
96
20
48
87
91
170
114
90
28
78
104
104
89
86
134
21
11
135
108
122
107
57
11
16
86
116
145
68
151
163
42
146
36
112
77
49
55
176
66
164
139
111

103
131
1
61
155
27
85
68
89
105
120
110
55
83
63
117
140
128
59
89
41
59
78
90
58
26
34
91
59
47
1
142
141
83
178
179
91
113
172
167
156
168
123
112
50
113
124
9
107
147
102

79
118
4
83
20
115
135
117
92
143
75
46
137
23
27
62
7
147
80
91
94
153
165
24
88
101
149
60
113
40
125
72
61
52
112
109
90
87
91
174
112
102
23
16
67
149
145
44
79
100
29

88
10
43
85
84
158
89
114
90
140
138
178
146
122
85
19
82
38
145
140
159
105
100
21
152
142
67
12
43
57
71
147
53
153
172
64
91
106
88
168
174
16
21
96
120
163
76
90
88
108
42

4
134
106
133
125
7
105
69
71
110
111
63
84
98
96
100
72
98
107
119
111
126
142
124
172
83
95
85
163
71
93
72
24
107
157
81
58
173
1
155
149
91
85
148
141
73
75
178
8
35
115

117
126
167
94
141
30
141
129
96
30
136
93
134
46
3
120
98
25
76
30
40
143
118
178
165
170
46

Data Table E3.1. Distribution of phosphatized tissues in Sirius Passet. "0"=absent, "1"=present, "?"=uncertain.

(A) *Aaveqaspis inesoni*

Field number		No mineralization
SP-2016-48	A	1
SP-2016-108		1
SP-2016-141	A	1
SP-2016-201	B	1
SP-2016-522	A	1
SP-2016-533	A	1
SP-2016-698	F	1
SP-2016-781	A	1
SP-2016-878	E	1
Total		9
Frequency		100.00%

(B) *Arthroaspis bergstroemi*

Field number		Width (mm)	Oesophagus	Gut tract	Gut diverticula	Axial muscle	Extrinsic muscle	[illegible]	Gill lamella	Transverse bar	Indet. mineralizations	No mineralization
SP-2016-8	A	49.5	0	0	1	0	0	0	0	0	0	0
SP-2016-23	A	65.8	0	0	1	0	0	0	0	0	0	0
SP-2016-25	A	122.6	0	0	0	0	0	0	0	0	0	1
SP-2016-34		?	0	0	0	0	0	0	0	0	0	1
SP-2016-38	D2	?	0	0	0	0	0	0	0	0	0	1
SP-2016-42		?	0	0	?	1	0	0	0	0	0	0
SP-2016-45		?	0	0	0	1	0	0	0	0	0	0
SP-2016-46	G	107.2	0	0	1	1	0	1	1	1	0	0
SP-2016-140	B	?	0	0	0	1	1	0	1	1	0	0
SP-2016-160		50.5	0	0	1	1	0	0	0	1	0	0
SP-2016-169	B	?	0	0	1	0	0	0	1	0	0	0
SP-2016-185	I	?	0	0	1	0	0	0	0	0	0	0
SP-2016-195	A	?	0	0	0	0	0	0	0	0	0	1
SP-2016-221		?	0	0	0	0	0	0	0	0	0	1
SP-2016-236	A	71.1	0	0	1	0	0	0	0	0	0	0
Sp-2016-257		51.6	0	0	1	0	0	0	0	1	0	0
Sp-2016-259	A	67.7	0	0	1	0	0	0	0	0	0	0
SP-2016-261		?	0	0	1	0	1	0	0	0	0	0
SP-2016-276	A	81.3	0	0	1	1	0	0	0	0	0	0
SP-2016-284		84	0	0	0	0	0	0	0	0	0	1
SP-2016-286		?	0	0	0	0	0	0	0	0	0	1
SP-2016-290		123.6	0	1	1	0	0	0	0	0	0	0
SP-2016-324		32.8	0	0	0	0	0	0	0	0	0	1
SP-2016-396	B	?	0	0	0	1	0	0	0	0	0	0
SP-2016-401	A	?	0	0	1	0	0	0	0	0	0	0
SP-2016-401	C	?	0	0	0	1	1	0	1	1	0	0
SP-2016-458	H	104.2	0	1	0	0	0	0	0	0	0	0
SP-2016-483	A	119.5	0	0	1	1	0	0	1	0	0	0
SP-2016-488		?	0	0	0	0	0	0	0	0	0	0
SP-2016-504	B	31	0	0	0	0	0	0	0	0	0	1
SP-2016-535	A	113.8	0	0	1	0	0	0	0	0	0	0
SP-2016-540	A	?	0	0	1	1	0	0	0	0	0	0
SP-2016-546	B	?	0	0	0	0	0	0	0	0	1	0
SP-2016-550	A	59	0	0	1	0	0	0	0	0	0	0
SP-2016-555	A	117.2	0	0	1	0	1	0	0	0	0	0
SP-2016-562		122.3	0	0	0	0	0	0	0	0	0	1
SP-2016-602	A	27.9	0	0	0	0	0	0	0	0	0	1
SP-2016-613	A	158.9	0	0	0	0	0	0	0	0	0	1
SP-2016-627	D	49.6	0	0	1	0	0	0	0	0	0	0
SP-2016-627	E	48.3	0	0	1	0	0	0	0	0	0	0
SP-2016-672	A	39	0	0	1	0	0	0	0	0	0	0
SP-2016-674		25.2	0	0	0	0	0	0	0	0	0	1
SP-2016-683	C	?	0	?	1	?	?	0	0	0	?	0
SP-2016-695	A	91.2	0	1	1	?	?	0	0	0	?	?
SP-2016-704	A	82.8	1	0	1	0	0	0	0	0	0	0
SP-2016-730	A	113.3	0	0	0	0	0	0	0	0	0	1
SP-2016-742	A	94	0	0	0	0	0	0	0	0	0	1
SP-2016-742	B	68.7	0	0	1	0	0	0	0	0	0	0
SP-2016-800		44.5	0	0	0	0	0	0	0	0	0	1
SP-2016-821	A	65.1	0	0	1	0	0	0	0	0	1	0
SP-2016-924	A	116.5	1	0	1	1	0	0	0	0	0	0
SP-2016-954	B	71.7	0	0	0	0	0	0	0	0	0	1
SP-2016-1021	A	142.5	0	0	1	1	1	0	0	1	0	0
SP-2016-1023	A	44.1	0	0	1	0	0	0	0	0	0	0
SP-2016-1034	A	109.4	0	0	1	0	0	0	0	0	0	0
SP-2016-1044	D	?	0	0	0	0	0	0	0	0	0	1
SP-2016-1056	A	115	0	0	1	0	0	0	0	0	0	0
SP-2016-1082	A	?	0	0	1	0	0	0	0	0	0	0
SP-2016-1130		51	0	0	1	0	0	0	0	0	0	0
SP-2016-1138	A	?	0	0	1	0	0	0	0	0	0	0
SP-2016-1153		?	0	0	0	1	1	0	0	0	0	0
SP-2016-1164		95.8	0	0	0	0	0	0	0	0	0	1
SP-2016-316	A	35.4	0	1	1	0	0	0	0	0	0	0
Total			2	4	35	13	6	1	5	6	2	19
Frequency			3.2%	6.5%	56.5%	21.0%	9.8%	1.6%	7.9%	9.5%	3.3%	30.6%

(C) *Buenaspis forteyi*

Field number		No mineralization
SP-2016-18	D	1
SP-2016-29	A	1
SP-2016-101	D	1
SP-2016-103		1
SP-2016-143	E	1
SP-2016-152	A	1
SP-2016-209		1
SP-2016-225		1
SP-2016-289	D	1
SP-2016-292		1
SP-2016-362	B	1
SP-2016-380		1
SP-2016-396	A	1
SP-2016-401	M	1
SP-2016-404	B	1
SP-2016-408	B	1
SP-2016-461	A	1
SP-2016-512		1
SP-2016-543		1
SP-2016-547	B	1
SP-2016-561	B	1
SP-2016-581	G	1
SP-2016-592		1
SP-2016-600	D	1
SP-2016-621	A	1
SP-2016-663	B	1
SP-2016-679	A	1
SP-2016-704	E	1
SP-2016-708	D	1
SP-2016-771	A	1
SP-2016-784		1
SP-2016-844	B	1
SP-2016-845		1
SP-2016-906	A	1
SP-2016-927	B	1
SP-2016-930	F	1
SP-2016-957	A	1
SP-2016-989	B	1
SP-2016-999	L	1
SP-2016-1003	B	1
SP-2016-1004	B	1
SP-2016-1032	A	1
SP-2016-1043	A	1
SP-2016-1044	B	1
SP-2016-1065	C	1
SP-2016-1115	A	1
SP-2016-1121	Y	1
SP-2016-1122	A	1
SP-2016-1161	D	1
SP-2016-1203		1
SP-2016-1226	B	1
Total		51
Frequency		100.00%

(D) *Buenellus higginsi*

[illegible]

(H) *Molaria steini*

Field number		No mineralisation
SP-2016-330	B	1
SP-2016-956	D	1
SP-2016-1187		1
Total		3
Frequency		100.00%

(I) *Pauloterminus spinodorsalis*

Field number		Carapace height (mm)	Gut tract	Gut sack	Abdominal muscle	Transverse bars	No mineralization
SP-2016-18	C	16.2	0	0	0	0	1
SP-2016-29	B	19.4	0	0	0	0	1
SP-2016-62		10.5	0	1	1	0	0
SP-2016-112	B	6.7	0	0	0	0	1
SP-2016-270	C	8.5	0	1	0	1	0
SP-2016-299	B	5.7	0	0	0	0	1
SP-2016-410	E	9.6	1	0	1	0	0
SP-2016-447	B	11.7	0	0	0	0	1
SP-2016-478	B	11.3	0	0	0	0	1
SP-2016-480	D	11	0	1	0	0	0
SP-2016-481		9.8	0	1	0	0	0
SP-2016-523	B	6.8	0	0	0	0	1
SP-2016-617	A	10.1	0	1	1	0	0
SP-2016-671	A	21.3	0	0	0	0	1
SP-2016-705	C	9.8	?	0	?	?	?
SP-2016-705	E	14.7	1	0	0	0	0
SP-2016-718	A	12.4	0	0	0	0	1
SP-2016-743		9	1	1	0	?	0
SP-2016-750	A	9.7	0	0	0	0	1
SP-2016-788	C	12.3	0	0	0	0	1
SP-2016-801	D	11.2	0	1	0	1	0
SP-2016-861	D1	?	0	?	0	0	?
SP-2016-872	D	?	0	1	0	0	0
SP-2016-923		?	0	0	0	0	1
SP-2016-924	B	12.5	0	0	0	0	1
SP-2016-953	A	?	0	1	0	0	0
SP-2016-956		24	0	0	0	0	1
SP-2016-976		11	0	1	0	0	0
SP-2016-1038		12	0	0	0	0	1
SP-2016-1046	B	20.8	0	0	0	0	1
SP-2016-1075		12.5	0	1	0	1	0
SP-2016-1080	A	23.2	0	0	0	0	1
SP-2016-1147		11.1	1	1	0	1	0
Total			4	12	3	4	17
Frequency			12.5%	37.5%	9.4%	12.9%	54.8%

(J) *Sidneyia* [illegible]

[illegible]

Transverse bars	Gill lamella	Gill ?rod	No mineralization
0	0	0	0
0	0	0	0
0	1	1	0
?	?	?	0
0	0	?	0
0	0	0	0
0	1	0	0
0	0	0	0
0	1	0	0
0	0	0	0
1	0	0	0
0	0	0	0
0	0	0	0
1	1	0	0
0	0	0	1
0	0	0	0
1	1	0	0
0	1	0	0
1	0	0	0
1	1	0	0
0	0	0	0
1	0	0	0
0	0	0	0
0	0	0	0
1	0	0	0
0	0	0	0
0	0	0	0
1	1	0	0
0	0	0	0
0	1	0	0
1	1	0	0
0	0	0	0
1	0	0	0
1	0	0	0
0	1	0	0
1	0	0	0
0	1	0	0
0	0	0	0
1	1	1	0
0	1	0	0
0	1	0	0
1	0	0	0
0	0	0	0
0	0	0	0
0	0	0	0
0	0	0	0
0	0	0	0
1	1	0	0
1	0	0	0
0	0	0	0
0	1	0	0
0	1	0	0
0	0	0	0
0	0	0	0
1	0	0	0
0	1	0	0
0	1	0	0
0	0	0	0
0	0	0	0
0	0	0	0
0	0	0	0
0	0	0	0
17	20	2	1
27.87%	32.79%	3.33%	1.61%

(K) *Siriocaris trollae*

Field number		[illegible]	No mineralization
SP-2016-51		[illegible]	[illegible]
SP-2016-288		[illegible]	[illegible]
SP-2016-218, SP-2016-3[illegible]		[illegible]	[illegible]
SP-2016-527		[illegible]	[illegible]
SP-2016-702, SP-2016-7[illegible]		[illegible]	[illegible]
SP-2016-770		[illegible]	[illegible]
SP-2016-1108		[illegible]	[illegible]
SP-2016-329		[illegible]	[illegible]
SP-2016-377		[illegible]	[illegible]
Total		[illegible]	[illegible]
Frequency		[illegible]	[illegible]

(L) [illegible]

[illegible]
[illegible]

(M) cf. *Pambdelurion* sp. nov

Field number		Total width (mm)	Pharynx	Gut tract	Gut diverticula	Axial muscle	Extrinsic muscle	Indet mineralization	No mineralization
SP-2016-6	A	25	1	1	0	1	1	0	0
SP-2016-79	A	?	1	1	?	1	?	0	?
SP-2016-86	A	?	?	?	0	1	1	0	0
SP-2016-101	B	46.9	1	1	0	1	1	0	0
SP-2016-133		36.9	1	?	0	1	1	0	0
SP-2016-198		39.4	1	1	1	1	0	0	0
SP-2016-202	A	17.5	1	?	?	1	1	0	0
Sp-2016-285	A	45	?	1	0	1	1	0	0
Sp-2016-296	D	?	?	1	?	1	1	0	0
SP-2016-412		47.1	1	1	1	1	1	0	0
SP-2016-420	A	?	?	1	1	1	1	0	0
SP-2016-482	J	82	?	1	1	1	1	0	0
SP-2016-486		?	1	1	1	1	1	0	0
SP-2016-491	A	75.5	1	1	0	1	1	0	0
SP-2016-504	A	65.6	1	1	1	1	1	0	0
SP-2016-559		?	?	1	1	1	1	0	0
SP-2016-619		30.4	1	1	1	1	1	0	0
SP-2016-629		34.8	1	1	1	1	0	0	0
SP-2016-642		47	?	1	1	1	1	0	0
SP-2016-700	A	?	1	1	1	1	1	0	0
SP-2016-765	A	48.4	1	1	0	1	1	0	0
SP-2016-862	A	55.9	1	1	1	1	1	0	0
SP-2016-934	A	?	1	1	0	1	1	0	0
SP-2016-937	A	48.3	1	1	?	1	1	0	0
SP-2016-1020	A	43.1	1	1	?	1	1	0	0
SP-2016-1052	A	?	?	1	1	1	1	0	0
SP-2016-1083		?	?	?	?	1	?	1	0
SP-2016-1123	A	40	1	0	0	1	1	0	0
SP-2016-1126	A	?	?	1	?	1	1	0	0
SP-2016-1141	A	47.4	1	1	1	1	1	0	0
Total			20	25	14	30	26	1	0
Frequency			100.00%	96.15%	60.87%	100.00%	92.86%	3.33%	0.00%

(N) *Pambdelurion whittingtoni*

Field number		Total width (mm)	Pharynx	Gut tract	Gut sac	Gut diverticula	Axial muscle	Extrinsic muscle	Extrinsic frontal appendage muscle	Indet mineralization	No mineralization
SP-2016-124	A	87.4	?	1	1	?	0	0	?	0	0
SP-2016-247		87.3	0	1	0	1	1	1	0	0	0
SP-2016-343		?	?	?	?	?	?	?	?	1	0
SP-2016-528	A	63.4	?	0	1	0	0	0	?	1	0
SP-2016-594	A	115.5	?	1	1	0	0	0	?	0	0
SP-2016-606	C	89.7	?	1	1	0	?	0	?	1	0
SP-2016-682		101.1	?	1	0	0	1	0	?	1	0
SP-2016-707	B	68.5	?	1	?	1	0	1	?	0	0
SP-2016-751		77.1	0	1	0	1	0	0	1	0	0
SP-2016-848	A	38.2	?	1	0	1	1	1	?	0	0
SP-2016-862	B	?	0	1	0	?	0	0	0	0	0
SP-2016-1098		76.4	?	0	1	1	0	0	?	1	0
SP-2016-760	A	?	?	1	1	?	?	?	?	1	0
SP-2016-430	A	93.3	?	1	?	?	?	?	?	1	0
Total			0	11	6	5	3	3	1	7	0
Frequency			0.00%	84.62%	54.55%	55.56%	30.00%	27.27%	33.33%	50.00%	0.00%

(O) *Sirilorica* spp.

Field number		?Muscle	Indeterminate strand	Indet mineralization	No mineralization
SP-2016-3	A	0	0	0	1
SP-2016-75	F	0	0	0	1
SP-2016-85	B	0	0	0	1
SP-2016-99		0	0	0	1
SP-2016-101	E	0	0	0	1
SP-2016-107	E	0	0	0	1
SP-2016-174		0	0	0	1
SP-2016-248	B	0	0	0	1
SP-2016-252		0	0	0	1
SP-2016-254		0	0	0	1
SP-2016-262	A	0	0	0	1
SP-2016-266	C	0	0	0	1
SP-2016-277	C	0	0	0	1
SP-2016-358		0	0	0	1
SP-2016-361		0	0	0	1
SP-2016-381		0	0	0	1
SP-2016-382		0	0	0	1
SP-2016-394	A	0	0	0	1
SP-2016-409	B	0	0	0	1
SP-2016-497	J	0	0	0	1
SP-2016-578	A	0	0	0	1
SP-2016-625	A	0	0	0	1
SP-2016-649		0	0	0	1
SP-2016-655	B	0	0	0	1
SP-2016-665	A	0	0	0	1
SP-2016-689	A	0	0	0	1
SP-2016-713	E	0	0	0	1
SP-2016-728		0	0	0	1
SP-2016-758	B	0	0	0	1
SP-2016-783	A	0	0	0	1
SP-2016-798	C	0	0	0	1
SP-2016-823	B	0	0	0	1
SP-2016-839	A	0	0	0	1
SP-2016-852		0	0	0	1
SP-2016-867	A	0	0	0	1
SP-2016-874	C	0	0	1	0
SP-2016-880	B	0	0	0	1
SP-2016-891		0	0	0	1
SP-2016-913	A	0	0	0	1
SP-2016-922	I	0	0	0	1
SP-2016-941		0	0	0	1
SP-2016-942	E	0	0	0	1
SP-2016-984	C	0	0	0	1
SP-2016-1013	C	0	0	0	1
SP-2016-1026	E	0	0	0	1
SP-2016-1033	J	1	1	1	0
SP-2016-1040	F	0	0	0	1
SP-2016-1046	H	0	0	0	1
SP-2016-1053	B	0	0	0	1
SP-2016-1065	F	0	0	0	1
SP-2016-1088	B	0	0	0	1
SP-2016-1089		0	1	1	0
SP-2016-1151		0	0	0	1
SP-2016-1158	B	0	0	0	1
SP-2016-1173	C	0	0	0	1
SP-2016-1184	A	0	0	0	1
SP-2016-1186		0	0	0	1
SP-2016-1192	A	0	0	0	1
SP-2016-1199		0	0	0	1
SP-2016-1200		0	0	?	?
SP-2016-1211	B	0	0	0	1
SP-2016-1218		0	0	0	1
SP-2016-1219	A	0	0	0	1
Total		1	2	3	59
Frequency		1.59%	3.17%	4.84%	95.16%

(P) Palaeoscolecids spp.

Field number		Gut tract	No mineralization	Note
SP-2016-413	A	1	0	*Xystoscolex*
SP-2016-684	D	1	0	
SP-2016-786		0	1	
SP-2016-855		0	1	
SP-2016-878	B	1	0	
SP-2016-950		1	0	
SP-2016-1014	B	1	0	
SP-2016-1025		1	0	*Chalazoscolex*?
SP-2016-1070		1	0	*Xystoscolex*?
SP-2016-1106	A	1	0	*Xystoscolex*?
Total		8	2	
Frequency		80.00%	20.00%	

(Q) Amiskwiiform sp.

Field number		Muscle	Gut tract	?Nerve ganglion	No mineralization
SP-2016-47		1	0	1	0
SP-2016-374	B	1	0	0	0
SP-2016-495		0	0	0	1
SP-2016-500	A	1	0	0	0
SP-2016-501		0	0	0	1
SP-2016-909		0	0	0	1
SP-2016-940	A	1	1	0	0
SP-2016-1010	B	1	0	0	0
Total		5	1	1	3
Frequency		62.50%	12.50%	12.50%	37.50%

(R) Nectocaridid sp.

Field number		Muscle	?Nerve ganglion	No mineralization
SP-2016-184	F	1	1	0
SP-2016-308		0	0	1
SP-2016-493		1	1	0
SP-2016-541	B	0	0	1
SP-2016-590		1	1	0
SP-2016-761	A	0	0	1
SP-2016-1100	A	1	1	0
Total		4	4	3
Frequency		57.14%	57.14%	42.86%

(S) *Halkieria evangelista*

Field number		Gut tract	No mineralization
SP-2016-557		1	0
SP-2016-745		0	1
SP-2016-914		0	1
Total		1	2
Frequency		33.33%	66.67%

(T) Polychaetes spp.

Field number		Muscle	Gut tract	No mineralization	Note
SP-2016-30		0	0	1	*Phragmochaeta*
SP-2016-87	A	0	0	1	*Phragmochaeta*
SP-2016-104		0	1	0	
SP-2016-135	B	0	0	1	*Phragmochaeta*
SP-2016-136	D	0	0	1	*Pygocirrus*
SP-2016-156	A	0	0	1	*Phragmochaeta*
SP-2016-260	A	0	0	1	*Phragmochaeta*
SP-2016-340		0	0	1	
SP-2016-370	A	0	1	0	
SP-2016-401	G	0	0	1	
SP-2016-492	B	0	0	1	*Phragmochaeta*
SP-2016-492	C	0	0	1	*Phragmochaeta*
SP-2016-532	E	0	0	1	*Phragmochaeta*
SP-2016-536	A	1	0	0	*Phragmochaeta*
SP-2016-589		0	0	1	*Phragmochaeta*
SP-2016-593	A	0	0	1	*Phragmochaeta*
SP-2016-609	A	0	0	1	*Phragmochaeta*
SP-2016-680		0	0	1	
SP-2016-695	B	0	0	1	*Phragmochaeta*
SP-2016-921		0	0	1	*Phragmochaeta*
SP-2016-949		0	0	1	*Phragmochaeta*
SP-2016-1013	A	0	0	1	
SP-2016-1029		0	0	1	*Phragmochaeta*
SP-2016-1137	C	0	0	1	
SP-2016-1138	B	0	0	1	
SP-2016-1140	A	0	0	1	
SP-2016-1140	B	0	0	1	
SP-2016-1183		0	1	0	
Total		1	3	24	
Frequency		3.57%	10.71%	85.71%	

(U) Vetulicolians spp.

Field number		Gut tract	No mineralization	Note
SP-2016-14	B	0	1	
SP-2016-52	B	0	1	
SP-2016-112	A	0	1	*Ooedigera*
SP-2016-114		0	1	*Ooedigera*
SP-2016-143	B	0	1	
SP-2016-173	A	0	1	
SP-2016-183	A	0	1	
SP-2016-183	C	0	1	*Ooedigera*?
SP-2016-210		0	1	
SP-2016-217	B	0	1	
SP-2016-250	C	0	1	
SP-2016-270	F	1	0	
SP-2016-278		0	1	
SP-2016-310	D	0	1	
SP-2016-339	A	0	1	
SP-2016-377	A	0	1	
SP-2016-393	C	0	1	
SP-2016-401	H	0	1	
SP-2016-426	D	0	1	
SP-2016-430	F	0	1	
SP-2016-430	G	0	1	
SP-2016-441	C	0	1	
SP-2016-442	C	0	1	
SP-2016-455	A	1	0	
SP-2016-456	B	0	1	
SP-2016-478	A	0	1	
SP-2016-522	B	0	1	
SP-2016-583	A	0	1	
SP-2016-606	G	0	1	
SP-2016-669	C	0	1	
SP-2016-670	C1	0	1	
SP-2016-670	C2	0	1	
SP-2016-678	A	0	1	
SP-2016-713	D	0	1	
SP-2016-716	A	0	1	
SP-2016-747	C	0	1	
SP-2016-767	C	0	1	
SP-2016-795		0	1	*Ooedigera*
SP-2016-802	B	0	1	
SP-2016-808	A	0	1	*Ooedigera*
SP-2016-893	A	0	1	
SP-2016-964	A	0	1	
SP-2016-1011	A	0	1	*Ooedigera*
SP-2016-1033	C	0	1	
SP-2016-1046	A	0	1	
SP-2016-1078	A	0	1	
SP-2016-1080	C	0	1	
SP-2016-1162		0	1	
SP-2016-1173	A	0	1	*Ooedigera*
SP-2016-1188	B	0	1	
Total		2	48	
Frequency		4.00%	96.00%	

Data Table E3.2. Longitudinal extent of continuously phosphatized axial muscle by segments. "0"=absent, "1"=present. Seg *n* =segment number.

(A) *Arthroaspis bergstroemi*

Field number		**Cephalon**	**Seg 1**	**Seg 2**	**Seg 3**	**Seg 4**	**Seg 5**	**Seg 6**	**Seg 7**	**Seg 8**	**Seg 9**	**Seg 10**	**Seg 11**	**Seg 12**	**Seg 13**	**Seg 14**	**Pygidium**
SP-2016-45		0	0	0	0	0	1	1	1	1	1	0	0	0	0	0	0
SP-2016-46		0	0	0	0	0	0	0	1	1	1	1	1	1	1	0	0
SP-2016-140		0	0	0	0	0	0	1	1	1	1	0	0	0	0	0	0
SP-2016-160		0	0	1	1	1	1	1	1	1	1	1	0	0	0	0	0
Sp-2016-257		0	0	1	1	1	1	1	0	0	0	0	0	0	0	0	0
SP-2016-401		0	0	0	0	0	0	0	0	1	1	1	0	0	0	0	0
SP-2016-535		0	0	0	0	0	0	0	0	0	0	0	1	1	1	1	1
SP-2016-924		0	0	0	0	0	0	0	0	1	1	1	1	1	0	0	0
SP-2016-1021		0	0	1	1	1	1	1	1	1	1	1	0	0	0	0	0
Total		**0**	**0**	**3**	**3**	**3**	**4**	**5**	**5**	**7**	**7**	**5**	**3**	**3**	**2**	**1**	**1**
Frequency		**0.0%**	**0.0%**	**33.3%**	**33.3%**	**33.3%**	**44.4%**	**55.6%**	**55.6%**	**77.8%**	**77.8%**	**55.6%**	**33.3%**	**33.3%**	**22.2%**	**11.1%**	**11.1%**

(B) *Kiisortoqia soperi*

Field number		**Cephalon**	**Seg 1**	**Seg 2**	**Seg 3**	**Seg 4**	**Seg 5**	**Seg 6**	**Seg 7**	**Seg 8**	**Seg 9**	**Seg 10**	**Seg 11**	**Seg 12**	**Seg 13**	**Seg 14**	**Seg 15**	**Seg 16**
SP-2016-32		0	0	0	0	0	0	0	1	1	1	1	1	1	1	0	0	0
SP-2016-98		0	0	0	1	1	1	1	1	1	1	0	0	0	0	0	0	0
SP-2016-106		0	1	1	1	1	1	1	1	1	1	0	0	0	0	0	0	0
SP-2016-205		0	0	0	0	1	1	1	1	1	0	0	0	0	0	0	0	0
SP-2016-208		0	0	0	0	0	0	1	1	1	1	1	1	0	0	0	0	0
SP-2016-273		0	1	1	1	1	1	1	1	1	1	0	0	0	0	0	0	0
SP-2016-280	A	0	1	1	1	1	1	1	1	1	1	1	1	1	1	1	0	0
SP-2016-327		0	0	0	1	1	1	1	1	1	0	0	0	0	0	0	0	0
SP-2016-447		0	0	0	0	0	0	0	1	1	1	0	0	0	0	0	0	0
SP-2016-458		0	0	0	1	1	1	1	1	1	1	1	0	0	0	0	0	0
SP-2016-471		0	0	0	0	0	0	0	1	1	1	1	1	1	0	0	0	0
SP-2016-594	B	0	1	1	1	1	1	1	1	1	1	1	0	0	0	0	0	0
SP-2016-594	E	0	0	0	0	1	1	1	1	1	1	1	1	0	0	0	0	0
SP-2016-607		0	0	1	1	1	1	1	1	1	1	1	1	0	0	0	0	0
SP-2016-626		0	0	0	0	0	1	1	1	1	1	0	0	0	0	0	0	0
SP-2016-662		0	0	0	1	1	1	1	1	1	0	0	0	0	0	0	0	0
SP-2016-753		0	0	0	1	1	1	1	1	1	1	1	0	0	0	0	0	0
SP-2016-829		0	0	1	1	1	1	1	1	1	1	1	0	0	0	0	0	0
SP-2016-884		0	1	1	1	1	1	1	1	1	1	1	1	1	0	0	0	0
Total		**0**	**5**	**7**	**12**	**14**	**15**	**16**	**19**	**19**	**16**	**11**	**7**	**4**	**2**	**1**	**0**	**0**
Frequency		**0.0%**	**26.3%**	**36.8%**	**63.2%**	**73.7%**	**78.9%**	**84.2%**	**100.0%**	**100.0%**	**84.2%**	**57.9%**	**36.8%**	**21.1%**	**10.5%**	**5.3%**	**0.0%**	**0.0%**

(C) *Sidneyia* ? sp.

Field number		**Cephalon**	**Seg 1**	**Seg 2**	**Seg 3**	**Seg 4**	**Seg 5**	**Seg 6**	**Seg 7**	**Seg 8**	**Seg 9**	**Telson 1**	**Telson 2**
SP-2016-23	C	0	0	0	0	0	1	1	1	1	1	0	0
SP-2016-46	B	0	0	0	0	0	0	1	1	1	1	0	0
SP-2016-50	A	0	0	0	0	1	1	1	1	1	0	0	0
SP-2016-58	B	0	0	0	0	1	1	1	1	1	1	0	0
SP-2016-63		0	1	1	1	1	1	0	0	0	0	0	0
SP-2016-69		0	0	1	1	1	1	1	0	0	0	0	0
SP-2016-72		0	0	1	1	1	1	1	1	1	0	0	0
SP-2016-149		0	0	0	0	1	1	1	1	0	0	0	0
SP-2016-195	D	0	0	1	1	1	1	1	1	1	0	0	0
SP-2016-316	C	0	0	0	1	1	1	1	1	1	1	0	0
SP-2016-353		0	0	0	0	0	0	0	1	1	1	0	0
SP-2016-376	D	0	0	1	1	1	1	1	1	0	0	0	0
SP-2016-506	A	0	0	0	0	0	0	0	0	1	1	0	0
SP-2016-518		0	0	0	0	0	1	1	1	1	0	0	0
SP-2016-532	A	0	1	1	1	1	1	1	1	1	1	0	0
SP-2016-567	A	0	0	0	0	1	1	1	1	1	1	0	0
SP-2016-591		0	0	0	1	1	1	1	0	0	0	0	0
SP-2016-596	A	0	0	0	0	0	1	1	1	1	1	0	0
SP-2016-623	B	0	0	0	1	1	1	1	1	1	1	0	0
SP-2016-705	A	0	0	0	1	1	1	1	1	1	0	0	0
SP-2016-711	A	0	0	0	0	0	0	1	1	1	1	0	0
SP-2016-767	A	0	0	0	1	1	1	1	1	1	1	0	0
SP-2016-870		0	0	0	0	1	1	1	1	1	1	0	0
SP-2016-947	A	0	0	0	0	1	1	1	1	1	1	0	0
SP-2016-955	A	0	0	0	1	1	1	1	1	1	1	0	0
SP-2016-969	A	0	0	1	1	1	1	1	1	1	0	0	0
SP-2016-1001	A	0	0	1	1	1	1	1	0	0	0	0	0
SP-2016-1022	A	0	0	1	1	1	1	1	1	1	0	0	0
SP-2016-1055	A1	0	0	1	1	1	1	1	1	1	1	0	0
SP-2016-1131	A	0	0	0	0	0	0	1	1	1	1	0	0
SP-2016-1213	A1	0	0	1	1	1	1	1	1	0	0	0	0
SP-2016-1213	A2	0	0	0	1	1	1	1	1	1	1	0	0
Total		**0**	**2**	**11**	**18**	**24**	**27**	**29**	**27**	**25**	**18**	**0**	**0**
Frequency		0	6.25	34.375	56.25	75	84.375	90.625	84.375	78.125	56.25	0	0

(C) cf. *Pambdelurion* sp. nov.

Field number		**Head**	**Seg 1**	**Seg 2**	**Seg 3**	**Seg 4**	**Seg 5**	**Seg 6**	**Seg 7**	**Seg 8**	**Seg 9**	**Seg 10**	**Seg 11**
SP-2016-6	A	1	1	1	1	1	1	1	1	0	0	0	0
SP-2016-101	B	1	1	1	1	1	1	1	1	1	0	0	0
SP-2016-202	A	0	1	1	1	1	1	1	1	1	0	0	0
SP-2016-486		1	1	1	1	1	1	1	1	1	0	0	0
SP-2016-504	A	1	1	1	1	1	1	1	1	0	0	0	0
SP-2016-619		1	1	1	1	1	1	1	1	1	1	0	0
SP-2016-629		1	1	1	1	1	1	1	0	0	0	0	0
SP-2016-642		1	1	1	1	1	1	1	1	1	0	0	0
SP-2016-700		1	1	1	1	1	1	1	1	1	1	1	1
SP-2016-765	A	1	1	1	1	1	1	1	1	0	0	0	0
SP-2016-862	A	1	1	1	1	1	1	1	1	1	0	0	0
SP-2016-934	A	1	1	1	1	1	1	1	1	1	1	0	0
SP-2016-1123	A	1	1	1	1	1	1	1	1	1	1	0	0
SP-2016-1141	A	1	1	1	1	1	1	1	1	1	0	0	0
Total		**13**	**14**	**14**	**14**	**14**	**14**	**14**	**13**	**10**	**4**	**1**	**1**
Frequency		**92.9%**	**100.0%**	**100.0%**	**100.0%**	**100.0%**	**100.0%**	**100.0%**	**92.9%**	**71.4%**	**28.6%**	**7.1%**	**7.1%**

Data Table E4.1. Summary of bedding surface data.

Block	Bed	Surface area (cm^2)	Fossil abundance	*Isoxys volucris* abundance	Fossil density (per 1000 cm^2)	Isoxys density (per 1000 cm^2)	Fossil diversity (*n* taxa)	Fossil diversity (per 1000 cm^2)
A	1	723	45	27	62.2	37.3	11	15.2
A	2	729	20	14	27.4	19.2	5	6.9
A	3	751	9	5	12.0	6.7	2	2.7
A	4	759	34	26	44.8	34.2	8	10.5
A	5	812	22	11	27.1	13.6	9	11.1
A	6	828	25	10	30.2	12.1	9	10.9
A	7	702	36	24	51.3	34.2	6	8.6
A	8	794	29	15	36.5	18.9	7	8.8
A	9	899	26	13	28.9	14.5	7	7.8
A	10	921	37	23	40.2	25.0	6	6.5
A	11	896	13	2	14.5	2.2	6	6.7
A	12	959	30	10	31.3	10.4	7	7.3
A	13	879	20	9	22.8	10.2	5	5.7
A	14	949	8	3	8.4	3.2	5	5.3
A	15	975	27	6	27.7	6.2	9	9.2
A	16	982	24	16	24.5	16.3	6	6.1
A	17	969	13	7	13.4	7.2	4	4.1
A	18	935	28	15	29.9	16.0	6	6.4
A	19	986	17	4	17.2	4.1	9	9.1
A	20	1166	44	34	37.8	29.2	6	5.1
A	21	1056	16	7	15.2	6.6	6	5.7
A	22	1259	25	13	19.9	10.3	6	4.8
A	23	1162	58	36	49.9	31.0	7	6.0
A	24	1344	59	41	43.9	30.5	10	7.4
A	25	1034	27	12	26.1	11.6	9	8.7
A	26	1032	24	14	23.2	13.6	6	5.8
A	27	1162	28	14	24.1	12.0	7	6.0
A	28	1099	25	13	22.7	11.8	9	8.2
A	29	828	33	11	39.9	13.3	12	14.5
A	30	1195	23	11	19.2	9.2	9	7.5
A	31	847	25	10	29.5	11.8	9	10.6
A	32	1030	31	15	30.1	14.6	10	9.7
Total A		**30658**	**881**	**471**	**28.7**	**15.4**	**32**	**7.8**
B	1	736	14	11	19.0	14.9	3	4.1
B	2	886	15	12	16.9	13.5	4	4.5
B	3	1019	12	8	11.8	7.9	2	2.0
B	4	1138	89	71	78.2	62.4	6	5.3
B	5	1221	50	42	41.0	34.4	7	5.7
B	6	1277	67	54	52.5	42.3	10	7.8
B	7	1308	37	33	28.3	25.2	4	3.1
B	8	1259	29	13	23.0	10.3	7	5.6
B	9	1291	38	29	29.4	22.5	5	3.9
B	10	1276	19	10	14.9	7.8	4	3.1
B	11	1265	34	27	26.9	21.3	4	3.2
B	12	1329	54	32	40.6	24.1	8	6.0
B	13	1359	42	34	30.9	25.0	6	4.4
B	14	1306	22	19	16.8	14.5	3	2.3
B	15	1331	47	43	35.3	32.3	2	1.5
B	16	1342	54	47	40.3	35.0	6	4.5
B	17	1379	40	30	29.0	21.8	7	5.1
B	18	1273	38	30	29.9	23.6	5	3.9
B	19	1013	120	110	118.5	108.6	7	6.9
B	20	1363	29	19	21.3	13.9	6	4.4
Total B		**24369**	**850**	**674**	**34.9**	**28**	**24**	**4.4**
Total A+B		**55027**	**1731**	**1145**	**31.5**	**20.8**	**36**	**6.5**

Data Table E4.2. Bed-by-bed fossil counts.

		Arthropods									
	Bed	*Arthroaspis*	*Buenaspis*	*Buenellus*	*Campanamuta*	*Isoxys*	*Kiisortoqia*	*Kleptothule*	*Kleptothule* sp. nov.	Leanchoilid? Sp.	*Molaria*
Block A	1	0	1	0	2	27	1	1	0	1	0
	2	0	0	0	0	14	0	0	0	0	0
	3	0	0	0	0	5	0	0	0	0	0
	4	1	0	0	0	26	0	1	0	0	0
	5	0	0	1	0	11	2	1	0	0	0
	6	1	3	0	1	10	0	0	0	0	0
	7	0	0	0	1	24	0	0	0	0	0
	8	0	0	4	0	15	2	0	1	0	0
	9	0	0	1	3	13	1	0	0	0	0
	10	0	0	1	1	23	0	0	0	0	0
	11	0	0	3	0	2	0	1	0	0	0
	12	0	0	0	2	10	0	0	0	0	0
	13	0	0	0	0	9	0	1	0	0	0
	14	0	0	0	0	3	1	0	0	0	0
	15	0	1	0	4	6	0	1	0	0	0
	16	0	0	0	1	16	0	0	0	0	1
	17	1	0	0	0	7	0	0	0	0	1
	18	0	0	0	1	15	0	0	1	0	0
	19	0	0	2	2	4	0	0	0	0	1
	20	0	0	2	0	34	0	1	0	0	0
	21	0	1	0	0	7	0	1	0	0	0
	22	0	0	0	4	13	0	1	0	0	0
	23	0	0	9	4	36	0	0	0	0	0
	24	0	1	2	2	41	2	0	0	0	0
	25	0	1	0	2	12	3	0	1	0	0
	26	0	0	1	1	14	0	4	0	0	0
	27	0	0	2	4	14	0	1	0	0	0
	28	0	1	1	3	13	1	0	1	0	0
	29	0	0	0	6	11	1	0	1	0	0
	30	0	0	0	2	11	2	1	0	0	0
	31	0	0	0	3	10	0	0	0	0	0
	32	0	1	0	2	15	1	1	1	0	0
	Total	**3**	**10**	**29**	**51**	**471**	**17**	**16**	**6**	**1**	**3**
Block B	1	0	0	0	0	11	0	0	0	0	0
	2	1	0	1	0	12	0	0	0	0	0
	3	0	0	0	0	8	0	0	0	0	0
	4	0	0	0	2	71	0	0	0	0	0
	5	0	0	0	0	42	0	1	0	0	0
	6	1	0	1	4	54	1	0	0	1	0
	7	0	0	0	2	33	0	1	0	0	0
	8	0	0	0	1	13	0	0	0	0	0
	9	0	0	0	3	29	0	0	0	0	0
	10	0	0	0	2	10	0	0	0	0	0
	11	0	0	0	4	27	0	0	0	0	0
	12	0	0	0	3	32	0	1	0	1	0
	13	0	0	2	1	34	0	0	0	0	0
	14	0	0	0	2	19	0	0	0	0	0
	15	0	0	0	0	43	0	0	0	0	0
	16	0	0	0	2	47	1	0	0	0	0
	17	0	0	2	3	30	0	0	0	0	0
	18	0	0	0	0	30	0	0	0	0	0
	19	0	0	0	1	110	0	1	2	0	0
	20	0	0	0	3	19	0	0	0	0	0
	Total	**2**	**0**	**6**	**33**	**674**	**2**	**4**	**2**	**2**	**0**

		Arthropods					Lobopods		
	Bed	New arthropod ("Molly")	*Pauloterminus*	?*Sidneyia*	*Siriocaris*	Arthropoda indet	*Kerygmachela*	cf. *Pambdelurion* sp.	Lobopoda indet
Block A	1	1	0	1	0	4	0	0	0
	2	0	0	0	0	0	0	0	0
	3	0	0	0	0	0	0	0	0
	4	1	2	0	1	0	0	0	0
	5	1	0	0	0	1	0	0	0
	6	0	0	0	0	4	0	0	0
	7	0	1	0	0	1	0	0	0
	8	0	0	0	0	4	0	0	0
	9	0	0	0	0	4	0	0	0
	10	0	0	0	0	2	0	0	0
	11	0	0	0	0	4	0	0	0
	12	0	0	1	0	1	0	0	0
	13	0	0	0	0	1	0	0	0
	14	0	1	0	0	1	0	0	0
	15	2	1	4	0	5	0	0	0
	16	0	1	0	0	1	0	0	0
	17	0	0	0	0	0	0	0	0
	18	1	0	0	0	3	0	0	0
	19	0	1	0	0	0	0	0	0
	20	0	0	0	0	2	0	0	0
	21	1	0	1	0	3	0	0	0
	22	0	0	0	0	0	0	0	0
	23	0	0	2	0	1	0	0	0
	24	0	1	1	0	2	0	0	0
	25	0	0	2	0	1	2	0	0
	26	0	1	0	0	2	0	0	0
	27	0	0	0	0	1	0	2	0
	28	0	0	1	0	1	2	0	0
	29	1	2	3	0	1	1	0	1
	30	0	1	0	0	1	1	0	0
	31	2	2	1	0	0	0	0	1
	32	0	1	0	0	1	0	0	1
	Total	**10**	**15**	**17**	**1**	**52**	**6**	**2**	**3**
Block B	1	0	0	0	0	0	0	0	0
	2	0	1	0	0	0	0	0	0
	3	0	1	0	0	1	0	0	0
	4	0	2	0	0	0	0	0	0
	5	0	1	1	0	2	0	0	0
	6	0	1	0	0	0	0	0	0
	7	0	0	0	0	0	0	0	0
	8	0	1	1	0	4	0	0	0
	9	0	0	0	0	1	0	0	0
	10	0	0	0	0	1	0	0	0
	11	0	0	0	0	0	0	0	0
	12	1	0	0	0	1	1	1	0
	13	0	0	0	0	1	1	0	0
	14	0	0	0	0	0	0	0	0
	15	0	0	0	0	1	0	0	0
	16	0	0	0	0	0	0	0	0
	17	0	0	0	0	0	1	0	0
	18	0	0	0	0	0	0	0	0
	19	0	0	1	0	4	0	0	0
	20	0	0	0	0	0	1	0	0
	Total	**1**	**7**	**3**	**0**	**16**	**4**	**1**	**0**

		Sponges						Scalidophorans				
	Bed	cf. *Choia*	cf. *Lenica*	Sponge spicule indet	Demosponge indet	Saetaspongia	?Reticulose sponge	*Sirilorica*	*Xystoscolex*?	*Chalatoscolex?*	Indet priapulid?	Indet palaeoscolecid
Block A	1	0	0	0	1	0	0	0	0	0	0	0
	2	0	0	1	0	0	0	0	0	0	0	0
	3	0	0	0	0	0	0	0	0	0	0	0
	4	0	0	0	0	0	0	0	0	0	0	0
	5	0	0	1	0	0	0	0	0	0	0	0
	6	0	0	0	0	0	1	0	0	0	0	1
	7	0	0	0	0	0	1	0	0	0	0	0
	8	0	0	0	0	0	0	1	0	0	0	0
	9	0	0	0	0	0	0	1	0	0	0	1
	10	0	0	0	0	0	0	0	0	0	0	0
	11	0	0	0	0	1	0	0	0	0	0	0
	12	0	0	0	0	0	0	1	0	0	0	1
	13	0	0	0	0	0	0	0	0	0	0	1
	14	0	0	0	0	0	0	0	0	0	0	0
	15	0	0	0	0	0	0	0	0	0	0	1
	16	0	0	0	0	0	0	0	0	0	0	0
	17	0	0	0	0	0	0	0	0	0	0	0
	18	0	0	0	0	0	0	0	0	0	0	0
	19	0	0	0	0	0	0	0	0	0	0	1
	20	0	0	0	0	0	0	0	0	0	1	3
	21	0	0	0	0	0	0	0	0	0	0	0
	22	0	0	0	0	0	0	0	0	1	0	0
	23	0	0	0	0	0	0	0	0	0	0	1
	24	0	0	0	0	0	0	0	0	0	0	2
	25	0	0	0	1	0	0	0	0	0	0	0
	26	0	0	1	0	0	0	0	0	0	0	0
	27	0	0	0	0	0	0	0	0	0	0	1
	28	0	0	0	0	0	0	0	0	0	0	0
	29	0	0	0	0	0	0	0	0	0	0	2
	30	0	0	0	0	0	0	0	0	0	0	0
	31	0	0	0	0	0	0	0	0	0	0	1
	32	0	0	0	0	0	0	0	0	0	0	0
	Total	**0**	**0**	**3**	**2**	**1**	**2**	**3**	**0**	**1**	**1**	**16**
Block B	1	2	0	0	0	0	0	0	0	0	0	0
	2	0	0	0	0	0	0	0	0	0	0	0
	3	0	0	0	0	0	0	0	0	0	0	0
	4	0	0	0	0	0	0	0	0	0	0	1
	5	0	0	0	0	0	0	0	0	0	1	1
	6	0	0	0	0	0	0	1	1	0	0	0
	7	1	0	0	0	0	0	0	0	0	0	0
	8	0	0	0	0	0	0	0	0	0	0	3
	9	0	0	0	0	0	0	0	0	0	0	2
	10	0	0	0	0	0	0	0	0	0	0	0
	11	0	0	0	0	0	0	1	0	0	0	0
	12	0	0	0	0	0	0	0	0	0	0	0
	13	0	0	0	0	0	0	2	0	0	0	0
	14	0	0	0	0	0	0	0	0	0	0	0
	15	0	0	0	0	0	0	0	0	0	0	0
	16	2	0	0	0	0	0	0	0	0	0	0
	17	0	1	0	0	0	0	0	0	0	0	0
	18	0	1	0	0	0	0	0	0	0	0	0
	19	0	0	0	0	0	0	0	0	0	0	0
	20	0	0	0	0	0	0	2	0	0	0	0
	Total	**5**	**2**	**0**	**0**	**0**	**0**	**6**	**1**	**0**	**1**	**7**

		Polychaetes	Gnathiferans			Vetulicolians		Mollusca	Chordata	Indets
	Bed	Polychaete sp.	Amiskwiiform	Gnathiferan indet	Small chaetognath	Vetulicolians indet	*Ooedigera*	*Halkieria*	Chordata	Indet fossil
Block A	1	0	1	0	4	0	0	0	0	0
	2	0	0	0	1	3	1	0	0	0
	3	0	0	0	4	0	0	0	0	0
	4	0	0	0	1	1	0	0	0	0
	5	0	0	0	1	2	0	1	0	0
	6	1	1	0	1	0	0	0	0	1
	7	0	0	0	8	0	0	0	0	0
	8	0	0	0	1	1	0	0	0	0
	9	0	0	0	0	2	0	0	0	0
	10	2	0	0	5	0	2	0	0	1
	11	0	0	0	1	1	0	0	0	0
	12	0	0	0	3	10	0	0	0	1
	13	0	0	0	2	0	6	0	0	0
	14	0	0	0	1	0	0	1	0	0
	15	0	0	0	2	0	0	0	0	0
	16	0	0	0	1	1	0	0	0	2
	17	0	0	0	0	3	0	0	0	1
	18	0	0	0	3	0	0	1	0	3
	19	0	0	0	3	1	1	0	0	1
	20	0	0	0	0	0	1	0	0	0
	21	0	0	0	2	0	0	0	0	0
	22	0	0	0	4	2	0	0	0	0
	23	0	0	0	3	1	0	0	0	1
	24	0	0	0	4	1	0	0	0	0
	25	0	0	0	1	0	0	0	0	1
	26	0	0	0	0	0	0	0	0	0
	27	0	0	0	3	0	0	0	0	0
	28	0	0	0	1	0	0	0	0	0
	29	0	0	0	2	0	0	0	1	0
	30	0	0	1	1	0	1	0	0	1
	31	0	0	0	0	4	1	0	0	0
	32	0	1	0	0	3	0	0	0	3
	Total	**3**	**3**	**1**	**63**	**36**	**13**	**3**	**1**	**16**
Block B	1	0	0	0	0	1	0	0	0	0
	2	0	0	0	0	0	0	0	0	0
	3	0	0	0	0	0	0	0	0	2
	4	0	0	0	5	8	0	0	0	0
	5	0	0	0	0	0	0	0	0	1
	6	0	0	0	0	0	0	0	0	1
	7	0	0	0	0	0	0	0	0	0
	8	0	0	0	5	1	0	0	0	0
	9	0	0	0	3	0	0	0	0	0
	10	0	0	0	0	5	0	0	0	0
	11	0	0	0	0	1	0	0	0	1
	12	0	0	0	12	0	0	0	0	1
	13	0	0	0	0	1	0	0	0	0
	14	0	0	0	0	0	0	0	0	0
	15	0	0	0	0	3	0	0	0	0
	16	0	0	0	0	1	0	0	0	0
	17	0	0	0	1	1	0	0	0	1
	18	0	0	0	1	5	0	0	0	0
	19	0	0	0	0	0	0	0	0	0
	20	2	0	0	0	0	0	0	0	1
	Total	**2**	**0**	**0**	**27**	**27**	**0**	**0**	**0**	**8**

Data Table E4.3. Taphonomic data.

	Block A																																
Taxon / ***Bed***	**1**	**2**	**3**	**4**	**5**	**6**	**7**	**8**	**9**	**10**	**11**	**12**	**13**	**14**	**15**	**16**	**17**	**18**	**19**	**20**	**21**	**22**	**23**	**24**	**25**	**26**	**27**	**28**	**29**	**30**	**31**	**32**	**Total**
Arthroaspis bergstroemi articulated				1													1																**2**
Arthroaspis bergstroemi soft tissues						1											1																**2**
Arthroaspis bergstroemi disarticulated						1																					1						**2**
Buenaspis forteyi articulated	1					3									1						1			1	1			1				1	**10**
Buenellus higginsi articulated					1			3	1		2									1			7			1	1						**17**
Buenellus higginsi soft tissues					1			1	1		2								0	1			1			1	0						**8**
Buenellus higginsi disarticulated										1									1				1	2									**5**
Pauloterminus spinodorsalis articulated																1			1					1						1			**4**
Pauloterminus spinodorsalis soft tissues																			1														**1**
Pauloterminus spinodorsalis dislocated																															2		**2**
Pauloterminus spinodorsalis disarticulated																										1							**1**
Campanamuta mantonae articulated	1						1		2	1		1			2	1		1	1			2	3	1	2	1	4	3	5	2	3		**37**
Campanamuta mantonae soft tissues									2			1			3			1	1			2	3	1	2	1	4	3	5	1	3	0	**33**
Campanamuta mantonae dislocated																																	**0**
Campanamuta mantonae disarticulated															1	1		1	1														**4**
Kleptothule rasmusseni articulated	1			1							1		1		1					1	1	1				4	1			1			**14**
Kleptothule rasmusseni soft tissues																																	**0**
Sidneyia ? sp. nov. articulated															2						1		1	1	2				3				**10**
Sidneyia ? sp. nov. soft tissues												0			2								1	1	2			0	3				**9**
Sidneyia ? sp. nov. dislocated																															1		**1**
Sidneyia ? sp. nov. disarticulated																																	**0**
New *Leanchoilia* -like arthropod articulated																																	**0**
Kiisortoqia soperi articulated	1				2			1	1					1										2	3			1		2		1	**15**
Kiisortoqia soperi soft tissues	1								1					1										1	3					1		1	**9**
Indet arthropods articulated	2					1		2	1																	1						1	**8**
Indet arthropods soft tissues								0			0										0											1	**1**
Indet arthropods disarticulated						1																											**1**
New arthropod ("Molly") articulated				1	1										1			1			1										1		**6**
New arthropod ("Molly") soft tissues	0														1			1													1		**3**
Kleptothule ? sp. nov. articulated								1										1							1			1	1			1	**6**
Kleptothule ? sp. nov. sp soft tissues																																	**0**
Siriocaris trollae articulated				1																													**1**
Molaria steini articulated																1	1		1														**3**
Isoxys volucris articulated	8	7	1	7	2	5	5	4	6	5	1	3	1	1	3	2	4	6	2	15	2	6	13	11	6	3	2	5	4	6	3	5	**154**
Isoxys volucris soft tissues (phosphatized only)	4	0	0	0	1	0	1	0	1	2	0	1	0	0	0	0	0	0	0	0	0	0	0	2	0	0	0	0	0	0	2	4	**18**
Isoxys volucris disarticulated valve	4	1	0	4	3	2	8	0	2	2	0	1	3	2	1	5	2	2	0	14	3	4	5	10	2	3	5	1	4	1	2	2	**98**
Isoxys volucris non-crumpled	13	7	1	11	5	7	13	5	7	7	1	4	4	3	4	5	6	9	2	28	6	10	17	23	8	6	7	8	7	7	5	4	**250**
Isoxys volucris crumpled	0	1	0	1	1	1	0	0	0	2	0	1	0	0	2	3	1	0	1	2	0	0	1	2	0	1	1	0	1	0	0	2	**24**

	Block B																					**Total Block A+B**	**Inferred ecology**
Taxon / ***Bed***	**1**	**2**	**3**	**4**	**5**	**6**	**7**	**8**	**9**	**10**	**11**	**12**	**13**	**14**	**15**	**16**	**17**	**18**	**19**	**20**	**Total**		
Arthroaspis bergstroemi articulated																					**0**	**2**	Benthic
Arthroaspis bergstroemi soft tissues																					**0**	**2**	-
Arthroaspis bergstroemi disarticulated		1																			**1**	**3**	-
Buenaspis forteyi articulated																					**0**	**10**	Benthic
Buenellus higginsi articulated		1											1				2				**4**	**21**	Benthic
Buenellus higginsi soft tissues		1											1				2				**4**	**12**	-
Buenellus higginsi disarticulated													1								**1**	**6**	-
Pauloterminus spinodorsalis articulated			1																		**1**	**5**	Pelagic
Pauloterminus spinodorsalis soft tissues						1															**1**	**2**	-
Pauloterminus spinodorsalis dislocated				2	1	1															**4**	**6**	-
Pauloterminus spinodorsalis disarticulated																					**0**	**1**	-
Campanamuta mantonae articulated						2	2	1	2	2	4	3	1	2		2	2		1	2	**26**	**63**	Benthic
Campanamuta mantonae soft tissues				0		2	1	1	3	2	4	3	1	1		2	2			2	**24**	**57**	-
Campanamuta mantonae dislocated						1			1												**2**	**2**	-
Campanamuta mantonae disarticulated																					**0**	**4**	-
Kleptothule rasmusseni articulated					1		1														**2**	**16**	Pelagic
Kleptothule rasmusseni soft tissues					1																**1**	**1**	-
Sidneyia ? sp. nov. articulated					1			1													**2**	**12**	Benthic
Sidneyia ? sp. nov. soft tissues								1											1		**2**	**11**	-
Sidneyia ? sp. nov. dislocated																					**0**	**1**	-
Sidneyia ? sp. nov. disarticulated																			1		**1**	**1**	-
New *Leanchoilia* -like arthropod articulated						1						1									**2**	**2**	N/A
Kiisortoqia soperi articulated						1										1					**2**	**17**	Pelagic
Kiisortoqia soperi soft tissues																1					**1**	**10**	-
Indet arthropods articulated										1											**1**	**9**	N/A
Indet arthropods soft tissues																					**0**	**1**	-
Indet arthropods disarticulated													1								**1**	**2**	-
New arthropod ("Molly") articulated												1									**1**	**7**	Pelagic
New arthropod ("Molly") soft tissues																					**0**	**3**	-
Kleptothule ? sp. nov. articulated																			2		**2**	**8**	Pelagic
Kleptothule ? sp. nov. sp soft tissues																			2		**2**	**2**	-
Siriocaris trollae articulated																					**0**	**1**	Pelagic
Molaria steini articulated																					**0**	**3**	Benthic
Isoxys volucris articulated	4	5	4	42	18	21	24	6	11	4	9	14	21	7	15	24	16	15	51	5	**316**	**470**	Pelagic
Isoxys volucris soft tissues (phosphatized only)	2	2	0	13	2	5	0	2	3	0	0	0	5	0	2	20	4	3	20	3	**86**	**104**	
Isoxys volucris disarticulated valve	2	1	1	3	6	7	0	1	4	1	2	4	3	2	4	8	5	5	2	6	**67**	**165**	**-**
Isoxys volucris non-crumpled	3	7	4	42	18	25	21	8	11	4	10	13	17	8	19	27	16	19	43	9	**324**	**574**	**-**
Isoxys volucris crumpled	3	1	1	13	4	3	3	0	4	0	2	2	5	1	2	4	2	1	14	1	**66**	**90**	**-**

Data Table E4.4. *Isoxys volucris* size measurements used for mixture analysis.

Block	Bed	Size (mm)
Block A	Bed 1	4.2
Block A	Bed 1	4.9
Block A	Bed 1	8.8
Block A	Bed 1	8.8
Block A	Bed 1	9.3
Block A	Bed 1	9.7
Block A	Bed 1	9.8
Block A	Bed 1	10.3
Block A	Bed 1	10.6
Block A	Bed 1	11.3
Block A	Bed 1	11.7
Block A	Bed 1	11.8
Block A	Bed 1	11.8
Block A	Bed 1	11.9
Block A	Bed 1	12.3
Block A	Bed 1	15.2
Block A	Bed 2	4.8
Block A	Bed 2	4.9
Block A	Bed 2	6.8
Block A	Bed 2	7
Block A	Bed 2	9.7
Block A	Bed 2	10.9
Block A	Bed 2	12.1
Block A	Bed 2	12.2
Block A	Bed 2	12.5
Block A	Bed 2	13.6
Block A	Bed 3	7.2
Block A	Bed 4	6.5
Block A	Bed 4	6.7
Block A	Bed 4	7
Block A	Bed 4	8
Block A	Bed 4	8.5
Block A	Bed 4	8.6
Block A	Bed 4	8.7
Block A	Bed 4	8.8
Block A	Bed 4	10
Block A	Bed 4	10.1
Block A	Bed 4	10.8
Block A	Bed 4	11.7
Block A	Bed 5	8.4
Block A	Bed 5	9.1
Block A	Bed 5	9.3
Block A	Bed 5	11.1
Block A	Bed 5	11.1
Block A	Bed 5	12
Block A	Bed 6	5.5
Block A	Bed 6	6.4
Block A	Bed 6	7.3

Block A	Bed 6	7.4
Block A	Bed 6	7.7
Block A	Bed 6	9.3
Block A	Bed 6	9.8
Block A	Bed 7	5.5
Block A	Bed 7	6.8
Block A	Bed 7	7
Block A	Bed 7	8.2
Block A	Bed 7	9.3
Block A	Bed 7	9.7
Block A	Bed 7	10.1
Block A	Bed 7	10.9
Block A	Bed 7	11.1
Block A	Bed 7	11.4
Block A	Bed 7	11.4
Block A	Bed 7	12.3
Block A	Bed 7	13.8
Block A	Bed 7	14.1
Block A	Bed 8	6.9
Block A	Bed 8	8.8
Block A	Bed 8	12.1
Block A	Bed 8	14.1
Block A	Bed 9	7.8
Block A	Bed 9	9.1
Block A	Bed 9	9.1
Block A	Bed 9	10.6
Block A	Bed 9	12.1
Block A	Bed 9	12.7
Block A	Bed 9	13.7
Block A	Bed 10	4.4
Block A	Bed 10	4.8
Block A	Bed 10	6.8
Block A	Bed 10	8.2
Block A	Bed 10	8.7
Block A	Bed 10	8.8
Block A	Bed 10	11
Block A	Bed 10	11.9
Block A	Bed 10	13.7
Block A	Bed 11	5.4
Block A	Bed 11	14.1
Block A	Bed 12	5.5
Block A	Bed 12	6.3
Block A	Bed 12	8.1
Block A	Bed 12	11.3
Block A	Bed 12	12.3
Block A	Bed 12	16.9
Block A	Bed 13	7.5
Block A	Bed 13	9.1
Block A	Bed 13	9.6
Block A	Bed 13	10.2

Block A	Bed 13	12.6
Block A	Bed 13	14.3
Block A	Bed 14	9.5
Block A	Bed 14	9.7
Block A	Bed 15	7
Block A	Bed 15	7.5
Block A	Bed 15	8
Block A	Bed 15	10.2
Block A	Bed 16	4.9
Block A	Bed 16	5.9
Block A	Bed 16	7.8
Block A	Bed 16	8.1
Block A	Bed 16	8.5
Block A	Bed 16	9.8
Block A	Bed 16	12.3
Block A	Bed 16	14.8
Block A	Bed 17	7.7
Block A	Bed 17	8.5
Block A	Bed 17	8.8
Block A	Bed 17	9.7
Block A	Bed 17	10.4
Block A	Bed 17	11.4
Block A	Bed 17	12.8
Block A	Bed 17	13.1
Block A	Bed 18	4.3
Block A	Bed 18	7.4
Block A	Bed 18	8.8
Block A	Bed 18	8.9
Block A	Bed 18	10.7
Block A	Bed 18	10.9
Block A	Bed 18	11.7
Block A	Bed 18	15.9
Block A	Bed 19	8.1
Block A	Bed 19	10.4
Block A	Bed 20	3.9
Block A	Bed 20	6.1
Block A	Bed 20	6.1
Block A	Bed 20	6.5
Block A	Bed 20	7.4
Block A	Bed 20	7.5
Block A	Bed 20	8
Block A	Bed 20	8.2
Block A	Bed 20	8.3
Block A	Bed 20	8.7
Block A	Bed 20	9
Block A	Bed 20	9.1
Block A	Bed 20	9.1
Block A	Bed 20	9.4
Block A	Bed 20	10
Block A	Bed 20	10.1

Block A	Bed 20	10.1
Block A	Bed 20	10.2
Block A	Bed 20	10.2
Block A	Bed 20	10.2
Block A	Bed 20	10.3
Block A	Bed 20	10.7
Block A	Bed 20	10.8
Block A	Bed 20	11.4
Block A	Bed 20	11.6
Block A	Bed 20	12.2
Block A	Bed 20	12.3
Block A	Bed 20	14.4
Block A	Bed 20	15
Block A	Bed 20	15.2
Block A	Bed 20	16.3
Block A	Bed 20	16.9
Block A	Bed 21	5.9
Block A	Bed 21	7.8
Block A	Bed 21	10.2
Block A	Bed 21	11.2
Block A	Bed 21	11.6
Block A	Bed 21	11.9
Block A	Bed 22	5.1
Block A	Bed 22	6.2
Block A	Bed 22	7.3
Block A	Bed 22	8
Block A	Bed 22	10.1
Block A	Bed 22	10.8
Block A	Bed 22	11
Block A	Bed 22	15.2
Block A	Bed 22	16
Block A	Bed 22	16.9
Block A	Bed 23	3.5
Block A	Bed 23	4.1
Block A	Bed 23	5.8
Block A	Bed 23	6.8
Block A	Bed 23	7.5
Block A	Bed 23	8
Block A	Bed 23	8.3
Block A	Bed 23	8.7
Block A	Bed 23	8.8
Block A	Bed 23	9
Block A	Bed 23	9
Block A	Bed 23	9.5
Block A	Bed 23	9.5
Block A	Bed 23	9.7
Block A	Bed 23	10.7
Block A	Bed 23	13.5
Block A	Bed 24	5
Block A	Bed 24	5.5

Block A	Bed 24	5.9
Block A	Bed 24	6.4
Block A	Bed 24	6.4
Block A	Bed 24	6.6
Block A	Bed 24	7.4
Block A	Bed 24	7.4
Block A	Bed 24	7.5
Block A	Bed 24	7.7
Block A	Bed 24	8.7
Block A	Bed 24	9.3
Block A	Bed 24	9.7
Block A	Bed 24	9.7
Block A	Bed 24	10
Block A	Bed 24	10.3
Block A	Bed 24	10.5
Block A	Bed 24	10.5
Block A	Bed 24	10.5
Block A	Bed 24	10.6
Block A	Bed 24	11.1
Block A	Bed 24	11.1
Block A	Bed 24	11.2
Block A	Bed 24	11.3
Block A	Bed 24	12
Block A	Bed 24	12.4
Block A	Bed 24	12.7
Block A	Bed 24	12.7
Block A	Bed 25	7.4
Block A	Bed 25	7.6
Block A	Bed 25	8.2
Block A	Bed 25	8.5
Block A	Bed 25	9.5
Block A	Bed 25	10.6
Block A	Bed 26	6.3
Block A	Bed 26	8.3
Block A	Bed 26	8.3
Block A	Bed 26	9
Block A	Bed 26	10
Block A	Bed 26	11
Block A	Bed 27	8.9
Block A	Bed 27	8.9
Block A	Bed 27	9
Block A	Bed 27	9.1
Block A	Bed 27	10
Block A	Bed 27	10.2
Block A	Bed 27	10.7
Block A	Bed 27	14.7
Block A	Bed 28	5.5
Block A	Bed 28	6.2
Block A	Bed 28	7.4
Block A	Bed 28	10.1

Block A	Bed 28	10.7
Block A	Bed 28	11.5
Block A	Bed 28	11.8
Block A	Bed 28	12.3
Block A	Bed 28	13.3
Block A	Bed 28	15.9
Block A	Bed 29	3.9
Block A	Bed 29	7.6
Block A	Bed 29	8.2
Block A	Bed 29	8.3
Block A	Bed 29	8.9
Block A	Bed 29	9.9
Block A	Bed 29	10.4
Block A	Bed 29	10.5
Block A	Bed 29	16.8
Block A	Bed 30	4
Block A	Bed 30	4.5
Block A	Bed 30	7.5
Block A	Bed 30	10.1
Block A	Bed 30	10.2
Block A	Bed 30	12.7
Block A	Bed 31	6.3
Block A	Bed 31	7.7
Block A	Bed 31	9.2
Block A	Bed 31	9.7
Block A	Bed 31	11.2
Block A	Bed 32	6.4
Block A	Bed 32	7.1
Block A	Bed 32	7.1
Block A	Bed 32	7.8
Block A	Bed 32	8.2
Block A	Bed 32	8.4
Block A	Bed 32	8.4
Block A	Bed 32	9.3
Block B	Bed 1	8.4
Block B	Bed 1	10.4
Block B	Bed 1	10.8
Block B	Bed 1	14.5
Block B	Bed 2	9.4
Block B	Bed 2	9.8
Block B	Bed 2	10.4
Block B	Bed 2	10.5
Block B	Bed 2	11
Block B	Bed 2	11.6
Block B	Bed 2	11.8
Block B	Bed 3	8.2
Block B	Bed 3	9.2
Block B	Bed 3	7.8
Block B	Bed 3	9.4
Block B	Bed 4	2.2

Block B	Bed 4	2.4
Block B	Bed 4	2.8
Block B	Bed 4	2.8
Block B	Bed 4	2.8
Block B	Bed 4	2.8
Block B	Bed 4	2.8
Block B	Bed 4	3.1
Block B	Bed 4	3.1
Block B	Bed 4	3.2
Block B	Bed 4	3.3
Block B	Bed 4	3.9
Block B	Bed 4	4.1
Block B	Bed 4	4.2
Block B	Bed 4	4.3
Block B	Bed 4	4.3
Block B	Bed 4	4.4
Block B	Bed 4	4.5
Block B	Bed 4	4.6
Block B	Bed 4	4.6
Block B	Bed 4	4.7
Block B	Bed 4	4.7
Block B	Bed 4	4.8
Block B	Bed 4	5
Block B	Bed 4	5.2
Block B	Bed 4	5.3
Block B	Bed 4	5.3
Block B	Bed 4	5.5
Block B	Bed 4	6
Block B	Bed 4	6.4
Block B	Bed 4	7.5
Block B	Bed 4	7.6
Block B	Bed 4	8.1
Block B	Bed 4	8.2
Block B	Bed 4	8.3
Block B	Bed 4	8.3
Block B	Bed 4	8.5
Block B	Bed 4	8.5
Block B	Bed 4	8.7
Block B	Bed 4	9.3
Block B	Bed 4	9.5
Block B	Bed 4	10.6
Block B	Bed 4	11.4
Block B	Bed 4	11.4
Block B	Bed 4	12.4
Block B	Bed 4	12.5
Block B	Bed 4	12.6
Block B	Bed 4	13.6
Block B	Bed 4	15.5
Block B	Bed 5	3.1
Block B	Bed 5	4.1

Block B	Bed 5	5.2
Block B	Bed 5	5.3
Block B	Bed 5	5.3
Block B	Bed 5	5.5
Block B	Bed 5	7
Block B	Bed 5	7.2
Block B	Bed 5	7.5
Block B	Bed 5	7.8
Block B	Bed 5	8.4
Block B	Bed 5	8.6
Block B	Bed 5	11
Block B	Bed 5	11.1
Block B	Bed 5	11.2
Block B	Bed 5	11.2
Block B	Bed 5	11.2
Block B	Bed 5	11.5
Block B	Bed 5	11.6
Block B	Bed 5	11.6
Block B	Bed 5	13.1
Block B	Bed 5	14.3
Block B	Bed 6	2.4
Block B	Bed 6	3.2
Block B	Bed 6	3.2
Block B	Bed 6	4
Block B	Bed 6	4.2
Block B	Bed 6	4.9
Block B	Bed 6	5.2
Block B	Bed 6	5.6
Block B	Bed 6	5.7
Block B	Bed 6	5.9
Block B	Bed 6	6.1
Block B	Bed 6	6.8
Block B	Bed 6	7.6
Block B	Bed 6	7.9
Block B	Bed 6	7.9
Block B	Bed 6	8
Block B	Bed 6	8.1
Block B	Bed 6	8.3
Block B	Bed 6	8.4
Block B	Bed 6	9.3
Block B	Bed 6	9.8
Block B	Bed 6	10.2
Block B	Bed 6	10.4
Block B	Bed 6	10.5
Block B	Bed 6	10.6
Block B	Bed 6	12.3
Block B	Bed 6	12.9
Block B	Bed 6	13.4
Block B	Bed 6	13.5
Block B	Bed 6	14.2

Block B	Bed 6	16.8
Block B	Bed 7	1.8
Block B	Bed 7	3.4
Block B	Bed 7	4.4
Block B	Bed 7	6
Block B	Bed 7	6.8
Block B	Bed 7	8
Block B	Bed 7	8.2
Block B	Bed 7	9.3
Block B	Bed 7	9.3
Block B	Bed 7	9.4
Block B	Bed 7	9.9
Block B	Bed 7	10.6
Block B	Bed 7	10.8
Block B	Bed 7	11.1
Block B	Bed 7	11.2
Block B	Bed 7	11.3
Block B	Bed 7	11.6
Block B	Bed 7	12.3
Block B	Bed 7	12.4
Block B	Bed 7	12.9
Block B	Bed 7	13.1
Block B	Bed 7	13.1
Block B	Bed 7	13.7
Block B	Bed 7	15.6
Block B	Bed 8	8.7
Block B	Bed 8	9.1
Block B	Bed 8	9.3
Block B	Bed 8	10.3
Block B	Bed 8	10.5
Block B	Bed 8	10.9
Block B	Bed 9	3.2
Block B	Bed 9	4.5
Block B	Bed 9	6.3
Block B	Bed 9	6.7
Block B	Bed 9	6.9
Block B	Bed 9	7
Block B	Bed 9	7.4
Block B	Bed 9	8.4
Block B	Bed 9	8.6
Block B	Bed 9	8.9
Block B	Bed 9	10.9
Block B	Bed 9	10.9
Block B	Bed 10	7
Block B	Bed 10	8.7
Block B	Bed 10	10.1
Block B	Bed 10	11.6
Block B	Bed 10	11.8
Block B	Bed 11	3.6
Block B	Bed 11	4.7

Block B	Bed 11	4.9
Block B	Bed 11	5.1
Block B	Bed 11	5.3
Block B	Bed 11	8
Block B	Bed 11	8.3
Block B	Bed 11	10.7
Block B	Bed 11	12.2
Block B	Bed 11	13.1
Block B	Bed 11	13.8
Block B	Bed 12	5.9
Block B	Bed 12	6.9
Block B	Bed 12	7.1
Block B	Bed 12	8.6
Block B	Bed 12	9.7
Block B	Bed 12	10.1
Block B	Bed 12	10.1
Block B	Bed 12	10.3
Block B	Bed 12	10.6
Block B	Bed 12	10.6
Block B	Bed 12	10.8
Block B	Bed 12	11.9
Block B	Bed 12	12
Block B	Bed 12	12.3
Block B	Bed 12	12.4
Block B	Bed 12	12.7
Block B	Bed 12	14.1
Block B	Bed 12	15.2
Block B	Bed 12	15.3
Block B	Bed 13	3.9
Block B	Bed 13	4.1
Block B	Bed 13	4.7
Block B	Bed 13	6
Block B	Bed 13	6.4
Block B	Bed 13	6.5
Block B	Bed 13	7.4
Block B	Bed 13	8.3
Block B	Bed 13	8.6
Block B	Bed 13	8.7
Block B	Bed 13	8.8
Block B	Bed 13	8.9
Block B	Bed 13	9.3
Block B	Bed 13	9.4
Block B	Bed 13	9.8
Block B	Bed 13	9.9
Block B	Bed 13	10.4
Block B	Bed 13	10.8
Block B	Bed 13	11.4
Block B	Bed 13	13
Block B	Bed 13	13
Block B	Bed 13	13.4

Block B	Bed 13	14.7
Block B	Bed 13	15.1
Block B	Bed 14	4.9
Block B	Bed 14	6.1
Block B	Bed 14	7.7
Block B	Bed 14	8.9
Block B	Bed 14	9
Block B	Bed 14	9.9
Block B	Bed 14	10.5
Block B	Bed 14	11
Block B	Bed 14	13.4
Block B	Bed 14	13.5
Block B	Bed 14	15.3
Block B	Bed 14	16.2
Block B	Bed 15	3
Block B	Bed 15	3.8
Block B	Bed 15	4.9
Block B	Bed 15	5.8
Block B	Bed 15	6.2
Block B	Bed 15	7.7
Block B	Bed 15	8.4
Block B	Bed 15	8.6
Block B	Bed 15	8.7
Block B	Bed 15	9.1
Block B	Bed 15	9.6
Block B	Bed 15	9.6
Block B	Bed 15	9.9
Block B	Bed 15	10.5
Block B	Bed 15	10.6
Block B	Bed 15	10.8
Block B	Bed 15	11.7
Block B	Bed 15	12.2
Block B	Bed 15	12.5
Block B	Bed 15	12.7
Block B	Bed 15	12.7
Block B	Bed 15	13.7
Block B	Bed 15	14.5
Block B	Bed 15	15.5
Block B	Bed 16	4.7
Block B	Bed 16	4.8
Block B	Bed 16	5.2
Block B	Bed 16	5.5
Block B	Bed 16	5.8
Block B	Bed 16	6.2
Block B	Bed 16	6.4
Block B	Bed 16	6.6
Block B	Bed 16	6.7
Block B	Bed 16	7
Block B	Bed 16	7
Block B	Bed 16	7.3

Block B	Bed 16	7.3
Block B	Bed 16	7.8
Block B	Bed 16	8.1
Block B	Bed 16	8.1
Block B	Bed 16	8.5
Block B	Bed 16	8.9
Block B	Bed 16	8.9
Block B	Bed 16	9.7
Block B	Bed 16	9.8
Block B	Bed 16	10.2
Block B	Bed 16	10.3
Block B	Bed 16	10.4
Block B	Bed 16	10.5
Block B	Bed 16	10.8
Block B	Bed 16	10.8
Block B	Bed 16	11.1
Block B	Bed 16	12.6
Block B	Bed 16	13.8
Block B	Bed 16	15.3
Block B	Bed 16	17.1
Block B	Bed 17	2.8
Block B	Bed 17	5.6
Block B	Bed 17	6.1
Block B	Bed 17	6.5
Block B	Bed 17	9.5
Block B	Bed 17	9.5
Block B	Bed 17	9.7
Block B	Bed 17	10.1
Block B	Bed 17	10.4
Block B	Bed 17	12.2
Block B	Bed 17	12.3
Block B	Bed 17	12.4
Block B	Bed 17	12.5
Block B	Bed 17	15
Block B	Bed 17	15.4
Block B	Bed 17	15.5
Block B	Bed 17	16.4
Block B	Bed 17	16.7
Block B	Bed 18	3.1
Block B	Bed 18	3.4
Block B	Bed 18	3.5
Block B	Bed 18	4.9
Block B	Bed 18	5
Block B	Bed 18	6.8
Block B	Bed 18	6.9
Block B	Bed 18	7.1
Block B	Bed 18	7.7
Block B	Bed 18	7.9
Block B	Bed 18	8.4
Block B	Bed 18	8.4

Block B	Bed 18	8.6
Block B	Bed 18	9.5
Block B	Bed 18	9.6
Block B	Bed 18	10.4
Block B	Bed 18	10.6
Block B	Bed 18	10.8
Block B	Bed 18	10.8
Block B	Bed 18	11
Block B	Bed 18	13.1
Block B	Bed 18	13.8
Block B	Bed 19	2.3
Block B	Bed 19	2.5
Block B	Bed 19	2.6
Block B	Bed 19	2.6
Block B	Bed 19	2.6
Block B	Bed 19	2.9
Block B	Bed 19	2.9
Block B	Bed 19	3.3
Block B	Bed 19	3.3
Block B	Bed 19	3.4
Block B	Bed 19	3.5
Block B	Bed 19	3.5
Block B	Bed 19	3.5
Block B	Bed 19	3.6
Block B	Bed 19	3.6
Block B	Bed 19	3.7
Block B	Bed 19	3.9
Block B	Bed 19	3.9
Block B	Bed 19	4.2
Block B	Bed 19	4.2
Block B	Bed 19	4.2
Block B	Bed 19	4.2
Block B	Bed 19	4.3
Block B	Bed 19	4.5
Block B	Bed 19	4.7
Block B	Bed 19	4.7
Block B	Bed 19	4.9
Block B	Bed 19	5.2
Block B	Bed 19	5.2
Block B	Bed 19	5.3
Block B	Bed 19	5.4
Block B	Bed 19	5.7
Block B	Bed 19	6
Block B	Bed 19	6.2
Block B	Bed 19	6.3
Block B	Bed 19	6.3
Block B	Bed 19	6.4
Block B	Bed 19	6.4
Block B	Bed 19	6.6
Block B	Bed 19	6.8

Block B	Bed 19	6.8
Block B	Bed 19	7
Block B	Bed 19	7
Block B	Bed 19	7.4
Block B	Bed 19	8
Block B	Bed 19	8.3
Block B	Bed 19	8.4
Block B	Bed 19	8.5
Block B	Bed 19	8.6
Block B	Bed 19	8.8
Block B	Bed 19	8.9
Block B	Bed 19	9.2
Block B	Bed 19	9.3
Block B	Bed 19	9.3
Block B	Bed 19	10.6
Block B	Bed 19	11.9
Block B	Bed 20	4.7
Block B	Bed 20	7.7
Block B	Bed 20	7.9
Block B	Bed 20	9.1
Block B	Bed 20	9.9
Block B	Bed 20	11.3
Block B	Bed 20	11.4
Block B	Bed 20	12.1
Block B	Bed 20	12.5
Block B	Bed 20	12.6